Cell derived-Extracellular Matrix Scaffolds with Polylactic Acid Microcarriers for Tissue Engineering and Cell Therapy

Tesis doctoral

presentada per obtenir el títol de Doctora per la Universitat Politècnica de Catalunya al programa de Doctorat en Enginyeria Biomèdica. Departament de Ciència dels Materials i Enginyeria Metal·lúrgica. Aquest treball va ser realitzat a l'Institut de Bioenginyeria de Catalunya, sota la co-direcció de la **Dra. Elisabeth Engel** i el **Dr. Miguel Ángel Mateos-Timoneda**.

Realitzada per la

Irene Cano Torres

Barcelona, Desembre 2018 · Vol. I

A mis queridos padres y hermana, y a ti, Pepe,
por estar siempre ahí.

Agradecimientos

Y eso que parecía que este momento nunca iba a llegar… pero aquí me encuentro, pensando en quiénes han estado ahí en todo este camino. Y a pesar de lo 'duro' que pueda ser un doctorado, cuando pienso en todo lo vivido, y en las personas con las que lo he compartido solo puedo sonreír y sentirme muy afortunada. Por supuesto, en primer lugar, pienso en Eli y Miguel, que me disteis la oportunidad de hacer el doctorado en el campo en el que quería especializarme, y me acogisteis con muchísimo cariño desde el minuto uno. Siempre me habéis acompañado y apoyado en todo. La verdad es que pocos 'noes' he oído de vuestra parte. Gracias por la oportunidad de aprender, asistir a congresos, viajar, conocer gente y ¡divertirme! Muchas gracias por cuidarme tanto.

La verdad es que el entorno en el grupo y en IBEC han sido inmejorables. No solo por los instrumentos e instalaciones a nuestra disposición, que aunque muy de vez de en cuando, y por supuesto, solo para momentos cruciales fallaban… siempre nos han facilitado la labor científica. Pero sobretodo por las personas, porque siempre te acababas encontrando a alguien dispuesto a echarte una mano. Y una de ellas ha sido Sole, que siempre se ha involucrado en la causa, aunque no le tocara en nada. ¡Mil gracias Sole! Por los ensayos con huevos, los cortes, immunos, histologías, reactivos, por el orden, la paciencia, por todo, gracias. Agradezco también a los veteranos del grupo Oscar, Xavi, Aitor y Riccardo por todos sus consejos. Gracias Riccardo porque, aunque fueran unos pocos meses como mentor, siempre me he sentido orgullosa de continuar tu legado en IBEC. A ti Aitor, gracias, por lo mala influencia que fuiste como compañero de pasillo (espero que se note la ironía).

A mis compañeros de laboratorio, y también amigos. Agradezco de todo corazón haber compartido todo este tiempo con vosotros Claudia, Joan, Sergi, Jesús y Gerard. Porque hemos sido un grupo especial, por tantos momentos compartidos, por las consultas de dudas científicas y de la vida, por los ánimos y el apoyo, y por las tantas risas que nos hemos echado. Ha sido un placer coincidir y vivir esta experiencia con vosotros. Además, debo agradeceros que secundarais muchos de mis momentos de inspiración creativa, dando rienda suelta a esa vertiente más artística. Agradezco también haber coincidido con Anna Crespo y Ágata, por ser buenas amigas y compañeras. Cómo no, a mis queridas rubias Cris y Jeni, que han sido como hermanas para mí. Sé que todas nos hemos apoyado en los momentos que nos necesitábamos, pero, por la parte que me toca, ¡gracias! Por

aguantarme y por compartir tanto. Nada de esto hubiera sido igual sin vosotras. Y gracias a esta bonita amistad, me hicieron integrante a medias de Core Facilities. Gracias Isa, Laura, Ramona, Tania e Inma, por vuestra labor y sobretodo amistad. Os echaré de menos. Será difícil encontrar un trabajo próximo en el que me sienta tan a gusto como me he sentido en IBEC.

Estoy muy agradecida al grupo de Terapia Celular del CSIC, al que me uní discretamente y con la escusa de usar el biorreactor de Olaia, y acabé metiéndome de lleno con las pruebas de los microtejidos en el cerebro. Gracias Olaia, Marta, Lourdes, Oscar, Nuri y Jero, por la ayuda y aprendizaje, pero en especial, ¡gracias Cris! Mil gracias por todo lo que he aprendido contigo, por tantas horas de trabajo con los ratones, por tu apoyo y desparpajo andaluz.

No quisiera acabar sin agradecerle a mi familia todo el apoyo y confianza, a todos, hermana, abuelos, tíos, suegra y cuñados, pero sobretodo a mis padres por todo lo que habéis hecho por mí. Os doy las gracias por la educación recibida a todos los niveles, sé que ha sido un gran esfuerzo y que siempre habéis intentado darme lo mejor, para que tuviera las mejores oportunidades. Barcelona, Londres, lo que quisiera, siempre me habéis dado mucho más de lo que hubiera hecho falta. Gracias de corazón.

Y a Pepe, cómo no, por entender el sacrificio que representaba esta tesis, y por no dejar que me rindiera. Gracias por estar a mi lado. Te debo varias semanas de vacaciones, algún año extra de juventud y cuidarte tanto como tu has hecho conmigo.

Abstract

Organ shortage for transplantation and the need for new therapies for the treatment of tissular damages have driven the development of an exciting field in research, called tissue engineering (TE). Its potential entails future strategies that will allow the development of functional substitutes for damaged tissues, obtained *in vitro* under risk-free environments, using autologous cells that will integrate within the host aiding in the regeneration and restore of the lost function. However, still current efforts have to deal with several restraints in order to achieve that paradigm.

The aim of this thesis focuses in the development of *in vitro* tissue analogues with millimetric size (microtissues), using the inherent ability of cells to secrete their own extracellular matrix (ECM) when they are seeded on a biocompatible scaffold. In this case, we have used polylactic acid (PLA) microcarriers (MCs) (80 -120 μm in diameter) as scaffold. PLA has been an extensively used as a biomaterial applied in medicine, as it is a biodegradable and biocompatible synthetic polymer. Moreover, we have used a green, non-toxic method for the preparation of PLA MCs that allows a high control over size and distribution. The use of these MCs provides cells with an ideal three-dimensional environment for proliferation and secretion of ECM components, which are different than when exposed to conventional tissue culture plates. Likewise, the use of MCs in the formation of microtissues allows their aggregation (as building blocks) into bigger constructs or macrotissues, with high interconnectivity and porosity, as well as the feasibility to adapt to different shapes.

Firstly, in this thesis we have studied different methodologies for the seeding of cells on MCs, and the latter formation of microtissues to define the best parameters for a homogeneous seeding and extensive ECM deposition. For that purpose, we have used a spinner flask bioreactor promoting a more uniform cell-MC colonization, and ECM deposition. After optimization, we have evaluated the obtained ECM microtissues, assessing their components and possible applications. In that case, we introduced the use of commercially available-gelatine microcarriers for a comparative with PLA MCs. We assessed whether the secreted ECM differed when using each MCs type. And we could confirm that the scaffold choice influences cellular behaviour and secreted matrix, favouring osteogenic with gelatine MCs or potentiating angiogenic capacity with a mixture of gelatine and PLA MCs.

One of the biggest hurdles that halt the introduction of TE constructs into clinical applications is the vascularization process for the survival of cells once implanted. The arrival of nutrients and oxygen must be favoured by a rapid *in vivo* vascularization. To aid in this process, we have studied the formation of co-cultured microtissues with mesenchymal stem and endothelial cells, together with PLA MCs. We were able to confirm the presence of both cell types in the microtissues, but there were no clear evidences that the presence of endothelial cells enhanced microtissue vascularization in mice models.

Finally, we used cell-derived ECM microtissues as a platform for the introduction and survival of therapeutic cells in an anti-tumoral model. Microtissues acted like a reservoir for these cells, allowing migration towards the tumour providing their bystander therapeutic effect. The results of this study demonstrated the efficiency of PLA microtissues obtained from therapeutic cells in stopping tumour progression. Moreover, a rapid microtissue vascularization was observed, which favoured cell survival.

To summarise, this thesis describes the fabrication of cell-derived microtissues, created from seeding cells on PLA microcarriers as a favourable strategy in tissue engineering, as well as a tool for the delivery and survival of therapeutic cells for anti-tumoral applications.

Resumen

La escasez de órganos disponibles para trasplantes y la falta de terapias para el tratamiento de algunas lesiones tisulares han llevado al desarrollo de un campo de investigación muy potente, la ingeniería de tejidos (TE). Futuras estrategias permitirán desarrollar y disponer de nuevos sustitutos para tejidos dañados, construidos de forma segura, a partir de nuestras propias células y totalmente funcionales que se integrarán en nuestro cuerpo ayudando a regenerar y restaurar la función perdida. No obstante, para que este futuro se materialice aún son necesarios muchos esfuerzos que lidien con las limitaciones que de momento nos encontramos.

El objetivo de esta tesis es el desarrollo *in vitro* de análogos de tejidos (microtejidos), utilizando la capacidad de las células de secretar su propia matriz extracelular (ECM) cuando son sembradas sobre un andamio biocompatible. En este caso, hemos utilizado micropartículas de ácido poliláctico (PLA) como andamio. Se trata de un material extensamente aplicado para uso médico, por su biodegradabilidad y biocompatibilidad. Además, para su producción utilizamos reactivos ecológicos y no tóxicos. El uso de estas partículas proporciona a las células un entorno tridimensional ideal para proliferar y secretar proteínas y otros componentes de la ECM, diferentes a cuando se las expone a entornos en dos dimensiones. Asimismo, su uso en TE permite la agregación de diferentes microtejidos para la creación de constructos más grandes, presentando una alta interconectividad y porosidad, así como una elevada facilidad para adaptarse a diferentes regiones.

Inicialmente, en esta tesis estudiamos diversos métodos de sembrado y de formación de microtejidos para configurar los parámetros para la obtención de un sembrado extenso y homogéneo. Esto nos llevó a determinar que el uso de un biorreactor de agitación promueve un mejor sembrado cosa que luego conlleva a una secreción más homogénea de ECM por el microtejido. Una vez optimizado, caracterizamos las matrices obtenidas, evaluando sus componentes y sus posibles aplicaciones. En este caso, utilizamos otras micropartículas comerciales para su comparativa con nuestras partículas de PLA. Evaluamos si las matrices obtenidas sembrando las mismas células eran diferentes y pudimos observar, cómo la elección del andamio influye en el comportamiento celular y en la matriz secretada favoreciendo en unos casos la diferenciación osteogénica o en otros su potencial angiogénico.

Una de las mayores limitaciones en la aplicación clínica de los constructos de TE, es su vascularización. La llegada de nutrientes y oxígeno debe ser favorecida mediante una rápida vascularización *in vivo* para la supervivencia de las células del constructo. Para favorecer este proceso, estudiamos la creación de microtejidos cocultivados con células mesenquimales y endoteliales, juntamente con las micropartículas de PLA. Pudimos demostrar la presencia de ambas células en el constructo, aunque no observamos una clara diferencia en cuanto a vascularización una vez implantados en ratones, con la presencia de las células endoteliales y sin ellas.

Por último, estudiamos el uso los microtejidos como plataforma para la introducción y supervivencia de células terapéuticas en un modelo subcutáneo tumoral. Los microtejidos actúan como reservorio de estas células, permitiendo la migración hacia el tumor, y así en proximidad provocar su efecto terapéutico. Los resultados de este estudio demostraron la efectividad de los microtejidos de PLA creados por las células terapéuticas, a través de la disminución del volumen de los tumores. Además, pudimos observar una rápida vascularización favoreciendo la supervivencia celular.

En conclusión, esta tesis describe la fabricación de microtejidos derivados de células, sembradas sobre partículas de PLA como estrategia favorable para ingeniería de tejidos, así como herramienta para la supervivencia y liberación de células terapéuticas en un modelo anti-tumoral *in vivo.*

Contents

Abstract / Resumen ..... ***vii / ix***

List of figures ..... **xv**

List of tables ..... **xx**

List of equations ..... **xx**

Chapter 1. General introduction, motivation and thesis outline **1**

Chapter 2. Introduction and state of the art **5**

2.1 Tissue Engineering 5

2.1.1 Cells *6*

2.1.2 Biomaterials *8*

2.1.3 Physicochemical stimuli *10*

2.2 Extracellular matrix scaffolds 12

2.2.1 Extracellular matrix scaffolds for the creation of functional tissues *13*

2.2.2 Cell-derived matrices for phenotype maintenance in cell culture. *17*

2.2.3 ECM models for basic biological research. *18*

2.3 Polymer microcarriers scaffolds 18

2.3.1 Types of polymer microcarriers *18*

2.3.2 Microcarrier fabrication methods *20*

2.3.3 Biomedical applications of polymeric microcarriers *25*

2.4 Microtissue vascularization strategies 28

2.5 Microtissues for anti-tumoral cell therapy 32

2.5.1 Bystander cell therapy against tumour *32*

2.5.2 Biomaterials used for the delivery of bystander cell therapy *33*

2.6 Bioluminescence as non-invasive imaging technique 34

2.7 Thesis Objectives 39

Chapter 3. Study of PLA microcarrier cell seeding technique for microtissue formation.....41

3.1 Introduction 41

3.2 Materials and methods.....43

3.2.1 Cell Culture and Expansion.....43

3.2.2 Microcarrier fabrication.....43

3.2.3 Biofunctionalization of the surface of microcarriers.....44

3.2.4 Microcarrier seeding in static conditions.....44

3.2.5 Morphology and size examination.....45

3.2.6 Microcarrier seeding in dynamic conditions.....45

3.2.7 Vital staining and MC colonization rate.....46

3.2.8 Scanning electron microscopy.....46

3.2.9 Statistical analysis.....47

3.3 Results 47

3.3.1 PLA microcarrier characterization.....47

3.3.2 Microtissue size evaluation in static conditions.....49

3.3.3 Microscopic evaluation of scaffolds produced in static conditions.....51

3.3.4 Spinner flask microcarrier colonization.....54

3.3.5 Extracellular matrix deposition after spinner flask bioreactor.....57

3.4 Discussion 58

3.5 Conclusions 64

Chapter 4. Cell-derived extracellular matrix scaffolds: microcarrier choice influences ECM deposition and functionality.....67

4.1 Introduction 67

4.2 Materials and methods.....69

4.2.1 Cell culture and expansion.....69

4.2.2 Microcarrier preparation.....69

4.2.3 Microtissue fabrication *70*

4.2.4 Vital staining and MC colonization rate *70*

4.2.5 Osteogenic induction *71*

4.2.6 Cell proliferation assessed by Picogreen dsDNA assay kit *71*

4.2.7 Total protein quantification *71*

4.2.8 Scanning electron microscopy (SEM) *72*

4.2.9 Immunofluorescent analysis of MT *72*

Reference number from Abcam catalogue. *73*

4.2.10 Analysis of alkaline phosphatase (ALP) activity *73*

4.2.11 Glycosaminoglycan quantification *73*

4.2.12 Real Time PCR *74*

4.2.13 Stromal derived factor-1α ELISA *75*

4.2.14 Chick chorioallantoic membrane (CAM) assay *75*

4.2.15 Statistical analysis *76*

4.3 Results 76

4.3.1 Microtissue fabrication using PLA, Cultisphere S and a mixture of both microcarriers *76*

4.3.2 Microtissue characterization with normal medium *82*

4.3.3 In vivo angiogenic potential characterization of microtissues using CAM model 88

4.3.4 Microtissue evaluation under osteogenic induction *90*

4.3.5 Evaluation of cell-homing chemokine SDF-1α expression *94*

4.4 Discussion 95

4.5 Conclusions 100

Chapter 5. Microtissue vascularization using a co-culture strategy 103

5.1 Introduction 103

5.2 Materials and Methods 105

5.2.1 Cell isolation, expansion and lentiviral transduction 105
5.2.2 Microcarrier preparation 105
5.2.3 Evaluation of HUVEC – microcarrier adhesion 105
5.2.4 Co-cultured microtissue fabrication 106
5.2.5 Vital staining for microcarrier colonization 106
5.2.6 Total DNA proliferation 107
5.2.7 Scanning electron microscopy 107
5.2.8 Flow cytometry 107
5.2.9 In vivo subcutaneous implantation 107
5.2.10 Bioluminescence imaging 108
5.2.11 Immunofluorescence 108
5.2.12 Histologies 109
5.2.13 Perfused bioreactor 109
5.3 Results 110
5.3.1 HUVEC adhesion to PLA microcarriers in static conditions 110
5.3.2 Co-culture microtissue formation by independent spinner flasks 110
5.3.3 Initial hAMSC MT pre-formation and later HUVEC seeding 114
5.3.4 Co-cultured microtissues promoted vascularization in vivo 116
5.3.5 Perfusion assisted macrotissue formation 118
5.4 Discussion 119
5.5 Conclusions 122

Chapter 6. Anti-tumoral microtissue application 125
6.1 Introduction 125
6.2 Materials and Methods 126
6.2.1 Cell isolation, expansion and lentiviral transduction 126
6.2.2 Microcarrier preparation 126
6.2.3 Microtissue fabrication 127

6.2.4 TK-hAMSCs quantification (Total DNA and BLI) *127*

6.2.5 Tk-hAMSC-microtissue SEM evaluation *127*

6.2.6 Transwell migration assay and decellularization *128*

6.2.7 In vivo TK-hAMSCs-MTs plus GCV treatment against subcutaneous PG-PC3 tumours *128*

6.2.8 Histologies *129*

6.2.9 Statistical analysis *130*

6.3 Results 130

6.3.1 Tk-hAMSCs-MT production, cell quantification and viability *130*

6.3.2 hAMSCs migration capacity was not enhanced when decellularizing and reseeding microtissues *132*

6.3.3 TK-hAMSCs-MTs were available up to 42 days after in vivo subcutaneous implantation *135*

6.3.4 TK-hAMSCs-MTs plus GCV inhibited PG-PC3 tumour progression *136*

6.3.5 TK-hAMSCs-MTs were irrigated by blood vessels and allowed TK-hAMSCs migration *138*

6.4 Discussion 141

6.5 Conclusions 144

Chapter 7. Conclusions 145

Scientific contributions **..... 147**

Bibliography **..... 151**

List of figures

Figure 2.1 Tissue engineering paradigm 6

Figure 2.2 Schematic representation of different bioreactors.....12

Figure 2.3 Cell culture methods for the preparation of cell-derived decellularized matrices 14

Figure 2.4 Chemical structure of the monomeric units of L-lactide, D-lactide, Glycolide and ε-Caprolactone.....20

Figure 2.5 Microcarrier fabrication via emulsion-solvent evaporation.....21

Figure 2.6 Porous polymeric microcarriers.....22

Figure 2.7 Microcarrier fabrication techniques I.....23

Figure 2.8 Microcarrier fabrication techniques II 24

Figure 2.9 Modular TE approaches using polymer MCs 28

Figure 2.10 Schematic representation of the processes for vascular development 29

Figure 2.11 Non-invasive imaging techniques.....35

Figure 2.12 Real-Time monitoring of luciferase-expressing cells 37

Figure 2.13 Tumorigenic cells expressing luciferase for bioluminescent *in vivo* monitoring.....38

Figure 3.1 Microcarrier preparation and characterisation 48

Figure 3.2 Immunofluorescent images of PLA MPs after surface biofunctionalization with collagen type I.....48

Figure 3.3 Macroscopic morphology and size of PLA microtissues prepared in static conditions 50

Figure 3.4 Area analysis of the MT obtained in the U-shaped 96 well plates.....51

Figure 3.5 Scanning electron microscopy images of U96 MT after 21 days in culture 52

Figure 3.6 Scanning electron microscopy images of 24w MT after 21 days in culture 53

Figure 3.7 Transversal sections of 24w MT observed by scanning electron microscopy 54

Figure 3.8 Microcarrier colonization parameters under study 55

Figure 3.9 Microcarrier colonization evaluated over time in a spinner flask bioreactor 56

Figure 3.10 SEM images of MT obtained after dynamic MC colonization and formed in ultra-low attachment 24 well plates for 21 days 58

Figure 4.1 Fluorescent microscope images of calcein-AM vital staining of colonized microcarriers, after 6h of intermittent agitation in spinner flask bioreactor 77

Figure 4.2 DNA and protein content characterization of MTs.....78

Figure 4.3 SEM micrographs of PLA, Mixed and Cultisphere S MTs at days 7, 14 and 21 80

Figure 4.4 Cell morphology evaluation on MTs after 21 days of formation 81

Figure 4.5 Cell morphology evaluation on magnified images for Cultisphere S and PLA MTs.....82

Figure 4.6 Immunofluorescent characterization of fibronectin after 21 days in culture 83

Figure 4.7 Quantification of immunofluorescent signal of expressed collagens type I, II, III and IV in PLA, CultiSphere and Mixed MTs.....84

Figure 4.8 Immunofluorescence of sliced microtissues assessing for collagen I, II, III and IV expression.....85

Figure 4.9 GAGs and ALP quantification.....86

Figure 4.10 Gene expression analysis of rMSCs in MTs developed with PLA, Cultisphere S and Mixed microcarriers.....88

Figure 4.11 CAM *in vivo* assay 89

Figure 4.12 Vascular area density (pixels/mm^2) of implanted MTs and controls in the *in vivo* CAM assay 90

Figure 4.13 Characterization of osteogenic MTs 91

Figure 4.14 Scanning electronic microscopy images of Mixed and Cultisphere MT after 7, 14 and 21 days in osteogenic medium 92

Figure 4.15 Gene expression profile of Mixed and Cultisphere MTs under osteogenic induction.....93

Figure 4.16 Stromal cell derived factor 1 alpha secretion into the medium analysed by an ELISA assay, and normalized to total DNA for each timepoint and condition 94

Figure 5.1 HUVEC static seeding on PLA and Cultisphere S MCs 110

Figure 5.2 Vital staining of hAMSCs and HUVEC cells seeded on PLA microcarriers in spinner flask bioreactor.....111

Figure 5.3 Co-culture MT evaluation.....112

Figure 5.4 Flow cytometry analysis of cells in MTs.....113

Figure 5.5 Analysis of CD31 expression of hAMSCs on TCP under different culture mediums.....114

Figure 5.6 Characterization of Co-culture MT obtained from the pre-formation of hAMSCs-MT and then HUVEC cells were seeded on top after one week.....115

Figure 5.7 Non-invasive imaging of RLuc-expressing cells in hAMSC-MT and Co-culture-MT, subcutaneously implanted in SCID mice.....116

Figure 5.8 *In vivo* MT implantation 117

Figure 5.9 Histological analysis of implanted MT.....118

Figure 5.10 Macrotissue formation monitoring inside a perfused bioreactor 119

Figure 6.1 Tk-hAMSCs cells expressing Rluc.....130

Figure 6.2 Evaluation of cell number in Rluc-Tk-hAMSCs-MT 131

Figure 6.3 TK-hAMSCs-MT observation with scanning electron microscope after 14 days in culture 132

Figure 6.4 Transwell migration assay assessing therapeutic hAMSCs mobility from MTs towards PG-PC3 derived medium.....133

Figure 6.5 Decellularization and recellularization of hAMSC-derived MTs.....134

Figure 6.6 Evaluation of AMD3100 in blocking CXCR4/SDF-1α migratory axis to enhance mobility towards prostate cancer cells stimuli.....135

Figure 6.7 *In vivo* survival of TK-hAMSCs-MT implanted dorsally.....135

Figure 6.8 *In vivo* TK-hAMSC-Mt implantation with GCV treatment against subcutaneous PG-PC3 tumours 137

Figure 6.9 Tumour size evaluation 138

Figure 6.10 Haematoxylin-eosin histological staining of TK-hAMSCs-MT treated with saline serum retrieved after 40 days of implantation 139

Figure 6.11 Histological H&E staining of PG-PC3 extracted tumours, after 40 days of dorsal subcutaneous implantation 140

Figure 6.12 Immunofluorescence showing CD31 positive cells inside the MTs conforming a tubular lumen structure 141

Figure 6.13 hAMSCs migration from MTs towards tumoral cells was observed using anti-human mitochondria antibody 141

List of tables

Table 2.1 Studies proving *in vitro* formation of ECM-derived scaffolds for tissue regeneration purposes.....15

Table 2.2 Commercially available MCs and some of their features 25

Table 4.1 List of antibodies used in the immunofluorescent analysis. 73

Table 4.2 RT-PCR programme for StepOne Plus Real-Time System. 74

List of equations

Equation 1 Definition of Microcarrier Colonization Rate.....46

Chapter 1

General introduction, motivation and thesis outline

Tissue engineering (TE) was defined three decades ago as an exciting and promising field of biomedicine aimed at elucidating new therapies for the repair, replacement and regeneration of tissues and organs that the body is not able to restore (Langer, 1993). Many efforts have been already made during these years, and a few TE products have successfully reached the market (Place, 2009). Skin, cartilage and bone TE products from allogenic sources were initially used, although more and more autologous therapies are now being implemented. Notorious clinical advances have used autologous cells seeded on poly(lactic-co-glycolic-acid) sheets to develop functional bladders (Atala, 2006). However, native complexity of tissues and organs considering the diversity of cells, the extracellular intricate network and the vascularization system render as the main hurdles for the creation of engineered tissues. Nevertheless, simplified strategies combining cells and scaffolds have been successful for cases that do not require extensive vascularization (Place, 2009).

Regulatory, ethical and financial issues have also represented important hindrances in TE commercialization. In Europe, the European Medicines Agency (EMA) regulates TE products as advanced therapy medicinal products (ATMPs) (Regulation (EC) No 1394/2007). For the sake of safeguarding public health, the production, distribution and uses of ATMPs face high regulatory requirements. Moreover, large amounts of time, money and resources have to be forestalled, making their road towards commercialization a rough path. Nonetheless, exciting prospects are being depicted for the next up-coming years. Market analysts have forecasted the global TE field to reach 10.000 million euros by 2022, meaning a 2-fold increase since 2016 (Grand View Research, 2018). Moreover,

increasing aging population, the emergence of new technological advancements, and the arousal of funds intended to the field are the key factors driving this new market scenario. Global life expectancy has increased 5.5 years, reaching 72 years (from 2000 to 2016, according to WHO) thanks to different medical advances and global control policies over some diseases. However, consequences of this elderly population implicate arising risks in the prevalence of age-associated diseases such as cardiovascular and orthopaedic disorders, together with an increase in diabetes, obesity, hypertension and trauma injuries, incrementing the need for medical procedures. Likewise, the emergence of technological advancements such as 3D tissue engineering, organ-on-a-chip technologies, replacement of embryonic cells with proliferative stem cells, lithography, laser tweezers, among others, are contributing to promote advances in the field of TE. Also, increased social awareness and public knowledge, as well as the arousal of grants both by governments and private sector are fostering the TE market to exciting paradigms.

Driven by this situation, this thesis was contemplated for the development of a TE strategy in which functional microtissues were derived from the extracellular matrix (ECM) secretion of cells seeded on polymeric microcarriers. Potentially, this strategy would result in the implantation of the engineered construct and its integration within the injured site, to eventually, overcome the lack of tissue donors and the problems of donor-receiver compatibility, by using autologous cell sources. The generation of ECM derived constructs allows a closer replication of the complex tissue architecture and arrangement found in nature, as well as the unlimited production of functional substitutive tissues.

To begin with, *Chapter 2* gathers a literature review of the main topics developed in this thesis. It summarises basic knowledge in the field of TE, together with microcarrier fabrication techniques and their applications in modular tissue engineering. Moreover, the latest strategies for the vascularization of engineered constructs are covered, as well as, a brief overview on the application of these scaffolds for anti-tumoral therapies.

In *Chapter 3* we investigated the appropriate methodology for the generation of microtissues using PLA microcarriers. Two seeding techniques, static and dynamic, were discussed. Also, for each of these techniques, different parameters were studied such as the proportion of cells - microcarriers, the total amount of microcarriers used, and different static platforms in which microtissues. Additionally, some agitating parameters were compared.

Chapter 4 englobes the characterization of cell-derived ECM scaffolds fabricated using polylactic acid microcarriers, gelatine microcarriers and a mixture of both types.

The evaluation of the secreted proteins such as collagens, or proteoglycans, as well as the osteogenic and angiogenic potential demonstrated that secreted ECM were different depending on the choice of the microcarrier. This chapter highlights the importance of ECM characterization prior to the determination of microtissue function, as the choice of MCs influences secreted ECM.

In *Chapter 5* a co-culture strategy was developed for evaluating microtissue vascularization upon *in vivo* implantation. The generation of a microtissue using human adipose-derived mesenchymal stem cells (hAMSCs) together with human umbilical cord endothelial cells (HUVEC) was investigated. Different co-culture microtissue formation procedures were evaluated, and finally, histological assessment of the implanted microtissues were used to determine the vascularization performance.

Chapter 6 describes the application of cell-derived microtissues for the delivery of therapeutic cells in a bystander anti-tumoral therapy. Therapeutic cells were able to produce a microtissue on PLA microcarriers, which was then implanted near a growing tumour. Cells migrated towards the tumour and delivered the therapeutic agent and eventually caused its regression.

Finally, *Chapter 7* summarizes the conclusions achieved at each chapter, and states future perspectives that arise from the investigation performed in this thesis.

This doctoral thesis was mainly developed at the Institute of Bioengineering of Catalonia (IBEC), at the group of Biomaterials for Regenerative Therapies, under the supervision of Dr. Elisabeth Engel and Dr. Miguel Ángel Mateos-Timoneda. *In vivo* experimental research, in Chapter 5 as well as the anti-tumoral strategy described in Chapter 6 were performed at the Instituto de Química Avanzada de Cataluña – CSIC (Barcelona) in the group of Cellular Therapy, with Dr. Cristina Garrido as close collaborator.

Chapter 2

Introduction and state of the art

2.1 Tissue Engineering

Tissue engineering is an interdisciplinary field of research focused in the development of functional constructs to restore, maintain or improve damaged tissues and organs by applying principles of engineering and life sciences combining three basic elements: cells, scaffolds and bioactive molecules (Langer, 1993). TE is integrated in the field of regenerative medicine, and although they are sometimes interchanged, the latter is a broader term that includes other approaches such as the single transplantation of genetic engineered cells, or the targeting of developmental pathways of stem cells as means of therapy (Daar, 2007).

Foreseen outcomes of TE include the mitigation of critical shortage organs for transplantations, prevent immune responses involved in organ compatibility and reduce related medical costs via the fabrication of functional biological structures. The classical or top-down approach in TE (*Figure 2.1*) involves the isolation of primary cells either from the same patient (autograft) or from healthy donors (allograft), and their expansion *in vitro*. Afterwards, cells are seeded on porous scaffolds, which provide structural support and present biochemical signals to exert specific cellular behaviours (release of growth factors, binding to bioactive molecules, etc). Prior to clinical implantation, seeded scaffolds are induced to mature under specific and controlled environmental conditions. Paradigmatically, upon implantation, gradual tissue regeneration is encompassed with progressive scaffold degradation and bioresorption achieving total tissue restoration. Nevertheless, modifications of the classical approach include strategies in which *in vitro* expanded cells are seeded on the scaffold and straightaway implanted, avoiding

maturation procedures in the bioreactor; as well as direct scaffold implantation in which *in vivo* cell recruitment is desired (Nair, 2011).

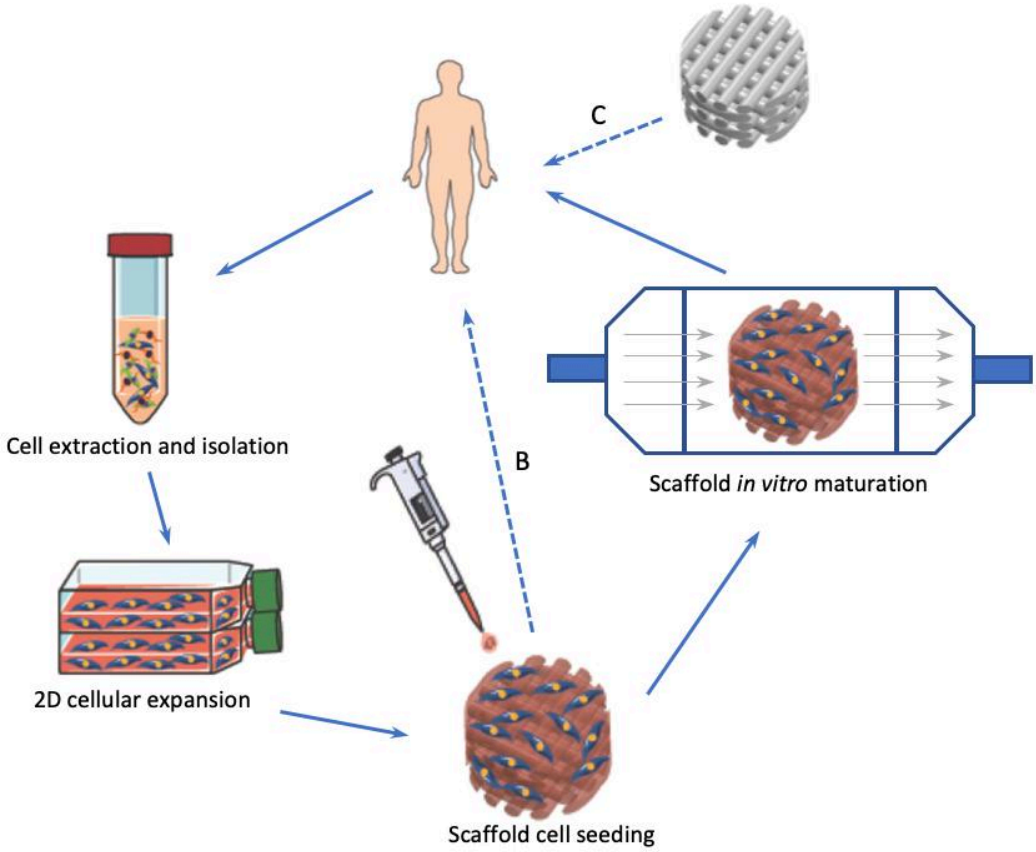

Figure 2.1 Tissue engineering paradigm. First, cells are extracted and isolated from the patient. To obtain large amounts of cells, these are expanded in vitro. Afterwards, cells are seeded onto the scaffold, which are then kept in in vitro controlled conditions for proliferation and maturation prior to reimplantation to the injured site (Langer, 1993). (B) Alternative strategies entangle the implantation of cell-laden scaffolds, without in vitro maturation processes, or (C) direct implantation of the scaffolds which promote host cellular ingrowth for an in-situ colonization. Adapted from (Pereira, 2015).

In their willing to recapitulate functional tissues, TE takes as basic elements those observed in native tissues: specialized cells which are entangled within a network named extracellular matrix (ECM) together with trapped or soluble signals, used in cell-cell contacts and paracrine communications. Detailed information on the basic TE elements (cells, biomaterials and signals) is next reviewed.

2.1.1 Cells

Multiple cell types can be used in TE, and the choice is always linked to the tissue being replicated. The simplest option is to obtain fully differentiated cells from the patient (autologous), avoiding incompatibilities and adverse immune responses when further

implanted after engineered construct formation. However, this strategy is mostly encompassed with limitations in cell availability, donor-site morbidity, and the possible diseased state of the patient. Also, somatic cells face insufficient or void proliferation rates, thus restricting *in vitro* expansion. However, advances in the field of progenitor/stem cells have opened up numerous alternatives for cell sourcing. Stem cells have self-renewal capacity and own the potential to differentiate into different phenotypes. For instance, human embryonic stem (ES) cells, which are obtained from blastocysts have the potential to differentiate into all three embryonic germ layers and own unlimited division potential. However, as a result to their allogenic origin, immune suppressing drugs are required. At the same time, their use arouses ethical concerns due to the disruption of the embryo following cell extraction (Thomson, 1998), and their clinical application is limited due to the risk for tumour formation, characteristic for pluripotency (Herberts, 2011; Przyborski, 2005).

On the other hand, mesenchymal stem cells (MSCs) which possess multi-lineage differentiation potential have rapidly attracted attention due to their versatile sourcing. MSCs can be found in almost any tissue type and they are easily accessible (*i.e.* bone marrow aspirates, skeletal muscle, connective tissue, human trabecular bones, adipose tissue, periosteum, foetal blood and liver, and umbilical cord blood) (Oh, 2011). Although some MSCs exist at a very low frequency in their native tissues, once isolated, they can be potentially expanded without losing their multipotentiality. Different multipotent stem cells can be committed into osteoblasts, chondrocytes, adipocytes, endothelial cells, nerve cells, heart myocytes, hepatic cells, or into virtually any cell phenotype (Beltrami, 2003; Crisan, 2008; Gage, 2000; Pittenger, 1999; Stock, 2008). Also, MSCs are of great interest to regenerative therapies as they have been demonstrated to exert anti-inflammatory and immunomodulatory effects in allogeneic T cells (Klyushnenkova, 2005). In addition, MSCs display an innate ability to home to areas of inflammation via the stromal cell-derived factor alpha (SDF-1α or CXCL12) and its receptor CXCR4 axis, as well as via the immune regulatory cytokine transforming growth factor beta (TGFβ) (da Silva Meirelles, 2009). Once in the injured site, they accelerate the repair process by promoting infiltration of immune cells, modulating angiogenic response and supporting cellular growth and proliferation (Nwabo Kamdje, 2016). MSCs homing is also observed towards tumoral tissues, and although their effect can be either supportive or inhibitory in tumour progression (Rivera-Cruz, 2017; Zimmerlin, 2013), several strategies are using MSCs in cell therapies in anti-tumour approaches (see Section 2.5).

In 2006 and 2007, induced pluripotent stem cells (iPSC) described as reprogrammed somatic cells presenting ES cell-like properties, emerged as the ultimate cell source for regenerative therapies (Okita, 2007; Takahashi, 2006). Takahashi and Yamanaka, considered as the fathers of iPSC, transfected adult fibroblasts with specific factors (Oct4, Sox2, Klf4, c-Myc, Nanog and Lin28), obtaining cells that exhibit ES cell morphology, growth properties, self-renewal, could differentiate the three germ-lines and expressed ES cell marker genes (Okita, 2007; Takahashi, 2006). In addition to fibroblast, several somatic cells have been already reprogrammed into iPSC for regenerative therapies, *in vitro* tissue modelling and drug screening (Yoshida, 2010). Several newly emerged technological advances in iPSC generation have replaced Yamanaka's virus-based reprogramming method, associated with incomplete reprogramming and tumour formation, by using: epigenetics, microRNA manipulation, episomal vectors and other nonviral vectors (Ji, 2016). Despite all these efforts, low efficiency in iPSC generation and the appearance of chimeras, together with the manifestation of epigenetic aberrations and immune intolerances have put the use of iPSC aside from clinical applications (Yoshida, 2010), motivating further investigations to unravel iPSC technology potential.

2.1.2 Biomaterials

Biomaterials were firstly used as mere tissue substitutes providing structural support in missing or injured tissues, like the prostheses in hip replacement, screws or metallic dental implants (Migonney, 2014). Nowadays, a huge importance is attributed to biomaterial-cell interactions for successful accomplishments. Considering that stem cells can exercise as therapeutic agents in regenerative medicine, when directly administrated in the desired location, they are easily washed away and less than 10% of injected cells survive (Scudellari, 2009). Biomaterial scaffolds must take on the instructive role to support cell viability enhancing cell residence time in the target tissue and exerting specific cellular behaviours. Temporary environment hold by materials should allow cell colonization, attachment and proliferation, as well as extracellular matrix synthesis. Also, scaffolds should be permissive with host cell infiltration and remodelling for the correct construct implantation, vascularization and in the end, adequate tissue regeneration.

The appropriate choice of a biomaterial and its properties are pivotal in any TE strategy and they should match physical, chemical, biological and structural features found in the tissue being treated or in the developing stages of that same tissue (Martin, 2014). Scaffolds must be biocompatible, and upon implantation, they must provoke reduced or

controlled inflammation, avoiding encapsulation and rejection. Also, biodegradation of the scaffolds must be thoroughly controlled, and the resulted by-products should not elicit any harmful effects on the body.

Mechanical properties of native tissues elicit specific responses on cell behaviour (Discher, 2005; Engler, 2006), for that reason, engineered scaffolds should consider targeted tissue stiffness and elasticity. Likewise, architectural features have to be considered in scaffold design. For instance, surface roughness or the presence of groove and ridge structures both at the micro- and nanoscale, influence specific cell functions. Cell-spreading and orientation are reflected in focal adhesion morphology and size, as well as in cytoskeleton distribution, affecting cell differentiation by mechanotransduction (Abagnale, 2015; Kim, 2014; Schenke-Layland, 2009). Moreover, three-dimensional scaffolds, conceived to better replicate native tissue dimensionality, were able to modulate cell morphology and behaviour differently to conventional 2D surfaces (Caddeo, 2017). 3D scaffolds should present high degree of porosity and proper pore interconnectivity to allow the migration of cells and the diffusion of nutrients and oxygen towards the inner part, as well as the removal of waste products.

Polymeric biomaterials are widely used in TE. Both natural and synthetic polymers allow the fabrication of devices with a broad range of bioactivity, biomimicry, biodegradation, and cell interactive properties (Nair, 2007; Tang, 2014). The use of natural components such as collagen, gelatine, elastin, chitosan, chitin, silk, and hyaluronic acid, provide intrinsic biological information for the guidance of cell behaviour. However, disadvantages of natural biomaterials include immunogenic responses, sourcing and purification issues, possible disease transmission and inferior biomechanical properties (Nair, 2007), although some modifications can be performed to control their degradation and support tissue formation. On the other hand, synthetic polymers can be easily produced and tailored into any suitable form. They can be obtained by controlled manufacturing and although their bioactivity is sometimes limited, their properties can be easily tuneable to fulfil specific purposes. Some of the mostly used synthetic polymers in TE include poly(lactic acid) (PLA), poly(glycolic acid) (PGA), polyethylene glycol (PEG) hydrogels, poly(caprolactone) (PCL), among others (Sisson, 2011; Tang, 2014).

A combined strategy of two or more biomaterial types in a composite material seeks for the complementation of their features to surpass specific limitations as the previously mentioned. For instance, the combination of ceramics, such as hydroxyapatite or calcium

nanoparticles with polymers such as PEG or PLA can generate bioactive materials with improved mechanical properties, suitable degradation profiles and more powerful bone regeneration inducers (Navarro-Requena, 2017; Vila, 2013; Yunoki, 2007).

2.1.3 Physicochemical stimuli

A series of chemical or physical stimuli can be incorporated within the engineered construct. Several bioactive molecules are naturally entrapped in the cell environment in native tissues. The ECM acts as a reservoir of these molecules providing a milieu for the communication between resident cells. These bioactive molecules influence the regulation of physiological processes within the tissue as for instance cell proliferation, chemotaxis, angiogenesis or specific cell differentiation. Several approaches have described the use of growth factors coupled with scaffolds as powerful therapeutic agents in TE (Wang, 2017). PEG hydrogel encapsulating chondrocytes increased proliferation and matrix production when immobilizing TGF-β1 within the scaffolds (Sridhar, 2014). Local administration of growth factors and other signalling molecules usually face rapid diffusion from the application site, thus minimizing the impact on tissue healing. On the contrary, biomolecule immobilization and controlled release from biomaterials prevents this diffusion and allows clear impact on the cells (Leonard, 2017; Lin, 2017). Lee *et al.* described the incorporation of fibroblast growth factor (FBF) in PCL/gelatine nanofibers together with a BMP-2 containing PEG hydrogel showing stronger osteogenic commitment in human MSCs (Lee, 2014). Triggered release from scaffolds has been achieved by means of enzymatic action (Foster, 2017), and pH changes (Han, 2015), but also by infrared laser (Vöpel, 2015), radiofrequency (Bariana, 2014), drug-sensing hydrogels (Ehrbar, 2008), and magnetic-fields (Sung, 2016).

One of the big challenges in TE is the achievement of clinically relevant tissues. However, the lack of vascularization and diffusion limits in 3D constructs restrict their size. Dynamic cell culture is introduced to overcome mass transfer issues during *ex vivo* TE. Bioreactors are devices in which biological processes develop under closely monitored and tightly controlled environmental and operating conditions (*e.g.* pH, temperature, pressure, nutrient supply and waste removal). By conferring a dynamic agitation to the media, bioreactors generally alleviate limited diffusion of nutrients and the discard of waste products. Also, their high degree of reproducibility, control and automation have been key for the translation of bioreactors into large-scale applications (Martin, 2004). Bioreactors enhance cell seeding efficiency and proliferation (Yeatts,

2011), but also, because of shear stresses applied recapitulating the native environment, cell fate is modified (Chen, 2013b; Conway, 2013).

Spinner flask, rotating-wall vessels, hollow-fiber and perfused bioreactors are some of the most common bioreactors. Hollow-fiber bioreactors were designed to simulate the capillarity network found *in vivo*, attempting to maintain a more physiologic environment for cultured cells with regard to nutrient supply, metabolic waste removal, pH, while providing a stable pericellular microenvironment (*Figure 2.2*, A). Small tube-like filters are packed, and cells are embedded within the package where media is diffused from the small tubes. This type of bioreactor has been successfully used to maintain the function of highly metabolic cells, *e.g.* hepatocytes, by increasing the mass transport of nutrients and oxygen (Mueller, 2011). Rotating-wall vessel bioreactors are formed by two concentric cylinders where gas exchange is made through the inner static one, while the outer cylinder rotates (*Figure 2.2*, B). Rotation speed is adjusted so that scaffolds inside remain in a state of free-fall. Up-regulation of osteoblastic genes is caused although cell proliferation is not enhanced (Wendt, 2005). Spinner flask (*Figure 2.2*, C) consists in a glass media bottle where scaffolds can be immersed or suspended while nutrients and oxygen are agitated by a stir bar. They are effective at creating a homogenous media solution on the exterior of the scaffold alleviating mass transfer, however, they do no effectively perfuse media into its inside. Spinner flasks have been widely used for the expansion of anchorage-dependent cells in suspension using microcarriers (Chen, 2013a), as well as for the extensive vaccine and protein production (Alfred, 2011b; Merten, 2015).

Finally, perfused bioreactors consist on a closed tubing circuit where media is perfused through the scaffold. Their basic composition requires from a media reservoir, a pump, a tubing circuit and a perfusion chamber, which houses the scaffold (*Figure 2.2*, D). Besides enhancing nutrient and oxygen transfer in the periphery and the inside of the scaffold, during cell seeding, the perfused flow allows cell transportation through the porosity of the biomaterial yielding a highly uniform cell distribution (Vila, 2016). Moreover, several studies have demonstrated that hydrodynamic shear stresses appeared in perfusion system affect cell behaviour. Chondrocyte culture and matrix deposition (Davisson, 2002), as well as osteogenic fate of mesenchymal stem cells (Gomes, 2003) were positively affected by flow perfusion.

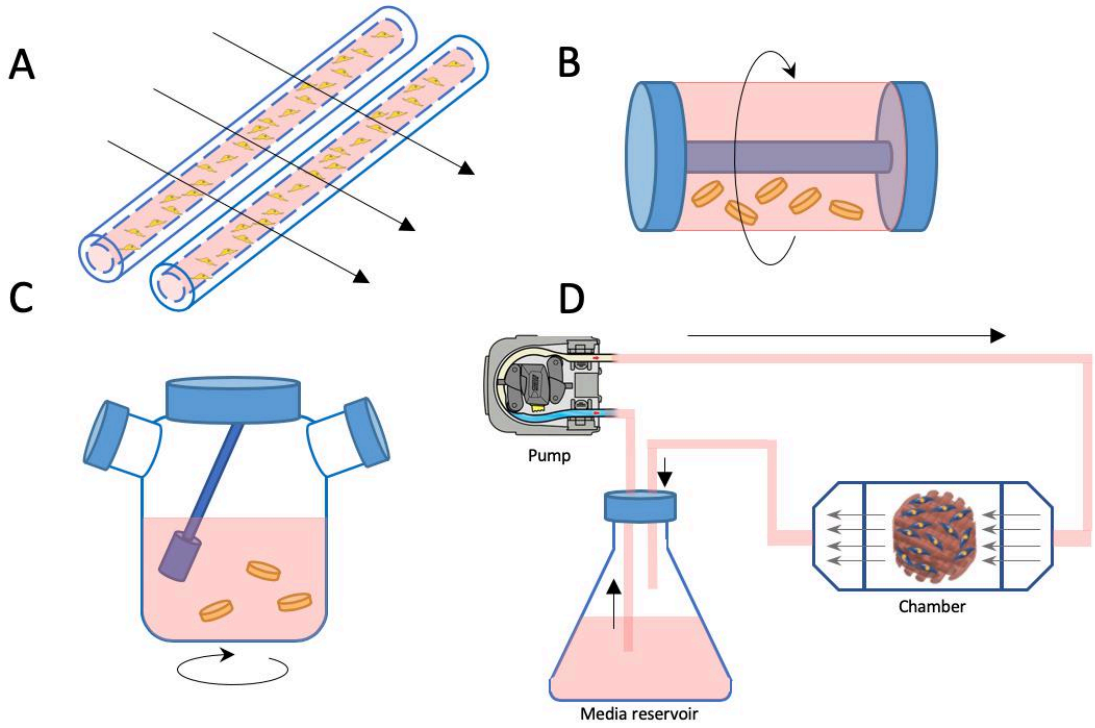

Figure 2.2 Schematic representation of different bioreactors. (A) Hollow-fiber bioreactors. (B) Rotating-wall bioreactors. (C) Spinner flask. (D) Perfusion system. Adapted from (Martin, 2004; Yeatts, 2011).

2.2 Extracellular matrix scaffolds

The production of ECM scaffolds from cultured cells renders a *promising* approach for the development of optimal structures aiming to guide appropriate neo-tissue formation. ECM was firstly thought to serve only as a structural support for locally living cells. Lately, the importance of ECM proteins (*i.e.* collagen, fibronectin, laminin, elastin, etc.) in regulating many aspects of cell behaviour was demonstrated (Cannas, 2004).

Bottom-up strategies have tried to create scaffolds with the same composition as that of native ECM by attaching tissue representative proteins to synthetic polymers (Dvir, 2011; Waldeck, 2011). Other approaches used modified natural polymers, whose components can be naturally found in ECM (Furth, 2007). However, it is an arduous task to completely mimic ECM because of its complex and dynamic composition. ECM is formed by several proteins and has an intricate microstructure. Moreover, it constantly changes as tissues develop, remodel, repair and age.

Native decellularized or *in vitro* cell-derived ECMs are ideal candidates to overcome ECM complexity. The main advantage of decellularized ECM from native tissues is that they keep its original structure. A wide variety of tissues and organs have already been used to obtain native decellularized scaffolds (heart, heart valves, blood vessels, lung,

trachea, skin, cornea, etc (Hoshiba, 2011). However, the restricted availability of tissues and organs for decellularization is their main limitation. Furthermore, the employment of decellularized ECM from other individuals (allografts) or even other species (xenografts) presents potential limitations, *i.e.* immunogenicity, possible presence of infectious agents, variability among preparations, and the inability to completely specify and characterize the bioactive components of the material (Furth, 2007).

To surpass these concerns, cell-derived ECM scaffolds can be produced *in vitro* directly from the patient's own cells, thus resulting in unlimited availability, and off-the-shelf technology, avoiding pathogen or immunological risks (Lu, 2011a). Cells cultured *in vitro* are able to deposit around them and on the biomaterial their own and specific extracellular matrix. These deposited molecules will modulate further depositions in neighbouring cell (Hoshiba, 2006). Also, during different cellular events like injury, wound healing, tissue development and cancer metastasis, cells mediate ECM remodelling, which can act as a target for biomaterial applications.

2.2.1 Extracellular matrix scaffolds for the creation of functional tissues

Tissue engineering scaffolds must take on the instructive role towards maintaining and controlling cell behaviour. They have to support seeded cells, allow them to find appropriate spaces, and provide physical and biological cues for adhesion, migration, proliferation, and differentiation. Eventually, cells will be able to replace them by their own matrices (Hoshiba, 2010b). Proof of concept is rapidly emerging for the hypothesis that ECM provides a template for tissue morphogenesis. Different studies have demonstrated that cell-derived ECM scaffold can guide the process of new tissue generation by exhibiting the intrinsic necessary cues.

Among bibliography, different approaches can be found for the preparation of cell-derived decellularized matrices (*Figure 2.3*). Jin *et al.* made a construct by combining pellet culture with a posterior expansion culture in a 6-well plate. This polymer-free scaffold was able to support cell viability and promote appropriate neo-cartilage formation (Jin, 2009). Similarly, Choi and colleagues efficiently induced chondrogenic differentiation of MSCs by acellular ECM developed by pellet culture (Choi, 2010). In contrast, PGA scaffolds by themselves could not promote expression of chondrogenic features; yet provoke hypertrophic changes, resulting unable to guide chondrogenesis.

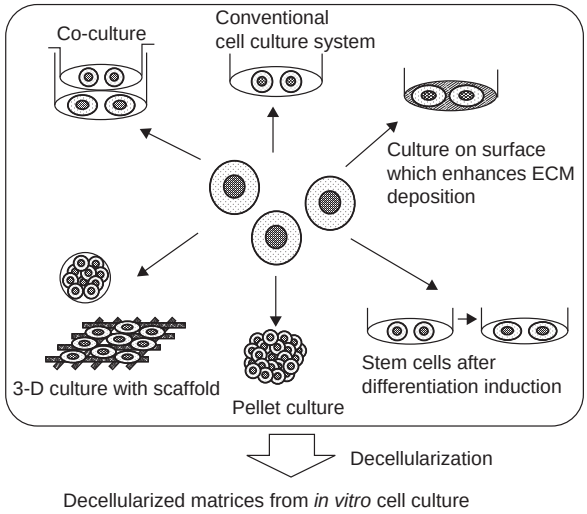

Figure 2.3 Cell culture methods for the preparation of cell-derived decellularized matrices. Some examples include the use of co-cultures for instance of alveolar epithelial cells with fibroblasts in a Matrigel for a basement membrane model; conventional TCP with highly producing cells such as fibroblasts; modified surfaces for ECM enhanced deposition; ECM formed by chondrocytes in a pellet culture; or the use of 3D scaffolds such as a titanium mesh used for the osteogenesis of MSCs. (Hoshiba, 2010b).

Conventional cell culture TCP has also been used to obtain ECM scaffolds. Narayanan *et al.* used a mouse MC-3T3 preosteoblast cell line to obtain an ECM, which was lately decellularized and disrupted to incorporate their elements into chitosan-alginate fibers. When implanted subcutaneously into severe combined immnodeficient (SCID) mice, they observed progressive ectopic bone formation and mineralization (Narayanan, 2009). Higuchi and fellows created a basement membrane by culturing a rat liver normal cell line overexpressing recombinant laminin. They were able to support differentiation of embryonic stem cells into endodermal lineage, and further to a pancreatic cell line (Higuchi, 2010).

Culture surfaces can be modified in order to enhance cellular properties. Soucy *et al.* used fibronectin-coated coverslips (2D) to increase cell adhesion and promote ECM secretion by confluent human foetal lung fibroblasts. After 7-10 days, they eventually obtained a dense and three-dimensional scaffold for tubulogenesis induction of HUVEC (Soucy, 2009).

Several researches are focusing their efforts towards the generation of 3D scaffolds for ECM deposition. Many studies have found differences in cell morphology, migration, adhesions, and signalling by comparing cellular behaviour in 2D versus 3D (Daley, 2008; Hakkinen, 2011). These findings state the importance of matrix dimensionality. Hence, cells are seeded in 3D scaffolds with the intention to closely resemble native dimensions

for ECM formation. Innumerable biomaterials have been used for that purpose such as microencapsulated collagen fibers (Cheng, 2009), titanium fiber mesh dishes (Datta, 2006; Pham, 2008), electrospun PCL microfibers (Liao, 2010), β-tricalcium phosphate (Kang, 2012), PLGA mesh dishes (Lu, 2011b), etc. Summarized information of their achievements can be found in *Table 2.1*.

Table 2.1 Studies proving *in vitro* formation of ECM-derived scaffolds for tissue regeneration purposes.

ECM cell source	**Reseed-cells**	**Matrix details**	**Decell. treatment**	**Ref.**
MSCs Chondrocytes Fibroblasts	-	PLGA mesh dish 5-6 days	Freeze-thaw + NH_4OH and Na_3PO_4	(Lu, 2011a)
MSCs Chondrocytes Fibroblasts	MSCs	PLGA mesh dish 5-6 days	Freeze-thaw + NH_4OH and Na_3PO_4	(Lu, 2011b)
Porcine chondrocytes	MSCs	Microencapsulation of collagen fibers and living cells (7 days)	Sodium deoxycholate	(Cheng, 2009)
Primary rat MSCs	MSCs	Ti-fiber mesh discs MSC culture in fluid shear stress (12 days)	Freeze-thaw	(Datta, 2006)
HUVEC	hMSCs	Beta-tricalcium phosphate 14 days	Triton + NH_4OH	(Kang, 2012)
Bovine chondrocytes	Rabbit MSCs	Electrospun PCL microfiber 9 days	Freeze-thaw	(Liao, 2010)
Dermal and saphenous vein fibroblasts	SMCs	Fibrous sheet rolled around a cylindrical mandrel (14-21 days)	Osmotic shock	(Bourget, 2012)
MSCs	MSCs	TCP 1-3 weeks	0.5% Triton + 20mM NH_4OH DNase I + RNase A	(Hoshiba, 2009)
MSCs Chondrocytes Fibroblasts	Articular chondrocytes	TCP 5-6 days	a)0.025% trypsine + 0.002% EDTA b)0.1% Triton in Tris-HCl DNase I + RNase A	(Hoshiba, 2011)
Three different breast cancer cell lines	breast cancer cells	TCP 7 days	0.1% Triton in Tris-HCl DNase I + RNase A	(Hoshiba, 2013)
Primary bovine chondrocytes P0-P2-P6	Chondrocytes	TCP 10 days	Tris-HCl, EDTA, 0.1% Triton 6h 37ºC	(Hoshiba, 2012)
Porcine articular chondrocytes	Rabbit chondrocytes	Pellet-type construct 3 weeks	3X Freeze (-20ºC)-thaw at 12h intervals	(Jin, 2009)
MC-3T3	hMSCs	ECM compounds incorporated into biological scaffolds based on polyelectrolyte complexation (1 week)	Sodium deoxycholate + Tris $MgCl_2$ + $CaCl_2$ + PMSF DNase I	(Narayanan, 2009)
Human foetal lung fibroblasts	HUVEC	Fibronectin-coated coverslips 7-10 days	Triton X-100 + NH_4OH DNase I	(Soucy, 2009)
3-y.o. and 18-y.o. mice femoral marrow cells	Freshly isolated bone marrow cells	Coverslip (2D) 15 days	Triton X-100 + 20mM NH_4OH	(Sun, 2011)

Human foreskin fibroblasts	hAMSCs	Electrospun scaffolds using sheet-derived ECM proteins and PCL 4 weeks	Sodium deoxycholate + Triton X100 6h incubation 37ºC & DNase	(Schenke-Layland, 2009)
Rat MSCs	Rat MSCs	Titanium fiber meshes 12 days Osteogenic medium	3x Freeze-thaw cycles	(Pham, 2008)
Human bmMSCs	MSCs	TCP culture and then disruption of ECM and transfer to PLG scaffolds (15 days)	0.5% Triton X100 in NH_4OH 5 min 37ºC + DNase I	(Decaris, 2012)
Rat bmMSC	Rat MSC	PCL fiber mesh Osteogenic medium 12 days	3x Freeze-Thaw cycles + 10 min ultrasonication	(Thibault, 2010)
MSCs	Pre-differentiated MSCs	PCL fiber meshes Flow perfusion bioreactor 12-16 days	(1) Freeze-thaw (2) Triton X-100 Freeze-thaw + EDTA	(Thibault, 2013)
Primary rat calvarian osteoblasts and dermal fibroblasts	*In vivo* study Calvarian defect	Synthetic hydroxyapatite MCs (20-60um) 21 days	0.5% Triton X-100 + NH_4OH Freeze-Thaw cycles	(Tour, 2011)
Adult human Dermal Fibroblasts	Bone MSC ADSC	Synthetic biphasic calcium phosphate ceramic granules (400-700um) 21 days	0.5% Triton X-100 + NH_4OH 3 min 37ºC	(Tour, 2013)
Porcine chondrocytes	Human foetal osteoblasts or human MSCs	Double emulsion method oil/water/oil Chondrocytes + gelatine microspheres + alginate (35 days) Alginate and gelatine removed	No decellularization	(Lau, 2012)
Primary mice chondrocytes	MSCs	2D expansion (3 weeks) + pellet formation (3 weeks)	Freeze-dry + DNase I	(Choi, 2010)

Abbreviations: bmMSCs (bone marrow Mesenchymal stem cells), Ti (Titanium), HUVEC (Human umbilical vein endothelial cells), DMX (dexamethasone), PCL (poly(ε-caprolactone)), PGA (polyglycolic acid), PLG (poly(lactide-co-glycolide)), ADSC (Adipose-derived stem cells), SMCs (smooth muscle cells), -y.o. (years old), MC-3T3(mouse osteoblastic cell line), MCs (microcarriers).

Another point to take into consideration is the stepwise differentiation process of stem cells into somatic cells. During tissue development, cells pass through different stages of maturation before acquiring final phenotype (Daley, 2008). While this happens, the surrounding ECM is dynamically remodelled to regulate stem cell functions. Although it is difficult to identify and isolate the matrices at different maturational stages, *in vitro* cultured MSCs can be useful to prepare ECM matrices with different osteogenic (Hoshiba, 2009; Kanke, 2014), or adipogenic commitment (Hoshiba, 2010a). In both approaches, early stage matrices were more favourable for adipogenesis and osteogenesis, than undifferentiated and late stage matrices. Nevertheless, osteogenic and adipogenic induction factors were required in each case.

2.2.2 Cell-derived matrices for phenotype maintenance in cell culture.

Some cell lines are unable to keep their cellular morphology and function as *in vivo* once harvested from their native niches. Maintenance of cell phenotype is dependent on microenvironmental signals. Development of cell-derived matrices represents a practical and ideal tool for obtaining the closest environment replicate *in vitro*.

Sinusoidal endothelial cells cannot be maintained in TCP without losing their phenotype. Sellaro *et al.* evaluated the ability of acellular native ECM from different tissues, such as liver, small intestine submucosa and bladder, to delay its loss. Only, liver derived ECM was able to maintain sinusoidal EC's phenotype for at least 3 days (Sellaro, 2007).

Similarly, a major concern for the *in vitro* culture of stem cells is the control of stemness maintenance. Due to limited number of these pluripotent cells in primary tissue, extensive passaging is required. Spontaneous suppression of differentiation and maintenance of stemness is prolonged when cultured in decellularized MSCs-derived matrices (Chen, 2007b; Lai, 2010). Lai *et al.* found lower levels of reactive oxygen species (ROS), fact that has been associated to contribute to the retention of MSC characteristics. Furthermore, ECM scaffold induced increased telomerase activity and thus avoided telomere reduction (Lai, 2010). Likewise, other stem cells have been cultured together with feeder layers, made upon cells, such as fibroblasts. Since the exposure to animal cells can lead to human health risks, Klimanskaya *et al.* have worked in an approach to avoid ES – feeder cells coculture, by creating a decellularized matrix formed by mouse embryonic fibroblasts. With this, ES were able to maintain their self-renewal ability and pluripotency intact even after 6 month of proliferation (Klimanskaya, 2005).

Age is also detrimental for stem cells quality. In consequence, ECM matrices derived from young cells differ in composition and functionality from those derived aged cells. Yun Sun and co-workers have deeply investigated young versus old matrices and found that aged MSCs restored their replication defects by exposure to an ECM made by marrow stromal cells from young animals. Moreover, the amount of ECM proteins created by both cells was the same, but their compositions were different, demonstrating the importance of each of the parameters that compose the ECM: elements, stiffness, distribution, etc (Sun, 2011).

2.2.3 ECM models for basic biological research.

Cell-derived ECM can also be applied as 3D models for research. These matrices closely mimic heterogeneity found *in vivo* but lack ethical and legal concerns encompassed in animal models. Besides, composition and physical properties can be manipulated to test hypothesis in ways that are not possible *in vivo* (Kutys, 2013). Cell behaviour in an environment that closely resembles that of *in vivo*. Hakkinen *et al.* performed research comparing 2D and 3D substrates willing to elucidate cell migration, morphology and adhesions (Hakkinen, 2011). Also, ECM models can be applied to study cancer mechanisms of invasion or test new drugs. Quiros *et al.* developed an ovarian stroma experimental model to support the study of stroma permissiveness in human ovarian neoplasies (Quiros, 2008).

2.3 Polymer microcarriers scaffolds

Microcarriers (MCs) are spherical particles with a diameter in the micron scale (10 to 1000 μm). However, they are generally bigger than cell size and smaller than 400 μm to maintain cells within the oxygen diffusion limits (which is 200 μm (Colton, 2014)). MCs have been extensively used for biomedical applications such as *in vitro* cell culture (Alfred, 2011a; Boo, 2011; Chen, 2015; Eibes, 2010; Frauenschuh, 2007; Jin, 2014; Schop, 2010), *in vivo* cell delivery (Chung, 2009; Hernández, 2010), drug delivery (Lu, 2015; Mohamed, 2008; Wong, 2018) and as biomaterials for the fabrication of TE scaffolds (Chau, 2008; Chen, 2011b; Georgi, 2014). Their fabrication is generally easy, and a wide variety of different materials is available for their creation.

2.3.1 Types of polymer microcarriers

Amongst the different MCs being developed (metallic, ceramic, polymeric) (Chau, 2008; Peticone, 2017), polymeric materials are mostly used because of their highly versatility, and ease for manufacturing. MCs fabrication methods allow the control of MC size in a reasonably simple and inexpensive manner. Also, features such as the surface porosity and the interior structures (hollow or interconnected internal porous) can be easily modulated. Polymeric MCs can be fabricated from natural (collagen, chitosan, alginate) (Zhou, 2016a) or synthetic polymers such as PLA, PGA, and their copolymer PLGA, PCL, PEG (Leong, 2015; Nair, 2007). Natural-derived polymers like polysaccharides and proteins from fungi, crustaceans, plants, or animals (Cipurkovic,

2018; Fernandez-Yague, 2015) possess appropriate bioactivity, supporting cell adhesion and proliferation. Moreover, they are biocompatible and biodegradable, generally by enzymatic activity (Chau, 2008). However, limitations appear by their poor mechanical properties and limited supply, thus becoming costly. On the contrary, synthetic polymers used for MCs production have demonstrated to be biocompatible and biodegradable. Degradation is driven by hydrolysis into non-toxic components which are eliminated from the implant site by normal metabolic pathways. Degradation rate can be adjusted to balance with tissue regeneration speed. Varying their chemical composition, crystallinity, molecular-weight and distribution, synthetic polymer degradation can be modulated from weeks to several years (Armentano, 2010). Although synthetic biopolymers lack cell recognitions sites, surface properties can be tailored to favour cellular adhesion and proliferation by coating with natural proteins such as collagen, fibronectin or RGD short peptides were enhanced cell attachment is obtained (Fabbri, 2017; Punet, 2013; Shekaran, 2016; Wang, 2017; Wronska, 2016). Compared to naturally-derived polymers, synthetic polymers can be obtained by more reproducible means under accurate control, thus avoiding uncontrolled immunological reactions seen with some natural polymers.

PLA is the world's mostly consumed biodegradable polymer (Institute for Bioplastics and Biocomposites, 2018). Growing as an alternative green food packaging polymer, PLA comes from renewable resources. Already approved by the Food and Drug Administration (FDA), PLA has been used as buffering agent, acidic flavouring agent, acidulant and as a bacterial inhibitor in many processed foods. For biomedical purposes, it has been used to produce screws, tacks and pins for bone fracture fixation, resorbable surgical sutures or implants as well as for the development of drug delivery systems (Cipurkovic, 2018).

PLA is an aliphatic polyester with a chiral centre, and therefore it has two stereoisomer forms, D- and L-form. Polymers composed of only one stereoisomer tend to be partially crystalline, because of the higher packing of the polymeric chains, whereas, mixtures of the D and L isomers tend to be amorphous (*Figure 2.4*). Depending on the proportion of each isomer (L/D), thermal and mechanical properties change, inducing different degradation rates. Thermoplasticy of PLA allows the fabrication of several scaffolds using different techniques: electrospun PLA films (Marti-Munoz, 2018; Mateos-Timoneda, 2014), solvent-casted films of PLA (Navarro, 2008), 3D printing scaffolds (Serra, 2013), and MCs (Levato, 2012). PLA degradation occurs via hydrolysis of the ester bonds, and by-products are removed by naturally occurring cell cycles. Compared

to other polyester biopolymers such as PGA, PLA degradation is slow and can take months or even years (Böstman, 2000). Copolymers between PLA and PGA, PLGA, have been created and extensively used to achieve intermediate degradation rates. The incorporation of PGA, a more hydrophilic polymer, provokes rearrangements in the structure of PLA, increasing hydrolytic degradation (Larrañaga, 2016). Other linear aliphatic polyesters, such as PCL and poly-(hydroxy butyrate) (PHB), show slower degradation rates which makes them less attractive for general TE applications, but more attractive for long-term implants.

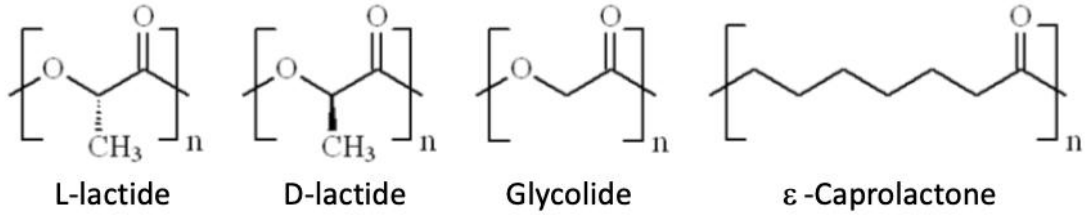

Figure 2.4 Chemical structure of the monomeric units of L-lactide, D-lactide, Glycolide and ε-Caprolactone (Larrañaga, 2016).

Although these biopolymers are known to be resorbable and biocompatible, massive release of acidic degradation may result in inflammatory reactions, as seen by Bergsma *et al.* in patients that had PLLA implants for 3 to 5 years. They observed a nonspecific foreign body reaction to the degraded PLLA material (Bergsma 1993, Bergsma 1995). Thus, degradation has to be thoroughly considered to avoid or reduce adverse reactions upon implantation.

2.3.2 Microcarrier fabrication methods

Amongst the different fabrication techniques, the most commonly used to obtain polymer MCs is the emulsion-solvent extraction/evaporation method (*Figure 2.5*) (Gupta, 2017). The polymer is initially dissolved in an organic solvent generating the 'oil phase', and then it is mixed with an immiscible water phase. Emulsification of the 'oil phase' is generated by physical methods such as homogenization or sonication. Speed during this homogenization process determines MCs size. In the following step, solvent is extracted into the water phase and further evaporated. Solvent extraction enriches the polymer in the oil phase until the droplets harden to become microspheres. In the last step, MCs are filtered or collected by centrifugation, washed and led dry or lyophilized. This single emulsion-solvent extraction method (O/W) allows the encapsulation of hydrophobic

bioactive molecules in the oil phase, such as dexamethasone in PLGA microspheres (Borden, 2002). Modifications of this method, incorporating a double emulsion $W_1/O/W_2$, allow the encapsulation of hydrophilic bioactive molecules (such as peptides, proteins, growth factors) in the MCs. This later method involves a first emulsification of a water phase W_1/O containing the desired molecule in the polymer dissolved oil phase. Then, this resulting solution is emulsified again in another water phase O/W_2, creating a second emulsion and allowing biomolecule-containing polymer to harden and form the MCs (*Figure 2.5*). For instance, Shi *et al.* described the incorporation of β-glycerophosphate and ascorbic acid, two hydrophilic components, in the first step W_1/O emulsion, being the 'oil phase' formed by a dexamethasone-methylene chloride solution with dissolved PLGA polymer. Second emulsification O/W_2 was added dropwise into a water solution containing poly(vinyl alcohol) (PVA), for the stabilization of the particles (Shi, 2010).

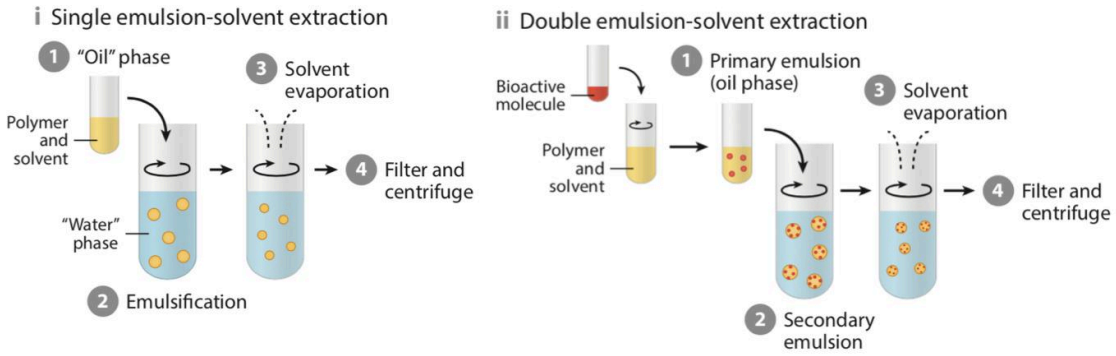

Figure 2.5 Microcarrier fabrication methods: (i) single emulsion-solvent extraction with only one phase O/W which allows the encapsulation hydrophobic molecules; and (ii) double emulsion-solvent extraction incorporating two phases $W_1/O/W_2$, allowing the incorporation of hydrophilic biomolecules (Gupta, 2017).

Porous MCs can be obtained by the addition of porogen molecules in one of the phases of MC formation (*Figure 2.6*). For instance, camphene is incorporated in a PCL solution. After microcarrier formation, camphene sublimates in ambient conditions leading to porous of a few microns or to interconnected channels in the inside if camphene concentration is increased (Hong, 2009). PLGA biodegradable porous microcarriers were formed by adding Pluronic F127, a water extractable porogen, obtaining solid in oil dispersed phase. During emulsification in the water phase, Pluronic is dissolved and extracted by water, leading to internal an surface porous without collapsing MC structure (Chung, 2009; Kim, 2006). Same procedure was followed by Cheng *et al.* who used calcium carbonate instead of Pluronic. This approach required the addition of gluconic acid lactone into the aqueous phase to interact with the porogen to release CO_2 forming

porous. Surface porosity was only achieved for compact PLGA microcarriers (Cheng, 2013). Other approaches used sodium chloride (Na, 2012) or ammonium bicarbonate (Chou, 2013) as porogens.

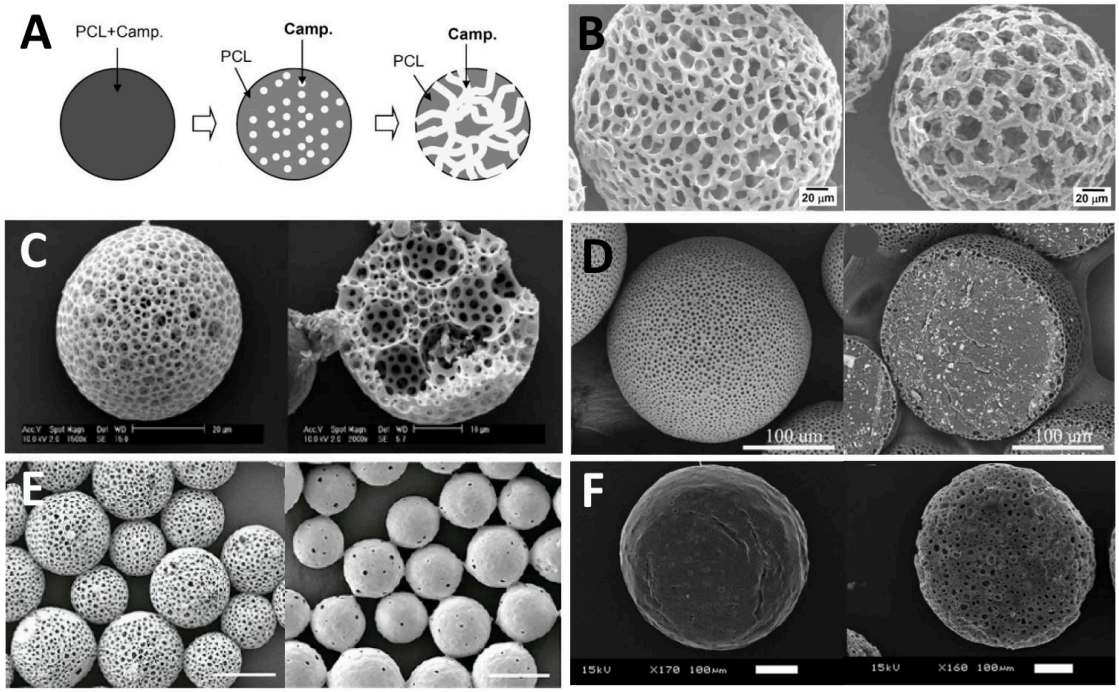

Figure 2.6 Porous polymeric microcarriers. (A) Schematic procedure of the fabrication of PCL porous carriers using camphene and (B) SEM micrographs of the resulting MCs. By using different camphene/PCL ratios different surface porous were obtained (Hong, 2009). (C) PLGA microcarriers with porous formed both in the inside and the surface by using Pluronic. Carriers did not collapse, and they were able to maintain the global spherical structure (Kim, 2006). (D) PLGA microcarriers using calcium carbonate as porogen agent. Because of a resistance from the oil matrix, the attracted water was confined to the outer shell of the microsphere and unable to enter into the inner part. So superficially porous PLGA-CC composite microcarriers were obtained (Cheng, 2013). (E) Methoxypoly(ethylene glycol)-poly-DL-lactide microcarriers were obtained by a water-in-oil-in-water double emulsion. By addition of sodium chloride porous structures were obtained, that allowed the incorporation of core materials such as proteins. Solvent swelling or infrared radiation were used to heal up the pore to close microcapsules (Na, 2012). (F) Ammonium bicarbonate solution was used to open porous on the surface of PLGA microcarriers during its production by emulsion, in a hepatocellular-specific approach (Chou, 2013).

Other possible procedures for the fabrication of MCs entangle the use of nozzles or injection-mediated methods. A fluid passing through a needle or pore, faces an inherent dynamic instability that leads to the break-up or atomization of the liquid (*Figure 2.7*, A) (Eggers, 2008). Based on that phenomenon, many droplet-generation techniques have been developed for MC formation such as fluid flow (Xu, 2009), precision particle fabrication using acoustic excitation (Berkland, 2001), spray drying (Baras, 2000), and electrospraying (Zhu, 2017). Fluids at the nozzle tip can generate droplets by dripping or stretching into laminar jets that will eventually break-up. Application of external fluid

flows, liquid/gas, immiscible with the polymer, aid in the controlled generation of droplets from the polymer solution. For that aim, two concentric nozzles can be coupled (*Figure 2.7*, B). The external flow exerts a force on the inner flow polymer solution pulling it in form of droplets, whose size will depend upon both flow rates. If the outer flow is higher, meaning it will pull the polymer solution in a stronger manner, particles are going to be smaller. Whereas, if the inner flow rate dispenses the polymer solution quicker, each particle will be formed by more polymer solution (thus obtaining bigger particles). Xu *et al.* obtained drug-loaded PLGA monodisperse sized particles by coflowing dichloromethane containing-polymer solution in water, combined with solvent extraction for the hardening of microcarriers (Xu, 2009) (*Figure 2.7*, C). Polymer jet disruption could be also performed by acoustic waves and electrical fields, being the first technique capable of a great control over microcarrier size (75-300µm) (*Figure 2.7*, D) (Berkland, 2001).

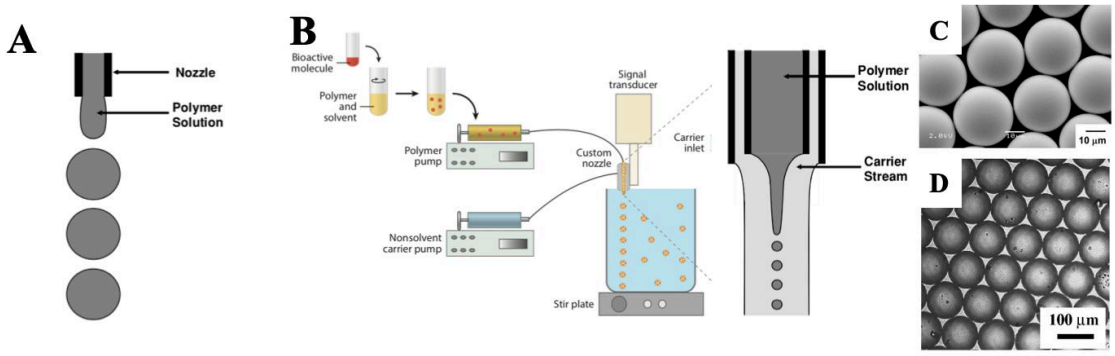

Figure 2.7 Microcarrier fabrication techniques: (A) Schematic scheme of the uniform-droplet generation by a single-nozzle approach and (B) Dual-nozzle approach with a carrier stream (Adapted from (Gupta, 2017)). (C) Example of the monodispersed carriers obtained by fluid flow-focusing device with a dual-nozzle. SEM image of biodegradable PLGA microcarriers (Xu, 2009). (D) Adaptation of the dual-nozzle approach: highly monodispersed and controllable PLGA microcarriers produced by combining polymer solution stream carrier and acoustic excitation breaking the stream into uniform droplets (Berkland, 2001).

Gas flow can be also coupled to pull polymeric solution to obtain microcarriers (*Figure 2.8*, A). Levato *et al.* used nitrogen gas coaxial flow to break-up polymer solution into microdroplets that felt into a 1% PVA aqueous solution for hardening by solvent extraction and evaporation (Levato, 2012). Modulation of the MC size was ligated to the nitrogen flow, the density of the polymer solution and the dispensing flow rate. Interestingly, this work also described the replacement of toxic organic solvents, widely used in synthetic polymer preparation, such as chloroform (Hong, 2009; Jin, 2014) or methyl chloride (Luciani, 2008; Shi, 2010), by the green biodegradable solvent ethyl lactate. This water-miscible solvent holds approval from the FDA as aroma for food

industry as it does not represent any potential risk for human health, neither for ecosystem when discarded (Clary, 1998).

Moreover, small particle fabrication techniques include electrospraying and spray-drying. Both methodologies are able to modulate particle size distribution with polymer concentration, however, irregular MCs are obtained. Electrosprayed particles were used for the treatment of pulmonary cancer due to efficient lung deposition and encapsulated-drug delivery (Zhu, 2017) (*Figure 2.8*, B). Spray-drying has been proven for successful scale-up processing and large operations, and they have been used for the long-lasting release of vaccines (*Figure 2.8*, C).

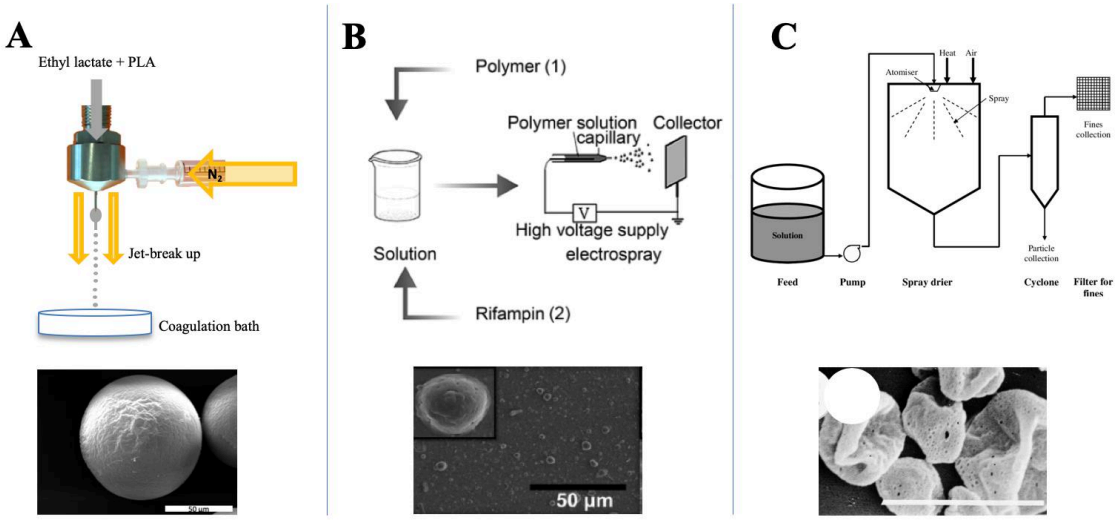

Figure 2.8 Microcarrier fabrication techniques II: (A) Schematic representation of the procedure used by Levato et al 2012 for the preparation of PLA microcarriers using ethyl lactate as green solvent. A dual nozzle is used where the polymer solution is extruded through the inner pore and a gas nitrogen flow is applied through the outer pore. Polymer jet breaks up into droplets that fall into a water bath where PLA microcarriers gelifies. Reduced polydispersed PLA microcarriers were obtained by using ethyl lactate in a solution jet break-up and solvent displacement method (Levato, 2012). (B) Electrospraying technique was used to prepare inhalable PLGA microcarriers encapsulating anti-lung cancer drugs (Zhu, 2017), as well as drug-loaded PLA microcarriers (Lu, 2015). (C) Spray-drying technology was used to manufacture PLA microcarriers. Atomization of the polymer solution through a spray nozzle is rapidly followed by spray-air contact and drying of the droplets. Although irregular carriers were obtained, they were able to encapsulate proteins (Baras, 2000). Scheme from (Burey, 2008).

Together with the custom-made MCs, a wide variety of commercial MCs is available. The most commonly used commercial particles are described in *Table 2.2*.

Table 2.2 Commercially available MCs and some of their features (Chen, 2013a; Rafiq, 2016).

Microcarrier	Matrix	Coating	Diameter (µm)	Porosity
SoloHill	Polystyrene	Collagen	125-212	Non-porous
SoloHill FACT III	Polystyrene	Cationic porcine collagen I	125-212	Non-porous
ProNectin® F	Polystyrene	Recombinant fibronectin	125-212	Non-porous
MicroHex™	Polystyrene	Nunclon™ surface	125x25	Non-porous
Cultisphere S	Gelatine	None	130-380	Macroporous
Cytodex 1	Dextran	DEAE	247-248	Non-porous
Cytodex 3	Dextran	Porcine collagen I	141-211	Non-porous
Cytopore 1 and 2	Cellulose	DEAE	200-280	Micro/Macroporous

DEAE (Diethylaminoethyl).

2.3.3 Biomedical applications of polymeric microcarriers

Due to its high surface area per volume ratio, they have been widely used in *in vitro* **cell cultures** to overcome conventional culture limitations. TE approaches need large amounts of cells to achieve clinical therapies (10^6 to 10^9 cells per treatment) and 2D traditional cultures would require a lot of space and surface area, becoming a challenging option. Also, the large-scale production of recombinant proteins and viruses in vaccine production requires large amounts of producing cells (Merten, 2015; Rourou, 2009). MCs cultivation of anchorage-dependent cells on suspension cultures has brought light to these matters. The use of stirred bioreactors in which MCs are suspended has reduced laboratory space and handling steps for cells, decreasing costs and contamination risks. Also, the use of bioreactors allows for a more reproducible cell culture and environmental parameters (pH, oxygen and nutrient concentrations) can be easily controlled (Schop, 2010). Also, and commonly attributed to the use of bioreactors, scaling-up would be an interesting and easy option for the propagation of more cells if needed. Besides, MCs culture facilitates cell propagation avoiding the use of proteolytic enzymes as cells are able to transfer to freshly added carriers in a continuous culture (Leber, 2017; Rafiq, 2018).

Different cell types have been successfully expanded using MCs: ESC, iPSC, hMSC from different origins, endothelial cells (ES), cancer cells, etc (Alfred, 2011a; Badenes, 2016; Leong, 2015; Lock, 2009). High proliferation yields have been reached when culturing cells on polymer MCs, showing superior cell-fold expansions (Alfred, 2011b; Mei, 2010; Schop, 2010; Yuan, 2014). MCs supported cell phenotype retention in stem

cells (Lock, 2009; Shekaran, 2015), as well as enhanced osteogenic (Levato, 2014) and chondrogenic (Lin, 2016) differentiation efficiency compared with conventional 2D cultures when using MCs.

MCs have been extensively used in **drug delivery** applications due to their ability in encapsulating drugs or bioactive molecules and enhancing administration efficacy. They provide both a large surface area-to-volume ratio and spatiotemporal control over the release. Work performed during the last decades has led to the creation of novel carriers, both at the micro- and nanoscale, with greater control over the release profile, protection of the encapsulated drugs or proteins from enzymatic degradation, enhancement of peptide stability and site-specific targeting. Attenuation of initial burst release has been achieved by modifying surface porosity, internal pore size and distribution (Mohamed, 2008), whereas some approaches have coated polymeric MCs with other polymers, such as PLA coating for PLGA microcarriers (Matsumoto, 2005), or PEG coatings for PCL nanoparticles (Layre, 2006). Ligand binding on the surface of polymeric carriers has also led to active targeting to specific receptors, however this strategy is generally used for the active uptake of nanocarriers (Vhora, 2014). MCs mediated drug delivery has been applied in a variety of different fields. To name a few examples: delivery of pro-inflammatory cytokines from PLA microcarriers for the generation of an immune response against melanoma and sarcoma tumour models (Sabel, 2007); insulin MC encapsulation for the treatment of diabetes mellitus (Wong, 2018); and smart drug release of PLGA nanoparticles coated with DNase I against bacterial biofilm infections (Baelo, 2015).

Cell therapies rely on the ***in vivo*** **delivery of cells** providing a specific cellular activity to the injured site. Deficient protein production leading to diseases such diabetes (insulin), anaemia (erythropoietin), or haemophilia (factors VIII and IX) could benefit from this treatment (Hernández, 2010). Also, cell therapy can be implemented for cancer therapies, where genetically modified cells with therapeutic agents are closely brought to the tumour site (Bagó, 2013a). Moreover, delivered cells could aid in the healing process of injured tissues in a TE approach. MCs have been proposed for the delivery of cells through a minimally invasive technique, easily adapting to defective sites and elongating cellular presence for the local and sustained delivery of cell-mediated treatments. Cells can be found attached to the surface of the carriers or within the pore structure in the case of porous microcarriers, allowing cell expansion on stirred cultures coupled with direct transplantation, generally using biodegradable and biocompatible MCs (Cirone, 2002;

Correia, 2017; Endres, 2010). Cell encapsulation aims to physically isolate cells from the outside protecting them from the host immune system, avoiding the use of immunosuppressive agents, although diffusion of nutrients, oxygen and therapeutic molecules is still allowed. Hydrogels are mostly used for cell encapsulation, being alginate, chitosan, collagen, agarose, and PEG some of the most used biomaterials (Hernández, 2010).

In addition to the above-mentioned applications, MCs can be packed together, alone or in combination with other materials to yield porous three-dimensional structures that can serve as **scaffolds for modular TE**. Complete mimicry of native tissues or organs is of extreme complexity, and top-down strategies usually fail in reproducing heterogeneity found *in vivo*. In fact, tissues such as liver, muscle, spleen, bone, and cartilage are characterized by repetitive functional units, which are assembled hierarchically across multiple length scales to finally form the tissue/organ (Liu, 2012; Nichol, 2009; Zorlutuna, 2013). For that reason, bottom-up or modular tissue engineering are proposed to enable facile incorporation of complex multiscale modularity into man-made tissue constructs. Therapies based on the modular fabrication of scaffolds using cell-laden microparticles as building units appear to be promising alternative to address limitations in traditional top-down approaches. Also, instead of only looking for structural support from polymeric materials, specialized environments recapitulating the native extracellular matrix of targeted tissue is of upmost importance.

PCL microcarriers, for instance, were orderly and randomly assembled and sintered forming porous interconnected 3D scaffolds to investigate functional vascular network formation (Rossi, 2016) (*Figure 2.9*, A). Also, MCs can be dispersed into hydrogel or polymer matrices providing controlled delivery of bioactive molecules (Roam, 2015) or increasing mechanical properties and introducing cues to allow cell anchorage or exert changes in cell behaviour (Levato, 2014). Another option is the use of cell-laden microcarriers as building blocks for modular tissue engineering based on the self-assembling intrinsic cell mechanism. Cell-seeded microcarriers are prone to form aggregates under appropriate conditions (cell/MC concentration, culture media conditions, cell type…) termed as microtissues (Chen, 2011b; Mei, 2010; Palmiero, 2010; Tang, 2008; Urciuolo, 2011) (*Figure 2.9*, B and C). For microtissue formation, cells are preferably seeded on microcarriers in dynamic conditions to favour homogeneous colonization (Matsunaga, 2011) (*Figure 2.9*, D). Next, some approaches describe the formation of little MC aggregates via cell-cell interactions in spinning bioreactors

(Chung, 2009; Declercq, 2013), although others manifest the need for static conditions and proximity between carriers for that aim (Twal, 2014; Urciuolo, 2011). General consensus is found for macrotissue formation, in which assembling of the modular microtissues is successfully achieved when confining them in the chamber of a perfused bioreactors (Chen, 2011b; Chen, 2014; Kou, 2016; Luo, 2014; Totaro, 2016; Wang, 2014) (*Figure 2.9*, E).

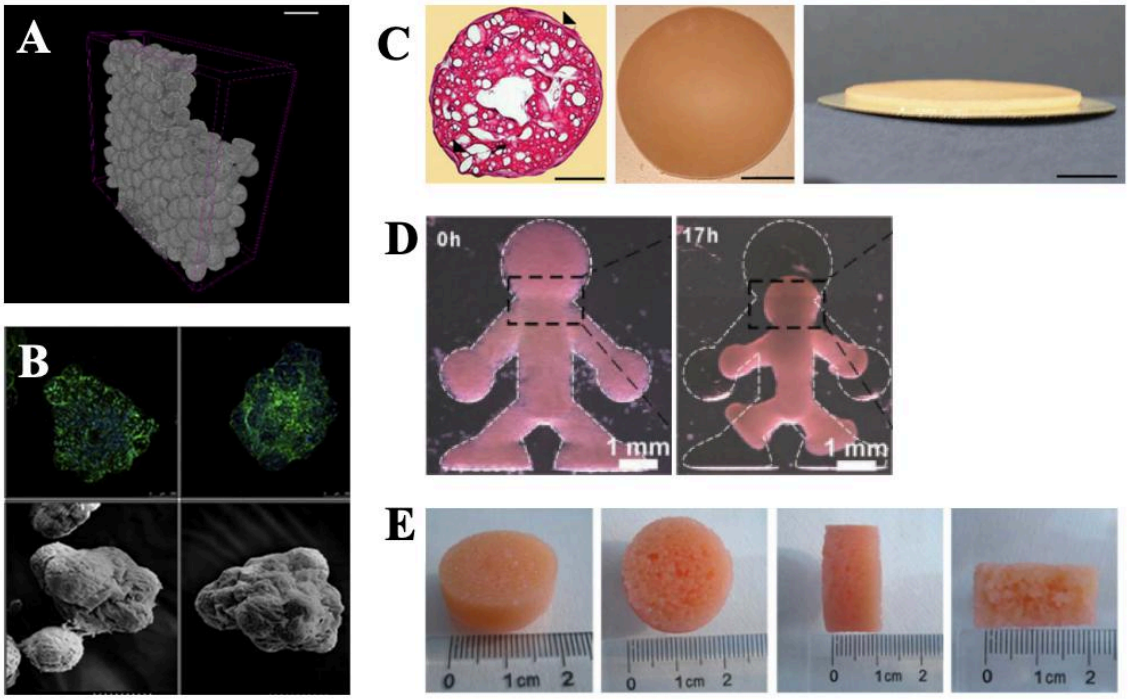

Figure 2.9 Modular TE approaches using polymer MCs. (A) Randomly sintered PCL MCs observed by microCT images (Rossi, 2016). (B) Microtissues formed by the aggregation of Cultisphere gelatine MCs (Chen, 2011b). (C) Microtissues prepared by seeding cells on macroporous gelatine MCs and assembling them by confinement in a maturation perfused chamber (Urciuolo, 2011). (D) Use of moulds for the rapid construction of macroscopic cell-MCs 3D scaffolds. Shrinkage of the resulting tissue was clearly observed after 17h (Matsunaga, 2011). (E) Macrotissue formation from human MSC-laden microcarriers through *in vitro* perfusion culture in a cylindrical chamber, obtaining centimetre-sized constructs (Chen, 2014).

2.4 Microtissue vascularization strategies

Despite the advances in TE during the last decades, translation into the clinical is still limited to a few examples, most of them related to low vascularized tissues, such as epidermis and cartilage. Passive oxygen and nutrient diffusion limits, both from nearby vessels and from culture medium, rely between 100 – 200µm in distance (Carmeliet, 2000). Generation of bigger macrotissues requires an adequate system to actively supply these much-needed resources to all the cells in the construct. *In vitro*, bioreactors have the ability to mitigate this limitation, allowing relevant clinical volumes (Chen, 2014;

Urciuolo, 2011). However, upon *in vivo* implantation rapid invasion from host vasculature has to be achieved (Janssen, 2006).

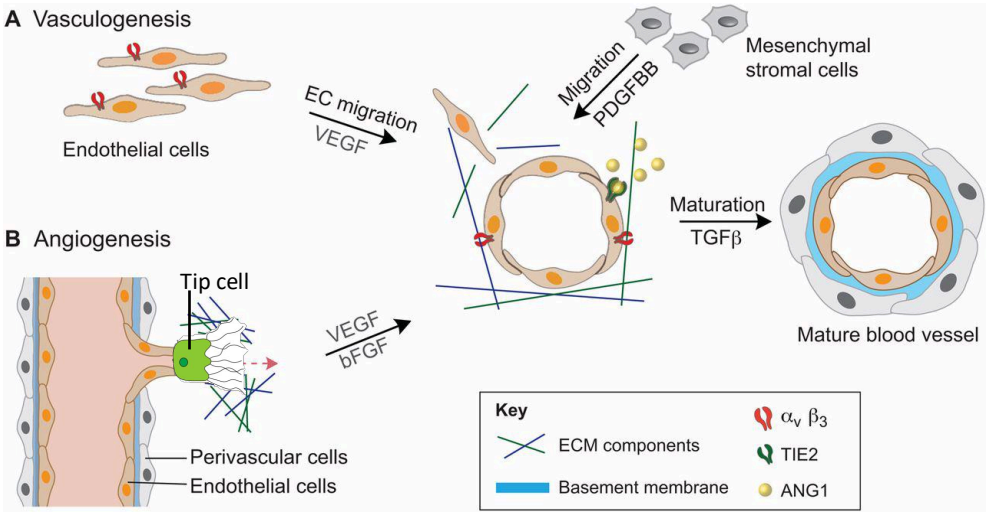

Figure 2.10 Schematic representation of the processes for vascular development. (A) During vasculogenesis, endothelial cells migrate to form lumens by a `process mediated by VEGF. Then maturation of the newly formed vessels is performed together with recruited MSCs. (B) During angiogenesis, quiescent vessels are activated and new vasculature sprouts and elongates. Proangiogenic factors stimulating initial sprouting are VEGF and bFGF. Adapted from (Geudens, 2011; Park, 2014).

Vascular development in the body is performed by two different processes: vasculogenesis and angiogenesis (*Figure 2.10*). During vasculogenesis, new blood vessels emerge from endothelial cell (EC) precursors, that migrate under the induction of vascular endothelial growth factor (VEFG) to form lumen structures, resulting in primary small capillaries. For the maturation of these capillaries, perivascular cells are needed to closely support endothelial wall. ECs secretion of platelet derived growth factor (PDGF) recruits nearby MSCs that in turn release angiopoietin 1 (ANG1), stimulating mural coverage and basement membrane deposition. Further MSCs release of TGFβ induces full vessel coverage with perivascular cells and inhibits EC proliferation. During angiogenesis, new vessels are developed by sprouting from pre-existing mature vessels. Quiescent cells are activated by VEGF and fibroblast growth factors (bFGF) stimulus and a tip cell is specified to lead the sprouting process. Neighbouring cells undergo proliferation, elongation and lumenization after the tip cell, involving complex cell-cell interactions and basement membrane remodelling for the formation a nascent vessel. Final stages require the recruitment of perivascular cells to mature new vessels walls, similarly to described above in the vasculogenesis, by means of PDGF secretion (Park, 2014).

Specific cell-cell interactions, ECM remodelling, signalling via growth factors as well as oxygen availability play a crucial role in early vascular development (Geudens, 2011). Relying on rapid neovascularization of engineered constructs upon *in vivo* implantation is a major drawback for clinical translation of TE constructs. For that purpose, studies are pursuing the incorporation and controlled release of pro-angiogenic factors from biomaterials to enhance *in situ* therapeutic vascularization. These strategies have to be thoroughly designed to avoid uncontrolled delivery which leads to disorganized, leaky and haemorrhagic vessels (Jain, 2005). For that reason, delivery of various sets of pro-angiogenic (VEGF) and pro-maturation (PDGF) factors in a spatio-temporal manner achieved blood vessel formation and maturation. Combination of two biopolymers with different degradations rates was used for the sequential delivery of two growth factors, *i.e.* PDGF-loaded PLG microcarriers immersed in VEGF containing alginate solution creating layers. Implantation of millimetre-sized cell-free scaffolds on mice demonstrated increased vessel density over 2 weeks, while effects on vessel maturity were observed out to 6 weeks due to the slower release of PDGF (Chen, 2007a).

In contrast with the *in situ* vascularization approach, acceleration of vasculogenesis and anastomosis with the host vasculature was observed with *in vitro* pre-vascularization of constructs. Mainly, efforts have been focusing in mimicking the scenario that exists during normal vascular development *in vivo*, meaning ECM environment and cell-cell interactions. Extracellular matrix in blood vessels is highly structured and specialized, named basement membrane (BM). Vascular BM relies between the endothelial cells and the perivascular cells, configurating the walls contributing to the structural vessel stability (Kalluri, 2003). Main components include laminin, heparan-sulphate proteoglycans and nidogen/entactin, although predominant component in vascular BM is collagen type IV (Petitclerc 2000; Davis and Senger 2005; De Smet 2009) from (Bahramsoltani, 2014). In fact, synthesis and deposition of collagen type IV by endothelial cells have been shown to be indispensable for vascular formation and maturation in vivo (Bonanno, 2000). Increased collagen IV secretion and extracellular deposition were found to couple with ongoing angiogenesis, whereas discontinuance of angiogenesis was associated with collagen IV presence restricted to intracellular compartments (Bahramsoltani, 2014). Functional relevance of collagen IV was further demonstrated when reduced levels of tube assembly were observed in tube formation assay after the blockage of collagen IV deposition (Zhou, 2016b). Nonetheless, collagen type IV influence in angiogenesis has been demonstrated to be both pro-angiogenic and inhibitory of vascular formation (Kalluri, 2003). In mature endothelium, cells are quiescent and bound to a highly

crosslinked vascular BM, where only certain domains of the proteins are exposed to the cells. In contrast, during neovascularization, ECM remodelling occurs by activated proteases together with other angiogenic modulators, exposing specific fragments of collagen IV chain isoforms inducing anti-angiogenic effects (Karagiannis, 2007; Mundel, 2014). Dose-dependent effects were described by Bonanno *et al.*, were intermediate concentrations (30µg/ml) of collagen IV promoted neovascular formation but high concentrations (300 µg/ml) exerted no growth, but stabilization of vascular vessels (Bonanno, 2000). This findings manifest that the same proteins can modulate distinct functional behaviours on vascular endothelial cells during different stages of the angiogenic process by modifying their structural configurations (Kalluri, 2003).

Mimicry of cell-cell interactions occurring in neovascularization is being extensively applied for TE. As described above, the formation of new blood vessels requires endothelial and mesenchymal stem cells playing a combined role. Direct cell-cell contact and mutual communications via growth factors happen in the initialization stages, during remodelling and at the final maturation stages (Geudens, 2011). Co-culture of endothelial cells or endothelial progenitor cells together with perivascular cells has been studied. Zhou *et al.* observed increased endothelial cell survival and tube formation demonstrating the importance to use both cell types (Zhou, 2016b). Also, co-culture of MSCs or progenitor cells with ECs supported the perivascular role of mesenchymal-derived cells, which was necessary for proper vessel network formation (Fuchs, 2007; Li, 2013; Melero-Martin, 2007). More evidences supporting the use of MSCs to obtain perivascular cells were found, demonstrating the dual role of MSCs in acting as supportive cells and endothelial progenitor cells (Pill, 2015; Portalska, 2012).

The use of MCs in modular TE approaches with the aim of vascularization has been successfully demonstrated. Taking in advantage the feasibility of encapsulating active biomolecules in MCs, Brudno *et al.* described the sequential delivery of pro-angiogenic factors followed by pro-maturation factors from Cytodex 3 MCs, mimicking natural events (Brudno, 2013). Moreover, coculturing of different types of cells is easily adapted to MCs culture. Investigations have reported several strategies including simultaneous or sequential seeding of MSCs and HUVEC on MCs in spinner flasks (Zhang, 2017), as well as patterned micromodules and degradable MCs (Zhong, 2017). Twal *et al.* for instance, fabricated tubular tissue constructs using plastic moulds and disposing cellularized MCs as adhesive building blocks (Twal, 2014). Coculture strategies described the use of HUVEC and hepatocytes (McGuigan, 2006), HUVEC and pancreatic

islets (Vlahos, 2017), smooth muscle cells (SMCs) and ES (Leung, 2007), but also several strategies include the use of MCs made from gelatine (Dikina, 2018), or chitosan (Tiruvannamalai-Annamalai, 2014) with more than two cell types in complex cultures. Interestingly, Dikina *et al.* described the fabrication of a tri-cultured and prevascularized cartilage rings, fusible into tubes, providing a framework for microvasculature formation *in vivo* (Dikina, 2018). Finally, another vascular strategy in which MCs are involved requires the incorporation of cell-laden MCs into fibrin hydrogen for a correct cellular entrapment and mechanical support. Endothelial cell sprouting and lumen formation confirmed the vascularity of this modular approach after 14 days *in vitro* (Peterson, 2014).

2.5 Microtissues for anti-tumoral cell therapy

2.5.1 Bystander cell therapy against tumour

Bystander cell therapy emerged as a sophisticated therapeutic approach against advanced cancer (Moolten, 1986). Genetically modified cells incorporating suicide genes were capable of inducing death not only to themselves but also to neighbouring untransfected cells. Suicide genes encode for enzymes that have the ability to transform harmless prodrugs into toxic metabolites. Different suicide gene/prodrug combinations are being studied, however the most extended one is the use of herpes simplex virus thymidine kinase (TK) in combination with the prodrug ganciclovir (GCV) (Kraiselburd, 1976). GCV prodrug is innocuous to mammalian cells, however when phosphorylated (pGCV) by viral TK, it becomes a synthetic analogue of 2'-deoxy-guanosine, which can be incorporated into DNA. Incorporation into DNA inhibits its replication and causes cellular death by apoptosis (Reardon, 1989).

Bystander cell therapy occurs through cell-cell contact by gap junctions between the therapeutic cells and the tumour cells, resulting in the transfer of the pGCV (Van Dillen, 2002). Also, when therapeutic cells carrying suicide genes are self-affected by pGCV, apoptotic vesicles containing the phosphorylated drug could spread the toxic effect to nearby untransduced cells (Colombo, 1995). Guerra-Rebollo *et al.* proved distant cytotoxic effects carried out by extracellular vesicle releasing, when treating tumour cells with conditioned medium from TK-hAMSCs exposed to GCV (Bello-Morales, 2018; Guerra-Rebollo, 2018). Cells presenting a rapid proliferative state, such as tumoral cells, are more prone to suffer ganciclovir-associated death. For that reason, minimal adverse

effects are observed in healthy cells as well as therapeutic cells, which are generally found in quiescent states in adult tissues (Guerra-Rebollo, 2018).

TK-presenting cells together with GCV administration has been investigated against different tumour types such as prostate cancer (Vilalta, 2009), uterine adenocarcinoma (Kunishige, 1999), melanoma (Xiao, 2017), colorectal cancer (Kucerova, 2007) or glioblastoma (Colombo, 1995; Guerra-Rebollo, 2018; Nakamizo, 2005). Glioblastoma is an aggressive malignant brain tumour with a poor prognosis (12 to 15 months of median patient survival) (Wen, 2008). Surgical resection is the main treatment, however, due diffusive nature of glioblastoma as well as the rapid therapeutic and chemotherapy resistance acquired from remaining cells, recurrence is inevitable (Young, 2015). Stem cells are able to migrate towards gliomas even through normal brain parenchyma (Aboody, 2000; Nakamizo, 2005). They are able to target microscopic tumours, migrate and engraft to them for the delivery of bystander therapy (Hung, 2005). However, controversy over the use of MSCs for tumour therapy was raised because of the potential of these cells in stimulating invasion and metastasis (Belmar-Lopez, 2013; Zimmerlin, 2013). Nevertheless, safety has been proven after Guerra-Rebollo *et al.* demonstrated effective therapeutic effect even with populations were as much as 25% of the inoculated cells were not therapeutic (untransduced with TK gene). In that situation, no pro-tumorigenic effects were observed (Guerra-Rebollo, 2018).

2.5.2 Biomaterials used for the delivery of bystander cell therapy

Human adipose derived mesenchymal stem cells (hAMSC), which are excellent candidates for autologous cell-based therapies, have also been demonstrated to be good cellular vehicles for the delivery of bystander therapy (Guerra-Rebollo, 2018; Kucerova, 2007; Vilalta, 2009), performing same tropism towards gliomas as bone marrow derived MSCs (Pendleton, 2013). However, direct implantation of therapeutic cells after glioma tumour resection is followed by a rapid clearance of cells, reducing the therapeutic efficacy. In order to enhance their retention in the cranial cavity, a few strategies have introduced the use of biomaterials (Bagó, 2016a; Bagó, 2016b; Kauer, 2012). Hydrogel forming materials such as the one used by Kauer *et al*. based on a thiol-modified hyaluronic acid and a thiol reactive cross-linker (polyethylene glycol diacrylate) provided attachment and reduced diffusion of neural stem cells when implanted after tumour resection. Moreover, it retained high concentration of therapeutic cells and allowed cell

migration. Diffusion of the killing agent was also permitted through the hydrogel, which in this case was the apoptosis inductor TRAIL, delaying tumour regression and significantly increasing survival of mice (Kauer, 2012). A fibrin-based matrix was also used for the encapsulation of therapeutic hMSCs. Bagó *et al*. used commercially available TISSEEL sealant applied clinically to achieve haemostasis in patients (Bagó, 2016a). By using TISSEEL, they observed a 2-fold initial retention increase, and a 3-fold prolonged persistence of the therapeutic cells compared to free cell incorporation. Cellular migration was allowed from the hydrogel towards glioma cells, inducing substantial tumoral killing, and prolonging mice survival from 15 to 36 days. However, limitations of this assay rely in the unknown optimal degradation rates of the implanted fibrin matrix and restrained scalability when large animal models are used (Bagó, 2016a). Another approach applied electrospun nanofibrous PLA scaffolds to large defects after tumour resection allowing for the coverage of the surface (Bagó, 2016b). This methodology left void space for post-operative fluid, minimizing intracranial pressure. Interestingly, the use of this biomaterial extended therapeutic cell survival and retention in the site of implantation, avoiding serial inoculation as seen in other approaches (Alieva, 2012). Tumour size was reduced the first 6 days; however, robust suppression was not maintained, and recurrence of tumours appeared. hMSCs migration from the biomaterial or cytotoxic efficiency of the strategy (TRAIL-induced apoptosis) were suggested as limiting factors.

2.6 Bioluminescence as non-invasive imaging technique

Avoiding destructive analysis procedures on TE constructs represents an advantageous feature both for *in vitro* and *in vivo* approaches. The use of non-invasive imaging techniques allows the reduction of samples under study, facilitating procedures and lowering research costs. Also, when investigation is performed on animals, experimental monitoring can be followed in real time avoiding animal suffering as repetitive exploration can be performed in the same individuals, meaning an appealing feature for ethical concerns. Non-invasive imaging techniques allow both the spatial and temporal distribution of a molecular probe and related biological processes, providing meaningful numerical measures of biological phenomena. Some non-invasive imaging techniques are magnetic resonance imaging (MRI) (Floeth, 2008), computed tomography (Su, 2014), ultrasound (Correa, 2004), positron emission tomography (PET) (Floeth, 2008) or optical imaging (fluorescence (Mehta, 2008) and bioluminescence (Vila, 2013)) (*Figure 2.11*).

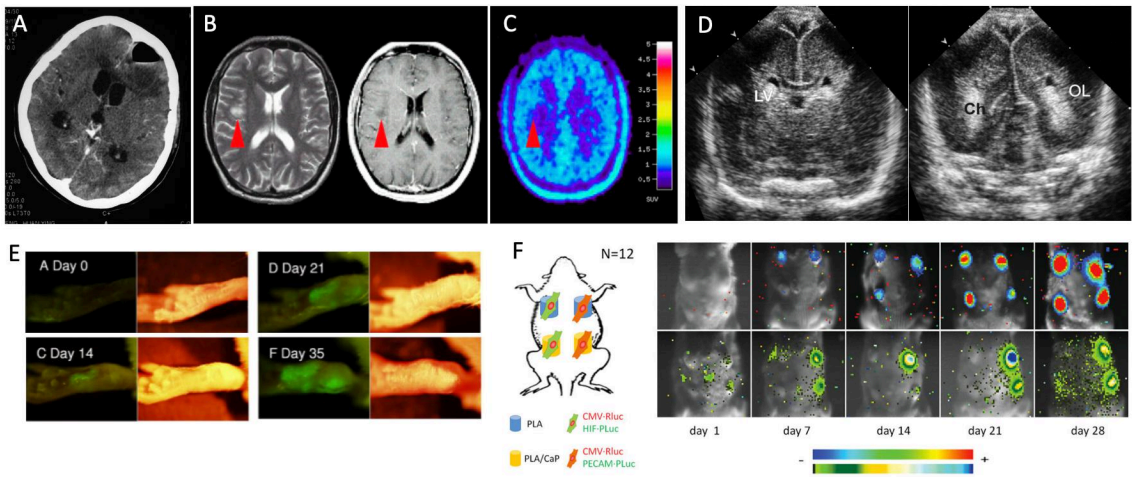

Figure 2.11 Non-invasive imaging techniques. (A) Brain computed tomography (CT) showing a lesion with air-fluid level in the left frontal lobe (Su, 2014). (B) Magnetic Resonance image and (C) Axial PET scan of a healthy young volunteer (Floeth, 2008). (D) Ultrasound of a neo-natal brain (Correa, 2004). (E) Mouse footpad fluorescence and bright-field images indicating Leishmania infection over time (Mehta, 2008). (F) Bioluminescence progression of Rluc constitutive expression (upper row) and inducive expression of Pluc (bottom row) demonstrating cell differentiation on PLA and calcium containing PLA scaffolds (Vila, 2013).

Advances in molecular and cell biology techniques have propelled non-invasive molecular imaging. Optical imaging has been widely used for *in vitro* and *ex vivo* analysis such as immunofluorescence of fixed samples, histologies of sliced tissues, etc. Although these techniques are affordable and stablished in any biological laboratory, they are tedious, and several proceedings are needed, moreover, signal is not always quantifiable. They represent a static moment of the biological process; thus, temporary monitoring requires from several different samples enlarging volume of work and resources. The alternative is the use of non-invasive optical techniques. Initially, they require sophisticated molecular techniques to genetically modify cells and animals to introduce fluorescent or light-emitting probes (for bioluminescence). However, once it is fully established, functional and efficient, imaging obtaining is quicker and less labour-intensive.

Fluorescence imaging requires the use of fluorescent protein-labelled antibodies, or the genetical introduction of genes encoding for naturally derived fluorescent proteins (FP) such as the green fluorescent protein (GFP) from the jellyfish *Aequorea Victoria*, or FPs found in marine anemone (*Discosoma striata*), reef coral (*Heteractis crispa*) or crustacea (*Copepoda Pontellidae*). Once cells are genetically modified to incorporate the FP, they do not require from the introduction of any substrate, but they need for an excitation source. FP have been used for the study of protein interactions, monitoring gene

expression in developmental biology, localizing specific proteins, among others (Chudakov, 2005).

Bioluminescent emission, on the other hand, requires from a luciferase-catalysed reaction, which turns molecular oxygen and a specific substrate into light and other by-products. More than 700 genera in nature exhibit bioluminescence activity, mostly marine species. However, luciferase enzymes coming from the sea pansy *Renilla reniformis* and North American firefly *Photinus pyralis* are the most used (de Almeida, 2011). Each of them catalyses different substrates (coelenterazine and D-luciferin, respectively), allowing for specific and independent detection even when using both luciferases in the same system. Light photons emitted from the cells have the capability to trespass 2 cm of tissue, which usually lacks from intrinsic bioluminescence (Massoud, 2003). For that reason, real-time monitoring of luciferase-expressing cells can help in the study of cell survival, cell interaction and specific targeting (*Figure 2.12*). Luciferase enzyme expression can be regulated by a constitute promoter (such as cytomegalovirus promoter) or with a tissue specific inducible promoter, which monitors changes in gene expression resulting from cell differentiation (Bagó, 2013b). Moreover, bioluminescence can be used for *in vitro* monitoring of cell-biomaterial interactions and bioreactor performance when using a transparent chamber. Cell distribution, proliferation and survival on a biomaterial for a long-term culture can be monitored without comprising neither the cells nor the construct. Also, time related changes in gene expression associated with cell differentiation (Bagó, 2013b; Vila, 2016).

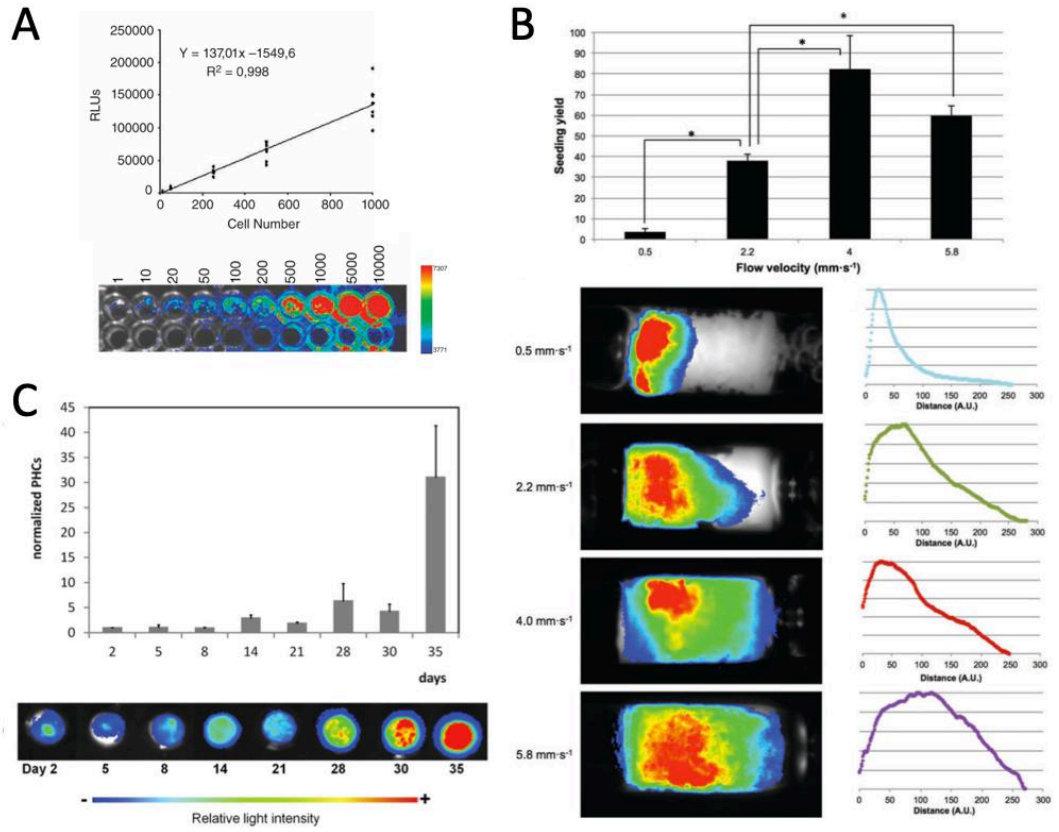

Figure 2.12 Real-Time monitoring of luciferase-expressing cells. (A) Correlation coefficient of luciferase activity from lysates of different quantities of cells (Gluc-hAMSCs) and the light produced, expressed in relative light units (RLUs). Below the graph, BLI imaging of serial dilution of Gluc-hAMSCs seeded in 96 well plates and a row of wells without cells included below (Vilalta, 2008). (B) Effect of fluid flow on cell seeding (Vila, 2016). (C) BLI monitored proliferation of hAMSCs seeded on CaP containing PLA scaffolds (Vila, 2013).

Bioluminescence can be also used to monitor bystander cells in anti-tumour therapies controlling both tumour and therapeutic cell fates, implanted in the same anatomical site (Alieva, 2012; Bagó, 2016b; Bagó, 2016a; Guerra-Rebollo, 2018; Li, 2018; Vilalta, 2009). Insertion of the specific luciferase genes can be done together with the genes encoding for the therapeutic response, thus allowing for the monitoring of proliferation and motion of bystander cells. Moreover, in tumour animal models, tumorigenic cells can be modified to express luciferase and thus assess tumour growth but also tumour recurrence (*Figure 2.13*). All of these is possible due to the correlation that exists between the number of cells and the bioluminescence signal detected (Guerra-Rebollo, 2018; Vila, 2013). However, due to the complexity of the luciferase-mediated reaction, where different molecules are involved (ATP, oxygen concentration, luciferin or coelenterazine, Mg^{2+}), and the influence of the number of metabolically active cells, the depth in the sample and the distance with the camera detector, as well as the optical properties of the

tissue can influence in intensity of bioluminescence signal. For instance, oxygen concentration in normal tissue is not the same as in injured or in tumoral tissue. Thus, for reliable BLI measurement it is important to know the cellular niche, interpret results carefully and be aware of changes in the path between the emitting cells and the camera, where oedemas, sutures or the natural animal growth can scatter the bioluminescence signal from one capture to the other (de Almeida, 2011).

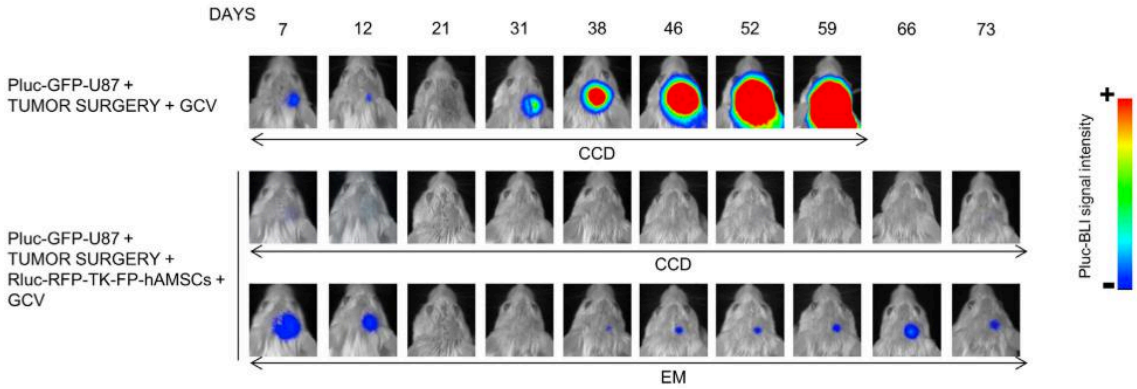

Figure 2.13 Tumorigenic cells expressing luciferase for bioluminescent *in vivo* monitoring. Pluc-GFP-U87 brain tumours implanted through a cranial window in SCID mice and surgically removed following a 21-day growth period. The brain cavity left by removing the tumour was filled (n = 4) or not (n = 4) with Rluc-RFP-TK-FP-hAMSCs in a human blood plasma matrix and subject to daily GCV treatment and weekly BLI to monitor tumour development. Representative BLI images showing development of Pluc-GFP-U87 tumours. BLI images at high sensitivity (EM) from the GCV-treated mice show the presence of Pluc-GFP-U87 cells. BLI images were superimposed on black and white images of the corresponding heads. Arbitrary rainbow colour scale depicts light intensity (red: highest; blue: lowest). From (Guerra-Rebollo, 2018).

Taking in consideration all the information displayed in the state of the art, we can state several points in which our investigation is needed. Even though several articles were published in the field of MCs for modular TE, there is no consensus in which is the best to use. Where some MCs have satisfactory biological performance, *e.g.* gelatine MCs, they are compromised for human applications because of their animal-derived origin. For that reason, controllable, biocompatible and biodegradable polymer PLA MCs are thought, and herein investigated, as suitable scaffold candidates for a modular TE strategy. This thesis compares different seeding parameters for the obtaining of the modular subunits (microtissues) in PLA MCs and compares the specific cell-derived matrices obtained upon the use of different MCs. Recent studies have already compared the proliferation rates and adherence of cells on different MCs, however, none of them has compared matrix composition after long-term cultures in MCs.

Moreover, a vascularization strategy was lacking for PLA MCs derived microtissues and a co-culture system was investigated. Although this strategy has been proved with other microcarriers, a correct vascularized strategy was lacking for this system.

Finally, we have here introduced for the first time the use of therapeutic cell-derived ECM scaffolds incorporating PLA microcarriers for the delivery of cell bystander therapy against prostate tumour progression. Other biomaterials were elsewhere described for the same aim, but this study offers proof of concept for the use of MC derived microtissues for the delivery of cytotoxic cells against tumours.

2.7 Thesis Objectives

The general objective of this work was to create cell-derived extracellular matrix scaffolds from cells cultured on PLA microcarriers.

The main purpose of this investigation is to create extracellular matrix (ECM) scaffolds from cellular aggregates cultured on poly(lactic) acid (PLA) microparticles (MP) in a dynamic bioreactor system. Once the scaffold is obtained, different methods of decellularization will be applied to acquire cell-free templates. Afterwards mesenchymal stem cells will be cultured on them for the production of functional tissues.

PLA microparticles will be elaborated as follows in Levato et al. 2012. Briefly, porous and biodegradable microparticles will be prepared extruding a polymer solution in a green solvent into a coaxial flow of nitrogen that induces the formation of a jet and its break up into droplets. Ethyl lactate which has been accepted by the FDA for its use as food aroma, is used as solvent. This procedure demonstrated to be homogenous and reproducible for obtaining PLA microparticles.

The strategy proposed here to overcome low seeding efficiencies and poor cell distributions seen in static cultures is the culture of cells using microcarriers in a spinner flask bioreactor. Different cellular lineages, such as fibroblasts, osteoblasts and endothelial cells will be seeded on the MP for adhesion and proliferation evaluation. Lately, in order to avoid the issue of mass transfer limit during *ex vivo* extracellular matrix deposition we will transfer the colonized microcarriers to a chamber connected to a perfusion system, allowing the formation of a clinical-relevant construct.

Once the cell derived scaffold is formed *ex vivo*, cells will be removed by means of different techniques (chemicals, physic or enzymatic) still in the perfused system, as well as the microparticles, in order to be left with the structure and components of the ECM.

Decellularization strategies will be closely evaluated as it is of utmost importance to prepare a desirable scaffold for implantation without eliciting adverse inflammatory and immune responses.

Subsequently, this matrix will be used as support for the culture of mesenchymal stem cells. The ECM will be then evaluated for its ability to guide cell proliferation and differentiation towards a specific phenotype, by means of the bioluminescence strategy and the constitutive or induced expression of luciferase enzymes.

To complete this project, we will perform different assays to characterize the biological scaffolds: topography, mechanical properties (stiffness, elasticity, and viscosity), ECM components, and concentration of immobilized growth factors.

Finally, we will seed mesenchymal stem cells in a co-culture with endothelial progenitor cells in order to evaluate the angiogenic/vascularity potential of the system.

Chapter 3

Study of PLA microcarrier cell seeding technique for microtissue formation

3.1 Introduction

In the pursuit of mimicking native tissues to restore or replace injured ones, efforts have been made towards modular Tissue Engineering (TE) where microstructural functional units (*i.e.* modules) are assembled to create complex tissue constructs. Across human biology, hierarchical combination of repetitive nano- or micro-sized modules define tissues in the millimetre scale but also larger structures such as organs in the macroscale (Lakes, 1993). Differently to traditional top-down strategies, modulation permits to integrate complexity into the engineered constructs in order to recapitulate the architecture of native tissues. Cell seeding in large scaffolds encounters poor cell distribution and colonization of the whole construct is limited to nutrient and oxygen diffusion (Carmeliet, 2000). However, high and uniform cell densities are found when small units are firstly created and then assembled to form engineered constructs (Chen, 2011b). Moreover, modularity represents a versatile method for the incorporation of multiple cell types. Cellular heterogeneity and physical arrangement can be directed by the assembly of simple building blocks obtained from using different cell lines (Leung, 2007; McGuigan, 2007b). Furthermore, survival of engineered constructs upon implantation requires a rapid vascular invasion to supply with vital resources. Inherent modularity of these techniques provides enhanced control over the assembling process allowing a permissive compactness for subsequent vascularization (Matsunaga, 2011; Rouwkema, 2009). To produce modular constructs, functional subunits can be created following different strategies such as cell-laden hydrogels (McGuigan, 2007a), cell-

sheets (Chen, 2016b; Liu, 2017), spheroids (Fennema, 2013), direct tissue printing (Levato, 2014), and cell-laden microcarriers (Declercq, 2013; Twal, 2014; Urciuolo, 2011; Zhong, 2017).

Microcarriers have been broadly used for different biomedical applications, not only as scaffolds for modular TE but also as tools for biomolecule and vaccine production in bioreactors *in vitro*, providing scale-up and controllable conditions for pharmaceutical industries (Gonsales da Rosa, 2012; Rourou, 2009); as drug delivery vehicles into targeted sites and triggered by specific signalling (Mohamed, 2008); and for *in vitro* cell expansion as their properties can be tailored to allow adhesion of anchorage-dependent cells (Eibes, 2010; Schop, 2010; Yuan, 2014). For the concern being discussed in this chapter, *i.e.* the use of microcarriers for modular tissue fabrication, cells and MCs are both integrated in a cell-derived extracellular matrix. Key events underneath this approach comprise the adhesion between cells and MCs, the interaction between cells, cellular proliferation and its inherent capacity in bridging MCs, and finally ECM protein deposition creating a fibrillar network.

Biocompatible synthetic polymers such as poly(lactic-acid) (PLA), polyglycolide and its copolymers (poly(lactide-co-glycolide) polymer (PLGA)) have been extensively investigated in biomedical applications as intravenous administration vehicles, resorbable sutures and implants (Nair, 2007). Its controlled manufacture and well-known composition, as well as they versatility and tuneable properties allow accurate control of its fabrication enabling their eventual approval by regulatory sources. Moreover, concerns on organic solvents used during PLA scaffold manufacturing were obliterated by the study performed by Levato *et al.*, where a novel green-solvent method for PLA MCs fabrication was described (Levato, 2012). Biodegradable, biocompatible and eco-friendly produced PLA microcarriers were characterized and proved satisfactory for cell attachment, and demonstrated to be supportive for cell proliferation after surface functionalization (Levato, 2015).

The aim of this work is to optimize cell seeding procedures on polylactic acid microcarriers for the subsequent obtaining of cell-derived microtissues (MT) to become the modules or small subunits in a modular TE strategy. Different MCs-cell seeding approaches are investigated, wherein static and dynamic procedures are compared. Main concerns in a correct MT production englobe microcarrier colonization and homogeneous cell distribution, MT size and shape, feasibility in producing large quantities of these modules and finally a correct ECM deposition. For that reason, different culture formats

are studied in static: 96 well plates, the use of PDMS moulds and 24-well plates. At the same time, different cell/MC seeding protocols were carried out for each of the above-mentioned static culture formats. Parallelly, dynamic microcarrier seeding is studied using a spinner flask bioreactor. Best settings concerning agitation regime, medium serum composition and cell/MC concentration are also herein elucidated. MTs obtained from static and dynamic protocols are compared to define the most efficient and feasible protocol for obtaining cell-derived ECM microtissues using PLA as small building blocks for modular TE.

3.2 Materials and methods

3.2.1 Cell Culture and Expansion

Bone marrow mesenchymal stem cells (MSCs) were isolated from long bones of 2-4 weeks old Lewis rats according to a previously published protocol (González-Vázquez, 2014). Passages between 4 and 6 were used in all experiments. Cell expansion was performed in T175 Nunclon™ flasks, using Advanced Dulbecco's Modified Eagle Medium (aDMEM, Gibco™) supplemented with 10% foetal bovine serum (FBS), 1% penicillin/streptomycin and 1% L-glutamine (Sigma).

3.2.2 Microcarrier fabrication

Poly(lactic-acid) was purchased from Purac® (Purasorb® PLDL 7038, The Netherlands). (-)-Ethyl-L-lactate (photoresist grade; purity > 99.0%) and polyvinyl alcohol (PVA, 9-10 kDa, 80% hydrolysed), as well as other products further mentioned were acquired from Sigma-Aldrich (Spain), unless otherwise stated.

PLA microcarriers were prepared by an emulsion/solvent evaporation technique, using ethyl-lactate as environmental-friendly solvent, as previously described (Levato, 2012). Briefly, a 3.5% w/v PLA in ethyl-lactate solution was extruded through a double-bore needle (inner 30G) (dispensing rate 10ml/h), where a coaxial flow of nitrogen was applied (outer 22G) (1 atm), breaking the solution jet into droplets. PLA MCs formed when droplets precipitated into a hydroalcoholic coagulation bath (70% v/v ethanol in water with 0.3% w/v poly-vinyl alcohol). Particles were left to harden in a stirring bath for 1 to 2 hours. Then, several rinses were carried out to remove solvent, using a 40μm pore

diameter sieve (CISA S.A, Spain). Particle size was obtained using a Leica E600 optical microscope and calculated employing *FIJI* software (Schindelin, 2012).

3.2.3 Biofunctionalization of the surface of microcarriers

Surface modification of PLA MCs was performed by covalently attaching human recombinant collagen type I (FibroGen, USA) in order to foster cellular response and adhesion to the material. Functionalization protocol followed three steps (Punet, 2013). Firstly, a controlled hydrolysis of the ester bonds of the PLA substrate was provoked for 10, 30 and 60 minutes respectively, with a 0,5M NaOH solution. Exposed COOH terminal groups resulting from surface hydrolysis were activated with an ethyl-(dimethylaminopropyl) carbodiimide / N-hydroxysuccinimide (0,1/0,2M EDC/NHS) solution in 70% ethanol for 2 hours. Activated microparticles were incubated in a collagen type I solution in PBS (100µg/ml collagen type I, overnight). Finally, functionalized MPs were washed and freeze-dried (Christ Alpha 1-4 LD, Freeze Dryers, UK) for preservation and kept in the fridge until used.

3.2.4 Microcarrier seeding in static conditions

Rehydration and disinfection of microparticles were done in 70% v/v ethanol for 12 hours prior to cell culture. Under sterile conditions repeated washings were performed with PBS until normal cell culture medium was added.

For the study of MT formation in static conditions, three different culture formats were investigated: (i) 96-well plates (Nunc, U-shaped bottom non-treated surface #262162), from now on U-96; (ii) polydimethylsiloxane (PDMS) moulds, that consisted in two 10x10mm layers of 5mm-thick one on top of the other. A 6mm in diameter centred hole was punched into the upper layer, and moulds were placed in 24-well plates; and (iii) ultra-low attachment 24-well plates (Falcon) tilted 30º degrees favouring accumulation of particles and cells in one side, from now on 24-W. Standard protocols were initiated with 3 mg MP per well. This was adapted for U-96 format reducing MP content in 6 times.

For each of these culture formats, three different cell/MCs seeding protocols were investigated: (a) control condition where 25,000 cells/mg MCs were seeded, (b) seeding 12,500 cells/mg MCs twice in the same well, leaving 20 minutes in between, and (c) 50,000 cells/mg MCs. Hydrated microparticles were placed in the wells or moulds and

let sink in all conditions. Medium excess was removed and rMSCs cell suspension was carefully added on top of the particles. Initially, minimum volumes were used in order to intensify cell-MP proximity. After 30 min normal volumes were reached. Cells were kept in a 37ºC, 5% CO2 humidified incubator. Cell medium was replaced every 2-3 days for as long as stated for the assays, reaching a maximum of 21 days.

3.2.5 Morphology and size examination

Microtissue morphology and size were evaluated using Leica stereomicroscope. Images were taken after 21 days in culture. Size was analysed using *FIJI* software (Schindelin, 2012) following the next steps. After setting the scale, *Adjust > Threshold* was used to discern between microtissue and background, creating a binary mask were background is 0 and MT is 255. *Analyze particles* was applied using a correct diameter inferior limit in order to avoid free particles. Then microtissue appeared selected as a ROI (region of interest). Area was calculated utilizing *Analyze > Measure*.

3.2.6 Microcarrier seeding in dynamic conditions

For dynamic microparticle seeding, a 250mL spinner flask device was used (BellCo, USA). The bioreactor consisted in a 140mm x 85mm glass flask, with two angled sidearms and a glass ball tube magnet for gentle agitation. Sigmacote® (Sigma-Aldrich, Spain), a silicone-based solution, was used to form a water-repellent thin film on the glass surface to avoid protein adsorption. Prior to sterilization in autoclave, spinner flask was thoroughly washed to remove toxic remainders using Cleaning solution (ES 7x MPBIO, #76-671-49). Already in aseptic conditions, hydrated microparticles were added alongside with 100ml of culture medium and cell suspension. Parameters under study in the spinner flask dynamic seeding concerning the inoculation phase were: (i) stirring regime, comparing 3- and 15-min 30rpm-agitation period, with 27 minutes at 0 rpm; (ii) serum content (0% or 10% FBS); and (iii) cell/bead ratio (8, 10 or 12 cells/bead). Then bioreactor spinner flask was placed on a multiple magnetic stirrer block (Biosystem 4 Direct, Thermo Scientific) located in a humidified incubator (5% CO2, 37ºC) for 6 hours. For all parameters, 1 ml sample was collected twice at the end of the spinner flask for vital staining. Moreover, long term spinner flask culture was investigated for 48 hours, where intermittent agitation (3min 30rpm, 27min 0rpm) was only maintained during the first 8 hours of inoculation, and then continuous stirring was applied for 48 hours. Vital

staining was also assessed by taking MC-cell samples from spinner flask after 4, 8, 24 and 48 hours.

Afterwards, 1ml sample was collected twice for vital staining, and the rest of colonized microcarriers were transferred to non-adherent 24-well plates in a 3mg MP/well concentration. Gentle manipulation was performed using 10ml pipette tips in order to avoid friction or cell-particle disruption. Plates were kept in a humidified incubator in a 30º titled position to promote microtissue formation for 21 days.

3.2.7 Vital staining and MC colonization rate

By the end of the inoculation phase in spinner flask bioreactor, two 1ml sample was collected twice for vital staining with Calcein AM (Thermo Fisher). Nonspecific estereases inside living cells transform non-fluorescent calcein into green-fluorescent molecules, which slowly leak out of the cells enabling their traceability. Briefly, after rinsing with PBS, cell-laden microcarriers were incubated for 15 min, at 37ºC, with a 2µM Calcein-AM solution in Dulbecco's Phosphate-Buffered Saline (DPBS) (Thermo Fisher, Spain). Fluorescent images were taken using E600 Leica microscope.

Cell-microparticle encounters during spinner flask culture could lead to single-cell-colonized particles. In order to dismiss unspecific attachments, we have described the concept of microcarrier colonization rate (MCR) as the number of microcarriers with three or more cells attached on them, divided by the total amount of microcarriers (Equation 1).

$$Microcarrier\ Colonization\ Rate = \frac{N^{o}\ of\ MC\ colonized\ by\ three\ or\ more\ cells}{Total\ MC\ number} x100$$

Equation 1 Definition of Microcarrier Colonization Rate

3.2.8 Scanning electron microscopy

Microtissue samples were taken after 21 days in culture. Firstly, they were fixed with 3% paraformaldehyde (PFA) for 10 min at 4ºC. After two PBS washes, microtissues were dehydrated in an increasing alcohol gradient before performing Critical Point Drying at the CCiTUB (Scientific and Technological Centers, University of Barcelona). Then, samples were mounted on sample holder and carbon sputtered. Morphological analysis and microtissue size were measured using ultra-high resolution filed emission scanning

electron microscopy (SEM,) (NOVA NanoSEM 230, FEI Company), available at the Platform of Nanotechnology of IBEC (Barcelona).

3.2.9 Statistical analysis

Data results were expressed as mean and standard deviation of the replicates (n=3, unless otherwise stated). Analysis of Variance (ANOVA) was used to statistically analyse conditions under study. And Sidak's multiple comparisons test was used to compare differences between groups. Significance level of $p \leq 0.05$ was selected. GraphPad Prism 6 was used to perform analysis.

3.3 Results

3.3.1 PLA microcarrier characterization

A two-step preparation technique was used to obtain PLA microcarriers. Extrusion of PLA/ethyl-lactate solution through a doubled-pore needle formed a jet of droplets. These fell in the coagulation bath and solidify to constitute microcarriers (Figure 3.1, A). As previously described (Levato, 2012), parameters affecting particle diameter concern the polymer concentration and the fluid flow rates at the dispensing stage. Microscope image analysis showed an average particle size of 81.85 ± 23.25 μm (Figure 3.1, B). MCs size was also investigated with SEM images, confirming size polydispersity and demonstrating Janus topography (Figure 3.1, C). MCs presented two different surface hemispheres, one smooth and the other displaying a wrinkled surface. No agglomeration between particles was found at any moment.

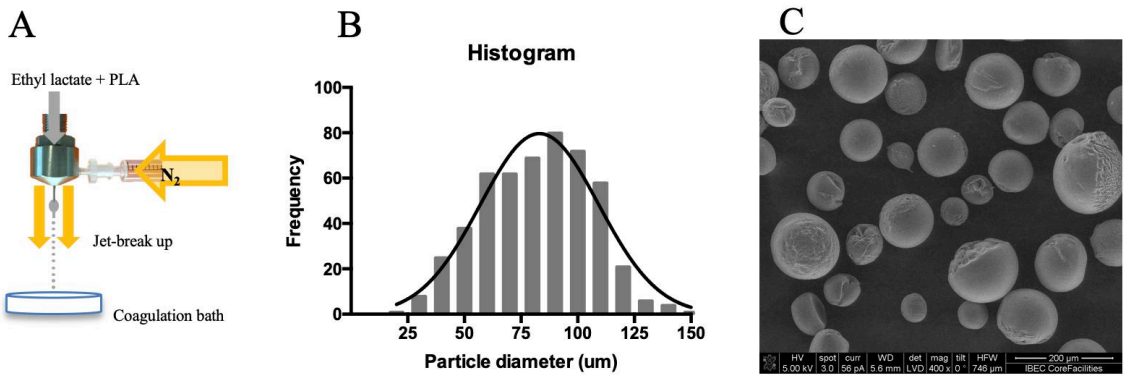

Figure 3.1 Microcarrier preparation and characterisation. (A) Schematic illustration representing experimental procedure. A 3.5% PLA (w/v) in ethyl lactate solution is extruded through the upper inlet and a nitrogen flow is applied through the coaxial inlet. Nitrogen pulls the solution forming a jet of droplets, that solidify in the coagulation bath (ethanol in water 70:30). (B) Microcarrier size distribution measured by optical micrographs. (C) SEM image showing PLA microcarriers and their Janus morphology.

Surface functionalization was performed using the zero-length crosslinkers EDC/NHS. The first step consisted in the partial hydrolysis of MC surface with NaOH in order to produce free carboxyl groups. Previous studies have shown that for functionalization of PLA films, 10 min of hydrolysis yielded the highest density of reactive groups available. However, here we studied longer incubation periods in order to assess higher protein grafting. Immunofluorescent images in Figure 3.2 showed higher amount of collagen protein attached to the surface after 60 minutes of activation rather than 10 or 30 min, in which no qualitative differences were observed.

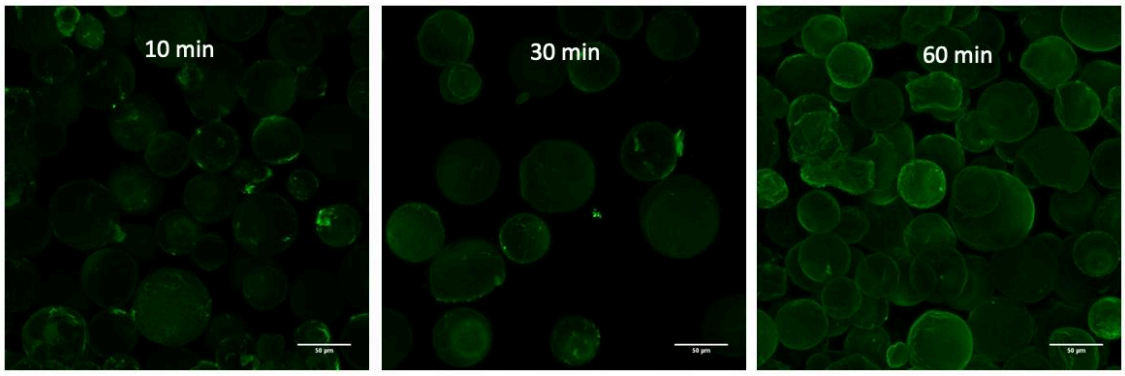

Figure 3.2 Immunofluorescent images of PLA MPs after surface biofunctionalization with collagen type I. In green, anti-collagen type I antibody assessing protein distribution on PLA MPs after 10, 30 and 60 minutes of surface hydrolysis with NaOH. Longer activation periods led to a more even protein distribution on their surface.

3.3.2 Microtissue size evaluation in static conditions

MSCs were seeded and cultured on PLA microcarriers using three different static formats: (i) U-96 well plates, (ii) PDMS moulds, and (iii) non-adherent 24-well plates; following three different cell/MP protocols (a) 25000 cells/mg MCs, (b) 12000 cells/mg MCs twice in the same well, and (c) 50000 cells/mg MCs. As can be observed in (Figure 3.3, A), cells adhered, proliferated and secreted ECM on microcarrier among all culture formats. However, only U96 well plates and non-adherent 24-well plates allowed the formation of macroscopically significant microtissues. PDMS moulds resulted unfruitful in that purpose, instead microcarrier were found dispersed around the moulds and cells were not only attached to microcarriers but also to PDMS (Figure 3.3, C).

ImageJ software was used to calculate MT sizes. In terms of cell seeding protocols, no significant differences were found for the size of microtissues formed in the U96 plates (Figure 3.3, B). However, for 24w plates, the two-times seeding protocol with a cell/MC final concentration of 25000 cells/mg MC yielded an average microtissue of 16.07 ± 2.83 mm^2, which was 1.8 and 2.1 times bigger than the MT obtained by the other two conditions (8.71 ± 2.40 mm^2 for 50000 cells/mg; and 7.58 ± 1.11 mm^2 for control condition, respectively). Only the later comparison was significantly different (p value ≤0,001).

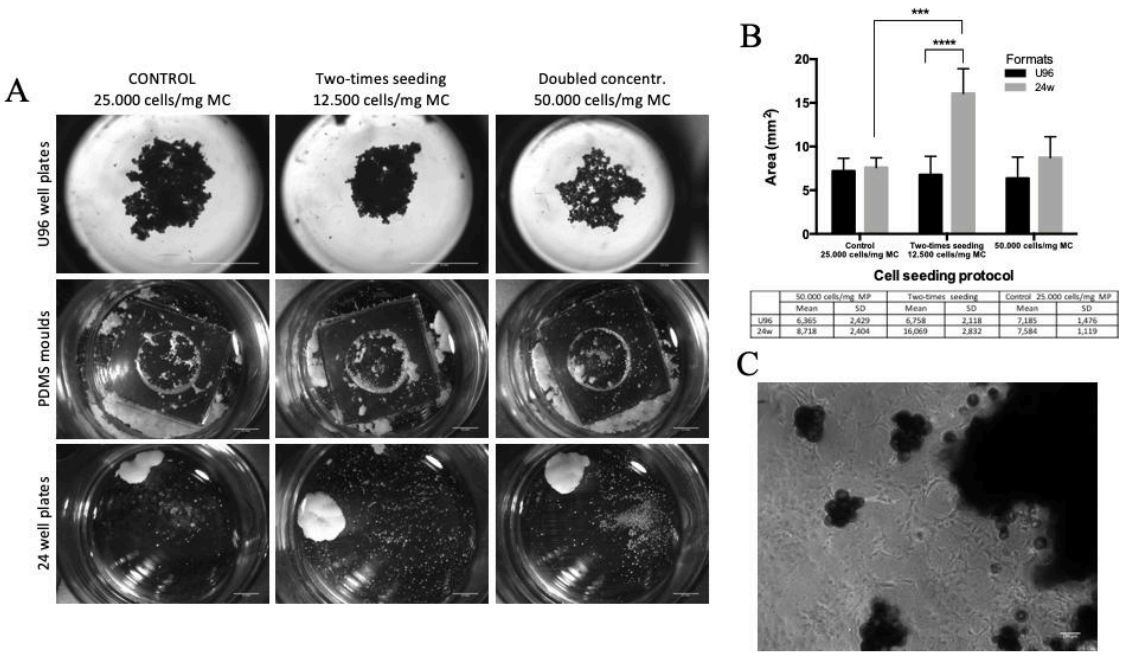

	50.000 cells/mg MP		Two-times seeding		Control 25.000 cells/mg MP	
	Mean	SD	Mean	SD	Mean	SD
U96	6,365	2,429	6,758	2,118	7,185	1,476
24w	8,718	2,404	16,069	2,832	7,584	1,119

Figure 3.3 Macroscopic morphology and size of PLA microtissues prepared in static conditions. (A) Leica stereomicroscope images of MT prepared via U96 well plates, PDMS moulds and 24 well plates using three different protocols: 25000 cells/mg MC, two-times seeding 12500 cells/mg MC and 50000 cells/mg MC. (B) Size of MT obtained using U96 and 24 well plates as culture formats via the different cell seeding protocols (***p≤0.001, ****p≤0.0001). (C) Cells attached to PDMS moulds instead of being exclusively attached on the MC surface.

When comparing between the two static seeding formats U96 and 24w plates, no significant differences were found for the control and the 50000 cells/mg MC protocols. Only the two-times seeding protocol in the 24 well plates rendered bigger scaffolds (2.7 times bigger in size, p value ≤0.0001) than the ones obtained by the same protocol but using U96 well plates. Interestingly, these results showed that U96 format was able to yield scaffolds as big as the ones from 24w but using 6 times less microcarriers and cells. Nonetheless, in all seeding conditions using U96, MC-free regions were observed in the scaffolds. The area of these regions was calculated and subtracted from total area as depicted in Figure 3.4. Although for the 50.000 cell/MC condition, more MC-free regions were found, final microtissue areas were the same. Considering that to reach this cell/MC ratio, MC content was reduced compared to control and two-times seeding protocols, smaller microtissues were expected. Instead, these were covering the same areas, but resulted less compact.

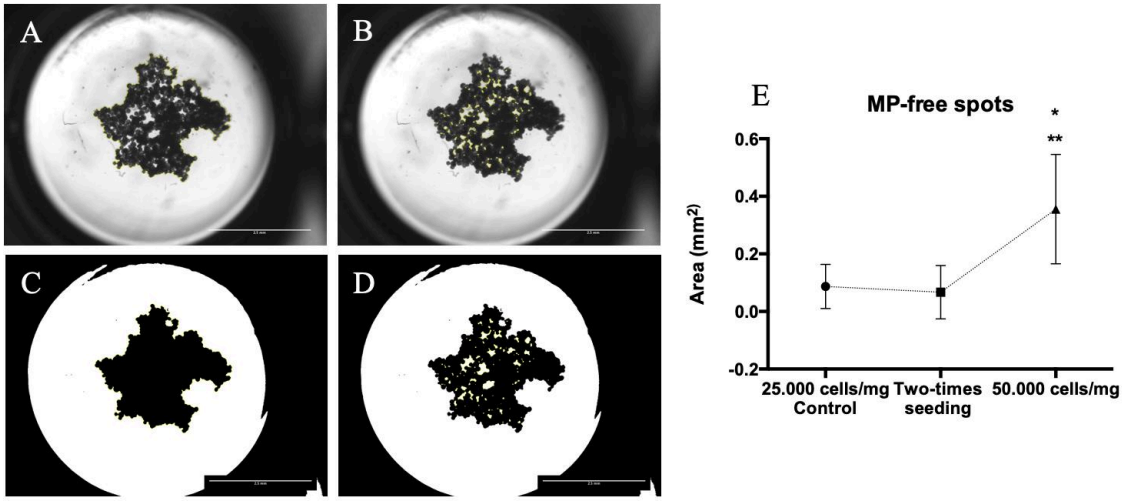

Figure 3.4 Area analysis of the MT obtained in the U-shaped 96 well plates. Detailed image processing for area analysis: raw MT images (A and B) were converted into binary (C and D) and they were used for area selection. (A) and (C) represent complete MT area selected, whereas (B) and (D) show microcarrier-free regions selected. Final MT area is expressed after the subtraction of microcarrier-free areas (D) from total area (C). (E) Graph representing the area within the microtissues that was not occupied by particles and cells (*i.e.* MC-free regions).

3.3.3 Microscopic evaluation of scaffolds produced in static conditions

Cell adhesion, spreading, interconnectivity and extracellular matrix deposition were analysed through surface SEM observations. Microtissues were formed in static conditions by U96 and 24w culture formats for 21 days. After that, they were fixed, dried and sputter covered with carbon before their study. For PDMS-formed MT little aggregates could be recovered for SEM analysis, although they were not relevant for the study (images not shown).

Detailed SEM examinations demonstrated that secretion of extracellular matrix after 21 days was not uniform upon the different culture formats. Microtissues seeded in U96 well plates exhibited non-complete cell-derived ECM layer on the surface when seeding in two times and the control condition (*Figure 3.5*, A, B); but it was not present at all when seeding at a 50000 cell/mg density (*Figure 3.5*, C). In the later condition, it could be observed how cells extended thin projections or filopodia in order to interconnect among different particles. Yet many of them appeared uncovered. Cell proliferation and ECM deposition were unsuccessfully achieved by this condition. For the two-time seeding and control conditions confluent cellular multilayers were observed, where cells maintained their typical flat and polygonal morphology. However, cellular limits were still visible suggesting proliferation prevailed over extracellular matrix deposition.

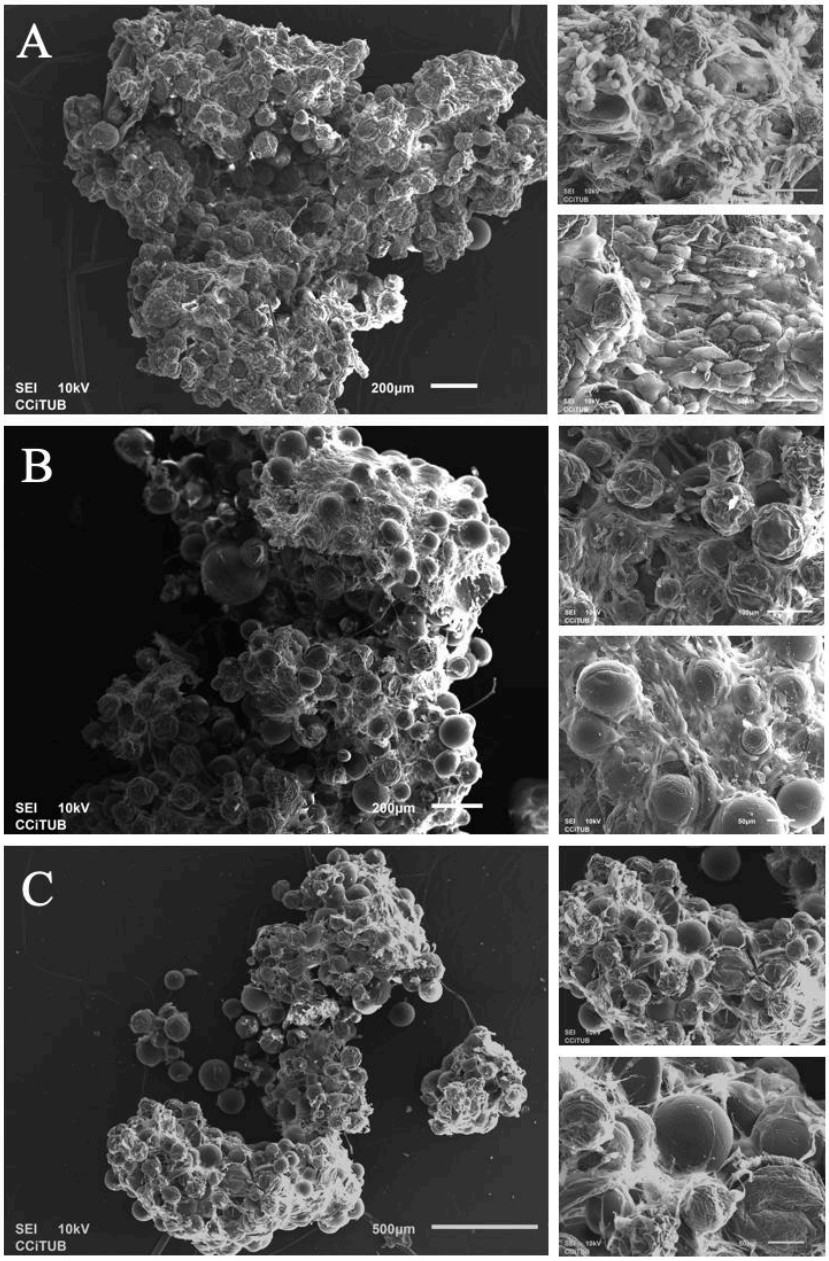

Figure 3.5 Scanning electron microscopy images of U96 MT after 21 days in culture. Images of the surface and closer magnifications for cell morphology evaluation. For (A) 25000 cells/mg MC seeding condition and (B) two-times seeding 12500 cells/MC, confluent cells appeared although cell morphology was still observable suggesting low ECM deposition; for the (C) 50000 cells/mg MC condition, lowest ECM deposition was observed, and cells showed elongated filopodia.

A completely different situation is found when observing microtissues from 24 well plates (*Figure 3.6*). A denser and more uniform ECM outer layer is secreted by cells around the particles. Actually, in some regions this layer was able to conceal microcarriers at the surface, providing a smooth wall/stratum. Because of the abundance of extracellular matrix, individual cells were not identified. When comparing the three

methodologies in which cells are seeded, no significant difference could be described. 25000 cells/mg MC microtissue had some thinner regions at its surface.

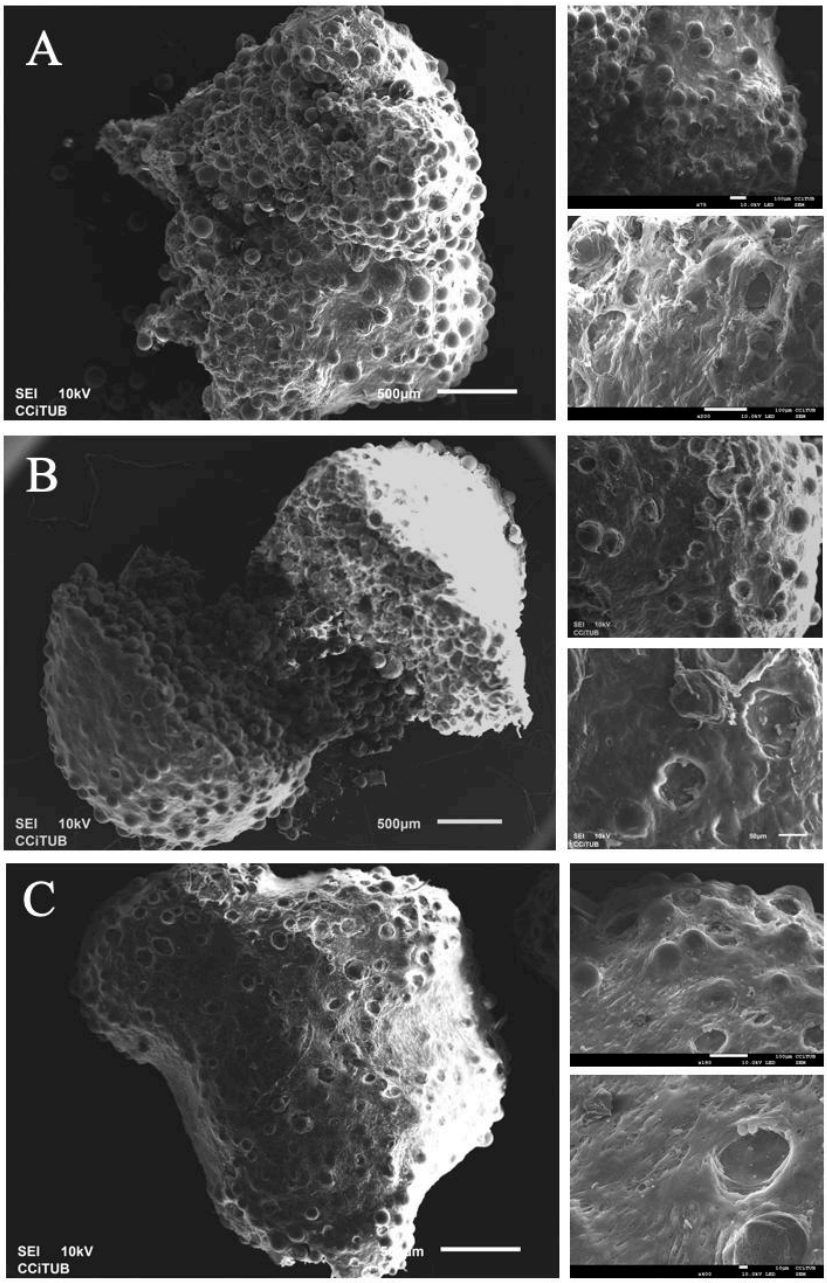

Figure 3.6 Scanning electron microscopy images of 24w MT after 21 days in culture. (A) 25000 cells/mg MC seeding condition. (B) Two-times seeding 12500 cells/mg MC and (C) 50000 cells/mg MC. For all conditions, ECM deposition was abundant and uniform all around the construct.

Transversal sections of 24w microtissues of all conditions exposed a fibrillar network in between the microcarriers (*Figure 3.7*). This was uniform all over the inner space, reaching as deep as 500-700µm for the 50000 cells/mg MC and two-times seeding conditions. For the control condition, some regions were observed with poor ECM deposition, mostly when reaching the core centre of the microtissue. The wrapping outer

layer was easily observed for all the studied circumstances. Smooth on its surface, the edge of the layer evidenced its fibrous nature.

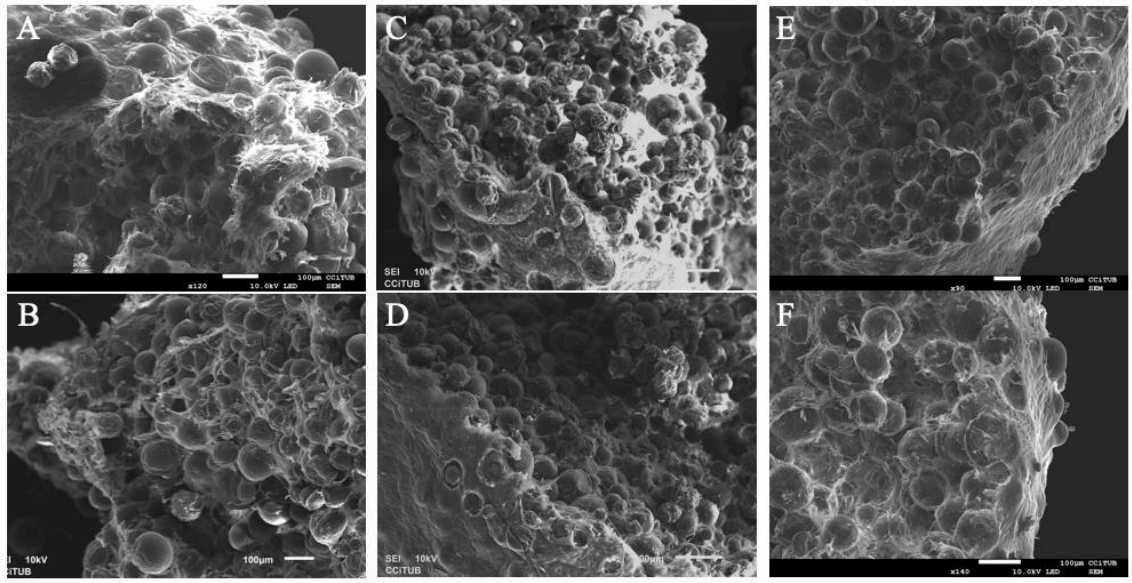

Figure 3.7 Transversal sections of 24w MT observed by scanning electron microscopy. (A, B) 25000 cells/mg MC seeding condition; (C, D) two-times seeding 12500 cells/mg MC and (E, F) 50000 cells/mg MC.

3.3.4 Spinner flask microcarrier colonization

Microcarrier colonization was further studied in dynamic conditions using a spinner flask bioreactor. Stirring regime, serum deprivation and cell-bead ratio were investigated as main parameters involved in the optimal particle colonization. Also, spinner flask culture was evaluated for 48h. Samples were taken out from spinner flask at stablished time points and attached cells were assessed by vital staining with Calcein AM. Particle colonization was determined as the number of colonized particles by the total amount of particles.

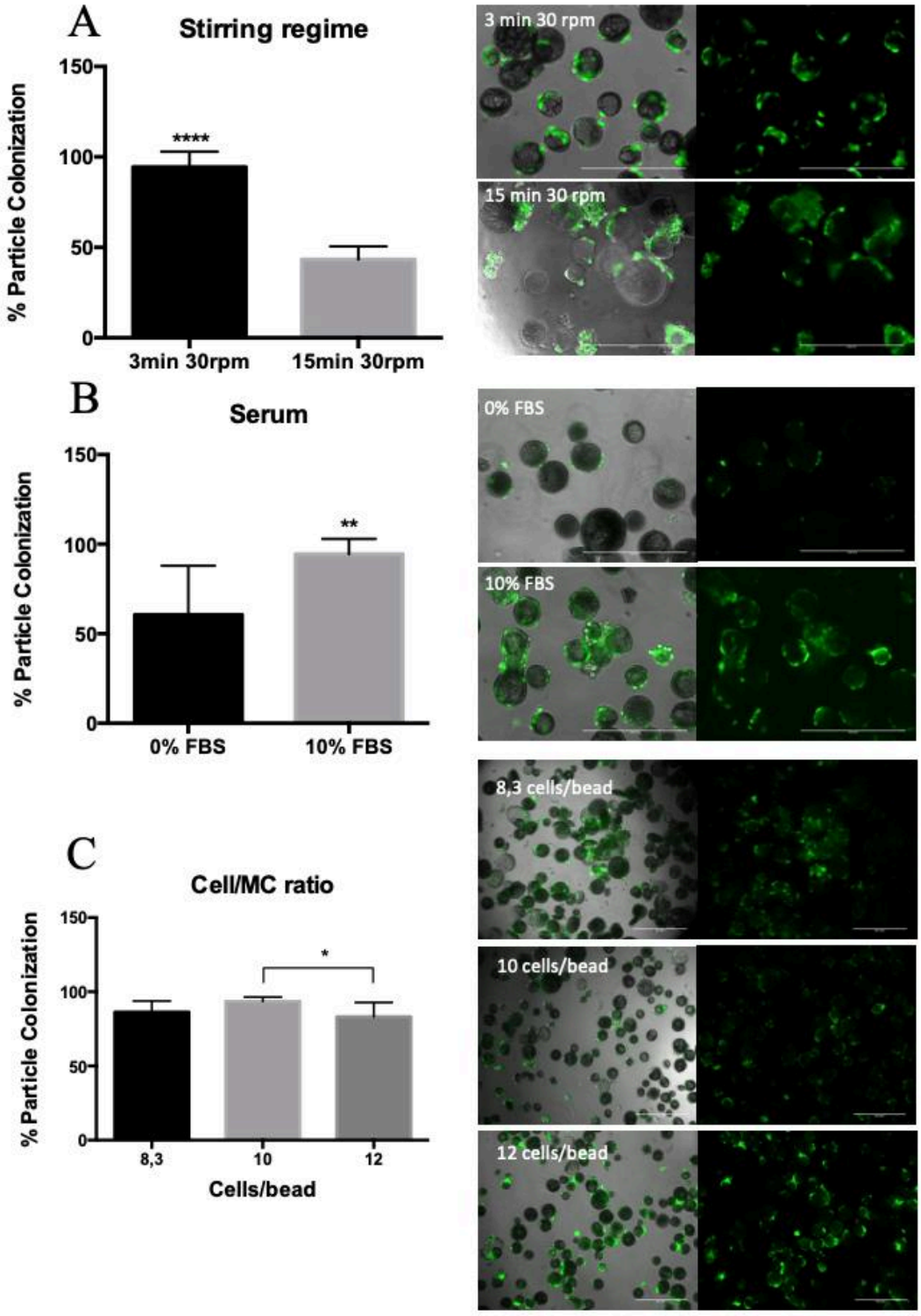

Figure 3.8 Microcarrier colonization parameters under study. (A) Stirring regime yielded a MCR of 94.4% for 3 min agitation and 43.3% for 15 min agitation; (B) Serum deprivation which decreased MCR to 60,6% whereas for 10% FBS it stayed at 94.4% MCR; and (C) cell/bead ratio with 86.3% MCR for 8.3 cells/bead, 93.6% MCR for 10 cells/bead and 83.2% MCR for 12 cells/bead. * p value ≤ 0.05, ** p value ≤ 0.01, *** p value ≤ 0.001. Scale bar 0.5 mm.

All cultures were stirred intermittently at 30 rpm. The duration of the agitation period was studied for 3 and 15 min. Then a static period was applied for 27 minutes. As shown in *Figure 3.8*, A, more MCs were colonized after 8h of applying a 3 min agitation regime (94.37% MCR), rather than 15 min, where only 43.29% of particles were colonized. Total deprivation of FBS showed a significant decrease in particle colonization in the inoculation phase compared to a normal 10% (v/v) concentration probably due to the adsorption of serum proteins onto the microcarrier surface (*Figure 3.8*, B). The impact of initial cell/bead ratio on microcarrier colonization efficiency was also evaluated. *Figure 3.8*, C shows no significant difference between 8.3 and 10 cells/bead. However, when increasing cell/bead ratio to 12 cells/bead, particle colonization decreased in significance with the previous result. In fact, an increased cell number provoked more cell-to-cell encounters, leading to higher amounts of self-aggregated groups of cells as observed in the calcein staining images (*Figure 3.8*, C).

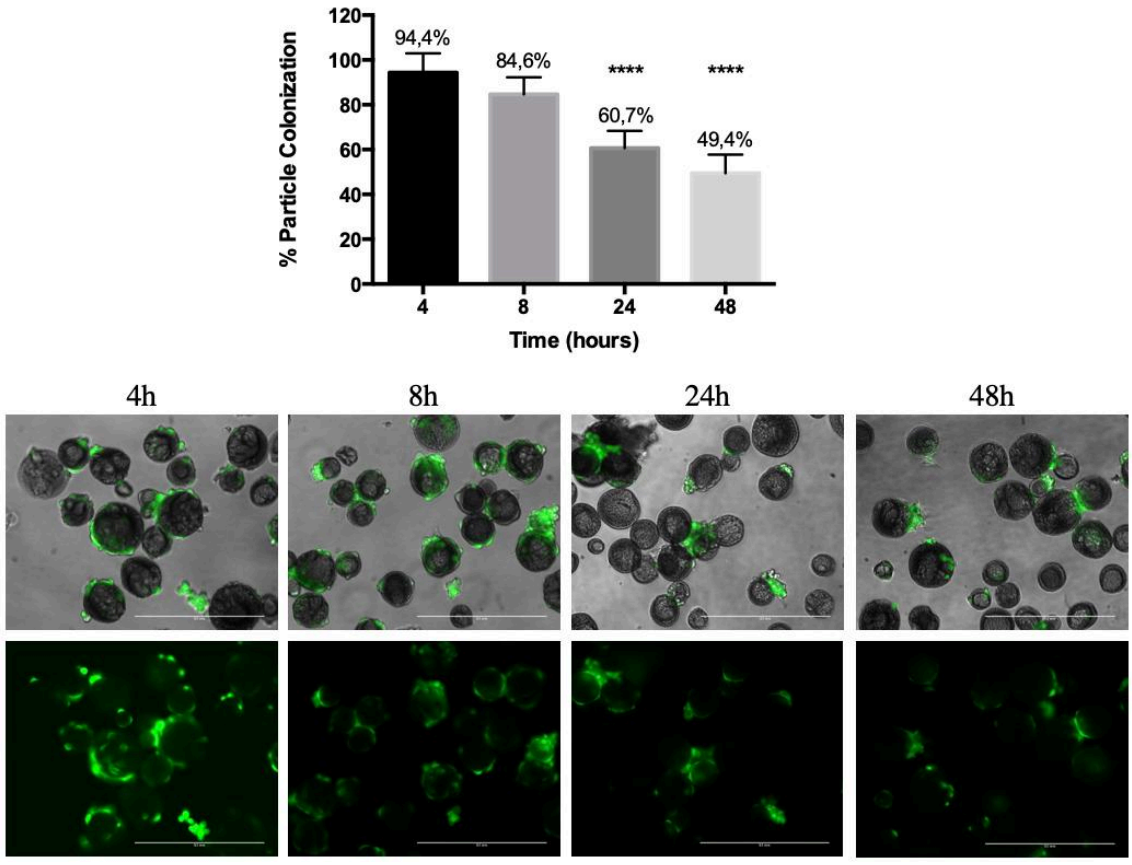

Figure 3.9 Microcarrier colonization evaluated over time in a spinner flask bioreactor. During the first 8 hours, an intermittent agitation regime was applied (3min 30rpm, 27min 0rpm). After that, continuous agitation was maintained at 30rpm. Green calcein AM vital staining was used to assess cells on top of particles. MC at 4 hours was 94.4%; at 8 hours was 84.6%; 60.7% MC at 24 hours and 49.4% MC at 48 hours. After 24 and 48 hours, number of colonized particles was significantly lower compared to the MC obtained at 4 hours (36% and 48% less, respectively). ****p value ≤ 0.0001. Scale bar 0.5mm.

Microcarrier colonization was also evaluated over a period of 48 hours. During the first eight hours, an intermittent agitation regime (3min 30rpm, 27min 0rpm). Then, continuous stirring (30rpm) was applied for 40h. Samples were collected at 4, 8, 24 and 48h to assess the number of colonized particles. Results showed a progressive decrease in particle colonization (*Figure 3.9*). During the discontinuous agitation, maximum yield was observed after the first 4 hours, where 94.4% of the MCs were colonized. The next four in intermittent stirring, colonization ratio saw a decreased of 10%, followed by another decrease of the 35% after 24 hours. Finally, the number of colonized microcarriers after 48h in spinner flask was cut in half compared to the first timepoint.

3.3.5 Extracellular matrix deposition after spinner flask bioreactor

In this dynamic microtissue strategy, MCs were firstly colonized in a spinner flask bioreactor, as described above. However, cell proliferation and extracellular matrix deposition leading to microtissue formation took place in static conditions. After determining the correct parameters for MC seeding, colonized MCs were transferred to ultra-low adhesion 24 well plates. Plates were placed in a humidified incubator, titled in 30º degrees provoking accumulation of microcarriers in one side, following the previously described protocol. After 21 days of culture, microtissues were collected and prepared for SEM analysis (*Figure 3.10*).

Unlike what happened in the 24 well plates in the static procedure, dynamic MC seeding allowed the total incorporation of carriers used in the assay into the microtissue, suggesting a homogeneous and favourable MCs colonization. The size of the MT obtained after using the spinner flask reached 4 to 7mm long x 1,5 to 2,5mm width x 0,5mm deep. ECM deposition was effective in forming microtissues, however, many MCs could still be noticed on the surface, meaning ECM deposition was effective for the cohesion of MCs into a construct, but not enough to cover them all. *Figure 3.10*, F shows how multiple cell layers were superposed, leaving some of the cell borders visible. In the transversal section (*Figure 3.10*, D) an abundant fibrillar network could be observed inside the microtissues.

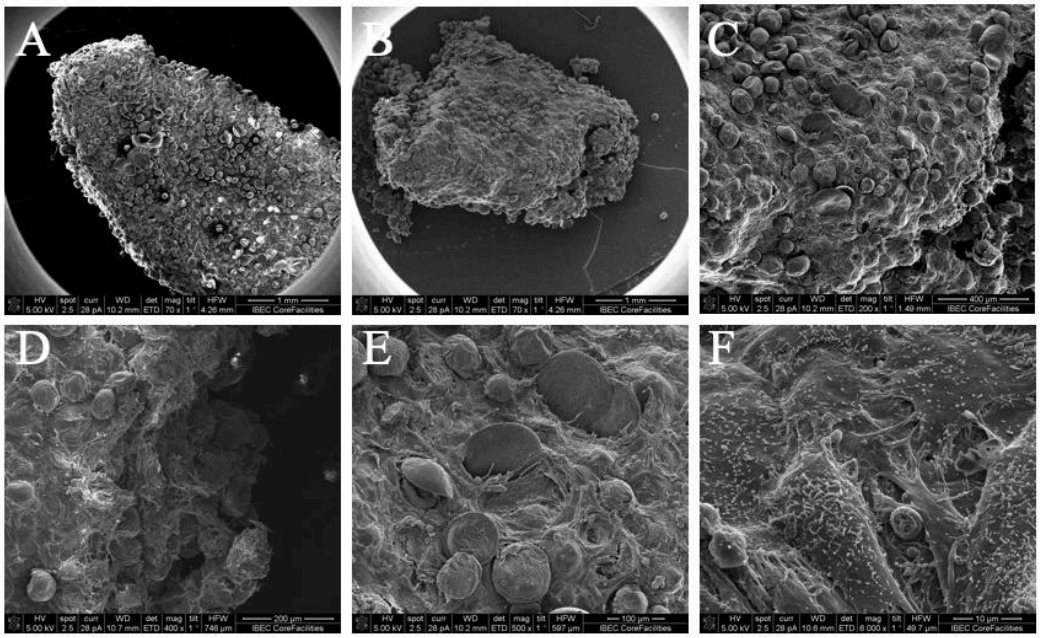

Figure 3.10 SEM images of MT obtained after dynamic MC colonization and formed in ultra-low attachment 24 well plates for 21 days. (A) and (B) images of the whole microtissue. ECM deposition gathered all MCs available in the culture. Although ECM was effective, at closer magnifications (C-E) MCs could be visible at the surface. (D) Shows fibrillar nature of the ECM deposited. (F) Multiple cells are superposed on the surface of the MT. Cells are perfectly spread and multiple filopodia are observed.

3.4 Discussion

Modular TE approaches are emerging as successful methodologies for the fabrication of biomimetic tissue substitutes. Following the aim of generating functional tissue modules, researchers have created microtissues from cellular aggregates, cellular sheets, cell-laden microgels or microcarriers (Elbert, 2011). Once obtained, microtissues are assembled to form macrotissues by means of random packing, stacking or directed assembly (Imparato, 2013). This study comprises the evaluation of the first step in the formation of modular microtissues using polylactic acid microcarriers. MC seeding was here investigated comparing static versus dynamic procedures in order to further obtain microtissues for TE.

Microcarriers offer physical support for cells to secrete ECM and develop *in vitro* microtissues which can be modulated as defect-filling materials, platforms for tissue characterization or for drug testing applications. In our study, we have determined the best parameters for the *in vitro* creation of cell-derived ECM-PLA microtissues. Biocompatible PLA microcarriers have been obtained following a green-solvent method in a coflowing fluid atomization process. Polydispersity in the PLA carriers found in our

experiments could add heterogeneity to our microtissues representing an advantage to better fit defects and adapt to injured sites.

Improving cell-adhesion properties of PLA MCs was necessary due to the lack of biological signals on their surface. Here, particles were exposed to 10, 30 and 60 min hydrolysis, and collagen type I recombinant protein was covalently bind through ECD/NHS solution. Confocal images demonstrated higher immunofluorescent signal corresponding to grafted collagen protein for the 60 min incubation. Previous investigations with PLA films reported a shorter hydrolysis incubation as optimal (30 min) and detrimental effects on longer periods due to the increment in roughness and subsequent steric hindrance of the attached proteins (Punet, 2013). Pseudo 3D environment displayed on PLA microcarriers may offer beneficial effect on overcoming steric hindrance of grafted proteins, thus allowing longer hydrolysis times than films. Microscopic images showed collapse of some particles and irregularity on its surface. Although hydrolysis modifies roughness on the surface of PLA films (Mateos-Timoneda, 2014), this fact could be herein observed for any incubation period suggesting it may be due to other steps in the processing of particles, such as the solidification in the aqueous bath or the freeze drying post-production step. 60 min hydrolysis was, from there on, used as the standard process for the first steps in PLA microcarrier functionalization.

Cell-derived microcarrier-assisted microtissue formation is based in the intrinsic capacity of cells in self-assembling during tissue development (Whitesides, 2002). Assembly of cells has been extensively used to study biological processes in oncology to evaluate drug efficacy and toxicity (Ishiguro, 2017; Perche, 2012); in stem cell biology for the production of specific cell lineages (Sart, 2014); and in tissue engineering with different approaches, both integrating biomaterials or not (Cesarz, 2015) (Gauvin, 2010), for the creation of functional tissues. Van Wezel *et al.* described that cells attached on microcarriers could join them together by cell bridging (VanWezel, 1967).

Static microtissue formation was conducted following three different formats: U-shaped 96-well plates, ideally considered for the high throughput manufacturing and restricted volume necessities; PDMS moulds that were considered to favour control over microtissue shape; and low-adhesion 24-well plates. Also, for each of the culture formats, three different seeding protocols were studied regarding cell/MC concentration: 25000 cells/mg MC chosen as control condition; then maintaining the same concentration, cells and MCs were added in two times in the same well, with the aim of facilitating cell-MC

encounters; and finally, doubling cell content (50000 cells/mg MC) increasing cell/bead ratio and favouring MCs cellular coverage.

Template assistance of cell-seeded microcarriers during macrotissue formation has been previously demonstrated in several occasions, using different moulds such as agar-based templates in form of tubular, disk and alphabetic letter-shaped (Wang, 2014), short tube agarose moulds (Twal, 2014), doll-shape PDMS moulds (Matsunaga, 2011), or silicon sandwich-like structures (Palmiero, 2010). In contrast with what we observed, all these strategies could easily form tissues in arbitrary shapes. Here the use of PDMS moulds did not resulted in the formation of microtissues. Instead, cells spread on PDMS and carriers were found randomly in the well, for all seeding protocols. Differences in which the success of this moulding method may rely, are found in the previous seeding of microcarriers using dynamic conditions. Matsunaga *et al.* reported the use of a doll-shape PDMS mould in which already cell-laden collagen beads were poured (Matsunaga, 2011). Also, Wang *et al.* used CultiSphere S microcarriers inoculated in spinner flask and cultured in agitation for 14 days prior to transference into a template-assisted perfusion chamber (Wang, 2014). Likewise, Palmiero *et al.* defined a strategy where dynamic cell-MC seeding was performed in spinner flask for up to 4 days before transferring into a silicon mould delimited by stainless steel rigid grids and incorporated into a perfused chamber to obtain dermal equivalent tissues (Palmiero, 2010). In our case, microcarriers were poured into the moulds and cells were later incorporated, thus cell-mould binding was also caused. Also, the use of grids or meshes would have facilitated the confinement of particles in the mould and so the formation of bigger constructs. Moreover, PDMS surface modification with Pluronic or chitosan could have also been used to prevent cell adhesion to PDMS moulds (Chambers, 2014).

The other investigated static formats, U96 and 24-well plates, were found feasible for the formation of microtissues. Differently to what we would expect, U96-format microtissues, which had 6 times less MCs and cells, occupied same area as the 24w-format MT, disregarding its volume and except for the two-times seeding protocol. Confinement of microcarriers in a reduced space is important for microtissue formation. Initially, cells attach to individual microcarriers but as they proliferate, they build bridges connecting them. The motivation behind the use of U-bottom shaped microwells was that they represented an ideal tool for agglutination of particles and cells, as well as they enabled high throughput microtissue manufacture (Chambers, 2014; Fennema, 2013; Futrega, 2015). Particles and cells were put together in each well and let for settling by

gravity in both formats U96 and 24w. In the case of U96 microwells, microtissues were less compact as they showed MC-free regions in between. SEM images corroborated lesser compactness and cohesiveness. ECM deposition was not abundant compared to 24w-microtissues, which did not show any MC-free regions in the middle of the constructs. U-shape configuration found in 96 well plates versus elongated V-shape found at the 24-well titled plates may have also contributed to the differences in microtissue production. Exact same ratio cell/MC was used adapted to the culture formats, and medium was exchanged previously to total nutrient consumption in all cases. However, U-shaped may have limited medium arrival to the aggregate. For 24 well plates, microcarriers firstly occupy half-moon shapes due to the inclination. In that position, extended cell-laden MC area is in contact with medium. As cell proliferation and ECM deposition occurs, cell contraction disposes MC in a rounded and more compacted shape. Contraction of cell-derived microtissues has been extensively reported due to forces exerted between cells and cell-ECM (Matsunaga, 2011; Rivron, 2012). Two-times seeding protocol in 24 well plates promoted significantly bigger microtissues compared to the control seeding condition and to U96 microwells. Although cell and microcarrier ratios were maintained in these two seeding protocols, seeding in two times might provide closer cell-particle encounter probably due to reduced medium volume. However, when studying this same protocol for U96 microwell format, bigger MT were not observed compared to control and doubled-concentration protocols. It has reported higher cell seeding efficiencies for low cell number and low seeding volumes (Leferink, 2016). Nonetheless, volume restriction is already small in 96 well plates, thus seeding in two times may not affect final MT formation. Moreover, during the 21 days of microtissue formation, 24 well plates offer more space and volume, permitting better exchange of medium and waste products, thus facilitating microtissue production. SEM images corroborated that all 24w microtissues were more consistent and abundant in ECM production and cell proliferation than U96 microtissues, disregarding seeding protocol. Therefore, 24-well plate formats yielded the best results in MT formation.

Generally, static seeding is described to be in detriment compared to dynamic seeding procedures yielding lower seeding efficiencies and poor cell distributions (Thibault, 2013). When seeding in static conditions, most of the cells stay close to the surface of the scaffold. Investigations seeding MCs in static conditions reported cell-MCs aggregation, but it did not lead to a 3D microtissues (Tseng, 2012). Declerq *et al.* however, used spinner flask bioreactor after static MC colonization for microtissue formation, where after 40 days in stirring aggregates of 0.55 – 2.6mm size were obtained (Declercq, 2013).

Agitated spinner flasks have been shown to improve cell distribution in microcarrier seeding as chances in cell-MC contact increase due to total microcarrier surface exposure. Also, agitation avoids the presence of concentration gradients which may delay or harm cell proliferation (Rafiq, 2016).

Parameters in microcarrier seeding using spinner flask bioreactor depend on the nature of the microcarrier and cell type, but also, they depend on the proper set-up of the bioreactor such as cell/MC concentration, serum content, agitation speed and regime. These parameters have been hereby studied in order to achieve a homogeneous and elevated MC colonization. Sample manipulation was initially based in detaching cells and separating them from the MC fraction through a cell strainer for further counting. However, this procedure was found to be challenging due to loss of cells and particles during handling. Instead, cell vital staining was done, and fluorescent images were taken to study MC colonization as defined above.

Intermittent agitation in spinner flask is nowadays widely used for MC cell seeding (Chen, 2011b; Chen, 2014; Mei, 2010; Twal, 2014; Wang, 2014). Improved attachment of MSCs using intermittent agitation was reported against continuous regime in Cultisphere S microcarriers (Yuan, 2014). When introducing agitation into the culture, cell-carrier random matching is favoured. Additionally, prolonged static intervals allow successful cell anchorage to the surface of the particle. Nonetheless, some authors have described similar efficiency results of synovial fluid MSC attaching to Cytodex 3 microcarriers when using continuous and intermittent agitation (Jorgenson, 2018). This discrepancy may be explained by the particular behaviour of every cell type against a specific microcarrier. In our work, two agitation regimes were studied (3 min or 15 min), both followed by the same static period of 27 min. The shortest agitation yielded best MC colonization reaching 94,4% of MCs with three or more cells attached on them, compared to only 43,3% in 15 min agitation. Although the time for settling, where cells have the opportunity to bind to microcarriers, was the same for both regimes, prolonged agitation periods after all may cause cells to detach or weaken cell-particle bindings. Also, for the 15 min agitation condition, increased number of cell clustering was observed, due to a more consistent cell-cell binding instead of cell-MC.

The presence of serum in culture medium is bound to concerns for the clinical use of *in vitro* produced cells. Therefore, cell expansion on MCs has been studied in serum-free conditions. However, we have observed that total deprivation of FBS lowered 30% of PLA MCs colonization. Contrarily, Yuan *et al.* reported increased attachment efficiency

on gelatine-based microcarriers in the absence of serum (Yuan, 2014), whereas Jorgenson *et al.* found no improvement when subtracting serum using dextran beads coated with denatured porcine-skin collagen in the inoculation phase, although it was accompanied by a prolonged lag phase (Jorgenson, 2018). Serum proteins, such as fibronectin, adsorb to the surface of microcarriers favouring cell attachment, which may have been our case. MCs of different origins present different abilities in the adsorption of serum proteins. Gelatine-based microcarriers, such as Cultisphere S, attract fibronectin (Brew, 1994), whereas Cytodex-1 and Cytopore-2 adsorbed majorly albumin (Mukhopadhyay, 1993), a non-adhesive molecule disfavouring cell binding. In the case of PLA, albumin unspecific adsorption is not able to displace covalently attached proteins such as fibronectin (Punet, 2013), and so we hypothesis that neither it does with covalent collagen. However, we decided to work with normal FBS concentration due to enhanced MC colonization.

Cell/MCs ratio is another parameter under study for spinner flask culture. To ensure all MCs are at least colonized by one or more cells, a cell/bead ratio higher than 1 is needed. On the other hand, when reaching a high cell/bead ratio, more cell-cell encounters are provoked causing unwilling cellular aggregates. Finding the appropriate ratio relays on the MC size and the available surface area. For instance, Cultisphere S microcarriers which present macroporous cavities where cells can attach internally (15000 cm2/g, 130-380µm), showed no differences in cell attachment between 5:1, 9:1, 60:1 cell:bead ratios (Yuan, 2014). Meanwhile, for smaller particles and continuous surfaces, such as our PLA microcarriers (2000 cm2/g), a ratio higher than 10 cells/bead was found to yield significant lower MC colonization, and more cell-cell aggregates were observed.

Prolonged agitated spinner flask culture was not able to support cell proliferation by our PLA microcarriers, as seen by the lowered MC colonization rates observed after 48h. We have demonstrated that by choosing the correct parameters, cell-MC binding could be favoured, however, prolonged agitated culture may provoke cell detachment from PLA microcarriers and therefore hinder cell proliferation. Spinner flask here was only introduced for homogeneous MCs colonization, whereas further ECM-deposition and microtissue production was followed in static conditions. Likewise, other researchers used spinner flask for particle colonization during 3 and 4 weeks respectively, prior to MT formation under perfusion (Chen, 2011b; Mei, 2010). Porous microcarriers have been successfully used for cell proliferation, offering shelter to cells against bioreactor agitation (Eibes, 2010). With that aim, the use of porogens in the fabrication of PLA microcarriers could be implemented. Camphene (Jin, 2014), calcium carbonate (Cheng,

2013), and other ethyl lactate insoluble salts, such as sodium chloride, glucose, sucrose, or calcium chloride could be used as candidates for the development of porous PLA MCs in future studies.

Comparing microtissues obtained after spinner flask colonization with the ones obtained under the best static conditions, *i.e.* 24w plates, similar MT were observed. The size of both MT was comparable (from 6 – 17.5mm2 and 7.6 – 16.1mm2, respectively), and ECM cell deposition was achieved both externally and in the inner space of MT. Two-times seeding procedure in static conditions and spinner flask agitation during MC inoculation allowed good colonization of particles and thus, cell bridging permitted encompassing of all the available microcarriers in the well. However, spinner flask colonization protocol presented superior benefits in terms of handling and automatization. Individually disposal of particles and cells into each 24-well for the static seeding, performed twice, became labour intensive, impractical for the technician and it increased variabilities in the manufacturing process. Therefore, the introduction of an agitated spinner flask for MC inoculation represented a more reproducible and scalable method for microtissue formation. Also, the number of microtissues obtained after spinner flask was substantially higher than by static means. Although transferring from spinner flask to 24 well plates was also performed manually, automatic liquid handling and dispensing pipettes can be easily adapted into laboratory daily use, reducing variability in MT formation.

3.5 Conclusions

In this work, we have defined the most appropriate MC colonization procedure for the formation of cell-derived PLA MCs microtissues. After improving biofunctionalization of MC surface, different MC cell seeding techniques were investigated. From the three different static procedures investigated (96w plates, PDMS moulds and 24w plates), we conclude that the use of non-adherent 24 well plates yielded microtissues with a better structure due to a more abundant ECM deposition and cell proliferation. Also, static seeding in two times for this same format generated bigger scaffolds. Parameters for MC colonization were set to: 3-minute agitation regime in between with 27 min in static, 10% FBS medium content and 8.3 cells/MC ratio, which stands for 10.000.000 cells for 100 mg MCs, as these yielded best results. Microtissues obtained from dynamic seeding, were homogeneously colonized and good cell proliferation and ECM deposition was observed. Comparing microtissues obtained by means of static and dynamic conditions, we can

conclude that using spinner flask bioreactor for MC colonization followed by static cell proliferation and ECM deposition, represents the best procedure for the generation of modules as first step in a modular tissue engineering approach.

Chapter 4

Cell-derived extracellular matrix scaffolds: microcarrier choice influences ECM deposition and functionality

4.1 Introduction

Organ shortage for transplantation has stimulated the development of new approaches in tissue engineering like the use of extracellular matrices as scaffolds. The extracellular matrix (ECM) is a complex network secreted by resident cells that gives structural support, but also regulates cellular functions such as proliferation, migration, differentiation and tissue homeostasis. It mediates cell-cell and cell-matrix communications and acts as reservoir of signalling molecules (Frantz, 2010). ECM is specific for each tissue type and is being constantly remodelled depending on the tissue state (injured, diseased, age, development) (Badylak, 2009). ECM matrices for tissue engineering can be obtained from native tissues or organs, harvested from the same patient, other species or cadaveric donors (Ott, 2008) and by different processes of decellularization, cells are removed maintaining the structure and composition (Bourgine, 2013; Gilbert, 2006). This strategy can provide complex organ-like structures, that otherwise would be very difficult to mimic *in vitro*. Moreover, they hold abundant biological signals for the subsequent reseeding cells and degrade into compatible substances (Badylak, 2009). However, risks of inflammatory and immunological reactions exist (Badylak, 2008; Cheng, 2014), as well as potential hazard of pathogen and disease transmission (Tomford, 1995).

The alternative to harvested native tissues is the *in vitro* production of ECM secreted by cultured cells, under pathogen-free conditions presenting more customizable features. Adequate recreation of *in vivo* environments in controlled *in vitro* conditions allows the generation of functional microtissues for the repair of injured tissues. Autologous cell-derived ECM can be designed in personalized strategies for the replacement and repair of impaired tissues (Lu, 2011a) or for the delivery of therapeutic cells. ECM microtissues enhance cellular adhesion and consequently cellular retention and integration compared to single delivered cells, becoming attractive for the application in cell-based therapies (Kelm, 2012). Additionally, cell-derived ECM can serve as platforms to aid in the phenotype maintenance (Sellaro, 2007) by mimicking the niches of stem cells to keep stemness phenotype otherwise lost upon traditional culture (Chen, 2007b; Lai, 2010). Cell-derived ECM can become models to study healthy and disease development but also, they can be applied for pharmaceutical purposes in diagnosis and drug screening (Quiros, 2008).

Cell-derived ECM scaffolds can be easily obtained from cells cultured as monolayers in 2D systems (Chen, 2007b; Fercana, 2017; Lai, 2010; Tang, 2013). Studies showed improved osteogenic responses when cells were reseeded, as well as delayed spontaneous commitment of MSC (Chen, 2007b; Lai, 2010). However, this approach holds limited capacity for mimicking the native 3D structure of ECM. For that reason, the use of biomaterials to instruct specific 3D configurations is of upmost importance. Moreover, increased cell-cell and cell-matrix interactions, that accompany 3D cell growth, exert different patterns on ECM expression compared to monolayer cultures (Daley, 2008; Hakkinen, 2011). Innumerable biomaterials have been used to produce cell-derived ECMs *in vitro*: collagen fibers (Cheng, 2009), titanium fiber mesh dishes (Datta, 2006; Pham, 2008), electrospun poly(ε-caprolactone) (PCL) microfibers (Liao, 2010), beta-tricalcium phosphate (Kang, 2012) and PLGA mesh dishes (Lu, 2011b) among others.

The use of microcarriers for the generation cell-derived ECM scaffolds holds great promise in TE. Used in modular approaches for the production of small functional subunits, they can be assembled to generate viable and clinically relevant constructs (Chen, 2011b; Luo, 2014). Microcarriers are valuable during all steps of a TE approach, from cellular expansion (Badenes, 2016; Eibes, 2010; Frauenschuh, 2007; Schop, 2010; Tan, 2016), through the formation of the functional modular units (Declercq, 2013; Dikina, 2015; Khan, 2015; Lu, 2011a; McGuigan, 2007c; Palmiero, 2010; Peticone, 2017), to the assembling of these in the formation bigger constructs for the final *in vivo*

implantation (Chen, 2014; Kou, 2016; Luo, 2014; Matsunaga, 2011; Mei, 2010; Wang, 2014). The election of the correct microcarrier has been previously studied in terms of cellular adhesion and expansion yields (Chen, 2011a; Frauenschuh, 2007; Rafiq, 2016; Sart, 2010; Yang, 2007). However, and to the best of our knowledge, there are no studies comparing the formation of modular units by the same procedure using different microcarriers. Properties of microtissues prepared with our custom-made PLA MCs, commercially available Cultisphere-S and a mixture of both MC types were herein explored. Characterization was performed for microtissues under normal growth medium where the capability to maintain undifferentiated phenotype was evaluated, as well as their angiogenic potential. Osteogenic phenotype was then induced, and cell response was assessed. We found that Cultisphere S microtissues enhanced spontaneous osteogenic differentiation by the end of the culture, and moreover, they increased and potentiated osteogenic response after induction. PLA and Mixed microtissues presented undifferentiated phenotypes but were not able to sustain osteogenic promotion even with inducers. On the other hand, Mixed microtissues presented elevated angiogenic potential in an *in vivo* model, together with increased Stromal derived factor-1α (SDF-1α) secretion favouring the cell-homing effect of microtissues.

4.2 Materials and methods

4.2.1 Cell culture and expansion

Bone marrow derived mesenchymal stem cells (MSCs) from Lewis rats were obtained and cultured as previously described in Chapter 3, section 3.2.1.

4.2.2 Microcarrier preparation

Polylactic acid microcarriers were prepared following the same jet-break up/solvent evaporation procedure as used in Chapter 3, section 3.2.2. Also, as previously stated human collagen type I recombinant protein (Advanced Biomatrix; San Diego, CA) was covalently link to its surface with the help of the zero length cross linkers, EDC/NHS carbodiimides. Prior to its use in cell culture, microcarriers were resuspended and sterilized in 70% ethanol aqueous solution (O/N agitation). Then, three repeated rinsing steps were performed with PBS in sterile conditions; centrifuging 800g for 5 min. MCs were pre-incubated with culture medium at 37ºC for 30 min.

Cultisphere-S gelatine microcarriers were obtained from Percell Biolytica (Astorp, Sweden). With a diameter ranging from 130 to 380 μm they present both superficial and internal porous, with and average pore diameter of 20 μm. Prior to cell culture, sterilization was performed following manufacturer's instructions. First, dry microcarriers were hydrated in calcium and magnesium free PBS (50 ml/g) for 1 h at room temperature, proceeding to autoclaving. PBS was substituted by culture medium and MCs were incubated at 37ºC, for 30 min prior to its use.

4.2.3 Microtissue fabrication

Microtissues were prepared using PLA microcarriers (PLA MT), Cultisphere S microcarriers (CultiS MT), and a combination of both PLA and Cultisphere-S microcarriers (1:1) (Mixed MT). For all three different MTs, fabrication procedure consisted in the same two steps: MC colonization in spinner flask followed by MT formation in static.

Microcarrier Colonization in Spinner Flask Bioreactor. Cells were harvested from T175 flasks (Nunclon) and resuspended in 100 ml culture medium. Ten million rMSCs were introduced together with 100 mg MCs, PLA or Cultisphere-S MCs, in a 250 ml spinner flask bioreactor, with 100 ml medium (Glass ball impeller; Bellco Glass, USA). For the Mixed condition, 50 mg PLA MCs and 50 mg Cultisphere S were added to the spinner flask. Bioreactor's stirring regime followed an intermittent pattern of 3 min with 30 rpm agitation, and 27 min with no agitation. Inoculation phase was maintained for 6 hours. Two 1 ml samples were taken from the bioreactor and vital staining with calcein was used to assess colonization rates.

Static Microtissue Formation. After 6h of intermittent agitation, colonized microcarriers were transferred into non-adherent 24 well plates (Falcon), 3 mg MCs/well. Once placed in the incubator, culture plates were titled 30º, to accumulate MCs in one side. Normal culture medium (advanced DMEM, 10% FBS, 1% step/pen) was carefully replaced every 2-3 days, avoiding microparticle agitation. Microtissue samples were collected after 1, 7, 14, 21 days of culture and proceeded for further assays.

4.2.4 Vital staining and MC colonization rate

Cell-laden microcarriers taken after inoculation phase from the bioreactor were rinsed with PBS and incubated for 15 min, 37ºC, with 2 μM Calcein-AM in Dulbecco's

Phosphate-Buffered Saline (DPBS) (Thermo Fisher, Spain). Fluorescent images were taken using E600 Leica microscope.

Microcarrier colonization rate was defined as the number of MCs with three or more cells attached on them, divided by the total amount of microcarriers, as seen in Chapter 3, section 3.2.7.

4.2.5 Osteogenic induction

Cultisphere-S and Mixed microtissues were subjected to osteogenic induction. For that aim, microtissue formation under normal conditions was performed for 7 days, including MC colonization in the spinner flask. After that, osteogenic medium consisting in 10^{-8} M dexamethasone, 10 mM β-glycerophosphate and 50 mM L-ascorbic 2-phosphate trisodium salt was used (all from Sigma). Medium was changed every 2 to 3 days, maintaining the osteogenic induction for 21 days, achieving a 28-day culture.

4.2.6 Cell proliferation assessed by Picogreen dsDNA assay kit

Cell increase in microtissues was evaluated by quantifying total DNA using Quant-IT Picogreen double-stranded DNA (dsDNA) assay kit (Invitrogen). Microtissues were collected at days 1, 7, 14 and 21 (and 28 days for the osteogenic induced MTs) and washed with PBS. Tris-EDTA (TE) buffer found in the assay kit, was diluted in DNase/RNase free Milli-Q water and used for freezing microtissue samples. Three freeze-thaw cycles were performed, freezing at -80ºC and thawing at room temperature. Microtissues were disrupted by both sonicating for 10s in ice and using micro-tube adapted pestles. Samples were centrifuged to remove MCs (5 min, 4000 g, 4ºC). Following manufacturer's instructions, samples were incubated with Quant-IT Picogreen reagent solution for 5 min at RT in the dark. Fluorescence was measured at 480/520 nm (excitation/emission) wavelengths, using a spectrophotometer plate reader (Infinite M200 PRO, Tecan). Calf thymus DNA solution was used as standard for DNA quantification.

4.2.7 Total protein quantification

BCA™ Protein Assay kit (Pierce, Thermo Scientific) was used to quantify total protein from the microtissues. Samples were collected at 1, 7, 14, 21 days and were homogenized. Supernatant was collected and used following manufacturer's protocol. In short,

homogenized samples were mixed with working reagent, and incubated at 37ºC for 30 minutes. Absorbance was measured at 562 nm using Infinite M200 PRO plate reader. Diluted albumin standards were used as calibration curve.

4.2.8 Scanning electron microscopy (SEM)

Scanning electron microscope (NOVA NanoSEM 230, FEI Company) was used to evaluate microtissue morphology: secreted ECM, cell distribution and MC inclusion in the microtissue. Samples were taken at different time points (7, 14, 21 days), and fixed with 4% paraformaldehyde (PFA) 10 min at 4ºC. After two PBS washes, microtissues were dehydrated in an increasing alcohol gradient before performing Critical Point Drying at the CCiTUB (University of Barcelona). Then, samples were carbon sputtered prior to SEM examination.

4.2.9 Immunofluorescent analysis of MT

Protein assessment of the ECM components in the different microtissues was examined by immunofluorescent analysis. Microtissues were collected after 21 days in culture and fixed in 4% PFA. Samples were then immersed in three different sucrose solutions (5%, 10% and 30% w/v) until they sunk. MT were further embedded in Tissue-Tek® O.C.T. Compound (Sakura® Finetek, VWR), and put in the -20ºC freezer for 3 hours, and then into -80ºC freezer for at least 24 hours. Cryosectioning was performed using Leica CM3050 S Research Cryostat (CCITUB). Three to five 25-µm thick MT sections were cut and displaced in SuperFrost Plus™ Adhesion slides (Thermo Scientific). These sections were kept in the freezer until imaging.

Prior to immunofluorescent incubation, slides were thaw and O.C.T was carefully removed. Permeabilization with 0,1% Triton (Sigma) in PBS-glycine (BioUltra, Fluka) was induced for 10 minutes. A blocking solution composed of 1% bovine serum albumin (BSA) and 10% goat serum in PBS-Glycine was used for 30 min. Overnight incubation with primary antibody solution (1/500 diluted in blocking solution) was followed at 4ºC (*Table 4.1*). Listing all primary and secondary antibodies used in this assay). Next day, slides were washed with PBS-glycine and secondary antibody was applied for 1 hour at RT, at dark (1/1000 dilution). Three intensive PBS-glycine washings were applied prior to 30-min, RT, dark, anti-actin staining. Phalloidin Rhodamine 574 nm (Cytoskeleton) was used at a concentration of 100nM. Nuclei staining with DAPI 1µg/ml was sustained

for 1 min. Finally, excess was removed, and PBS-glycine was used to wash slides, three times. Vectashield® Antifade Mounting Medium (Vectorlabs) was applied to seal with coverslips. Immunofluorescence images were taken with Zeiss LSM780 confocal microscope, at the IBMB-CSIC Molecular Imaging Platform.

Table 4.1 List of antibodies used in the immunofluorescent analysis.

Primary antibodies			Secondary antibodies		
Reactivity against	**Host**	**Reference**	**Reactivity against**	**Host**	**Reference**
Collagen I	Mouse	ab6308	Mouse	Goat	ab150117
Collagen II	Rabbit	ab34712	Rabbit	Goat	ab150081
Collagen III	Rabbit	ab7778			
Collagen IV	Rabbit	ab6586			
Fibronectin	Rabbit	ab2413			

Reference number from Abcam catalogue.

4.2.10 Analysis of alkaline phosphatase (ALP) activity

SensoLyte® pNPP colorimetric Kit (AnaSpec Inc, USA) was used to determine alkaline phosphatase enzymatic activity. Microtissues were firstly rinsed with PBS and then collected with assay buffer containing Triton X100 as established in the manufacturer's protocol. Micro-tube adapted pestles were used for manual homogenization. Samples were then centrifuged (15 min at 10000x g at 4ºC) and supernatant containing alkaline phosphatase was directly used for the enzymatic reaction with substrate solution in a 96-well plate. After 30 min incubation, absorbance was read at 405 nm using Infinite M200 PRO plate reader. Sample results were compared with ALP standard dilutions.

4.2.11 Glycosaminoglycan quantification

Blyscan™ Glycosaminoglycan Assay (Biocolor, UK) was used to quantitatively analyse sulphated proteoglycans and glycosaminoglycans (sGAG) in the different microtissues. First, sGAG were extracted from dried MTs using papain enzyme from papaya latex. Papain and all the reagents for the papain extraction solution were purchased from Sigma-Aldrich, unless otherwise specified. Papain extraction solution at a concentration of 4.76 nM was prepared in 0.2 M sodium phosphate buffer with 97.5 mM sodium acetate, 13.69 mM EDTA and 5 mM L-cysteine hydrochloride. Digestion was performed for 3 hours at 65ºC. Then, samples were centrifuged (10.000 g, 10 min) and 50 µl of supernatant plus 50 µl MilliQ water were transferred into 1.5 ml microtubes. Each condition was examined in triplicates. 1 ml of Blyscan dye reagent was added to each microtube, which were gently shaken for 30 min. In that step, sGAG-dye complexes

formed and precipitated. Tubes were centrifuged at 12000 rpm for 10 min, supernatant was discarded by carefully inverting and draining tubes. Pellet was dissolved adding 0.5 ml dissociation reagent and by vigorously agitation. Centrifugation at 12000 rpm, 5 min, removed foaming. 200 µl of each sample were transferred into a 96 micro well plate and absorbance was read using 656 nm filter. S-glycosaminoglycan concentrations were obtained using standard curve.

4.2.12 Real Time PCR

Microtissues were washed with PBS and collected after 1 and 21 days of culture for gene expression analysis. RNA extraction and purification were done using RNeasy® Plus Mini kit (Qiagen). Briefly, buffer RLT with β-mercaptoethanol were added to the samples and immediately froze (-80ºC). Prior to use, samples were thaw in a water bath at 37ºC and microtissues were homogenized using micro-tube adapted pestle. Also, QIAshredder columns (Qiagen) were used to homogenize samples and remove carriers. Next, gDNA eliminator columns removed genomic DNA. Several washing and centrifugation steps together with the RNeasy columns allowed RNA extraction in RNase-free water. Extracted RNA (0.5 µg) was used for cDNA synthesis using RT2 First Strand kit (Qiagen). Then gene amplification was performed in a StepOne Plus Real-time PCR system (Applied Systems) machine, using SYBR Green Mastermix (Qiagen) with the following primers, all from Qiagen: *Col1a1* (PPR42922A), *Col4a2* (PPR42703A), *Alp* (PPR52402A), *Runx2* (PPR53039B) and *Act* (PPR52391B). Cycling conditions were set as follows:

Table 4.2 RT-PCR programme for StepOne Plus Real-Time System.

Cycles	Duration	Temperature
1	10 min	95ºC
40	15 s	95ºC
	1 min	60ºC

Gene expression was normalized to *Actin* expression for each condition and relative amounts of RNA of each gene were expressed as fold increase calculated using the 2-AACT method. No RT- and no template controls were included on every plate.

4.2.13 Stromal derived factor-1α ELISA

SDF-1α expression in cell culture supernatant was evaluated by a Sandwich-ELISA kit (Elabscience) at days 1, 7, 14 and 21. Samples were centrifuged during 20 min at 1000 g at 2-8ºC to remove debris and insoluble particulate. Then, following manufacturer's directions, ½ diluted samples, standards and blank were added into the wells in the ELISA plate and incubated for 90 min at 37ºC. Next, detection biotinylated antibody solution was added to specifically bind to SDF-1α molecules in the samples. Further washings and conjugated Avidin-Horseradish Peroxidase (HRP) antibodies were introduced. Complexes created by Avidin-HRP antibody bound to biotinylated antibody, immobilized by SDF-1α interaction, will turn substrate reagent into measurable colour. Infinite M200 PRO plate reader spectrophotometer was used to detect optical density at 450 nm wavelength.

4.2.14 Chick chorioallantoic membrane (CAM) assay

CAM assay was used to study angiogenic potential of the cell-derived ECM scaffolds. Shell-less cultured ex ovo models were adapted from a previously described protocol (Deryugina, 2008), using collagen onplants. Fertilised chicken eggs were purchased from a local farm (Granja Gibert SA, Spain) and upon arrival they were horizontally placed in a humidified incubator at 37ºC. After 3 days, egg shell was aseptically and carefully cracked, transferring embryos into sterile petri dishes (15cm ∅). Embryos were kept back in the incubator for 6 days. On the ninth day of development, PLA, Mixed and Cultisphere-S microtissues formed after 14 days of culture, were prepared for implantation. Briefly, scaffolds were decellularized incubating for 30 min in 1% Triton X-100 in a 0.1% ammonium hydroxide (NH_4OH) solution. Also, a DNase I treatment was later applied (30 µg/ml) for 30 min at 37ºC.

Onplant preparation was carried out in sterile conditions using a parafilm-covered petri dish. Each of them consisted in a single 6mm circle nylon mesh (180µm, Merk Millipore) which guided onplant CAM position over time. Decellularized microtissues were carefully placed on top of nylon meshes, and they were embedded in rat tail collagen type I solution (Opticol, Cell Guidance Systems). Iced-cooled neutralized collagen is pre-mixed as stated by the manufacturer, and 30 µl of solution were prepared for each onplant. As negative control condition, polycaprolactone (PCL) irregular macroparticle (same macroscopic size as sample MTs) were used to simulate 3D microstructure. And as

positive control condition, 200 ng vascular endothelial growth factor (VEGF) were added into collagen embedding solution into PCL macroparticle onplants. Onplants were let to polymerize in a 37ºC incubator for 30-45 min. For the implantation, there were placed in areas containing fine vessels, avoiding large blood vessels. Five onplants were used per embryo and 6 to 10 eggs were used for each individual condition. After 3 more days of incubation, embryos were sacrificed by decapitation and 10% formalin solution was used to fix the CAM for 20-30 min. Subsequently, scaffolds and their surrounding CAM (1 cm around) were excised and images were taken with an Olympus MVX10 Macroscope (IRB Microscopy Facility, Barcelona). Angiogenic potential of microtissues was quantitatively measured by determining vascular density in microtissues. FIJI software was used following the script described in Annex 1.

4.2.15 Statistical analysis

Results were statistically analysed using GraphPad Prism 6 and expressed as mean and standard deviation of the replicates (n=3, unless otherwise stated). One or Two-way Analysis of Variance (ANOVA) were used. For each assay being analysed, the type of ANOVA is stated in results. Multiple comparisons test was performed using Tukey's tests. Significance level of $p < 0.05$ was selected.

4.3 Results

4.3.1 Microtissue fabrication using PLA, Cultisphere S and a mixture of both microcarriers

Microtissue formation was performed identically for the three conditions: PLA, Cultisphere S and Mixed microcarriers. First, rMSCs (10^4 cells/mg MPs) were seeded onto the microcarriers in spinner flaks bioreactors for 6 hours of intermittent agitation (3 min 30 rpm, 27 min 0 rpm). Calcein-AM vital staining showed cellular MC colonization. A complete colonization was only observed when using Cultisphere S (Figure 4.1), corroborating the characteristic well-performance of gelatine microcarrier in cell adhesion (Mei, 2010; Sart, 2013; Yuan, 2014). PLA microcarriers yielded a 70,07% of colonization, whereas by mixing both MCs types this was 80,71%. Although collagen covalent coating was enhanced in PLA MCs in our previous study (Chapter 3), it was not enough to perform a complete cell colonization here. Nevertheless, PLA MCs

performance was not decreased in the mixed condition even if the bigger carriers (Cultisphere S) provided 7.5 times more available surface than that of PLA MCs. For that reason, surface covalent functionalization of PLA microcarriers was considered successful. Importantly, cell clustering was avoided for all conditions, as individual cell attachment was achieved for all microcarriers.

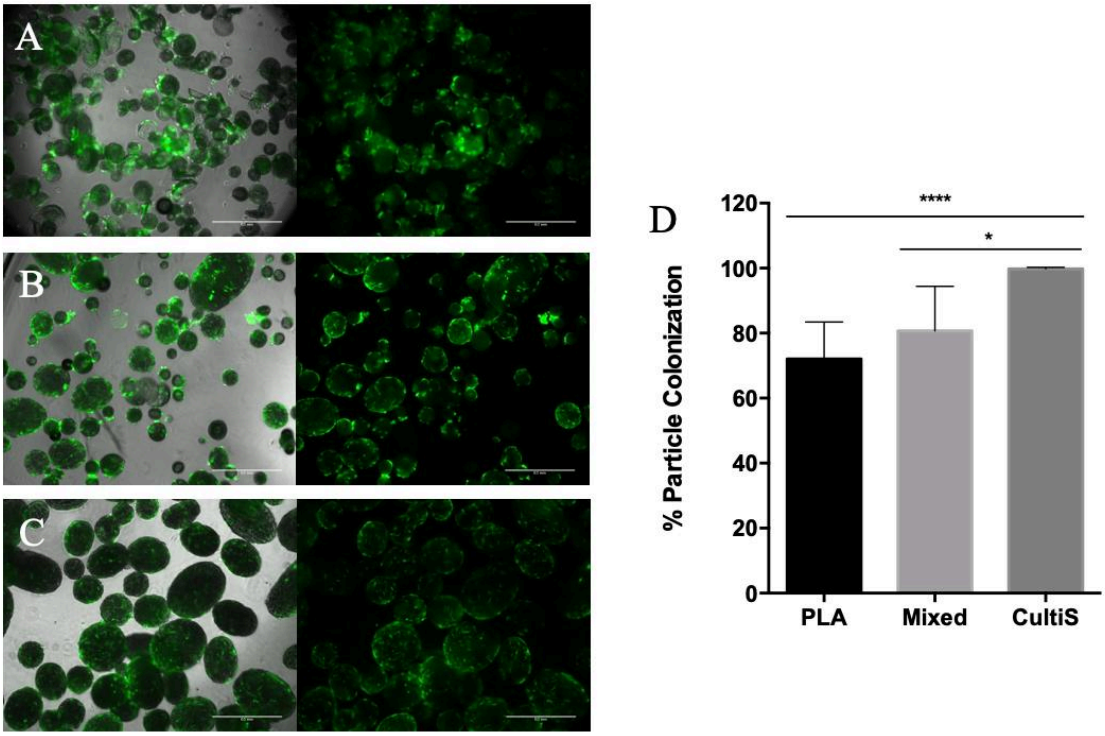

Figure 4.1 Fluorescent microscope images of calcein-AM vital staining of colonized microcarriers, after 6h of intermittent agitation in spinner flask bioreactor. (A) PLA MCs, (B) Mixed MCs 1:1 Cultisphere S and PLA, and (C) Cultisphere S MCs. (D) Percentage of particles being colonized by three or more cells for each of the spinner flask: 72,07% MC colonization for PLA, 80,71% for Mixed MCs and 99,8% for CultiS. *P value ≤ 0.05; ** P value ≤ 0.01; **** P value ≤ 0.0001. At least 4 images were taken for each spinner flask condition, and n=5 spinner flask were used for each condition.

After cell seeding, colonized MCs were transferred into static 24-well plates. These were kept in a 30ºC titled position and medium was changed every two to three days, leaving microcarriers and cells undisturbed. Normal growth medium was used for 21 days for the fabrication of modular microtissues. For all conditions, microtissue structures were already observable within the first week of culture. As shown in *Figure 4.2*, A, cellular proliferation was monitored by quantifying total DNA present in the samples at each time point. Results showed that Mixed microtissues significantly supported cell proliferation and almost doubled DNA amount after 14 and 21 days of culture (1.95 and 1.89 times, respectively) compared to day 1. Cultisphere S microtissues increased 1.38 times cellular DNA content during the first 7 days although it stayed constant for the rest

of the culture (1.38 and 1.47, at days 14 and 21 respectively). rMSCs population in PLA microtissues faced a lag phase without proliferation, however, proliferation was then observed for the following days. These results suggest initial cellular loss in PLA microtissues. Compared to the other two conditions, DNA was lower for all time points.

Protein secretion was also followed during the microtissue formation process as seen in *Figure 4.2*, B. Deposited protein was quantitatively evaluated, normalized by the total amount of DNA and finally expressed against day 1. Cultisphere and Mixed microtissues showed initial decrease in protein deposition, given by the increase in cell proliferation. Whereas in the case of the PLA MT, deposition increased for the first 7 days, because of cellular loss. Cells in PLA microcarriers were able to generate constructs for the first week because protein deposition made up for the limited cell proliferation. During the last week Mixed and Cultisphere MT increased protein deposition. Generally observed for all microtissue types, microcarriers were included in half-moon-shaped MT. As time progressed, microtissues experienced contraction from half-moon shapes to rounded or irregular shaped constructs (*Figure 4.2*, C).

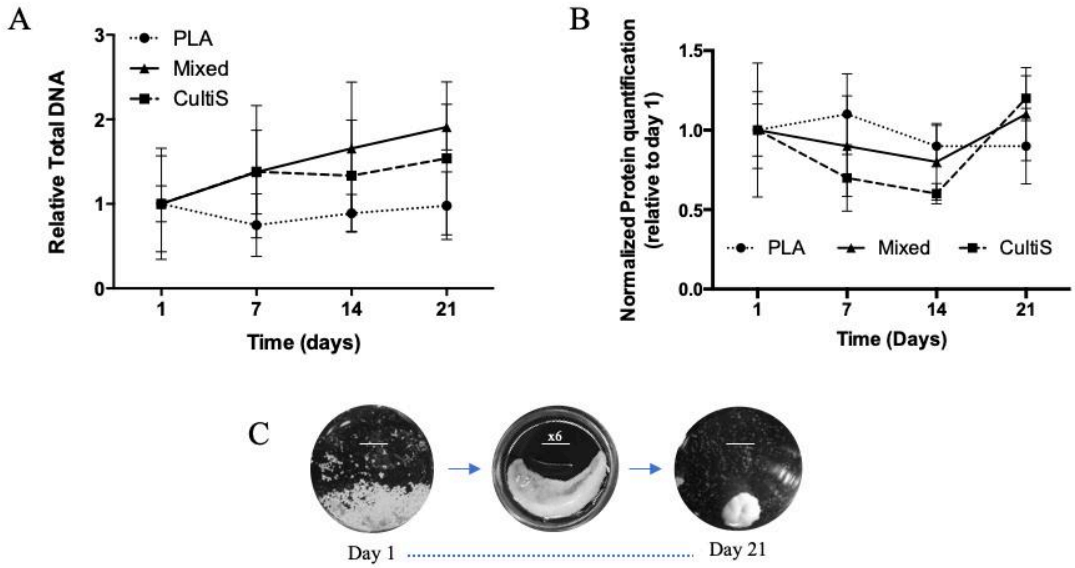

Figure 4.2 DNA and protein content characterization of MTs. (A) Total DNA quantification displayed relative to day 1 of each condition, for PLA, Mixed and Cultisphere microtissues. N=3, Two-way ANOVA was performed with Tukey's multiple comparison test, and no significant differences were observed. (B) Relative protein secretion against day 1 and normalized by the amount of total DNA. N=3, two-way Anova with Tukey's multiple comparisons test was performed. (C) Microtissue progression during static culture in 24 well plates (Image in the middle was taken placing the MT in a 96-well plate). PLA microtissue is pictured here: initially individual carriers were concentrated in a tilted culture plate, and progressively, half-moon shaped constructs were formed (around days 5-14). Towards the end of the culture period, constructs contracted forming rounded or irregular shapes. This happened for all microtissue types.

Complementarily, SEM micrographs were taken to observe ECM deposition (*Figure 4.3*). After 7 days, microtissue structures were found for all conditions. On PLA MT, MCs were observable even until the finalization of the cultivation process. Some of them remained partially uncovered, although they were able to resist post-cultivation sample manipulation, suggesting tight union into the secreted protein matrix. Consistently with proliferation and protein quantitative results, no substantial changes were observed on PLA MT surface from day 7 till the end of the culture. However, and contradictorily to quantitatively measurements, a construct was formed, suggesting that cells, although did not proliferate neither secrete higher amounts of proteins, were able to interact and bridge between carriers, forming a construct. In Mixed and Cultisphere S MT, carriers were still observable after 14 days. This phenomenon changed for the last time point, were ECM deposition and cell proliferation formed a dense layer covering and gathering all particles together, mostly concealing their presence.

Greater magnifications on SEM micrographs (*Figure 4.3*), focusing on the surface of MTs manifested different cellular morphology and disposition between different MT type. Cells on CultiS MT maintained their individual integrity, with marked cell limits and voluminous cytoplasm, in a cobblestone morphology. However, cells on Mixed and PLA MT were randomly organized, and no individual cellular limits were discerned suggesting closer contact between cells as well as cell immersion within the extracellular network. Some areas on the surface of these constructs were completely smooth, making cell identification impossible. Whereas for Cultisphere MT, rougher surface and extensive filopodia was observed. Further cellular morphology was observed by immunofluorescent images taken by a confocal microscope. A clearly distinctive trait was found for cells on Cultisphere S microcarriers.

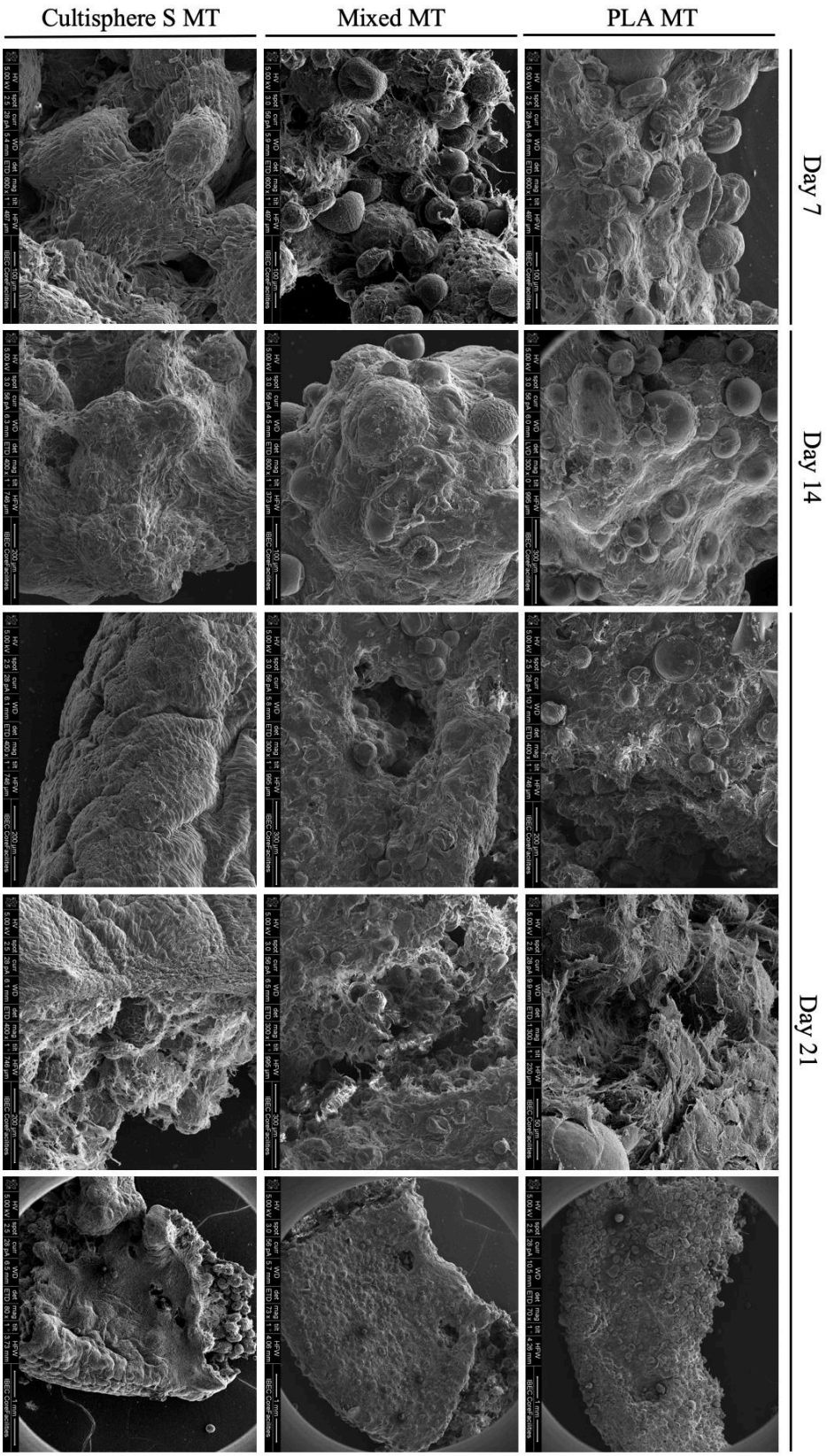

Figure 4.3 SEM micrographs of PLA, Mixed and Cultisphere S MTs at days 7, 14 and 21. At day 21, surface, interior and large view of MT are shown. On PLA microtissues, carriers were still observable at the surface even after 21 days of culture. For the other two conditions, MCs were concealed by day 21. Images at closer magnifications show how a dense ECM layer is gathering particles, and although there is ECM deposited in the inside, protein density is much lower and more fibrillar.

Actin filaments stained by phalloidin rhodamine, showed irregular and spindle-shaped cells on the surface and inside of CultiS MCs (arrowheads on *Figure 4.4*). However, when cellular bridging was formed between carriers and cells proliferated over the cell-deposited matrix, normal elongated and spread cytoskeleton was found. Moreover, cytoplasmic collagen I expression further confirmed this. Cultisphere microcarriers on Mixed microtissues were easily identified due to this specific cell morphology (*Figure 4.4* and *Figure 4.5*). Spread cytoskeleton was observed on cells cultured on PLA microcarriers surrounding individual particles and bridging others (*Figure 4.5*). PLA microcarriers clearly showed strong cell attachment as stress fibers clearly appeared after actin organization. Contrarily, irregular shaped cells and cortical actin accumulation were observed on cells present directly on Cultisphere S microcarriers. Additionally, expanded stress actin presenting cells appeared only in cells or deposited ECM bridging between carriers.

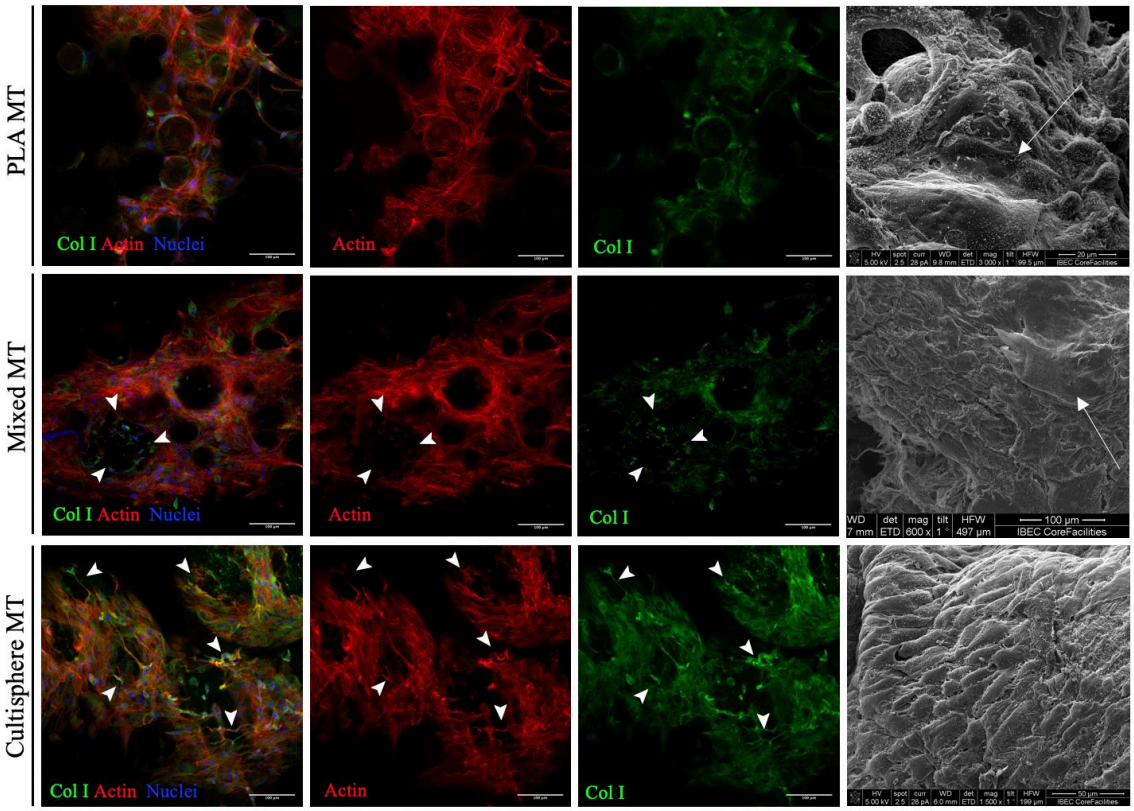

Figure 4.4 Cell morphology evaluation on MTs after 21 days of formation. Immunofluorescent images were taken using a Zeiss confocal microscope in hole microtissues. Arrowheads point to irregular and spindle-shaped cells found on the surface and inside Cultisphere S MCs. SEM images (column on the right) show microtissue surface. White arrows point to smooth areas where cell individual integrity is not possible to discern.

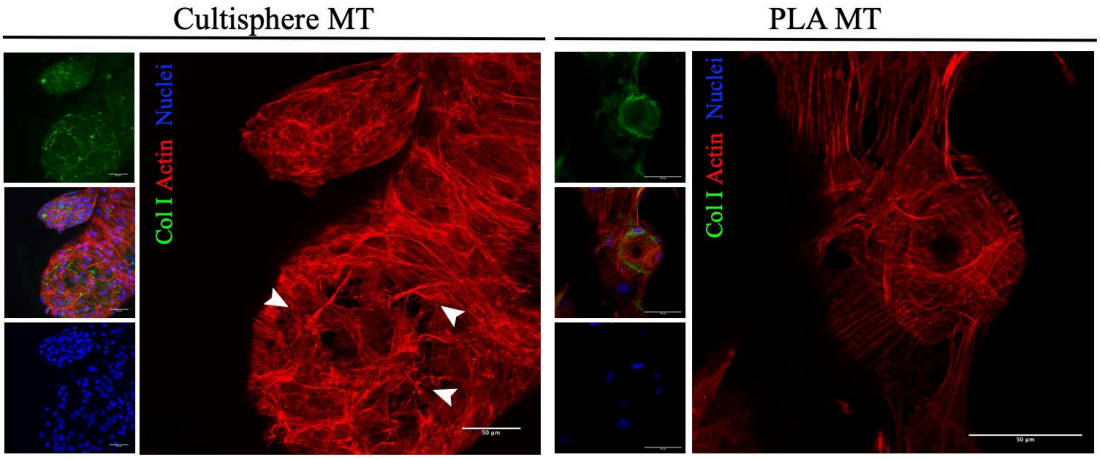

Figure 4.5 Cell morphology evaluation on magnified images for Cultisphere S and PLA MTs. Arrowheads point to irregular and spindle shape cytoskeleton in cells present at Cultisphere S MCs, whereas in PLA MCs cytoskeleton was perfectly spread.

4.3.2 Microtissue characterization with normal medium

Normal culture medium was used for 21 days for microtissue production. After that, constructs were collected and specifically processed for its characterization. For immunofluorescence analysis, MT were collected and cryosectioned in slides of 25 µm width. Presence of different ECM proteins was demonstrated. Fibronectin which is a fibrous glycoprotein with adhesive properties, and one of the first ECM proteins being released, was localized in all microtissue types and was intensively linked to Cultisphere microcarriers. *Figure 4.6* shows how fibronectin is localized in Cultisphere carriers exhibiting its internal structure as well as its perimeter. Moreover, secreted fibronectin was found between particles demonstrating the accumulation of a clear extracellular matrix. Cultisphere S carriers were also identified in Mixed microtissues, alternated with PLA. Cells or deposited ECM adapted to microcarrier shape as found in the Mixed MT image on the right, where they were found spread in a circular surface. PLA microtissues presented fibronectin as well, forming an intricated network gathering the particles. Weaker signal was observed in the inner space of the construct, as seen in the PLA image of the right.

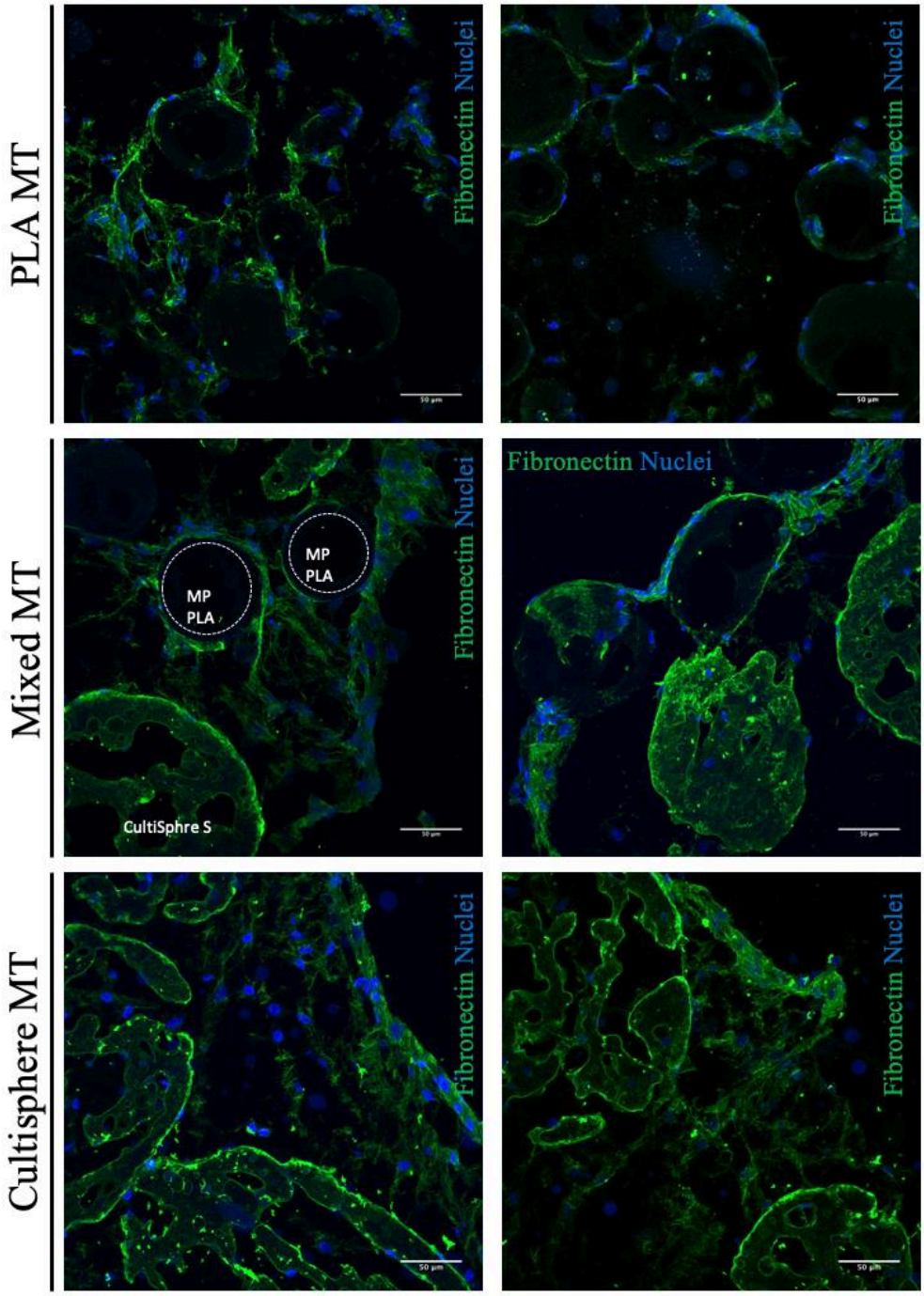

Figure 4.6 Immunofluorescent characterization of fibronectin after 21 days in culture. PLA is not stained, and spherical holes are observed. On the contrary, due to the gelatine nature of Cultisphere S MCs, fibronectin is adsorbed and this immunostained. Irregularities observed in Cultisphere carriers are due to macroporosity found inside them.

Next to fibronectin, collagens are also very important extracellular macromolecules. Their main functionality consists in providing structural support as well as cell adhesion sites. We have tested PLA, Cultisphere and Mixed microtissues for the presence of collagens I, II, III and IV (*Figure 4.7*). Immunofluorescent images were here taken in

sliced samples maintaining the same acquiring settings in the confocal microscope: laser intensity, pin hole aperture, and excitation/emission wavelengths. Image J software processing was used to quantify pixel intensity corresponding to each collagen signal and normalized it by the number of nuclei (DAPI-stained) in each sample. All three microtissue types followed the same pattern for collagen deposition were collagen type IV was the most secreted protein. Comparing between them, Mixed microtissues provided the highest collagen IV signal. However, a significant difference was only found between Mixed and PLA MT. Collagen III was the second most secreted protein in all constructs, and collagens I and II were the least expressed. CultiS MT promoted the highest collagen III production, with similar levels as to its collagen IV. It also significantly secreted more collagen II compared to PLA and Mixed MT, although presented the least collagen I production. PLA MT showed lower levels of proteins II, III and IV, but outreached CultiS MT with collagen I, similarly to Mixed MT.

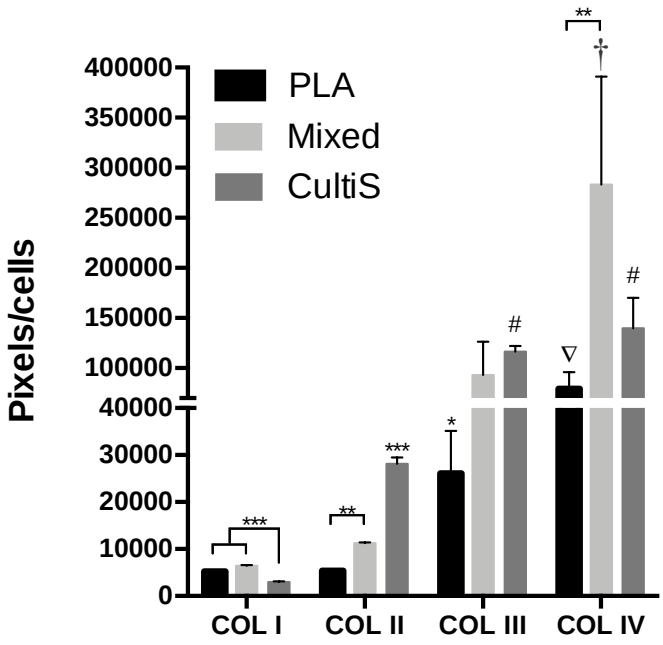

Figure 4.7 Quantification of immunofluorescent signal of expressed collagens type I, II, III and IV in PLA, CultiSphere and Mixed MTs. (* symbol indicates statistical differences in protein expression between microtissue types (*p value ≤ 0.01, **p ≤ 0.001, ***p ≤ 0.001). Other symbols represent statistical differences of collagen expression in the same MT. ∇ indicates COL IV was significantly increased compared to the other collagens in PLA MT; # means COL III and COL IV expression in CultiS was significantly higher than collagens I and II; † indicates COL IV expression in Mixed MT is significantly different from other collagens in the same MT type). At least four regions were studied for each microtissue type and collagen type. Two-way ANOVA with Tukey's multiple comparisons test was performed.

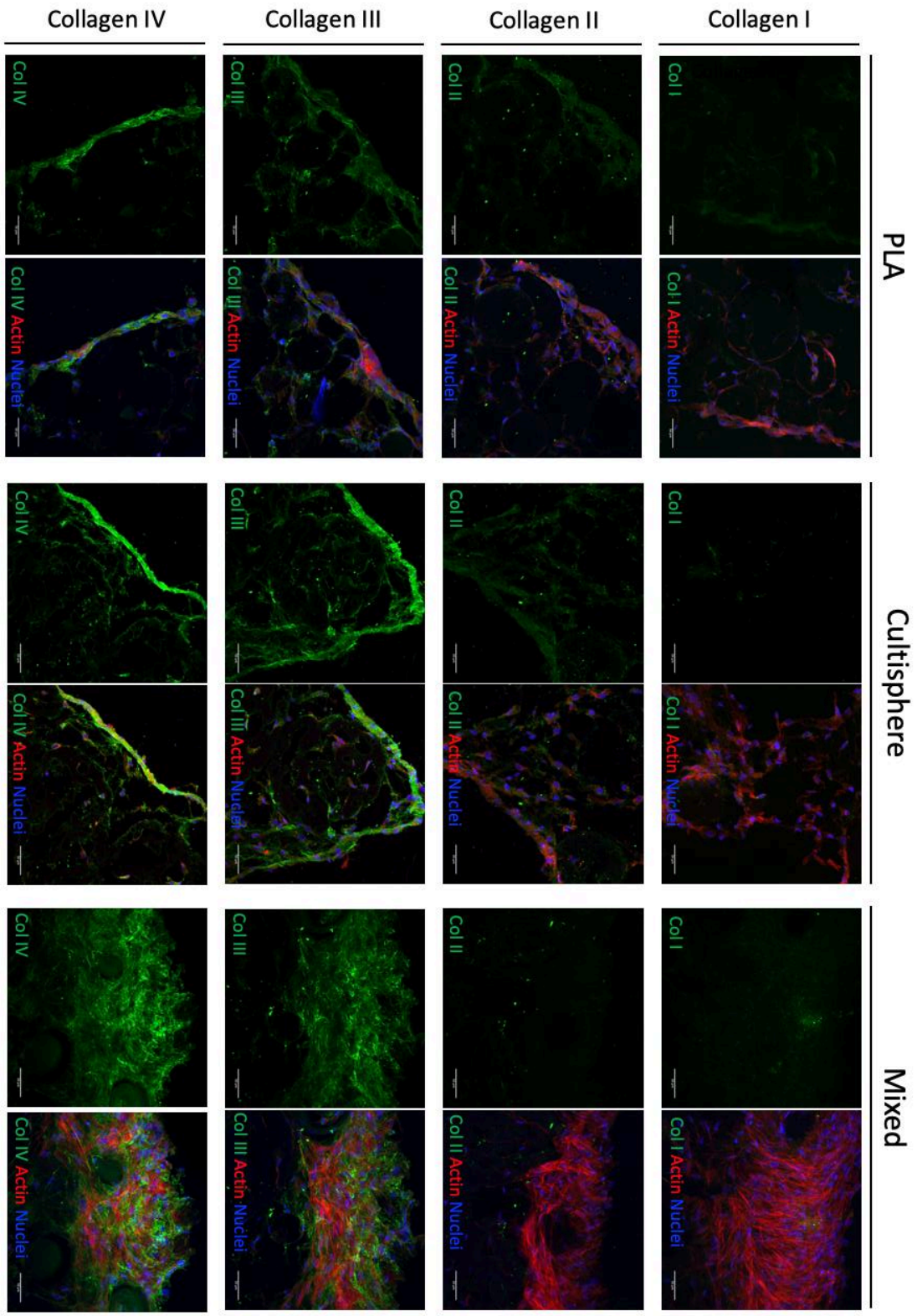

Figure 4.8 Immunofluorescence of sliced microtissues assessing for collagen I, II, III and IV expression.

Cross sections revealed the formation of a dense and thin layer surrounding the MT, both for PLA and Cultisphere conditions (clearly observed in CultiS MT for collagens III and IV (*Figure 4.8*)). Instead, Mixed microtissues showed a wider dense region,

observable both by ECM deposition and cellular actin, suggesting increased cell density and ECM depositions deeper towards the inside of the construct.

Further characterization consisted in the assessment of glycosaminoglycans (GAGs) present in microtissues. GAG, key elements in extracellular matrices, are based on polysaccharide chains capable of self-organizing, and associate with fibrous proteins such as collagen, forming large complexes and providing the tissue with the specific mechanical properties. Normalized GAGs by their dry weight, showed that both CultiS and Mixed conditions increased deposition within time (*Figure 4.9*, A). However, in PLA MT, GAGs did not increase from the first day but fluctuated along the culture with lower levels than day 1. Although, GAGs deposition was higher in CultiS MT, Mixed MT showed a higher relative increase from day 1, reaching 2.9-fold increase.

Early osteogenic differentiation marker alkaline phosphatase enzyme was evaluated with normal medium (*Figure 4.9*, B). Both Mixed and Cultisphere microtissues showed significant increased ALP activity compared to PLA MT, this increase was shifted from day 7 to day 14 for both conditions, suggesting a late spontaneous initiation for osteogenic profile.

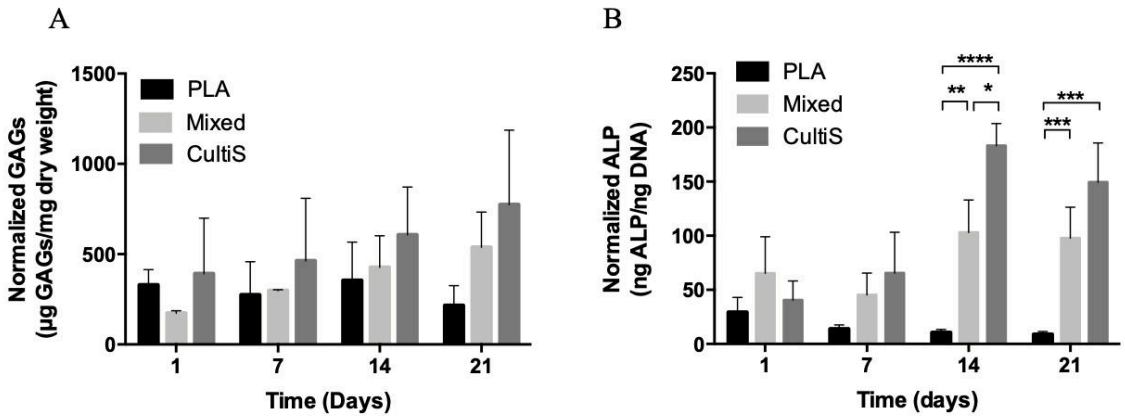

Figure 4.9 GAGs and ALP quantification. (A) Normalized GAGs with dry weight expressed relatively to day 1 value. (B) Normalized alkaline phosphatase enzyme amount with total DNA, relative to day 1. *Indicates significant (p value < 0.05) difference between the CultiS MT and PLA MT. For both analysis, two-way ANOVA with Tukey's multiple comparisons test was done.

Assessment of the relative expression of *Col I* and *Col IV*, *Alp* and *Runx2* genes under normal medium culture was performed comparing last day of culture with their first day (*Figure 4.10*). For Cultisphere MT, all genes were upregulated. Contrarily to immunofluorescent results where Cultisphere extracellular matrix had less collagen type I, 2-fold increased expression of this gene was observed, significantly higher than PLA

condition. This elevated messenger RNA (mRNA) might represent a late *Col I* gene activation for Cultisphere MT. On the other hand, 0,4-fold and 1-fold change for PLA and Mixed MT respectively, together with the low levels of secreted collagen I protein, indicate lack of induction for the production of this protein, probably due to its presence on PLA microcarriers. Although Mixed microtissues expressed and secreted a denser collagen IV extracellular matrix, gene expression compared to day 1 was not up-regulated. Although no quantitative experiments were performed on intermediate days (7-14 days), collagen type 4 deposition was already found in Mixed microtissues (by an immunofluorescence assay on day 7, data not shown). Early expression of this protein could be normalized by lower levels of mRNA by day 21. However, CultiS MT still showed 1.5-fold up-regulation, and although secreted levels of protein were lower compared to Mixed MT for that time, we have no data regarding intermediate timepoints.

Runx2 or Runt-related transcription factor 2, was evaluated due to its role in initializing MSC differentiation into osteogenic lineage. Up-regulation was only found for Cultisphere MT (2.1-fold). Also, osteogenic-related gene *Alp* expression was studied, and both CultiS and Mixed MT showed up-regulation, 1.9- and 3.1-fold respectively. Despite the higher gene up-regulation evidenced for Mixed MT, a major ALP activity was found for Cultisphere MT at that timepoint (*Figure 4.9*, B). Delayed up-regulation might be occurring, leading to higher levels of ALP activity if the cultured would have been extended for more than 21 days. Also, 1.2-fold increase of *Alp* gene in PLA MT did not correspond with the ALP activity expressed in cells, where levels were below day 1 (*Figure 4.9*, B).

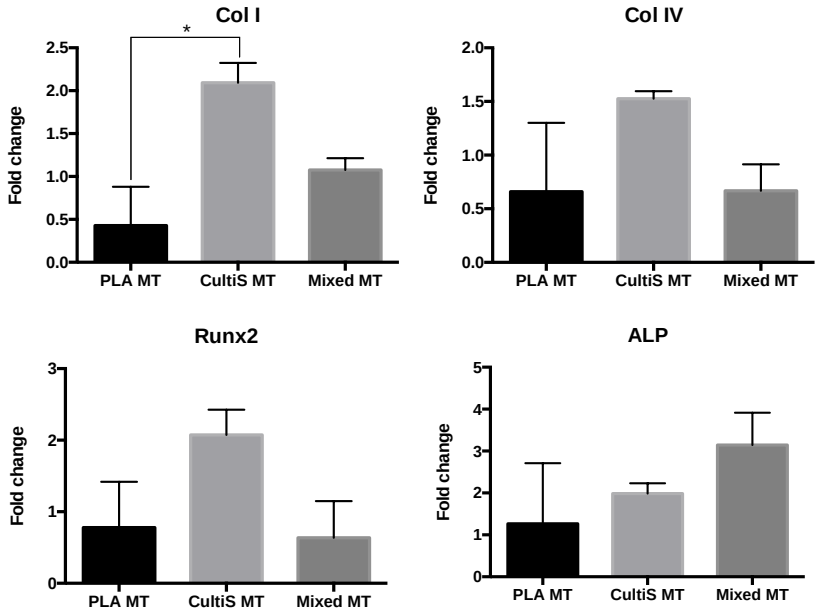

Figure 4.10 Gene expression analysis of rMSCs in MTs developed with PLA, Cultisphere S and Mixed microcarriers. Col I, Col IV, Runx2 and ALP genes were evaluated for its implication in osteogenesis and ECM formation, at days 21 of normal culture, and expressed compared to day 1. Actin expression was used as housekeeping gene. One-way ANOVA was performed for each gene, comparing the three MT conditions. * indicates significant different with a p value ≤0.05.

4.3.3 In vivo angiogenic potential characterization of microtissues using CAM model

In light of the abundant collagen IV found in secreted ECM on all microtissues, regardless microcarrier type, we decided to evaluate their angiogenic potential on a CAM *in vivo* model. During chick embryo's development, chorioallantoic membrane supports gas exchange with the outside, and suffers a rapid vascularization occurring on day third to day tenth of embryogenesis (E3 and E10, respectively) and, achieving fully differentiation by E13. Accessibility to the membrane for experimental manipulation and feasibility to engraft materials provides CAM as a robust experimental platform to study pro- and antiangiogenic properties of bioengineered constructs and in cancer research for drug development, among others (Nowak-sliwinska, 2015). Here PCL polymer was used to prepare irregular macroparticles matching the size of the microtissues (MT size). Despite being a biodegradable material, PCL has slow degradation rates and exerts no effects on CAM vascularization (Keshaw, 2010). Thereof, it was used as negative control. Addition of pro-angiogenic vascular endothelial growth factor (VEGF) to PCL scaffolds with 200 ng of VEGF was used as positive control for vascularization. On day E9 of development, microtissues prepared for 14 days were decellularized and implanted on CAM. After 3 days, scaffolds and CAM were fixed, excised and proceed to imaging and vessel quantification (*Figure 4.11*).

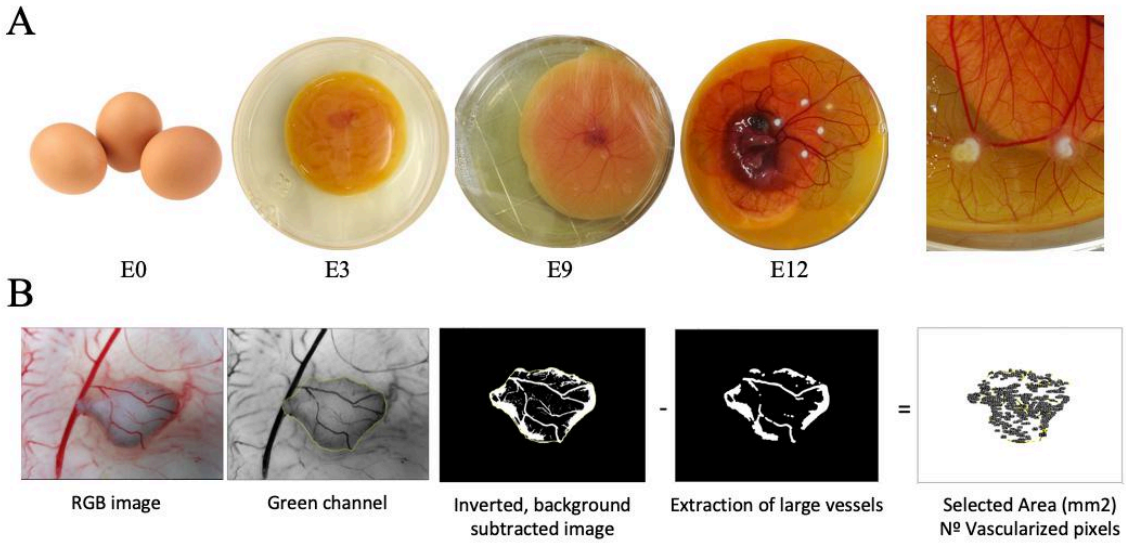

Figure 4.11 CAM *in vivo* assay. (A) Images of chick embryo at different stages of development. On day E9 microtissues were implanted, and then on day E12 they were harvested together with CAM and proceeded to angiogenic assessment. (B) Quantification procedure of the vascularization occurring in implanted scaffold. RGB images were taken on fixed and excised samples in an Olympus MVX10 Macroscope. On ImageJ software, RGB images were separated and green channel was considered to imaging processing. After the scaffold area was selected, background was subtracted, and large vessels discarded. These big vessels were not considered to be a result of angiogenic potential of the constructs, but they were found because of proximity. Following subtraction, pixels were quantified and normalized by scaffold size.

Mixed microtissues were found to be significantly vascularized (*Figure 4.12*). Proangiogenic capability of Mixed MT was as much potent as positive control (200 ng of VEGF). Cultisphere and PLA microtissues were significantly vascularized compared to negative control, but not as much as the effect of the positive control and Mixed MT. This result suggests that Mixed microtissues and the ECM secreted by cells on a mixture of both PLA and Cultisphere microcarriers could exert proangiogenic properties upon construct implantation *in vivo*.

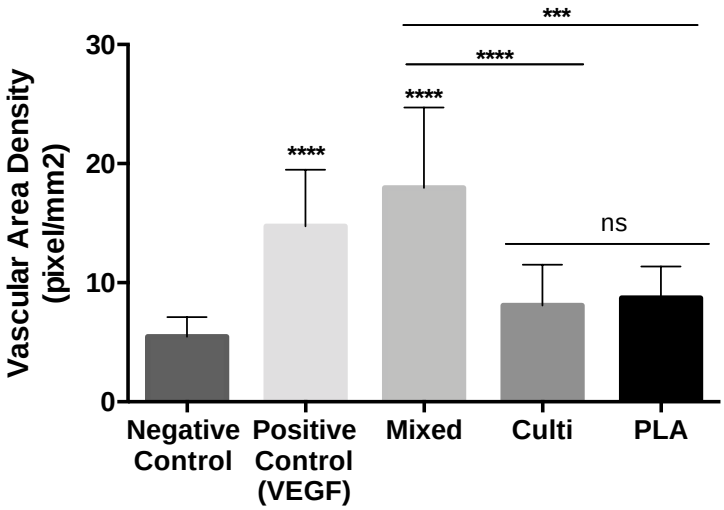

Figure 4.12 Vascular area density (pixels/mm^2) of implanted MTs and controls in the *in vivo* CAM assay. Positive VEGF control and Mixed condition showed elevated vascularized areas, significantly different to negative control (****p value ≤ 0.0001). Cultisphere and PLA microtissues were not significantly different to negative control but were significantly lower than Mixed condition (***p value ≤ 0.001, ****p value ≤ 0.0001). N=15-25. One-way ANOVA with Tukey's multiple comparisons test was performed for significant differences.

4.3.4 Microtissue evaluation under osteogenic induction

In order to investigate the effect of the chosen microcarriers on cell proliferation, osteogenic conditions were also evaluated during microtissue formation. As described before, microcarrier were seeded in intermittent agitation for 6h in a spinner flask bioreactor. In this case, only Cultisphere S and a mixture of PLA and Cultisphere MCs 1:1 were evaluated. Afterwards, colonized particles were trespassed to 24-well plates for the formation of microtissues in static conditions. Seven days with normal culture medium were followed with osteogenic medium for 21 days. Both CultiS and Mixed MT presented restricted cell proliferation after the first week of osteogenesis. However, on the following timepoints, cells significantly proliferated on CultiS MT whereas slightly decreased for Mixed MT (*Figure 4.13*). Higher proliferation observed in CultiS MT contrasted with protein deposition, which significantly decreased after 14 days in osteogenic medium. On the other hand, normalized protein deposition for Mixed MT experienced an increase in day 14 followed by a drop the next timepoint.

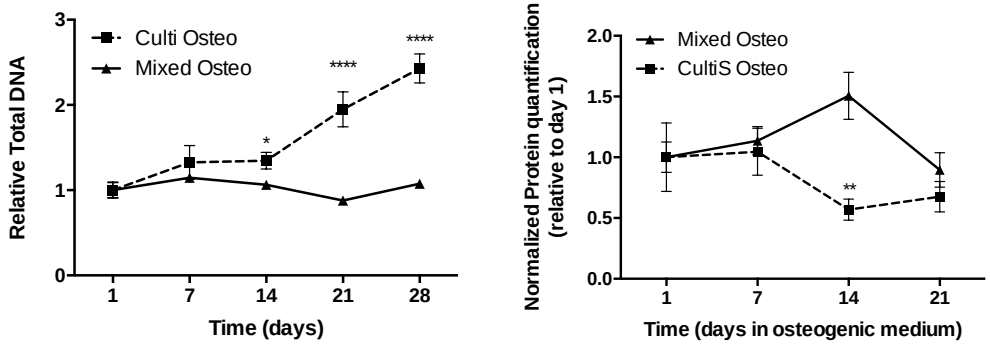

Figure 4.13 Characterization of osteogenic MTs. (A) Total DNA expressed relatively to day 1 in microtissues during osteogenic induction. Osteogenic medium was introduced after 7 days in culture. Significant difference with a p value < 0.05 was observed on day 14 between Cultisphere and Mixed MT. On days 21 and 28 of culture, CultiS relative increase was also significantly higher than Mixed MT (**** p value < 0.0001). (B) Protein quantification, normalized for DNA amount, and expressed relatively to day 1. Significant difference was observed for day 14 (** p value < 0.001).

SEM images show irregular ECM deposition on Mixed MT (*Figure 4.14*). Although individual cells are not discerned on its surface, similarly to what was observed for normal medium, microcarriers were not fully covered until last day. Also, irregular deposits on the surface were observed. In Cultisphere MT, microcarrier coverage was achieved earlier. Seven days after osteogenic induction, MC were covered. In concordance with the elevated proliferation, and low protein quantification, individual cells are observable on the surface of these microtissues. For both conditions, osteogenic induction resulted in less ECM deposition and smaller and less compacted microtissues were obtained, compared to normal medium incubation.

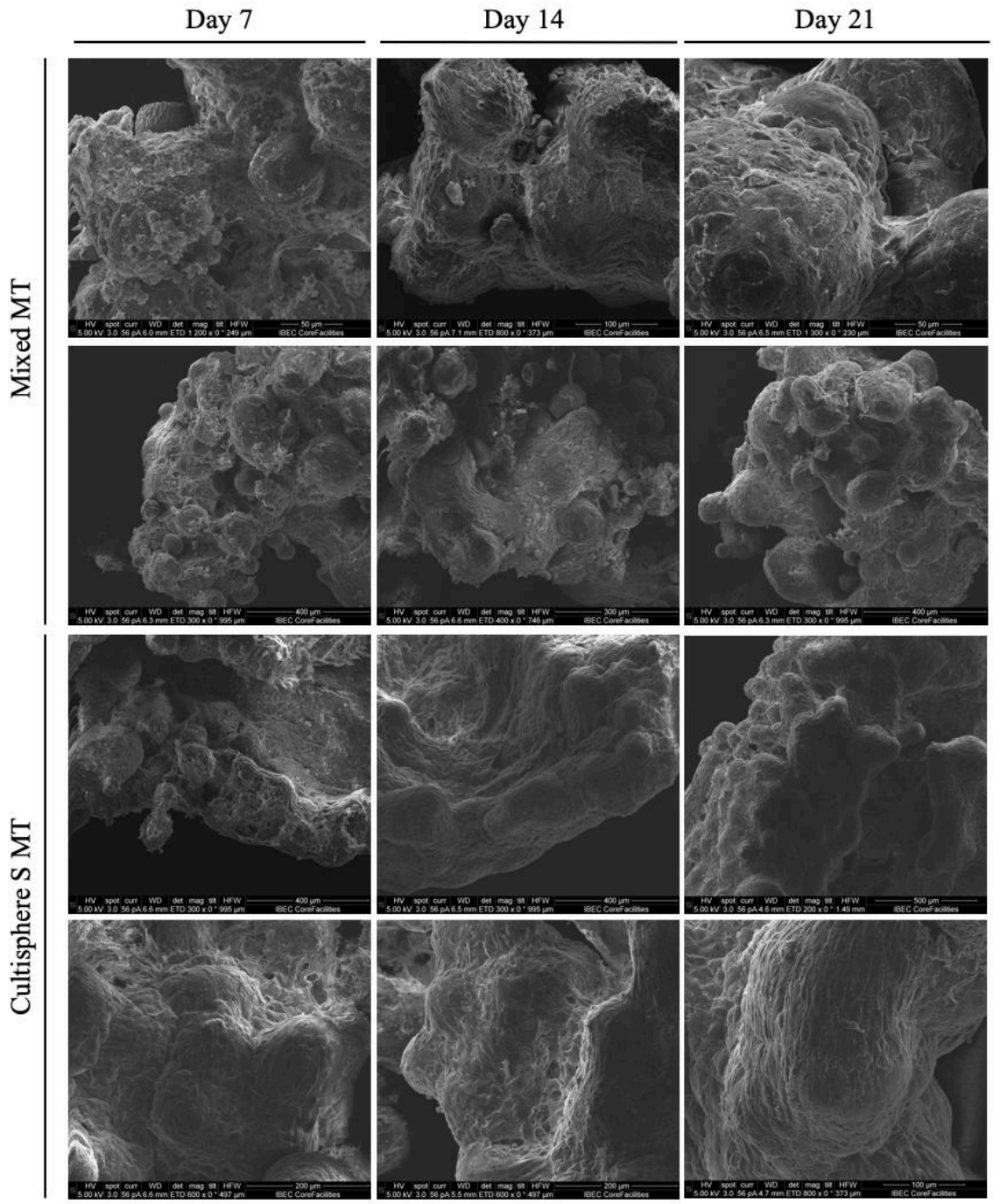

Figure 4.14 Scanning electronic microscopy images of Mixed and Cultisphere MT after 7, 14 and 21 days in osteogenic medium. Irregular ECM is observed in Mixed MT whereas smooth surface is found for Cultisphere S.

Real-time PCR was performed to analyse collagens I and IV gene expression in osteogenic Mixed and CultiS MT. The main collagen expected to be deposited in ECM, collagen type I, and the most abundant collagen found in MT formation with normal medium were investigated for 7, 14 and 21 days under osteogenic induction. Normal 2D cell culture with proliferating and osteogenic medium were also analysed. Gene

expression of microtissues in normal medium and on day 21 are also shown (*Figure 4.15*). Osteogenic induction caused down-regulation of collagen type I expression for all conditions. Although a negative progression was also observed by time regardless MT condition. Contrarily, *Col IV* gene expression was progressively up-regulated for osteogenic conditions. On day 21, Mixed MT expressed same fold regulation, regardless the medium used, whereas for 2D cell culture condition and CultiS MT, both under osteogenic induction, showed a significant up-fold compared to their normal medium counterparts. CultiS MT under osteogenesis was found to be 16-fold increase compared to day 1.

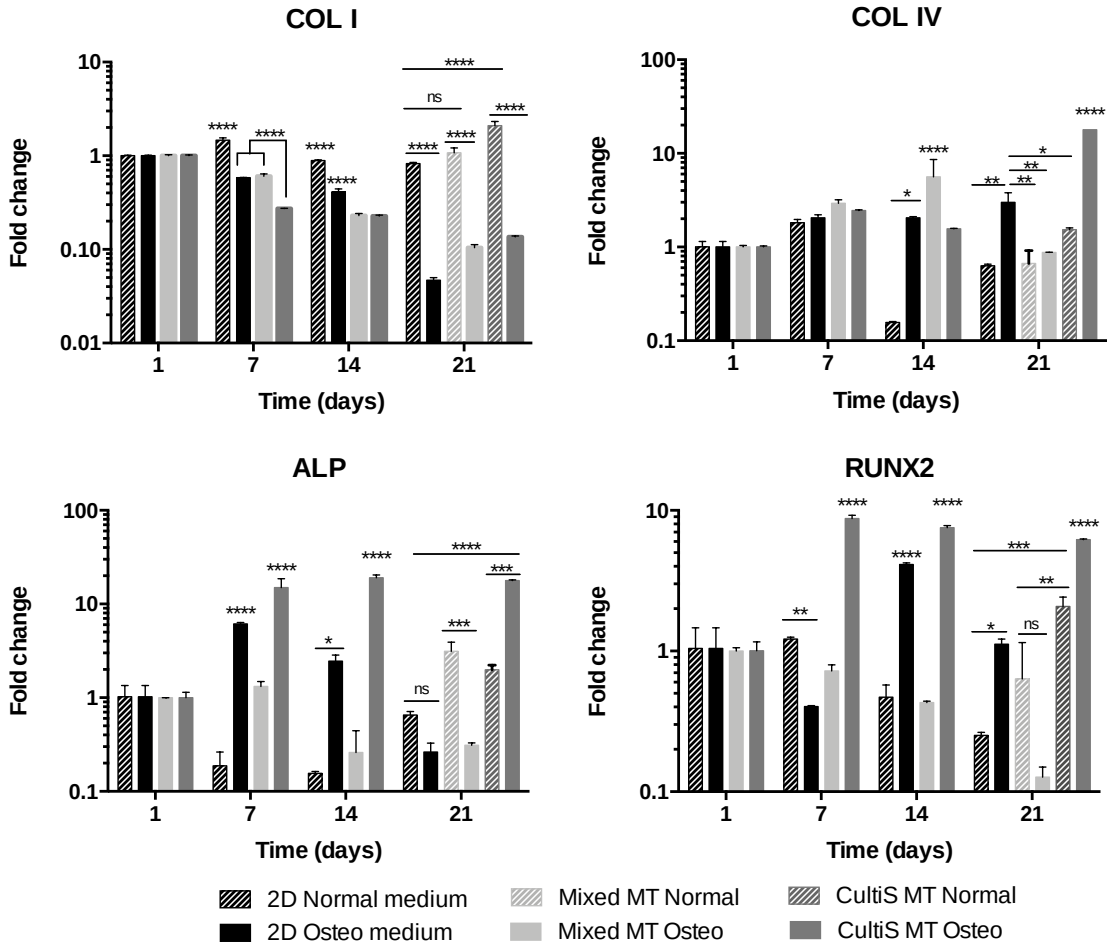

Figure 4.15 Gene expression profile of Mixed and Cultisphere MTs under osteogenic induction. Data from day 21 of normal culture medium is also displayed. 2D controls appear after normal and osteogenic induction. Fold expression is relative to day 1 of each condition. Significant differences between different conditions the same day are shown. Two-way ANOVA was evaluated with Tukey's multiple comparisons test. Fold change is displayed in log10 scale.

Osteogenic-related genes *Runx2* and *Alp* showed significant up-regulation for cells on Cultisphere MT (*Figure 4.15*). Both genes, related to early steps of osteogenic

differentiation increased after 7 days (8-fold for Runx2 and 15-fold for Alp), and were maintained up-regulated for all the induction. Mixed MT showed non-existent increase at any timepoint. Nonetheless, control condition in 2D, showed shifted up-regulation of this genes from day 7 to day 14. *Runx2* considered to be key in initiating osteogenic differentiation was 4-fold up-regulated on day 14, but it was not further maintained. In terms of *Alp* gene expression, osteogenic 2D control was significant up-regulated (6-fold) compared to first day. But also, as seen for *Runx2* it was not maintained. These results suggest osteogenic induction was initiated but not accomplished on cells cultured in tissue culture plates.

4.3.5 Evaluation of cell-homing chemokine SDF-1α expression

Stromal derived factor 1α plays a major role in MSC migration and cell-homing. Here we have evaluated the secretion of this chemokine into the medium by cells cultured on PLA, Mixed and Cultisphere microtissues for 1, 7, 14 and 21 days after normal culture medium, as well as Mixed and Cultisphere microtissues under osteogenic medium (for this condition, time expresses the days under osteogenic induction) (*Figure 4.16*). Continuous basal release was observed for PLA and Cultisphere MT in normal medium and Cultisphere MT osteogenic medium. Mixed microtissues were supporting SDF-1α increased secretion on cells. On day 7, highest expression was found for osteogenic Mixed MT, whereas on day 21, it was normal Mixed MT presenting increased levels.

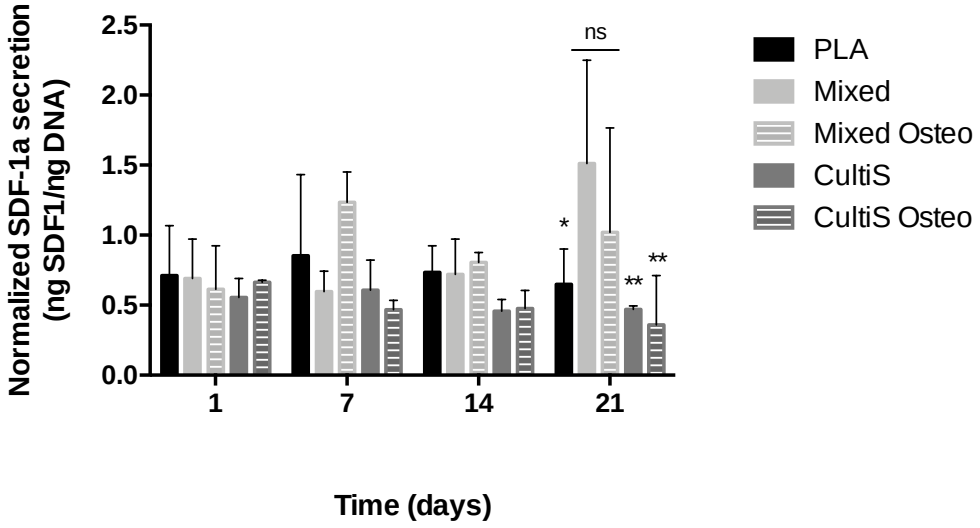

Figure 4.16 Stromal cell derived factor 1 alpha secretion into the medium analysed by an ELISA assay, and normalized to total DNA for each timepoint and condition. Significant differences were only found the last day for the Mixed MT cultured in normal growth medium with respect to PLA and Cultisphere in normal medium and Cultisphere MT in osteogenic medium. Two-way ANOVA with Tukey's multiple comparisons test was performed.

4.4 Discussion

In the last decades, decellularized *in vitro* cell-derived ECM (dECM) scaffolds have been postulated as promising choices in the development of biomimetic tissue engineering constructs (Badylak, 2009; Fitzpatrick, 2015; Zhang, 2016). The methodology by which cell-derived ECMs are obtained *in vitro* is usually mediated by the use of biomaterials that give support or instruct specific cell behaviours for the subsequent decellularization and posterior reseeding (Datta, 2006; Thibault, 2010; Tour, 2011). However, the selection for the most appropriate biomaterial to instruct ECM initial deposition is subjected to arbitrary choices.

In this study we have found that the use of different microcarriers to produced cell-derived ECM influence the characteristics of the obtained matrix. Although some similarities are raised, final functionality is affected by the interaction of the cells with the scaffolds and external added factors. We have observed that the mixture of Cultisphere and PLA microcarriers in the same microtissue induced the formation of undifferentiated constructs with pro-angiogenic potential. Moreover, Cultisphere S microtissues may be able to restore MSC multipotentiality, enhancing osteogenic phenotype even compared to 2D cultured cells.

The initial focus in the comparison of PLA and Cultisphere microcarriers relied on cell adhesion. Correct cell attachment to microcarriers is important for subsequent cellular processes such as survival, proliferation and cell behaviour (Rafiq, 2016; Tseng, 2012). Conducting screening studies of the most appropriate MCs for each application and cell type is essential (Frauenschuh, 2007; Rafiq, 2016; Schop, 2010). Microcarrier bulk composition, surface functionality and protein adsorption are all important factors mediating cell-MC attachment (Mateos-Timoneda, 2014; Punet, 2013). Both microcarrier types demonstrated to successfully work in cellular adhesion (Levato, 2015; Sart, 2011), however when directly compared, Cultisphere S shows better initial colonization rates (99.8% for Cultisphere and 80.71% for PLA microcarriers). Natural polymers, such as gelatine, inherently present appropriate biological cues favouring enhanced adhesion (Nair, 2007).

The insight of strong absorption of fibronectin into Cultisphere S, as seen by immunofluorescent analysis, where the particular Cultisphere S structure was clearly elucidated, made us think that protein serum absorption was mediating in cell adhesion performance. Although some authors recognized enhanced cell response of Cultisphere S in serum-free conditions (Eibes, 2010; Yuan, 2014), others sustained the importance of

fibronectin (present in serum) to absorb on gelatine carriers for the proper cell adhesion and cytoskeleton organization (Sart, 2013). Cellular adhesion to covalently-coated PLA MCs was also favoured with the presence of serum in the medium (as seen in Chapter 3). However, collagen coating may remain as the principal protein displayed on the surface of PLA. Different MSC affinity to ECM proteins may be responsible for varied attachment on these microcarriers, as fibronectin has been described to be the most affine protein to MSC, followed by collagen type I (Salasznyk, 2004; Tsuchiya, 2001). Nevertheless, similar colonization rates were obtained when PLA microcarriers were coated with fibronectin (data not shown), suggesting that bulk composition still influenced in cell performance (Rafiq, 2016).

In terms of cell proliferation, a consensus on the best microcarrier with a specific cell type does not exist, and contradictory results are found in literature. Whereas Rafiq *et al.* manifest poor sustained cell proliferation on Cultisphere (Rafiq, 2016), Sart *et al.* determined it worked better than dextran-based microcarriers Cytodex-3 (Sart, 2013). Our results are in concordance with Rafiq *et al.* and others (Grayson, 2004; Mei, 2010), manifesting that cell proliferation on Cultisphere arrived to a plateau after 7 days, probably due to restricted available surface (Rafiq, 2018). On the other hand, cell proliferation on collagen coated PLA MCs was previously proved in static culture (Levato, 2015), although restricted homogeneous distribution was found. For that reason, we implemented dynamic MC seeding (Chapter 3). However, limited proliferation was observed on PLA during the first 7 days, indicating the appearance of a lag phase. That situation was then mildly reversed. Extended microcarrier incubation in serum containing medium prior to inoculation could effectively reduce lag phase, enhancing cellular proliferation (Eibes, 2010). Unexpectedly, combination of both types of microcarriers allowed a sustained proliferation from the beginning until the last day of culture. We propose that the combination of both MC features helped improving cell performance: initial enhanced attachment promoted by Cultisphere, avoiding PLA's lag phase and then sustained proliferation probably due to surface availability.

Cell-laden microcarriers successfully aggregated forming microtissue constructs on all microcarrier conditions, mainly attributed to cell-cell interactions and ECM deposition (Frauenschuh, 2007; Mei, 2010) in what is considered a cell-derived extracellular matrix scaffold. The ECM is a highly specialized macromolecular network that provides structural and biomechanical support for cells along with biological cues influencing all levels of cell behaviour *i.e.* proliferation, cell migration, differentiation (Zhang, 2016).

ECM composition is specific for each tissue type and it is being continuously remodelled in order to adapt to different stages of development, aging and disease. Here, we have investigated the main ECM constituents in our microtissues including fibronectin, different collagens and glycosaminoglycans, and found that all three microtissues were positively expressing them, although in different intensities and distribution. Such differences promoted significant different microtissue functionalities.

Fibronectin is an abundant and ubiquitous ECM protein that organizes into fibrillar networks in a cell-dependent manner (Hynes, 1990). Blockage of fibronectin polymerization inhibits self-organization of multicellular structures *in vitro*, and the consequent microtissue formation (Sevilla, 2010). In here, PLA, Cultisphere and Mixed constructs exhibited an extended fibronectin extracellular matrix that allowed the formation of MTs. Also, cell-laden microcarrier contractility and microtissue geometry that evolved from free microcarriers, to half-moon shaped and finally to compacted structures were most probably mediated by fibronectin remodelling (Mao, 2005).

Collagen molecules are, together with fibronectin, the most abundant proteins in extracellular matrices, however their characteristic distribution depends on the nature of the tissue. Collagen type I is present almighty, and it is abundantly represented in bone, skin or tendon (Parry, 2017); collagen type II is specifically associated with the ECM of hyaline cartilage (Chen, 2016a); collagen type III is found in connective tissues; and collagen IV which is a non-fibrillar collagen, forms an interlaced network in basement membranes (Kadler, 2007). Quantitative collagen assessment in MC-mediated cell-derived microtissues demonstrated that collagens type I and II were the lowest expressed compared to collagens III and IV. Specifically, collagen type IV was the most abundant protein. Supporting our findings, another engineered approach found similar hMSCs behaviour on poly(ethylene terephthalate) (PET) fibrous scaffolds promoting extended secretion of extracellular fibronectin and collagen IV, and restricting collagen I expression (Grayson, 2004).

Basement membranes (BM) are specialized ECMs aiding in epithelial and endothelial cell growth, surrounding muscle and fat cells, and providing structural support for blood vessels and peripheral nerves (Kalluri, 2003). Type IV collagen is the most abundant component of the BM, and it is found together with laminin, heparan-sulphate proteoglycans and nidogen (Schittny, 1989). Mesenchymal stem cells are considered to importantly contribute to the synthesis of BM components including type IV collagen isoforms and laminin (Furuyama, 2000). Interestingly, hMSCs were secreting collagen

IV in an *in vitro* model of epidermal regeneration in combination with keratinocytes contributing to the reestablishment of the dermo-epidermal junction (Ojeh, 2014). Here, we have found that collagen IV expressing Mixed microtissues were able to induce a potent angiogenic response in the *in vivo* CAM assay, similar to 40 ng of VEGF. However, both Cultisphere and PLA microtissues, although expressing collagen IV, were not able to promote angiogenesis. We speculate that either the amount of collagen expressed, and the specific ECM organization had something to do with this diverted response. Broader and more prominent ECM found in Mixed MT may be enabling a laxer environment recapitulating initial steps in angiogenesis, whereas the sheet-like thin layer found in Cultisphere and PLA resembled a more mature BM. Upholding our observations, Nicosia *et al.* described that changes in the degree of collagenization of the ECM affected the calibre of the newly formed microvessels, and found that abundant interstitial collagen fibers raised more functional and mature capillaries (Nicosia, 1991). Moreover, collagen type IV plays an antagonist dual role in angiogenic processes, depending on the dose (Bonanno, 2000), and on the exposure of specific peptide fragments with anti-angiogenic properties because of reorganization of collagen IV network or by enzymatic cleavage (Mundel, 2014). Cryptic domains of collagen IV possess anti-angiogenic properties when exposed, and several anti-tumoral molecules have been developed after them: arrestin, canstatin and tumstatin (Kalluri, 2003; Karagiannis, 2007). These results encourage the use of Mixed microtissues in other *in vivo* models for in situ rapid vascularization.

In the characterization of PLA, Mixed and Cultisphere S microtissues we wanted to assess the spontaneous commitment of cells towards osteogenic profile. Numerous studies sustained that MSCs culture on spherical microcarriers helped in maintaining multipotency of these cells delaying spontaneous differentiation (Shekaran, 2015) and enhancing osteogenic phenotype after proper induction (Chen, 2011b; Goh, 2013; Levato, 2014; Shekaran, 2015; Yang, 2007). Low levels of early osteogenic genes Runx2, Alp and Col I together with decreased ALP activity suggested no spontaneous osteogenic induction in PLA microtissues with normal medium. Consistently, Tseng *et al.* corroborated no spontaneous osteogenesis in collagen-coated microcarriers (SoloHill) on rat bone marrow derived MSCs, however both human placenta derived multipotent cells, ESC-derived mesenchymal progenitor and C3H10T1/2 murine MSC cell line expressed up-regulated osteogenic genes (Tseng, 2012). Although cytoskeleton tension produced by circularity of MC is related to an osteogenic phenotype and given the fact that actin tension fibers were observed on PLA microcarriers, there was no correlation here with

spontaneous osteogenesis. Nevertheless, circularity effects might be lost after the first days of MT formation due to abundant ECM deposition. After the creation of bridges connecting different MCs, no sense of circularity might be felt by cells, and only a reduced number might still be in direct contact with surface shape. Assessment of PLA microtissues under osteogenic medium could unfortunately not be developed. Thus, we could not further assert their pro-osteogenic behaviour.

On the other hand, Cultisphere microtissues had increased ALP enzyme production in normal medium, together with up-regulated early osteogenic genes by the end of the culture, compared to the other two microtissues. Rubin *et al.* also found increased ALP activity of adipose derived MSCs on Cultisphere S microcarriers under normal medium although late stage marker in osteogenesis, calcium deposition, was never found (Peter Rubin 2007). These results could suggest either basal expression or slight initiation of spontaneous osteogenesis. In concordance with our results, after proper osteogenic induction, cells on Cultisphere microtissues developed successful osteogenic profile (*Alp* and *Runx2*). Osteogenesis was even more up-regulated than 2D controls. These observation could imply two things, first that Cultisphere S incremented the osteogenic effect, matching with what several papers declare (Goh, 2013; Levato, 2014; Shekaran, 2015; Yang, 2007); and second, that rMSCs had lost their multipotent phenotype, and Cultisphere-seeding allowed the multipotentiality restoration (Lai, 2010), the same way healthy or young ECM can restore aged cells (Sun, 2011). Nevertheless, calcium deposition assessment evidencing total osteogenic commitment would finally confirm the first, and the evaluation of different lineage multipotency commitment both in 2D cultured and Cultisphere would confirm the later.

Evaluation of Mixed microtissues showed synergistic results by the presence of both microcarriers. Basal ALP activity was also found, as well as up-regulation of *Alp* gene in normal medium similar to Cultisphere MT, together with *Col I* and *Runx2* down-regulation similar to PLA MT. Only, *Alp* gene was slightly upregulated by day 21. Yet, during osteogenic induction no signs of osteogenesis were elucidated. Levato *et al.* and Goh *et al.* described positive appearance of late osteogenic markers (osteocalcin) on cells attached to MCs, even without the expression of ALP (Goh, 2013; Levato, 2014). The reason for this behaviour is unknown, and again calcium deposition analysis would finally confirm or deny our guessing. However, persistent proliferation of MSCs on Mixed MT during osteogenesis suggests failed cell cycle arrest, and so no entry in the differentiation state (Ruijtenberg, 2016).

Interestingly, low levels of *Col1* gene expression on all microtissues were observed, probably due to the presence of collagen or collagen derived gelatine on MCs leading to an inhibitory effect on gene expression also described by Chen *et al.* (Chen, 2011b). Moreover, Declercq *et al.* found no restriction using the same gelatine-MCs, although up-regulation was mild (Declercq, 2013). However, 2D controls rMSCs controls here were also incapable of mediating up-regulation of *Col1*, suggesting incomplete or moderate osteogenic differentiation.

Finally, we decided to investigate the cell homing effect of the different microtissues, by assessing the levels of SDF-1α secretion. This chemokine plays a role in cell trafficking and homing of CD34+ stem cells (Lau, 2011), and within an injure, increased SDF-1α levels lead to their recruitment and retention. Furthermore, the incorporation of SDF-1α or SDF-1α-overexpressing cells into engineered scaffolds is shown to improve tissue regeneration (Lau, 2011; Thevenot, 2010). PLGA scaffolds combined with this chemokine shown reduced inflammation and decreased fibrotic responses towards the implants, as well as increased angiogenesis (Thevenot, 2010). MSCs constant expression of SDF-1α in bone marrow is attributed to the maintenance of cells in the stem cell niche (Potapova, 2008). Mixed microtissues in normal medium significantly peaked in SDF-1α expression over the other two microtissues. Therefore, upon implantation they will be able to maintain a cell-homing effect on implanted cells avoiding washout and favouring the regenerative outcome. We also hypothesize that this expression could have influenced in the angiogenic response seen in the CAM *in vivo* model, promoting the migration of CD34+ progenitor endothelial cells towards the construct.

4.5 Conclusions

Microcarrier culture and microtissue formation offers the opportunity to create cell-derived extracellular matrix scaffolds for modular tissue engineering approaches. It is important to precisely choose the microcarrier type that it going to support initial ECM deposition to meet functionality of the targeted tissue. We have seen that microtissues derived from Cultisphere S microcarriers are prone to osteogenic phenotype in normal medium, but also enhance osteogenesis when properly induced. On the other hand, PLA microtissues have shown no spontaneous osteogenic differentiation and failed in secreting a dense extracellular matrix due to a retarded cell proliferation. Interestingly, by mixing both types of microcarriers, Mixed microtissues were able to continuously

proliferate, secrete an abundant extracellular matrix and promote angiogenic properties for further vascularization. All these results reinforce the strong necessity of microcarrier screening prior to each specific case.

Chapter 5

Microtissue vascularization using a co-culture strategy

5.1 Introduction

Despite the great potential that TE approaches hold, translation into the clinics is still hampered. Limitations in the passive supply of oxygen and nutrients to the whole scaffold result in regions with cellular death. The solution to this problem requires the formation of new blood vessels to surpass this mass transfer constrain. During the last decades, vascularization has gathered plenty of efforts in the field of TE (Novosel, 2011; Rouwkema, 2008). Different strategies include the *in vitro* pre-vascularization of scaffolds (Kook, 2018; Verseijden, 2010) and the *in vivo* vascularization once the scaffold is implanted (Brudno, 2013; Portalska, 2012). The former strategies are based in the formation of pre-vascular structures when cultured under the right conditions and environment. For instance, nanofibrous patterned PCL/gelatine scaffolds promoted the alignment of HUVEC cells and the formation of functional microvessel structures along the fibers *in vitro* (Kook, 2018). Also, the correct stimuli of cells in hydrogels can trigger the formation of tubular structures that can be then anastomose to the host vasculature upon implantation (Zhou, 2016b).

The latter strategies rely on the invasion of the host vasculature upon implantation, and although it is a prolonged process that can take from days to weeks compromising cell survival, different strategies are designed to enhance and exacerbate *in vivo* vascularization. Parameters such as scaffold design (Rossi, 2016; Tao, 2009; Zhong, 2017), delivery of growth factors (Brudno, 2013; Chen, 2007a) and the co-culture of endothelial cells with supportive perivascular cells (Costa-Almeida, 2014; Saleh, 2011) have been explored to enhance *in vivo* vascularization.

Concerning the design of the scaffolds for the production of functional-microvessel structures, cell-laden microcarriers can offer advantageous features. MCs can be easily assembled into larger constructs in modular strategies offering great potential for the fabrication of virtually any tissue type (Dikina, 2018; Matsunaga, 2011; McGuigan, 2007a). Moreover, inherent porosity presented by the aggregation of MC provides a permissive environment for vessels to grow inside (Rossi, 2016; Tao, 2009). Also, cells laden on microcarriers can deposit an extended and intricate network of ECM providing with appropriate cell-adhesion sites for endothelial cells and promoting cell proliferation and protein synthesis for vasculogenesis and angiogenesis (Chen, 2016b).

The importance of a co-culture system for vascularization purposes relies in the mimicry of natural-happening events, in which both intimate cell-cell contacts and diffusible signalling molecules control vessel generation or sprout (Costa-Almeida, 2014; Fuchs, 2007). Among the different cells that have been co-cultured with endothelial (EC) or endothelial progenitor cells (*i.e*. pericytes, fibroblasts, smooth muscle cells, osteoblasts), MSCs have been extensively used (Klar, 2016; Kook, 2018; Melero-Martin, 2007; Pill, 2015). MSCs can contribute to the vascular stability displaying a pericyte-like phenotype (Crisan, 2008). Pericytes cover newly formed microvessels, that otherwise would regress. They also stablish direct physical contact with EC, contributing to the deposition of a specialized ECM (Costa-Almeida, 2014). In fact, some studies have demonstrated that only co-cultured HUVEC and MSCs spheroids were able to form vascular-like structures *in vitro* (Verseijden, 2010; Zhou, 2016b).

Here, we have investigated the fabrication of MTs formed by human adipose derived mesenchymal stem cells (hAMSCs) seeded on PLA MCs, as favourable microenvironments for vascular morphogenesis when co-cultured with human umbilical vein endothelial cells (HUVEC). First, we evaluated the best methodology for the preparation of co-cultured microtissues (CoC-MT), and found that independent seeding was not favouring HUVEC attachment to PLA MC. On the contrary, they could attach to the surface of preformed hAMSC-MT. Then, *in vivo* vascularization was assessed, and it was found that both microtissue types, hAMSC- and CoC-MT, yielded similar results.

5.2 Materials and Methods

5.2.1 Cell isolation, expansion and lentiviral transduction

HUVECs were purchased from Millipore™ (SCCE001). Cells were cultured in 175 cm^2 T-flasks (Nunclon™, ThermoFisher) with EndoGRO-LS complete culture media (Merk-Millipore, SCME001) at a cell density of 2500 – 5000 cells/cm^2. EndoGRO-LS contained reduced FBS and no VEGF at all.

hAMSCs were obtained from Jerónimo Blanco's group (Group for Cell delivery Therapies, IQAC-CSIC. Barcelona), following the procedure exposed by Vilalta *et al.* (Vilalta, 2008). In brief, adipose tissue was obtained in a cosmetic subdermal liposuction from a 44-year-old white lady. Lipoaspirates were rinsed with PBS, digested with collagenase I solution, and then after several rinsing and centrifugation steps, cells were resuspended in Ringer's lactate and tested positive for specific MSC surface markers (Vilalta, 2008). hAMSCs at passage 3 were transduced using lentiviral constructs CMV:hRluc:mRFP as previously described (Guerra-Rebollo, 2018). RFP expressing property was used for cellular fluorescent identification (Rluc-RFP-Tk-hAMSCs). Resulting cells were culture for expansion with Advanced Dulbecco's Modified Eagle Medium (aDMEM, Gibco™) supplemented with 10% FBS, 1% penicillin/streptomycin and 1% L-glutamine (Sigma-Aldrich), and 10 ng/ml recombinant basic human fibroblast growth factor (bFGF) (Peprotech, 100-18B).

5.2.2 Microcarrier preparation

Collagen functionalized-PLA MCs were prepared following the same procedure as in Chapter 3 (Levato, 2012). MCs were freeze dried and kept in the fridge. Prior to its use, PLA MCs were hydrated with 70% ethanol overnight. Ethanol was replaced with PBS in three rinsing steps, prior to the addition of complete culture medium for at least 30 min before cell seeding.

5.2.3 Evaluation of HUVEC – microcarrier adhesion

Initially, HUVECs were seeded onto PLA MCs in static conditions to evaluate cell adhesion. 1.5 mg MCs were incorporated into each well of a non-adherent 24-well plate (Corning® Costar ultra-low attachment) and let sink. Avoiding MCs removal, minimal

medium was left, and cells were placed on top in a concentration of 45000 cells/mg MC. After 30 min with minimum volume, 1 ml was added. Medium was changed every two to three days. Cultisphere S microcarriers (Percell Biolytica; Sweden) were used as control condition. By utilising same parameters, HUVEC cells performance with PLA microcarriers was evaluated compared to Cultisphere S. Samples of both microcarriers were taken after 1, 3 and 7 days, and cell content was evaluated by quantifying total DNA. Calcein vital staining was performed on samples at day 1 to evaluate cell adhesion and distribution on the MC.

5.2.4 Co-cultured microtissue fabrication

The fabrication of hAMSC and HUVEC co-culture microtissues was investigated following two methodologies. First, *independent spinner flasks* were used to individually seed each cell type onto PLA MCs. hAMSCs were seeded in a 10^5 cells/mg MC concentration using a 250ml - Bellco Glass spinner flask, with a final total volume of 100 ml, whereas HUVEC were seeded in another identic spinner flask in a 186.666 cells/mg MC concentration with 50 ml as final volume. After 6h of intermittent agitation (3 min at 30 rpm, 27 min at 0 rpm), colonized MCs from both spinner flasks were collected and transferred to non-adherent 24-well plates. Microtissues with HUVEC-MC, hAMSCs-MC and both HUVEC-MC and hAMSCs-MC 1:1 in the same well were produced. All wells contained 1.5 mg MCs. Co-cultured microtissues were grown using a 1:1 mixture of the individual mediums (co-culture medium). Medium was replaced every 2-3 days.

In the second methodology, hAMSCs-MT were initially prepared with PLA microcarriers, following the same spinner flask procedure and then transferred to 24-well plates in a 1,5 mg MC/well concentration. Then after 1 week of static microtissue formation, 150.000 HUVECs were seeded on top. In that precise moment, medium was changed to co-culture medium, and replaced every 2-3 days.

5.2.5 Vital staining for microcarrier colonization

After spinner flask microcarrier inoculation, and prior to transferring into 24-well plates for the static microtissue formation, two samples were taken. HUVEC-MC and hAMSCs-MC attachment was evaluated by vital staining using Calcein-AM (Thermo Fisher). Procedure followed as explained in Chapter 3, section 3.2.7.

5.2.6 Total DNA proliferation

Cell proliferation in microtissues was assessed quantifying total DNA using Quant-IT Picogreen double-stranded DNA assay kit (Invitrogen), following the same procedure as in Chapter 4, section 4.2.6.

5.2.7 Scanning electron microscopy

Scanning electron microscope (NOVA NanoSEM 230, FEI Company) was used to evaluate microtissue morphology as explained in Chapter 3, section 3.2.8. Fixed and dried samples were carbon sputtered prior to examination at the Platform of Nanotechnology of IBEC, Barcelona.

5.2.8 Flow cytometry

To assess the proportion of each cell type in the CoC-MT, a flow cytometry (FC) analysis was performed. Cells were firstly removed by incubating with trypsin-EDTA (Sigma-Aldrich) (10mM in DPBS) for 5 minutes at 37ºC. Then, microtissues were carefully disrupted with a pipette tip. and passed through 100 µm nylon mesh strainers (BD Biosciences) to separate the cells from the carriers. Afterwards, cells were centrifuged (300g 5 min) and resuspended in 0,5% BSA. Next, primary antibody incubation against human CD31 conjugated with APC (MACS, Miltenyi Biotec) was performed in a dilution of 1:11 for 10 minutes. Cells were washed, centrifuged and fixed in 1% paraformaldehyde (Electron Microscopy Sciences). HUVEC and hAMSCs trypsinized from monolayer cultures were used as controls for CD31 staining, positive for the first cells and negative for the later. hAMSCs expressing RFP could also be determined by FC without the addition of extra antibodies. CytoFlex Flow Cytometer Platform (Beckman Coulter) was used from the Flow Cytometry facility at the CCiTUB, Barcelona.

5.2.9 In vivo subcutaneous implantation

Dorsal subcutaneous implantation was performed in 6- to 8-week-old SCID mice purchased from Harlan Laboratories. Animal work and facilities were located in IQAC-CSIC, Barcelona, in the group of Cellular Therapies from Jerónimo Blanco, incollaboration with Dr. Cristina Garrido. Animal maintenance and experiments were

performed following the established guidelines of the "Direcció General del Medi Natural" from the Catalan government. Previously to implantation, animals were anesthetized with intra peritoneal injections of 0.465 mg/kg xylazine (Rompum; Bayer DVM) and 1.395 mg/kg ketamine (Imalgene; Merial Laboratorios). Two individual dorsal incisions (1cm) were excised in the middle of the back, at a symmetrical distance from the spine. By introducing the tip of the dissecting scissors, a pocket was created between the skin and the muscle. Using a spatula, 1week old hAMSC-MT and Co-culture-MT, after 1 day of HUVEC implantation, were individually introduced, placing one MT type in each subcutaneous pocket. Each mouse received two different microtissues, and the incisions were finally closed by suture. After 3, 7 and 14 days, mice were anesthetized for the retrieval of MT and euthanized. MT were investigated by non-invasive bioluminescence (BLI) signal while implanted, and by immunofluorescence imaging and histological staining after MT retrieval.

5.2.10 Bioluminescence imaging

For the *in vivo* hAMSC behaviour, monitored by non-invasive bioluminescence imaging, 150 µl of coelenterazine (0.1 ng/ml) in saline serum were intravenously administered. Images were immediately acquired. Light events were recorded and added by arrays of 4 x 4 adjacent pixels (binning 4 x 4) or exceptionally in binning 1 x 1, activating the Electron Multiplier (EM) function of the CCD camera ImagE-MX2 Hamamatsu Photonics system. Images were taken on days 1, 3, 7, 10 and 14 and analysed using Hokawo 2.6 software from Hamamatsu Photonics (Deutschland GmbH). Results were expressed as photon counts (PHCs) after substracting the background. Arbitrary colour bars representing standard light intensity levels were used to generate images.

5.2.11 Immunofluorescence

Implanted MT were extracted at specific time points by excising skin near to the implantation site. Then, samples were fixed in formalin solution (Sigma-Aldrich) overnight and subjected to different gradients of sucrose solution (10%, 20%, 30%). Similarly to the procedure in Chapter 4, section 4.2.9. OCT-embedded microtissues were frozen and cryosectioned in 10µm slices using Leica CM3050 S Research Cryostat (CCITUB). For immunofluorescent analysis, CD31 primary polyclonal antibody was used (Abcam ab28364), with Alexa 488 secondary antibody against rabbit (also from

Abcam, ab150081). Zeiss LSM780 confocal microscope from the IBMB-CSIC Molecular Imaging Platform was used to take images.

5.2.12 Histologies

Sectional histologies were performed by the Histopathology facility at IRB Barcelona. OCT embedded microtissues were cryosectioned in 5µm thick slices and carefully stained with haematoxylin and eosin. Moreover, CD31 immunohistochemistry was performed with DAB, avoiding organic solvents and excessive temperature to avoid PLA degradation. CD31 positive regions were analysed using QuPath software.

5.2.13 Perfused bioreactor

A perfused bioreactor containing a transparent chamber (PD3, Ebers Medical) was used to monitor macrotissue assembly and decellularization. The perfusion system consisted in a medium reservoir placed in a 37ºC heated bath, connected to a peristaltic pump and the transparent chamber, which was located inside an imaging compartment of a Hamamatsu Photonics ImagEM X2 System equipped with a C9100-23B camera. The perfusion system was mounted in sterile conditions, and 100 ml of aDMEM growing medium were added to the reservoir. Prior to the introduction of MTs, medium was pumped through the circuit at 30rpm. Then, ten hAMSC-MT were incorporated inside the transparent chamber, which was previously adapted with a nylon mesh (0,45 µm pore size) to confine microtissues and avoid free flowing through the circuit. Medium flow was kept constant during all the culture. For the visualization of cells using BLI, Rluc substrate Benzyl-coelenterazine (PJK GmbH) was added to the culture medium at a concentration of 2ug/L. Bright-field images were also taken to lately superpose BLI signalling. Several imaging captured BLI emitted photons until substrate consumption led to a decrease in the signal. Peak emission was considered for quantification in each time point.

MTs were kept in continuous perfusion for 13 days, when finally a decellularization solution was applied to the system. 1% Triton X-100 with 0,1% NH_4OH solution in PBS was added overnight for decellularizing. Next, medium was replaced by PBS to completely remove decellularization solution, and coelenterazine was added to evaluate remaining living cells.

5.3 Results

5.3.1 HUVEC adhesion to PLA microcarriers in static conditions

HUVEC cellular adhesion to PLA MCs was firstly evaluated in static conditions. As a control for good attachment the same procedure was evaluated with Cultisphere S gelatine MCs. Although total DNA concentration demonstrated similar levels of attached cells on day 1 for both MCs, calcein staining showed poor cell distribution on PLA MCs (*Figure 5.1*), and when culture was prolonged for 7 days, HUVEC proliferation was only sustained by Cultisphere, but no PLA.

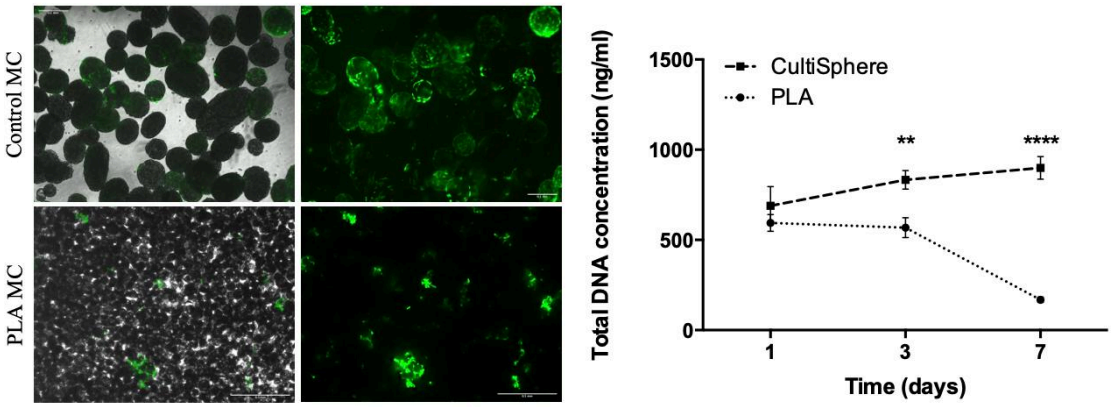

Figure 5.1 HUVEC static seeding on PLA and Cultisphere S (control) microcarriers. On the left, microscope images of living cells (calcein vital staining) showing cell adhesion and distribution on microcarriers after 1 day of culture. On the right, DNA concentration on control and PLA MC. After 3 and 7 days of static culture, control MC were able to sustain cell proliferation, whereas PLA MC could not. (**p value ≤0.01, **** p ≤0.0001).

5.3.2 Co-culture microtissue formation by independent spinner flasks

Although HUVEC cell distribution was not satisfactory on PLA MCs when seeding in static, DNA suggested that similar amounts of cells were present for both MCs after one day. In light of these results, we decided to implement dynamic spinner flask seeding to enhance cell distribution. At the same time, and in order to avoid physical competence, we decided to carry on independent spinner flasks for hAMSC- and HUVEC-MC colonization. After using same conditions, colonized microcarriers were evaluated with vital staining, and better cell adhesion was observed for hAMSCs to PLA. (*Figure 5.2*). HUVEC cell adhesion seemed to be weaker due to the spherical cell appearance and the formation of cellular aggregates, suggesting inadequate attachment. Nevertheless, MCs were transferred from spinner flask to non-adherent 24-well plates, obtaining co-cultured microtissues by mixing hAMSC-PLA and HUVEC-PLA microcarriers (1:1). At the same

time, hAMSCs-PLA MT and HUVEC-PLA MT were also produced. During microtissue formation, cell proliferation was observed at the end of the culture for hAMSC-MT and CoC-MT but not for HUVEC microtissues alone (*Figure 5.3*, A). Macroscopically, HUVEC MT were not properly assembled, correlating with the small amount of DNA found by day 16. Confirming HUVEC-PLA MCs attachment was not suitable for MT formation.

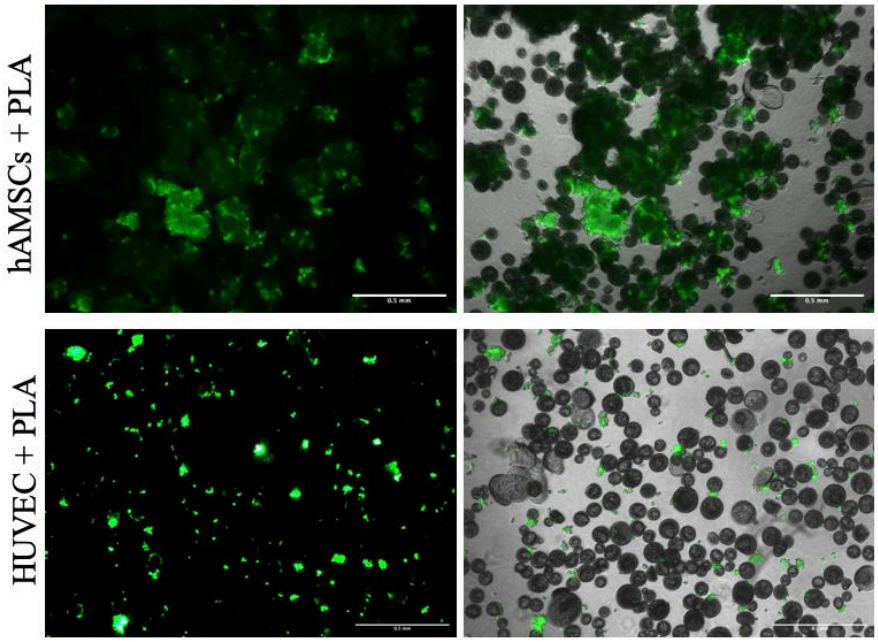

Figure 5.2 Vital staining of hAMSCs and HUVEC cells seeded on PLA microcarriers in spinner flask bioreactor. Intermittent agitation regime was applied for 6 hours. Samples were taken at the end of the dynamic inoculation.

After these results, we wanted to evaluate the presence of HUVEC in the CoC-MT. Therefore, immunofluorescence staining and FC assays were performed. CD31 or platelet endothelial cell adhesion molecule (PECAM-1) was used as a marker for HUVEC. Immunofluorescent images evaluated at day 16 of the co-culture showed CD31 diffusive signal and some intense points, as well as, irregular cytoskeleton rearrangement of cells. Actin morphology was both spread (arrowheads) but also rounded (dotted arrows) suggesting some cells were dying (*Figure 5.3*, B) . Intense CD31 signal points were close but did not correspond exactly to rounded cytoskeleton structures thus suggesting unspecific expression. All in all, HUVEC presence could not be confirmed.

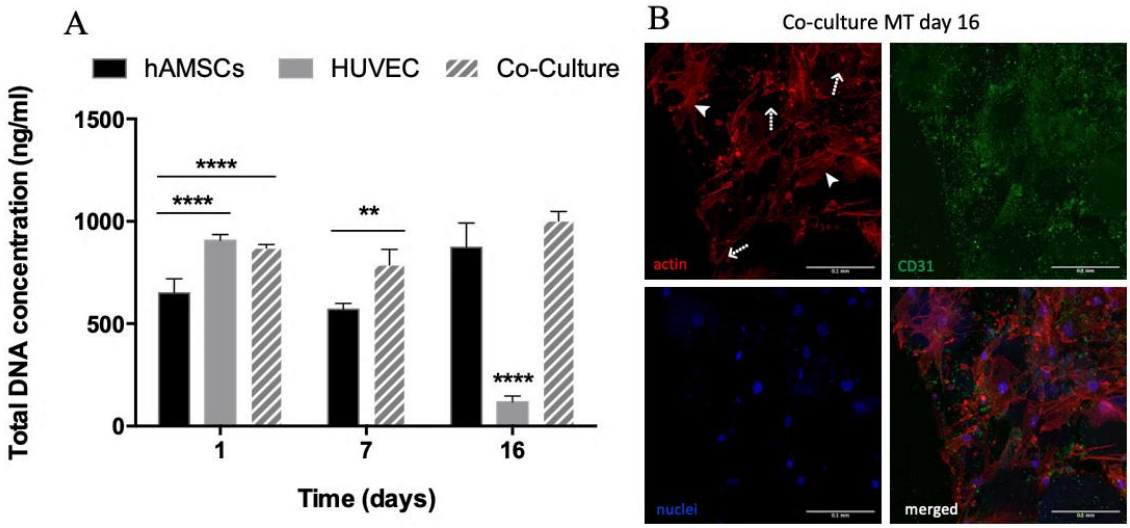

Figure 5.3 Co-culture MT evaluation. (A) Total DNA quantification of MTs obtained by dynamic microcarrier seeding, and static proliferation. hAMSCs MT, HUVEC MT and Co-culture microtissues were investigated for 16 days. At each time point, MT were collected and assess with Picogreen Total DNA quantification. Significant differences were assessed by Two-way ANOVA, and Sidak's multiple comparisons test. (**p≤0.01, ****p≤0.0001). (B) Immunofluorescence examination of Co-culture microtissues at day 16.

Additionally, cells harvested from 16-day-old MTs were taken to FC analysis. As control, HUVEC growing in monolayer were positively identified with CD31-APC antibody (*Figure 5.4*, A), and genetically modified hAMSCs were constitutively expressing RFP, therefore they were identified for that fluorescent wave length (*Figure 5.4*, B). When harvesting cells from hAMSC-MTs, 24.01% of cells were positively expressing both CD31 and RFP proteins (*Figure 5.4*, D), contrarily to what they did on monolayers (2.56%). However, when harvesting cells from CoC-MT, no sign of HUVEC or CD31-exclusively expressing cells was found (0.02%), and cells expressing both CD31-APC and RFP decreased to 5.13% (*Figure 5.4*, E). These results, which are in concordance with the immunofluorescent images, suggest that the production of a CoC-MT by seeding cells separately on PLA MCs was not successful, as no HUVEC cells were found after 16 days.

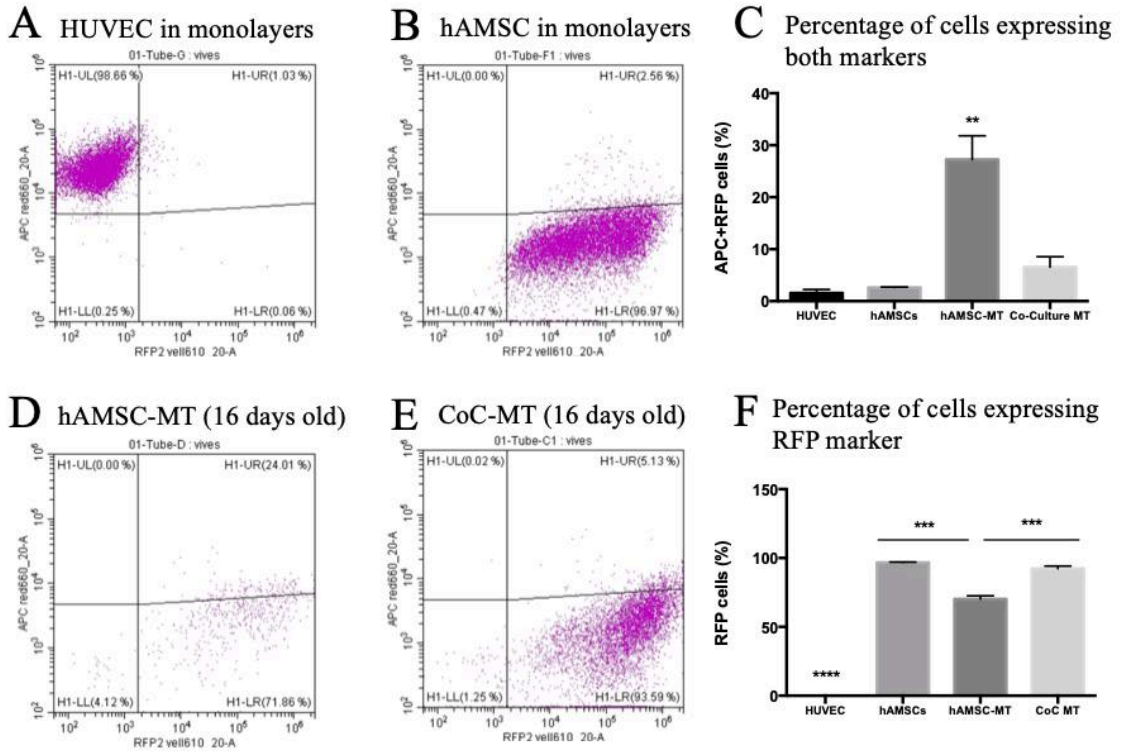

Figure 5.4 Flow cytometry analysis of cells in MTs. (A) HUVEC grown in monolayer with CD31-APC antibody staining. (B) hAMSCs constitutively expressing RFP in monolayer culture. (C) Percentage of cells expressing both markers CD31 conjugated with APC, and RFP. The percentage of cells expressing both makers in the hAMSC-MT was significantly higher than in any other conditions. (D) hAMSCs cells harvested from hAMSC-PLA MTs after 16 days of culture. (E) CoC-MT after 16 days. (F) Percentage of cells expressing RFP marker alone. As expected, HUVEC in monolayers were not expressing RFP at all. Elevated percentage of RFP-expressing cells in the CoC-MT suggested low or void present of HUVEC. Statistical evaluation was performed by one-way ANOVA with Tukey's multiple comparisons test with a p value of ** $p \leq 0.01$ and *** $p \leq 0.001$.

We hypothesized that the differential CD31-co-expression of hAMSCs was influenced by the environment. Cells growing on MCs showed increased CD31 cytoplasmic co-expression (24.01%) compared to cells harvested from monolayer (2.56%). When medium was replaced to co-culture medium in MTs, CD31 co-expression decreased (CoC-MT, 5.13%). To further estimate the influence of the different culture mediums on hAMSCs, these were seeded in monolayers on TCP, and kept with aDMEM medium, aDMEM supplemented with FGF (10ng/ml) and co-culture medium (1:1 aDMEM supplemented medium mixed with EndoGrow). Immunofluorescent analysis showed basal CD31 expression in the cytoplasm at day 1, but complete inhibition for all conditions at day 11 (*Figure 5.5*, A). Only, differential behaviour was observed in terms of cell proliferation, where the addition of FGF to aDMEM significantly enhanced hAMSCs replication after 7 and 11 days; and co-culture medium enhanced it even more

(*Figure 5.5*, B). These results manifest the potential effect of 3D environments in modifying cell behaviour, compared to traditional TCP.

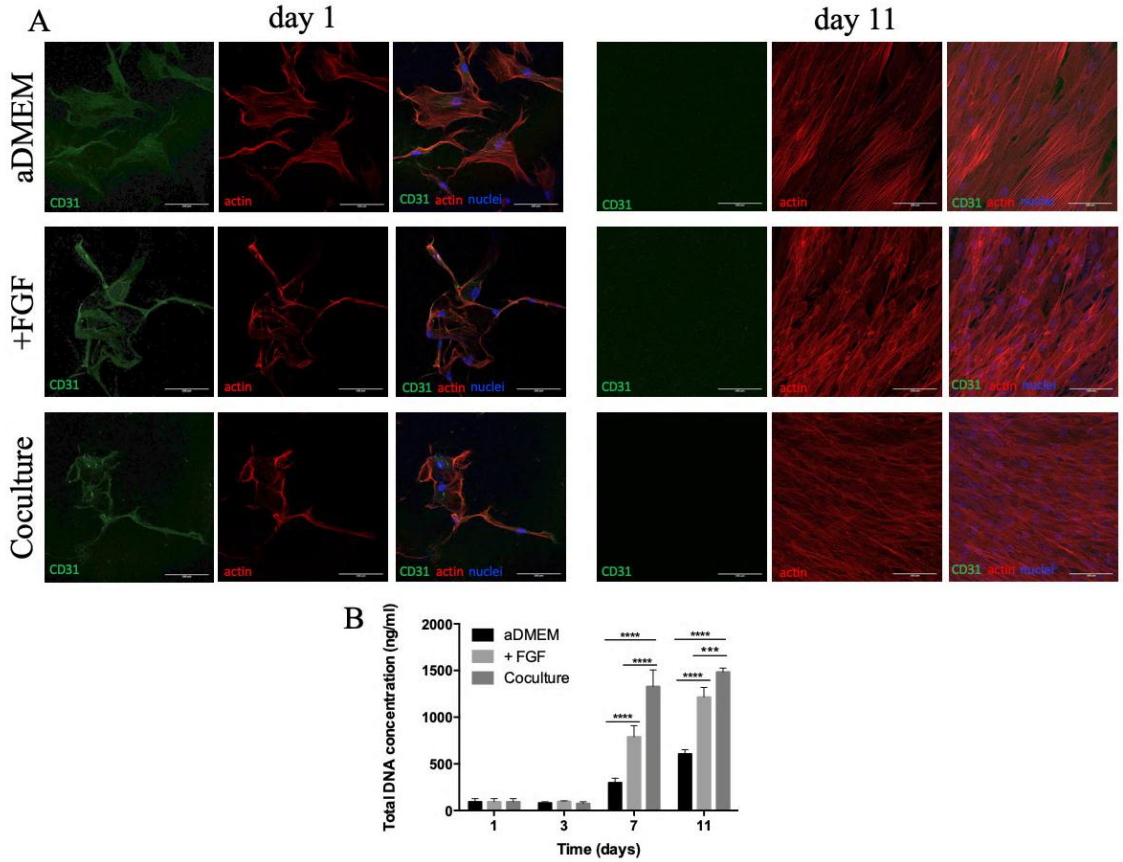

Figure 5.5 Analysis of CD31 expression of hAMSCs on TCP under different culture mediums. aDMEM, FGF-supplemented aDMEM and co-culture mediums were used (aDMEM always contained 10% FBS and 1% penicillin and streptomycin). (A) Confocal immunofluorescent images at day 1 showing cytoplasmic CD31 expression. No signal was observed after 11 days. (B) Total DNA concentration of hAMSCs cultured with the different mediums showed that after 7 and 11 days, the number of cells cultured with FGF-supplemented aDMEM and co-culture mediums was significantly higher than with aDMEM culture medium. (*** p value ≤ 0.001).

5.3.3 Initial hAMSC MT pre-formation and later HUVEC seeding

A second methodology for the obtaining of CoC-MTs was investigated. In here, hAMSCs-MT were firstly created with PLA MCs, and after one week, HUVEC cells were seeded on top. HUVEC adhesion was assessed by total DNA, immunofluorescence and FC. Total DNA was evaluated for both hAMSC-MT and CoC-MT one day after HUVEC seeding, and a significant increase was observed suggesting the presence of newly adhered cells (*Figure 5.6*, A). Analysis of MT surfaces with anti-CD31 antibody confirmed CD31-basal expression of hAMSCs in MT (*Figure 5.6*, B), confirming the previous FC results. But it also confirmed HUVEC presence on CoC-MT. CD31 was clearly found expressed on the cellular membrane, exhibiting characteristic cobblestone

like morphology (*Figure 5.6*, B). However, FC analysis for the quantitative evaluation of HUVEC and hAMSCs cells on CoC-MT showed no CD31-only-expressing cells (0%) (*Figure 5.6*, C). Similar results as those of the first FC analysis appeared on terms of cells expressing both CD31 and HUVEC marker and RFP-hAMSC marker on MT (4.21%). Nevertheless, considering the evidenced presence of HUVEC in the immunofluorescent images, we believe this FC outcome was related to the cell extraction procedure, which might have affected HUVEC cell integrity.

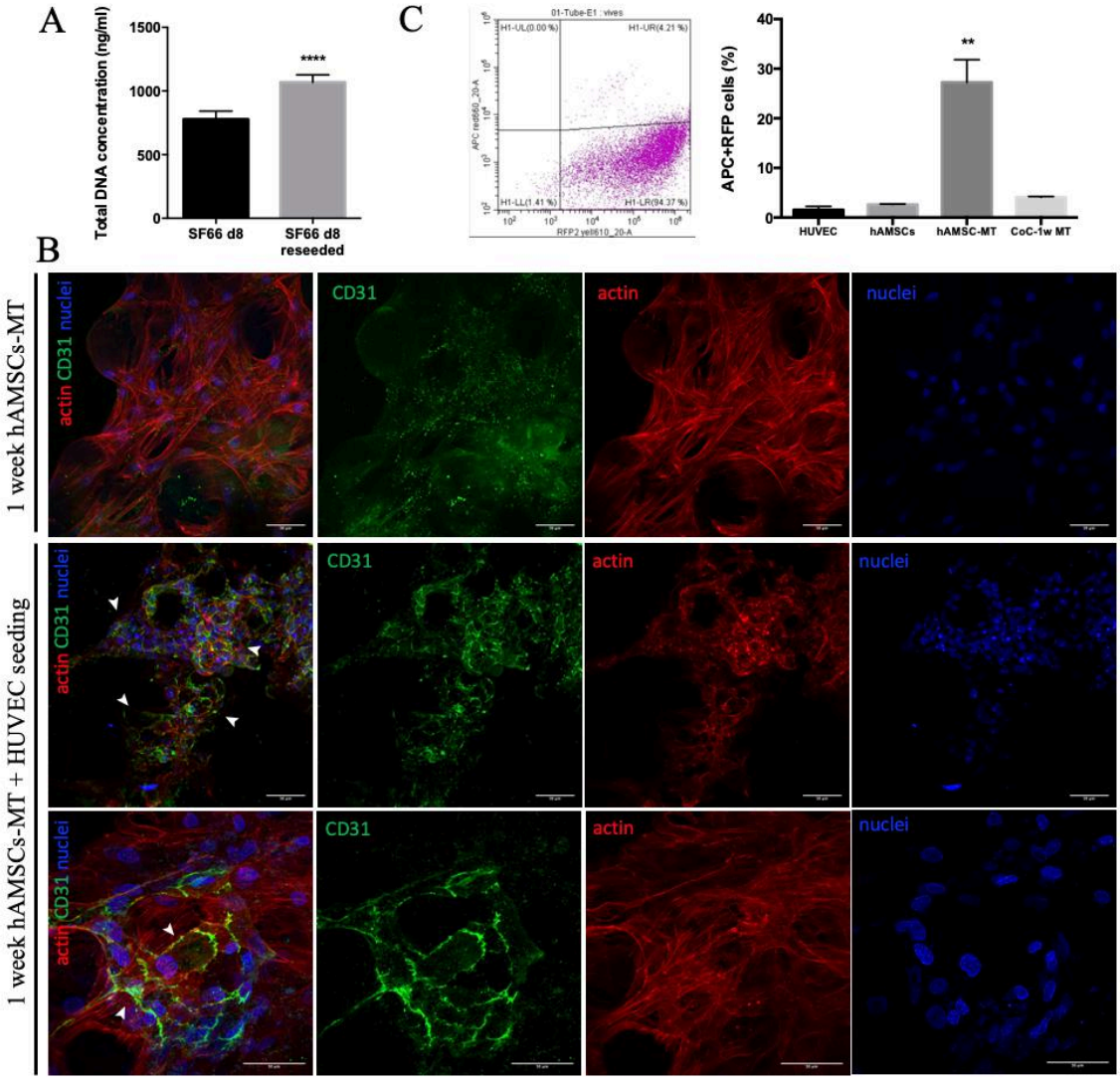

Figure 5.6 Characterization of CoC-MT obtained from the pre-formation of hAMSCs-MT and then HUVEC cells were seeded on top after one week. (A) Total DNA was quantified before and after HUVEC seeding. A significant difference with a p value smaller than 0.0001 was found. (B) Flow cytometry analysis of cells harvested from CoC-MT showed no signal for cells expressing only CD31 antibody (plot on the left), so no HUVEC cells were identified. Cells expressing both CD31-APC and RFP were shown on the graph at the right. hAMSCs cells on MT were expressing CD31 more abundantly compared to TCP. (C) Immunofluorescent analysis of MT before and after HUVEC seeding demonstrated basal CD31 expression by hAMSCs cells. However, cobblestone morphology was elucidated on top of the CoC-MT, positive for CD31, corroborating the presence of HUVEC cells.

5.3.4 Co-cultured microtissues promoted vascularization in vivo

After the confirmation of HUVEC on top of CoC-MT we decided to investigate its *in vivo* performance in favouring microtissue vascularization. For that aim, hAMSC-MT and CoC-MT were implanted on the back of 12 SCID mice. Each mouse received two microtissues, one of each type, with alternated positions (right or left). Evaluation of MT behaviour was performed blindly until the end of the analysis.

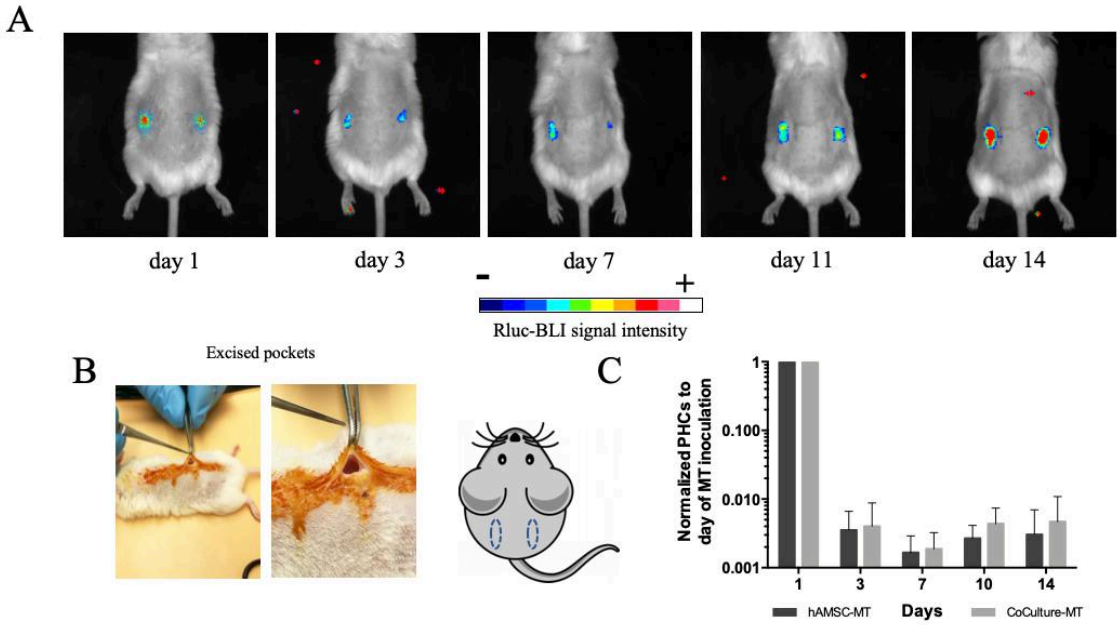

Figure 5.7 Non-invasive imaging of RLuc-expressing cells in hAMSC-MT and Co-culture-MT, subcutaneously implanted in SCID mice. (A) Representative BLI images showing Rluc activity from hAMSCs cells in MT, superimposed on black and white dorsal images of the corresponding mice. Colour bars illustrate relative light intensities (blue: low, red: high). (B) Insertion of MT in dorsal pockets. Two pockets were symmetrically excised per mouse. (C) Quantification of BLI photons (PHCs) normalized to day of implantation. No significant differences were observed.

The incorporation of *RLuc* transgene in hAMSCs allowed *in situ* and non-invasive follow up of implanted microtissues. Emitted photons recorded from BLI captures (*Figure 5.7*) showed an initial decrease during the first 7 days of implantation. Nevertheless, after 10 and 14 days, BLI increased for both MT types, although without significant differences. Bioluminescence is the product of the reaction of *Renilla luciferase* enzyme, transforming coelenterazine and oxygen. Coelenterazine, administered intravenously, arrives via blood vessel circulation towards the cells. Thus, the decrease in BLI signal corresponded to the restricted extension of blood vessel network on the MT during those days. After 10 and 14 days, BLI signal increased, and when microtissues were harvested after 14 days, extended vessel network was macroscopically observed on top (*Figure 5.8*, A). When histological sections were

examined with haematoxylin-eosin staining extensive blood vessel lumens and erythrocytes were observed on the surrounding of both MT types. Only one sample of each condition, from the four examined, presented in growth of vascular vessels stained after eosin (*Figure 5.8*, B).

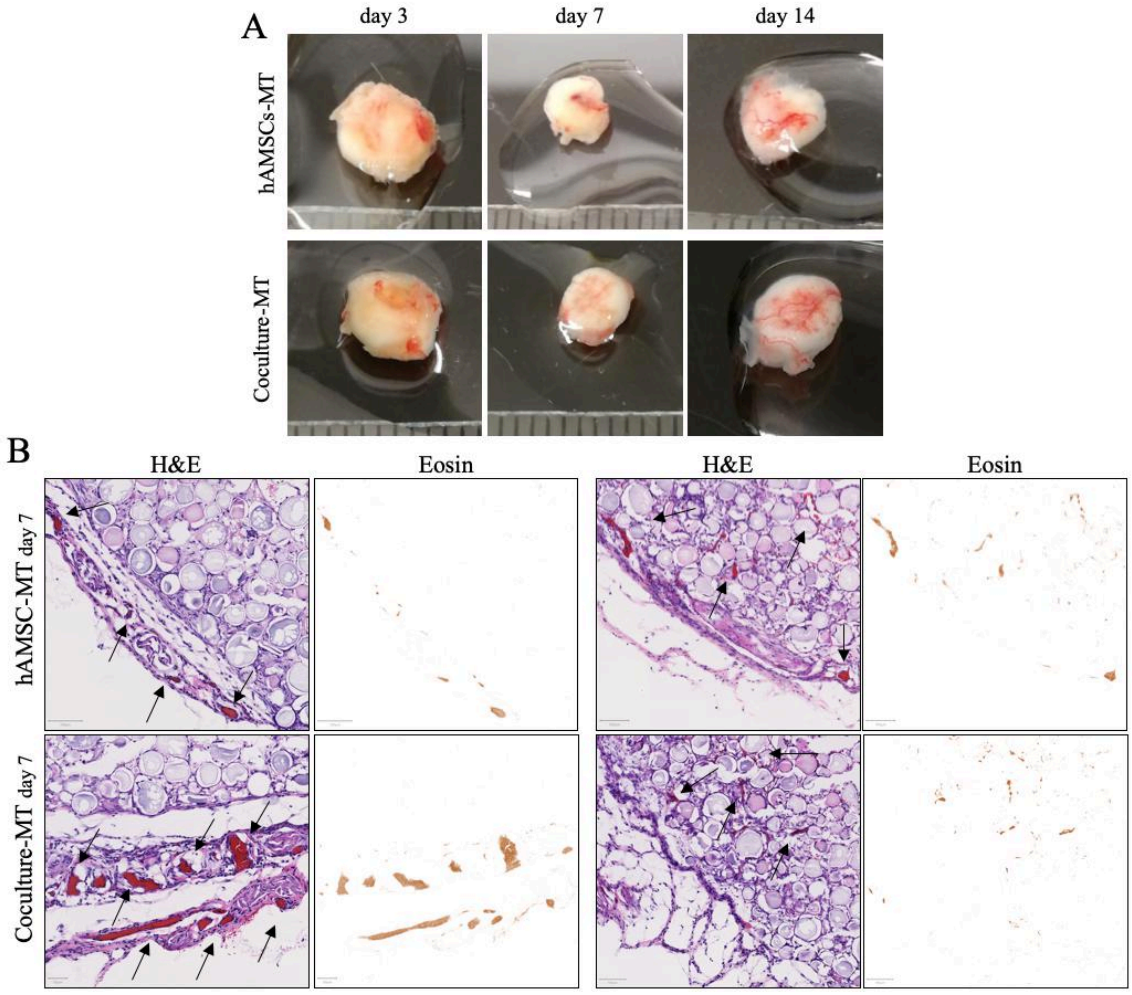

Figure 5.8 *In vivo* MT implantation. (A) Images of microtissues harvested from dorsal subcutaneous implantation after 3, 7 and 14 days for both conditions hAMSCs-MT and CoC-MT. (B) Haematoxylin-eosin staining of microtissue sections after 7 days of implantation. Eosin intense staining of erythrocytes allows the visualization of vascular lumen areas in the periphery of microtissues. From sections examined, only one microtissue of each type showed eosin positive lumen in the inside of microtissues (images on the right). Black arrows point at visible lumens.

Immunohistochemistry for CD31 on both microtissue types showed positive regions on the periphery, at 180-300 µm deep from the MT limit (*Figure 5.9*, A). Several regions resembling a tubular lumen appeared in all microtissues, however, CoC-MT presented some of them as deep as 870µm. Quantification of the CD31 positive pixels demonstrated that CoC-MT presented higher CD31 signal, however, no statistical differences were

observed after performing unpaired t-test (*Figure 5.9*, B). Immunofluorescence imaging corroborated CD31 regions with luminal morphology inside the microtissue region even after 2 weeks (*Figure 5.9*, C).

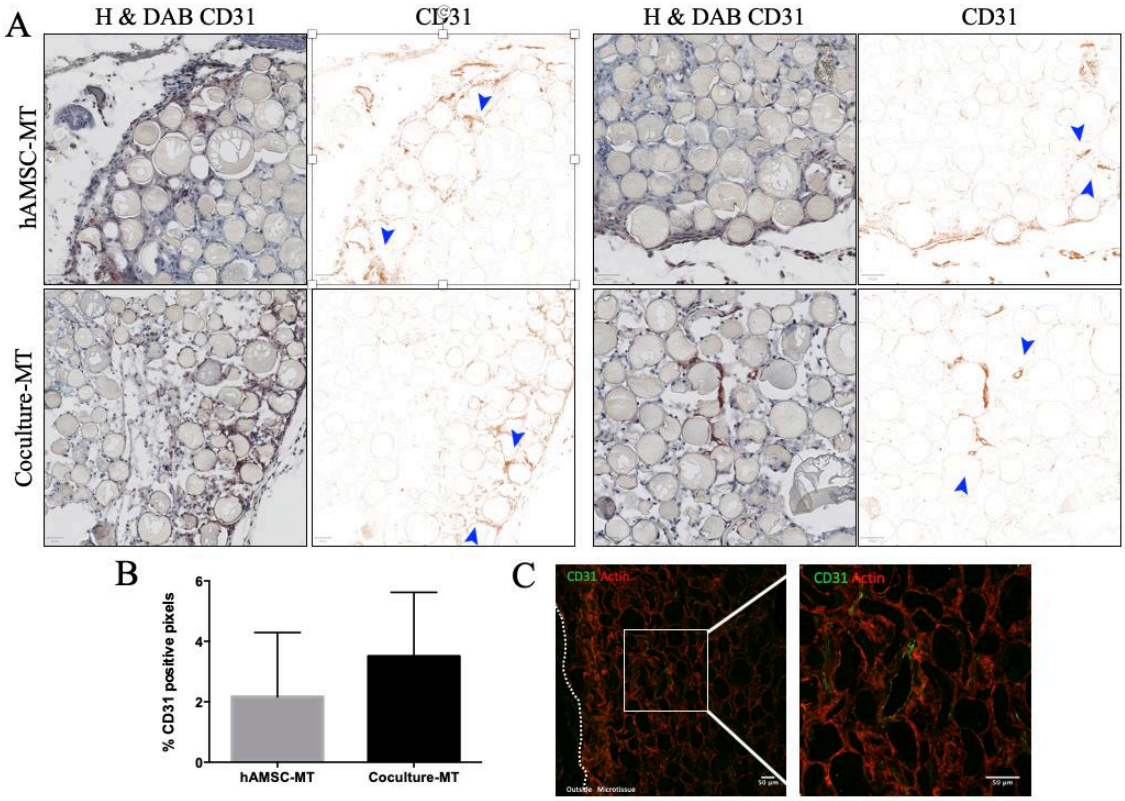

Figure 5.9 Histological analysis of implanted MT. (A) Immunohistochemistry for CD31 in microtissue sections after 7 days of implantation. Blue arrowheads point to luminal CD31 positive regions found inside microtissues. (B) Quantification of CD31 positive pixels, expressed as a percentage of all quantified pixels considering also haematoxylin-stained ones. (C) Immunofluorescence of a hAMSCs-MT after 2 weeks of implantation confirmed the presence of a CD31 regions contouring a luminal area.

5.3.5 Perfusion assisted macrotissue formation

The assembly of several MTs into a bigger construct, called macrotissue, was carried out in a perfused bioreactor. *RLuc* expression of hAMSCs was used to monitor cell performance in a proof-of-concept experiment. Several hAMSCs-MTs were introduced and confined in a transparent chamber of the perfused system (*Figure 5.10*), and at each type point, coelenterazine was introduced. Transformation of the substrate in the reaction catalysed by the luciferase enzyme, emitted photons that allowed the non-invasive and *in live* monitoring of living cells. Photon quantification demonstrated the survival and proliferation of cells inside the bioreactor, although a slight decrease was observed by day 13. Also, a decellularization protocol was here coupled, and the lack of BLI emission confirmed satisfactory cell death. Additionally, the aggregation of several MTs by the

end of the culture confirmed the initial formation of a macrotissue construct. Nevertheless, longer culture periods would be required for the complete aggregation of all the included MTs.

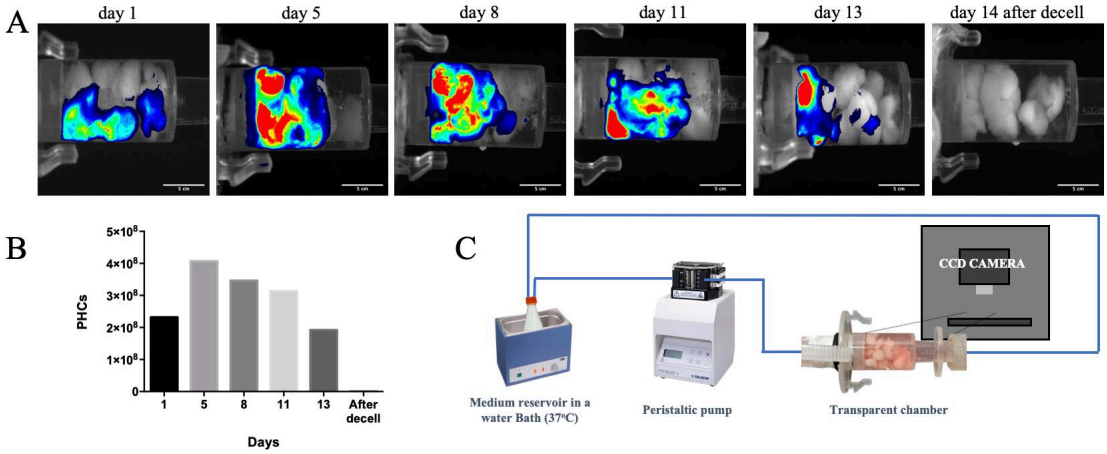

Figure 5.10 Macrotissue formation monitoring inside a perfused bioreactor. (A) Representative images of hAMSC-MTs inside a perfusion chamber. (B) BLI allowed the monitorization of cells in microtissues by the quantification of emitted photons. (C) Schematic illustration of the perfused bioreactor system consisting in a water bath where the medium reservoir is heated, a peristaltic pump, a transparent chamber to allow bioluminescent visualization, and a sensitive CCD camera to capture emitted photons.

5.4 Discussion

In this study we have investigated the feasibility of PLA MCs in the fabrication of CoC-MT for vascularization purposes. Preformation of a hAMSCs-MT facilitated HUVEC adhesion and spreading, establishing direct cell-cell contacts in a cobblestone morphology. Moreover, MC-based microtissues allowed the *in vivo* vascularization upon implantation and although differences were not significant, CoC-MT promoted higher CD31-vascular associated regions.

For the fabrication of CoC-MT, static HUVEC-MCs colonization was dismissed because of the limited homogenization and the appearance of cellular aggregates. For that reason, direct seeding of HUVEC cells in spinner flask was studied, however, not all MCs were colonized, and cells were not fully attached, resulting in the failure of the MT formation by this methodology. Adherence of HUVEC to synthetic biomaterials has always been a hurdle, and several efforts were previously made in that field (Feugier, 2005; Kaehler, 1989). A combination of fibronectin and type I collagen were proposed as the best cell adherence and spreading coatings, although the proportion of adhered cells was always low. As seen in our control condition using gelatine MCs, gelatine-coated surfaces or gelatine derived scaffolds have shown good HUVEC attachment as denatured

collagen presents the necessary cues for cell adhesion (Dikina, 2018; Kook, 2018; Zhang, 2017). In fact, Zhang *et al.* reported viable co-culture of MSC and HUVEC in the same spinner flask using gelatine MCs (Zhang, 2017). Other researchers have combined gelatine with PCL synthetic biopolymer in the creation of an electrospun nanofibrous scaffold were HUVEC and hAMSCs were satisfactorily co-cultured (Kook, 2018). Encapsulation was also demonstrated to be a good solution for HUVEC survival and cell proliferation. Dikina *et al.* and McGuigan *et al.* used collagen microspheres to encapsulate HUVEC and found good survival and cell performance for the further *in vivo* vascularization (Dikina, 2018; McGuigan, 2006). In our case, collagen type I coating was not enough for a correct HUVEC attachment, but instead, we took advantage of the *in vitro* cell-derived ECM secreted by hAMSCs on these carriers. HUVEC were seeded on top of the stable hAMSCs-MT and clear adherence and tight cell-cell contacts were here observed after CD31 expression. Previous experiments (data not shown) confirmed fibronectin, collagen type IV and laminin presence in hAMSC-MT, mimicking the native ECM environment and enhancing HUVEC cell adhesion.

Additionally, hAMSCs-MT prefabrication was considered for the introduction of perivascular-like cells in the construct. During natural vasculogenesis, endothelial cell precursors initiate the formation of lumen structures, that are lately supported by perivascular cells during maturation (Park, 2014). Crisan *et al.* described the existence of a subpopulation of human perivascular cells that expressed both pericyte and mesenchymal stem cell markers *in situ* (Crisan, 2008). That finding led to subsequent experiments demonstrating that both bone marrow and adipose-tissue derived MSCs supported HUVEC organization into prevascular-like structures when co-cultured *in vitro* (Verseijden, 2010). Thus, co-culture systems of HUVEC cells with hAMSCs may reflect the *in vivo* situation more adequately (Zhou, 2016b).

Interestingly, when characterizing the cells present in hAMSC-MT we found that hAMSCs expressed CD31, phenomena associated with the endothelial differentiation of those cells (Portalska, 2012). Culture medium used for these MTs consisted in aDMEM supplemented with bFGF, as the normal medium for their correct proliferation. As bFGF is a proangiogenic factor, we might have been inducing endothelial differentiation of hAMSCs. However, when investigating the effect of bFGF supplementation and co-culture medium in monolayers, hAMSCs did not expressed CD31 endothelial marker. In fact, initial basal expression was observed but after several days in culture, this was inhibited. Similarly, Portalska *et al.* described that under endothelial medium stimulation

(containing VEGF, FGF and PDGF), MSCs were not able to express CD31 and KDR markers, however, when combined with 24h incubation in Matrigel, the expression of those markers was triggered (Portalska, 2012). Kook *et al.* also manifested different cell behaviour in the 3D environment of PCL/gelatine electrospun fibers, where growth factors worked better due to cell interactions occurring in 3D (Kook, 2018). These observations highlight the importance of 3D environments to which cells are exposed, resembling native-ECMs. PLA MC-microtissues were able to enhance growth factor sensitivity or angiogenic potential of hAMSCs as they were providing with 3D environments. On the other hand, as CoC-MT were incubated with 1:1 mixed medium, they were exposed to lower bFGF concentration. 24h-incubation in less concentrated bFGF medium was sufficient to decrease CD31 expression of hAMSCs as seen in the decreased percentage of cells expressing both RFP and CD31 in FC analysis. It would be interesting to further characterize this endothelial-like phenotype of hAMSCs on PLA microtissues as these cells have been described to play both the role of endothelial cells that create vessels, as well as the role of pericytes that stabilize those vessels (da Silva Meirelles, 2009). In fact, endothelial-like MSC seeded on PLGA scaffolds were able to create capillary networks by their own, resulting in a higher number of vessels compared to normal MSCs (Portalska, 2012). This might explain the *in vivo* similar performance of our two MT types: hAMSCs-MT due to endothelial-like induction and CoC-MT due to the complementary contribution of both cell types.

The use of MCs for the fabrication of MTs is advantageous in the vascularization process as the inherent porosity created during aggregation between MCs facilitates vascular invasion (Zhong, 2017). Nevertheless, after the *in vivo* implantation of both hAMSCs-MT and CoC-MT in mice, only partial vascularization of the constructs was achieved. Although BLI signalling suggested the beginning of a cell population recovery after 10 days, low microvessel density was found once MTs were retrieved no matter the condition type. After histological analysis, and despite CD31 positive pixel quantification was higher for CoC-MT, both conditions had similar erythrocyte-eosin stained regions. Similarly, Lam *et al.* found that large volume implants of collagen co-cultured modules required longer periods for vascularization, and that vessels were concentrated at the periphery (Lam, 2015). Since host vessel ingrowth involves the simultaneous degradation and remodelling of the ECM, size but also density of the cell-derived ECM and the slow-degradation of PLA MCs might have delayed vascular ingrowth. Shorter MT fabrication might enhance remodelling permissiveness, although scaffold integrity should not be compromised.

Moreover, and very importantly, HUVEC correct survival must be further assessed and enhanced, since it dictates the level of graft-derived vascularization (Lam, 2015). We believe that prolonged *in vitro* cultivation of HUVEC on hAMSC-MT may lead to the creation of a stable pre-vascular network, instead of implanting right after HUVEC seeding. Another possible strategy for the improve of the vascularization of MT might involve changes in the nature of MCs. Sacrificial MCs with faster degradation rates, such as gelatine spheres (Zhong, 2017) should allow for more space inside the constructs, in an appropriate timing for host vascular invasion. Also, as a future approach, we might consider the encapsulation of growth factors, such as bFGF or VEGF in MCs and their sustained delivery to initiate vascularization steps (Brudno, 2013) or functionalize the surface of those with proangiogenic factors triggering vascular generation (Chiu, 2010). Brudno *et al* described the importance of a controlled and sequence in the delivery of specific vasculogenic factors, as the simultaneous delivery could inhibit vessel sprout. Moreover, they found that in the absence of any growth factors, PLG MC alone yielded the lowest microvessel density compared to the conditions that included specific vasculogenic growth factors (VEGF, Angiopoietin 2, Angiopoietin 1, and PDGF) (Brudno, 2013).

Finally, we have demonstrated that bioluminescence could assist macrotissue formation in a perfused bioreactor in a non-invasive manner. Perfusion enhances nutrient and oxygen transport, allowing the aggregation of bigger constructs (Chen, 2011b; Chen, 2014; Janssen, 2006). Interestingly, further experiments would include the introduction of endothelial cells in line, favouring homogeneous cell distribution (McGuigan, 2006; Vila, 2016), and, moreover, mimicking the blood fluid shear stress might achieve a more native environment for endothelial cells. Decellularization and reseeding could also be easily monitored.

5.5 Conclusions

All the efforts concentrated in the correct vascularization of engineered constructs reflect the complexity of this natural occurring process, and its importance for cell survival. The generation of hAMSCs-MT from cells cultured on PLA MCs offers vast opportunities in TE, fundamentally because of the secreted extracellular matrix. As we have found in this case, the cell-derived network of proteins has allowed the correct HUVEC seeding. Moreover, our results manifest the increased sensitivity of cells present in the MT to growth factors favouring angiogenesis. Although the strategy herein

presented was not capable of enhancing microtissue vascularization, our results offer interesting insights on what can be modified and improved for its total success.

Chapter 6

Anti-tumoral microtissue application

6.1 Introduction

Thymidine kinase expressing human adipose mesenchymal stem cells (TK-hAMSCs) plus ganciclovir (GCV) are promising vehicles for bystander therapy against tumour models in mice (Alieva, 2012; Meca-Cortés, 2017; Vilalta, 2009). TK catalyses the phosphorylation of the pro-drug nucleoside GCV. Incorporation of tri-phosphorylated GCV (pGCV), a thymidine analogue, into nascent DNA of proliferating cells results in chain termination and DNA polymerase inhibition leading to cell death by apoptosis (Okura, 2014). Bystander effect is mediated by direct cell to cell transfer of the pGCV cytotoxic agent through gap junctions (Nicholas, 2003; Touraine, 1998), by the release of pGCV in apoptotic vesicles (Freeman, 1993), and by the secretion of extracellular vesicles from TK-hAMSCs differentiated to vascular structures in the tumour microenvironment (Guerra-Rebollo, 2018). Although experimental results with TK-hAMSCs/GCV treatment are promising, the translation of this therapeutic strategy to clinic has shown limited results. After *in vivo* inoculation, the amount of TK-hAMSCs rapidly decreases, endangering the efficacy of the therapy as the quantity of therapeutic cells in the tumour area is essential.

Cell-derived ECM microtissues comprise a useful approach for bioengineering regenerative therapies (Hoshiba, 2010a; Mei, 2010; Thibault, 2013). MTs allow the implantation of functional living tissue replacements generated *in vitro* and produced by autologous cells (Atala, 2006; Lu, 2011a). In the current work we designed and produced cell-based MTs composed of TK-hAMSCs attached to biodegradable PLA MCs as described previously (Levato, 2012). PLA MCs became connected by extracellular matrix components secreted by TK-hAMSCs forming the MTs. MTs are biocompatible

and support proliferation of TK-hAMSCs. Moreover, MTs have flexible shape and size which facilitates their implantation and adjustment *in vivo*.

We explore the use of TK-hAMSCs-MTs as vehicles for bystander therapy with concomitant GCV administration against human PC3-prostate cancer subcutaneous tumour model in SCID mice. *In vivo*, subcutaneously implanted MTs were maintain TK-hAMSCs detectable longer than 42 days. The TK-hAMSCs-MTs integrated in the tissue, promoted neo-vascularization, and allowed stem cell migration toward tumour cells. TK-hAMSCs-MTs plus GCV effectively inhibit PC3 tumour growth, presenting as a promising scaffold for therapeutic mesenchymal cells.

6.2 Materials and Methods

6.2.1 Cell isolation, expansion and lentiviral transduction

hAMSCs were isolated as previously described (Vilalta, 2008) from the adipose tissue from sub-dermal liposuctions of an anonymous donor (Dr. Roca i Noguera aesthetic surgery team, Delfos hospital). hAMSCs and human PC3 prostate cancer cells (ATCC, CRL-1435) were grown in DMEM (Sigma) supplemented with 10% heat-inactivated FBS (Sigma), 2 mM L-glutamine (Sigma), 50 units/ml penicillin/ streptomycin (Sigma). Advanced DMEM (10% FBS, 1% penicillin and streptomycin, 1% L-glut) supplemented with 10 ng/ml bFGF was used to promote rapid hAMSCs proliferation as described before.

Cells were labelled using lentiviral constructs CMV:hRluc:mRFP:tTK (TK-hAMSCs) and CMV:Pluc:eGFP (PG-PC3). Lentiviral constructs were packaged in Hek-293T/17 cells (ATCC, CRL-11268), using viral envelope plasmid (pCMV-VSV-G; Addgene) and packaging construct (pCMV-dR8.2 dvrp; Addgene). For cell transduction, cells were incubated with the virions in culture medium containing 8 μg/ml polybrene (Sigma). After 48 hours fluorescent cells were sorted using an Aria^{TM} IIIFACS (BD).

6.2.2 Microcarrier preparation

PLA MCs were prepared as described in Chapter 3. Briefly, PLA dissolved in ethyl lactate was extruded through a double-pore needle applying a coaxial nitrogen flow. Droplets formed at the tip of the needle coagulate in an ethanol-water (70:30) bath with 1,5% PVA surfactant. Recombinant collagen type I was covalently attached to the surface

of microcarriers using zero-length cross-linkers (EDC/NHS). MCs were then lyophilized and kept in the fridge until use. Reconstitution of carriers consisted in drying with ethanol 70% overnight, and then progressively change solution to sterile PBS.

6.2.3 Microtissue fabrication

hAMSCs harvested from conventional T-flasks were seeded on PLA MCs using a spinner flask bioreactor with a glass ball impeller (Bellco). $1x10^6$ hAMSCs were incorporated with 100 mg MCs in 100 ml culture medium. Intermittent agitation (3 min 30 rpm and 27 min at 0 rpm) was prolonged for 6 hours and then 1,5 mg colonized MC per well were transferred to non-adherent 24-well plates. MTs were formed after 5-6 days of culture and kept until established for the different assays. bFGF-supplemented aDMEM medium was changed every two to three days.

6.2.4 TK-hAMSCs quantification (Total DNA and BLI)

TK-hAMSCs forming the MTs were quantified on days 1, 8, and 15 of culture by total DNA quantification (Picogreen total DNA quantification kit, Pierce Thermofisher) following the manufacturer standard protocol. MTs were first mechanically homogenized using an Eppendorf-tip plastic pestle in ice (as described in Chapter 4, section 4.2.6). Alternatively, cell proliferation was analysed by *in vitro* bioluminescence imaging (BLI). Coelenterazine (PJK-GmbH) was solubilized in NanoFuel solvent (Nanolight technology) following the commercial protocol (3.33 mg/ml) and stored at −80°C. For *in vitro* BLI measurements, medium was removed from the wells, washed with PBS. Immediately after the addition of coelenterazine (0.1 mg/ml) in PBS, images were taken using a detection chamber for high-efficiency ImagE-MX2 Hamamatsu Photonics system provided with an EM-CCD digital camera cooled at −80°C. Images were analysed using the Hokawo 2.6 image analysis software from Hamamatsu Photonics (Deutschland GmbH), and expressed as Photon counts (PHCs) after removing the background signal. Arbitrary colour bars representing standard light intensity levels were used to generate images.

6.2.5 Tk-hAMSC-microtissue SEM evaluation

Surface microtissue evaluation with SEM micrographs was performed following same procedure as in Chapter 3, section 3.2.8.

6.2.6 Transwell migration assay and decellularization

The effects of tumour-derived conditioned medium on stem cell migration were assessed using a transwell migration assay in a modified Boyden chamber. Cancer cell-conditioned medium was obtained after seeding PG-PC3 cells in 24-well plates at a concentration of 100000 cells/well. Upon adhesion, low-serum containing medium (DMEM 1% FBS) was added and left for 48h. Medium was recovered and filtered prior to the assay. Cell migration capacity from TK-hAMSCs-MT and from re-seeded MTs was assessed. For the later condition, MT decellularization was performed after 8 days of culture using 1% Triton X-100 in a 0.1% ammonium hydroxide (NH_4OH) solution and applying a DNase I treatment for 30 min (30 µg/ml, 37ºC). Recellularization with 50000 TK-hAMSCs/MT was followed after intensive PBS washings, and kept for one week before the assay. Moreover, TK-hAMSCs-MT and recellularized-TK-hAMSCs-MT were incubated with AMD3100 (20 µg/ml) for 30 min prior to the migration assay.

TK-hAMSCs-MT, TK-hAMSCs-MT incubated with AMD3100, recellularized-TK-hAMSCs-MT and recellularized-TK-hAMSCs-MT-AMD3100 were placed in Corning FluoroBlok™ Cell culture inserts (0.8 um pore size, VWR) and embedded in 100 µl of Opticol™ rat tail collagen I (Cell guidance systems). Gelification during 30 min at 37ºC allowed the formation of a continuous 3D environment for migration. Then, they were covered with 100 µl of low-serum medium. Inserts were placed in the companion plates, and the lower chambers were filled with 550 µl of low-serum medium (control), PG-PC3-condicioned medium or 100 ng/ml PDFG-bb. hAMSCs were allowed to migrate for 48 h. Afterwards, cells at the bottom of the inserts were fixed in 4% PFA, and MT and collagen gel were removed from the upper chamber. Cell nuclei were stained with DAPI, and the number of migrating cells was counted using a fluorescence inverted microscope. FluoroBlok inserts shielded top chamber cells fluorescent signal, allowing a more accurate quantification of migrating cells.

6.2.7 In vivo TK-hAMSCs-MTs plus GCV treatment against subcutaneous PG-PC3 tumours

TK-hAMSCs-MTs were subcutaneously implanted on the back of five SCID mice (four TK-hAMSCs-MTs/mice). *In vivo* TK-hAMSCs behaviour was monitored by non-invasive BLI. Images were acquired immediately after intravenous administration of 150 µl of coelenterazine (0.1 mg/ml) in saline serum, by adding together the light events

recorded by arrays of 4 × 4 adjacent pixels (binning 4 × 4) or exceptionally in binning 1 × 1; and activating the Electron Multiplier (EM) function of the CCD camera. Images were taken on days 0, 3, 7, 11, 14, 18, 27, 32 and 42 after TK-hAMSCs-MTs inoculation.

First, animals were anesthetized by intraperitoneally injections of xylazine (Rompum®, Bayer DVM) 0.465 mg/kg and ketamine (Imalgene®, Merial Laboratorios) 1.395 mg/kg. PG-PC3 (5×10^5) were subcutaneously inoculated at the back (anterior position) of SCID mice (n = 12). On the 6^{th} day after tumour inoculation TK-hAMSCs-MTs were implanted next to the tumour (n = 9) and 24 h later mice were treated intratumorally either with 200 µl saline serum (n = 4) or 200 µl GCV (Cymevene®, Roche; 10 mg/ml) (n = 5). Controls were considered as PG-PC3 tumour-bearing mice not receiving any treatment (n = 3). Tumour progression was weekly monitored by *in vivo* BLI. Images were acquired 15 minutes after i.p. injection with 150 µl of luciferin substrate (16.7 mg/ml). D-luciferin (Regis Technologies) stock solution was prepared at a concentration of 16.5 mg/ml in PBS and stored at −20°C. Tumour volume (evaluated by calliper measuring in three diameters) was calculated with the following formula: $L \times H \times W \times \pi/6$ (L: length, H: height, W: width) (Richtig, 2004).

6.2.8 Histologies

After euthanizing the animals, TK-hAMSCs-MTs were harvested and washed with physiological serum and fixed with formalin solution for 24 hours, immersed in 10%, 20% and 30% of sucrose (J.T. Bakers) solution to cryoprotect the tissues, and then embedded in O.C.T (Tissue-Tek). Fixed tissues were sliced in 5-10 µm sections and mounted on glass slides. DAPI (1:1000) (Invitrogen) staining was performed for detection of cell nuclei. Immunofluorescent detection of RFP+ cells was performed on the 10 µm thick sections using mouse monoclonal antibody against RFP (1:500) (ab65856, Abcam) and Alexa 647 donkey anti-mouse (1:1000) (ab150107, Abcam). GFP+ cells were detected with chicken polyclonal antibody anti-GFP (1:500) (ab13970, Abcam) and goat Alexa 488 anti-chicken (1:1000) (ab150169, Abcam). Endothelial cells were labelled using rabbit anti-CD31 (1:500 dilution) (ab28364, Abcam) and secondary goat anti-rabbit antibody, conjugated with Alexa Fluor 488 (1:1000) (ab150081, Abcam). Also, 5 µm-sliced samples were stained with haematoxylin-eosin at the Histopathology facility at IRB Barcelona.

6.2.9 Statistical analysis

GraphPad Prism 5 Software was used for the statistical analysis of BLI data. When data could be adjusted to a normal distribution the T-test was applied for 2 group comparisons, one-way Anova for more than two groups, and two-way Anova to compare more than two treatment groups at different times. Statistically significant differences (*) were considered when $p \leq 0.05$.

6.3 Results

6.3.1 Tk-hAMSCs-MT production, cell quantification and viability

PLA MCs were produced as previously described in Chapter 3, by a solution jet-break up and solvent displacement method (Levato, 2012) and covalently functionalized with collagen type I. Then, luminescent (*Renilla luciferase*), fluorescent (RFP) and cytotoxic (HVS-Tk) transduced hAMSCs (Tk-hAMSCs) were seeded on PLA MCs following the same procedure as in previous chapters, in which colonization is performed under agitation parameters in a spinner flask bioreactor. Tk-hAMSCs in PLA MCs culture was extended for 18 days, and cell-derived ECM microtissues were produced (1.5 mg MCs/MT). When cultured in tissue culture plates, BLI signal emitted by *Renilla luciferase* expressing Tk-hAMSCs was quantitatively correlated with the number of cells (*Figure 6.1*).

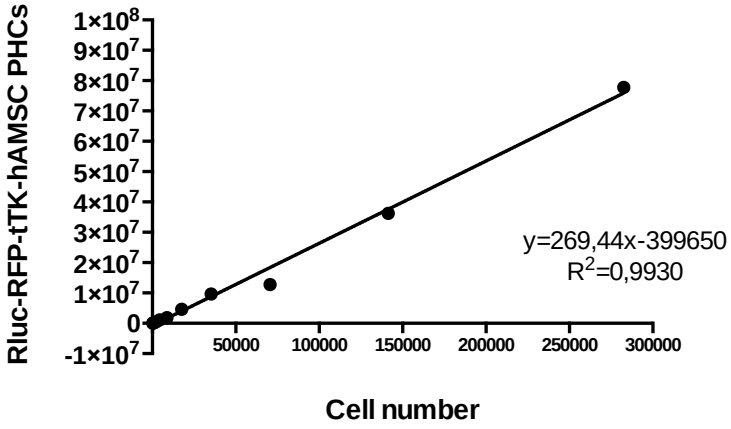

Figure 6.1 Tk-hAMSCs cells expressing Rluc. Cell quantification by total DNA and BLI signal.

For MC culture, proliferation of MT-forming Tk-hAMSCs cells was also correlated with emitted BLI signal (*Figure 6.2*, A), allowing its monitoring and quantification by

Rluc-BLI for *in vitro* and *in vivo* experimentation. Increased cell number was observed both by BLI and total DNA Picogreen assay. From day 7 until day 18 cell number was kept constant. Microtissue macroscopic morphology shifted from half-moon shape to spherical appearance as seen from day 14 (*Figure 6.2*, B).

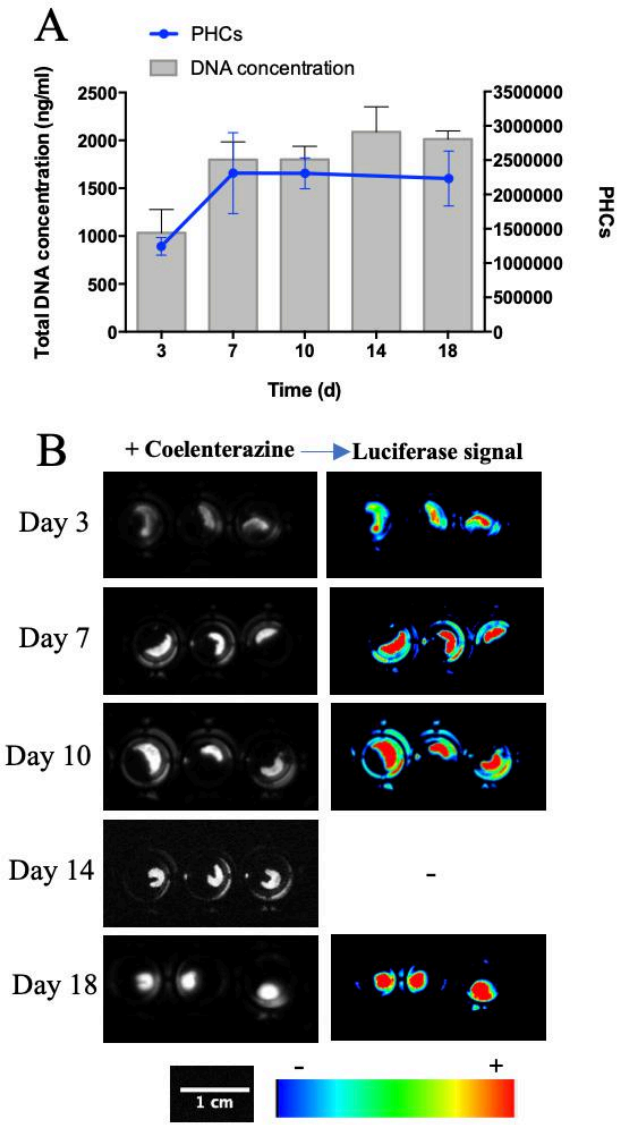

Figure 6.2 Evaluation of cell number in Rluc-Tk-hAMSCs-MT. (A) Cell proliferation on microtissues evaluated by total DNA quantification and BLI emission. Quantitative results of both measurements, showed correlated behaviour, allowing monitoring of cell number in microtissues by BLI signal. (B) Representative images from Rluc-Tk-hAMSCs-MT taken after coelenterazine addition, and luciferase BLI signal overlaid (on the right). The colour bar shows arbitrary standard rainbow colour scale used to depict light intensities (red highest; blue lowest; black no signal).

TK-hAMSCs-MTs were also evaluated using SEM imaging after one week of culture. Microtissues reached 5.5 mm long and 2 mm wide (*Figure 6.3*, A and B). At higher magnifications, spread cell morphology was observed together with a smooth surface on all the MT (*Figure 6.3*, C). Although MCs were still evidenced, cells and secreted matrix

covered most of them (*Figure 6.3*, D). Also, cross-sectional images showed dense ECM deposition in the inside of the constructs (*Figure 6.3*, E).

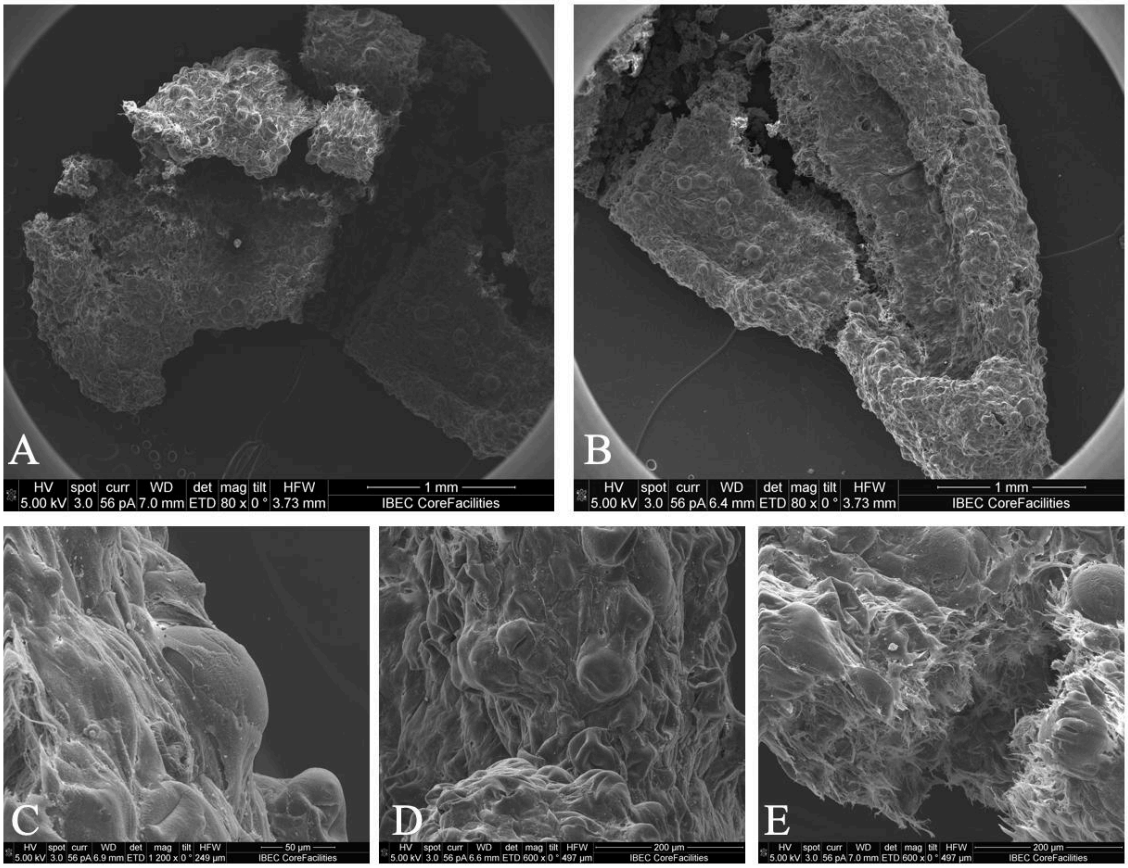

Figure 6.3 TK-hAMSCs-MT observation with scanning electron microscope (SEM) after 14 days in culture. (A) and (B) show two segments of the same MT. Dimensions of MT achieved 5.5 mm long and 2 mm wide. (C) and (D) showed smooth surface of MTs. Cells are elongated on top of microcarriers. After 8 days in culture, microcarrier silhouette could still be observed on the surface. (E) MT transversal section showing fibrous ECM deposition in the inside.

6.3.2 hAMSCs migration capacity was not enhanced when decellularizing and reseeding microtissues

hAMSCs migration capacity from microtissues towards tumour chemotactic stimuli was evaluated through a transwell migration assay (*Figure 6.4*, A). Although PG-PC3 conditioned medium yielded higher number of migrating cells than LS-medium (83 and 51 cells, respectively), no significant differences were observed. PDGF-bb potently induced mobilization after 831 cells migrated from the microtissues towards the bottom of the insert (*Figure 6.4*, B). In order to promote tropism of cells from microtissues, we decided to evaluate whether recently seeded cells in a cell-derived MT were less entrapped in the matrix, and thus more able to mobilize towards prostate cancer stimulation. For that, decellularization of hAMSCs-MTs was achieved with Triton X-

100, ammonium solution and DNase I treatment (*Figure 6.5*, A). And then, therapeutic Tk-hAMSCs cells were efficiently reseeded on top (*Figure 6.5*, B). Results after 48 h of transwell culture showed no significant increased migration compared to normal microtissues for any of the conditions (*Figure 6.4*, B). Instead, PC3 migration was decreased for recellularized microtissues.

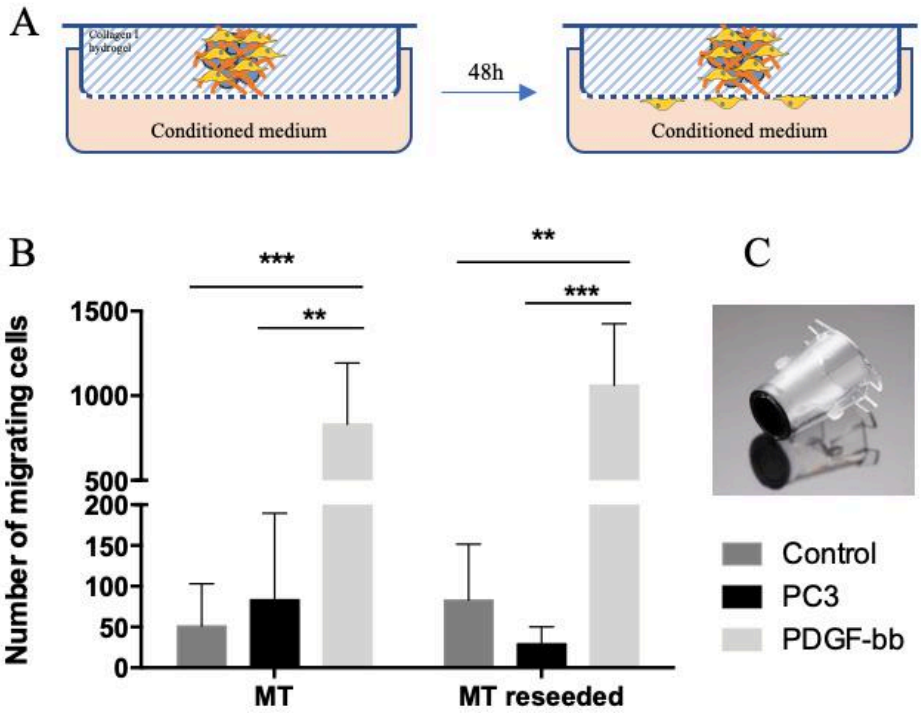

Figure 6.4 Transwell migration assay assessing therapeutic hAMSCs mobility from MTs towards PG-PC3 derived medium. (A) Schematic representation of the transwell migration assay. Upper part of the chamber (or insert), was filled with collagen type I forming gel, and MTs were embedded. Lower chambers were filled with low serum (LS)-medium, PC3 conditioned medium and PDGF-bb containing medium (100ng/ml). Migration was allowed for 48 hours. (B) Quantification of migrating cells showed significant PDGF-bb induced mobilization. And higher migration for PC3-induced medium compared to low serum, although no significant differences were observed between them. Considering decellularization and reseeding of microtissues, Tk-hAMSCs mobility capacity (compared to normal MT) was not increased. Instead, lower mobility towards PC3-medium was observed. (**p≤0.01, ***p≤0.001) (C) Image of a FluoroBlok™ insert with dark membrane to facilitate the identification of migrating cells.

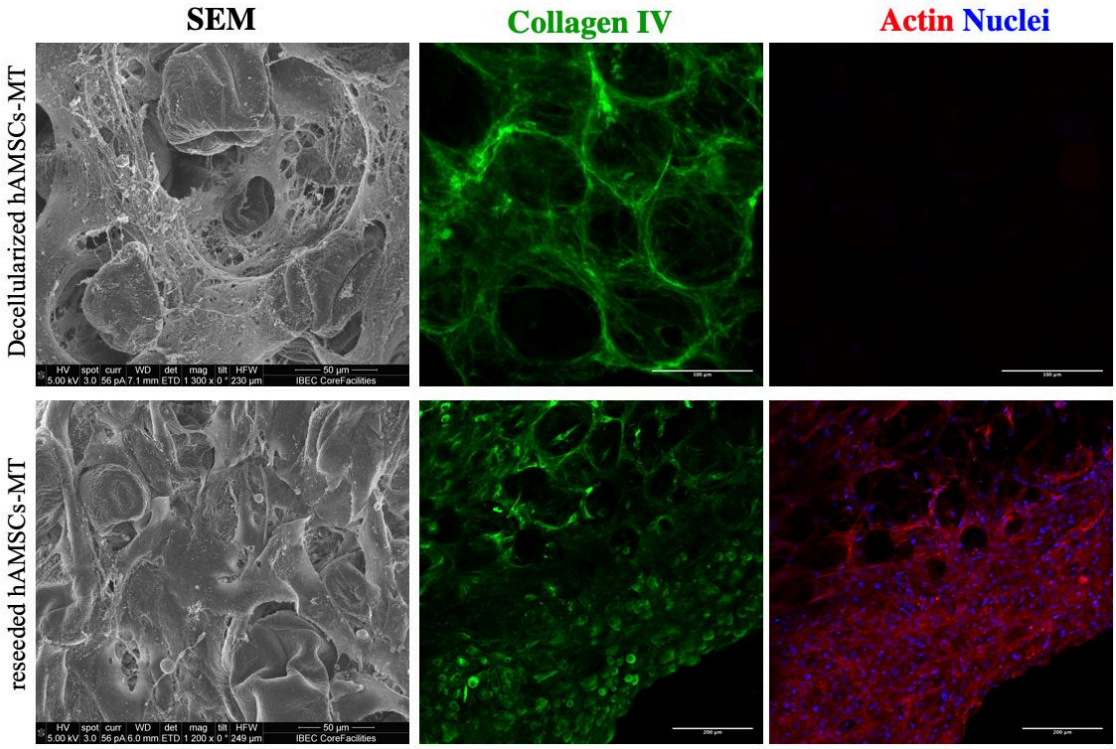

Figure 6.5 Decellularization and recellularization of hAMSC-derived MTs. First, SEM imaging showed intricate network that was left after decellularizing, which was positive for collagen IV (immunofluorescence imaging). No actin or nuclei signalling were found. Upon reseeded Tk-hAMSCs cells on microtissues, intricate ECM network was not observed, but instead smoother surface was found, in sign of cells spreading covering the matrix. Collagen type IV assessment by immunofluorescence showed network like structures, but also cytoplasmic expression on newly added cells, corroborated by actin and nuclei signal.

In light of the low mobilization efficiency from cells both in MT and after reseeding, we considered the preconditioning with CXCR4 antagonist, AMD3100. This compound blocks CXCR4/SDF-1α axis, which modulates the cell homing effect seen in MSCs niches, improving cell migration towards external stimuli. We found that 30 min AMD3100 incubation increased migration without stimuli (LS-serum condition; from 51 to 144 migrating cells), and with PDFG-bb growth factor (from 831 to 1124 cells) (*Figure 6.6*). However, hAMSC migration from microtissues towards PG-PC3 conditioned medium decreased from 81 to 59 migrating cells. Nevertheless, no significant differences were found for any of the conditions. When assessing the same effect in reseeded microtissues, AMD3100 incubation increased Tk-hAMSCs migration with PC3 (29.5 to 122 migrating cells) and without stimuli (82 to 306 cells). But had no effect on PDGF-bb migratory stimulation. Despite differences found, they were not significant enough.

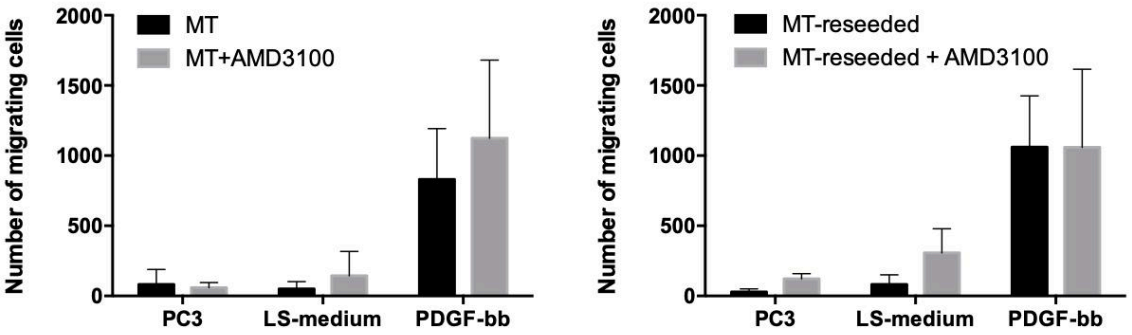

Figure 6.6 Evaluation of AMD3100 in blocking CXCR4/SDF-1α migratory axis to enhance mobility towards prostate cancer cells stimuli. Although some differences were observed after the addition of ADM3100, no significance appeared due to high standard deviation.

6.3.3 TK-hAMSCs-MTs were available up to 42 days after in vivo subcutaneous implantation

To test the availability of TK-hAMSCs *in vivo*, TK-hAMSCs-MTs were implanted in the back of five SCID mice (4 TK-hAMSCs-MTs per mice), and TK-hAMSCs were monitored by *in vivo* Rluc-BLI. On the three first days a strong cell wash-out was detected and the number of cells decreased. Later, TK-hAMSCs slightly proliferated until day 10 post-implantation, since then the amount of TK-hAMSCs decreased but were detectable at least until day 42 (*Figure 6.7*).

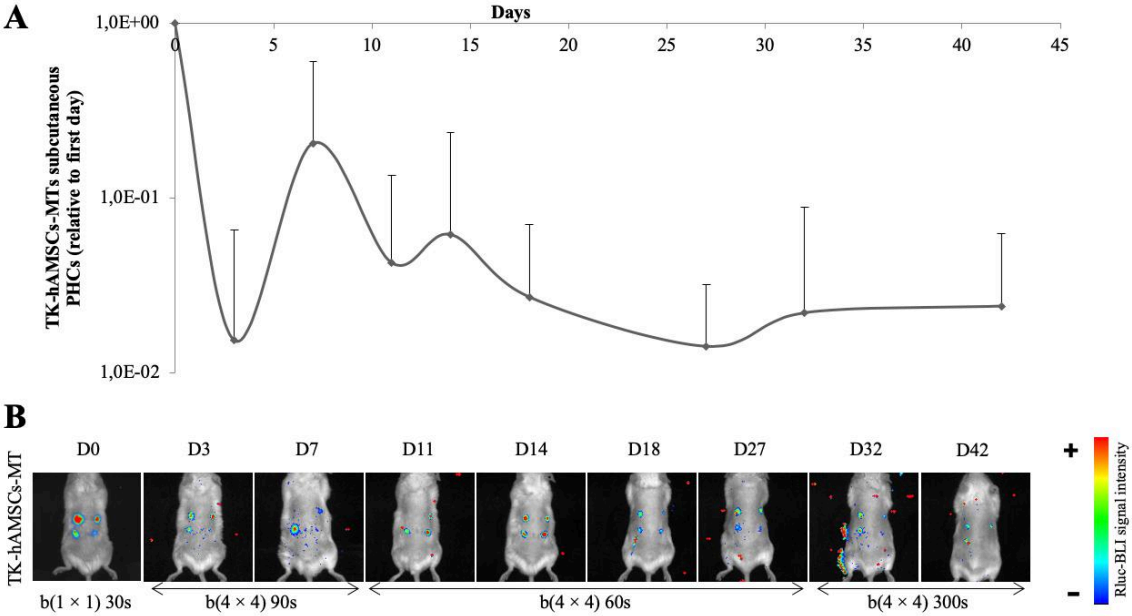

Figure 6.7 *In vivo* survival of TK-hAMSCs-MT implanted dorsally. Four MTs were implanted per mice (n=6) and monitored for 42 days. (A) BLI signal quantification related to first day of implantation. (B) Non-invasive bioluminescence signal was overlaid on the corresponding black and white images of the mouse. Colour bar indicates arbitrary standard rainbow colour scale used to depict relative light intensities.

6.3.4 TK-hAMSCs-MTs plus GCV inhibited PG-PC3 tumour progression

To test anti-tumor capacity of TK-hAMSCs-MTs plus GCV bystander treatment, PG-PC3 cells (5×10^5) were subcutaneously inoculated and six days later TK-hAMSCs-MTs were implanted in the proximity of growing tumours. Treated mice received daily intratumoral injections of 200 µl GCV (10 mg/ml) (n = 5). Tumour progression was weekly monitored by *in vivo* BLI (*Figure 6.8*, A) and compared with PG-PC3 bearing mice (control group; n = 3) or PG-PC3 bearing mice treated with TK-hAMSCs-MTs plus intratumoral saline serum injections (200 µl) (n = 4). TK-hAMSCs-MTs plus GCV bystander treatment inhibited tumour progression obtaining BLI values 2.6 times less intense (*Figure 6.8*, B) and a volume 4 times smaller than control group (*Figure 6.9*). TK-hAMSCs-MTs plus intratumoral saline serum did not affect tumour progression compared with control mice. Mice were sacrificed on day 40 after PG-PC3 cell inoculation and tumours were harvested and histologically analysed. Microtissues were strongly integrated into the subdermal surrounding tissue and blood vessels were visible on the surface of the MTs (*Figure 6.9*).

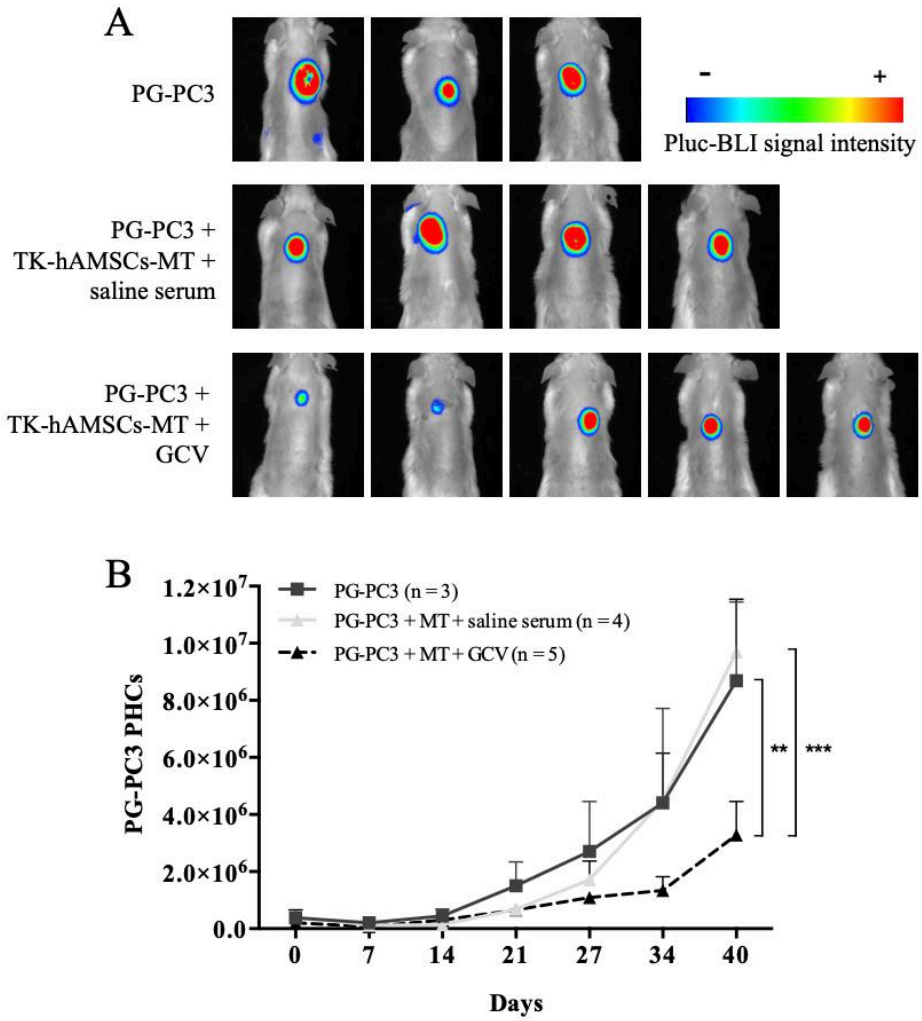

Figure 6.8 *In vivo* TK-hAMSC-Mt implantation with GCV treatment against subcutaneous PG-PC3 tumours. (A) PG-PC3 follow-up by bioluminescence imaging by PLuc BLI signal. (A) Representative BLI signal of Pluc expressing PG-PC3 cells superimposed on black and white images of the corresponding mice. (B) BLI signal quantification. Animals treated with GCV showed significantly less signal.

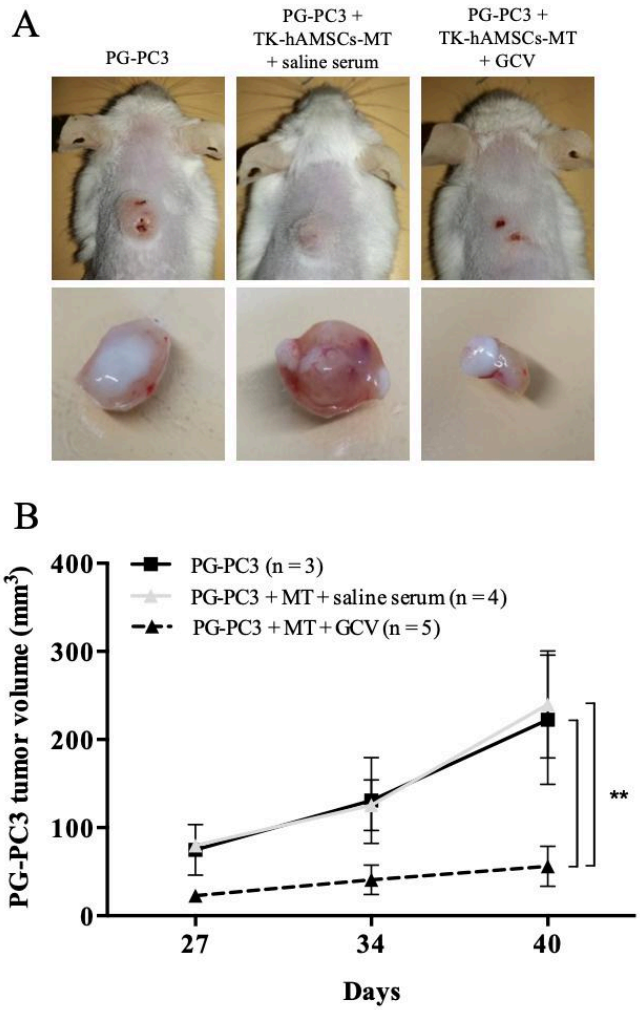

Figure 6.9 Tumour size evaluation. (A) Images of experimental animal with subcutaneous tumour and MT (except for PG-PC3 control) dorsal implantation. Down, extracted-tumour gross view. (B) Tumour volume measurements using tumour diameter and tumour height with the formula 4/3·πa2b, were a is half the diameter of the tumour and b is the tumour height.

6.3.5 TK-hAMSCs-MTs were irrigated by blood vessels and allowed TK-hAMSCs migration

PG-PC3 tumours and TK-hAMSCs-MTs were harvested after 40 days of dorsal implantation. Haematoxylin and eosin staining showed extensive vascularization in the inside of the TK-hAMSCs-MTs for both GCV and SS treated conditions (*Figure 6.10*). Eosin intrinsic affinity to erythrocytes exhibited bright red spots throughout the construct, even 1 mm inside, corresponding to vascular lumens. On the contrary, PG-PC3 tumours presented a high cellular density although erythrocyte-containing lumens were discretely found in peripheric areas (*Figure 6.11*), confirming hypoxic environments that characterize solid malignant tumours.

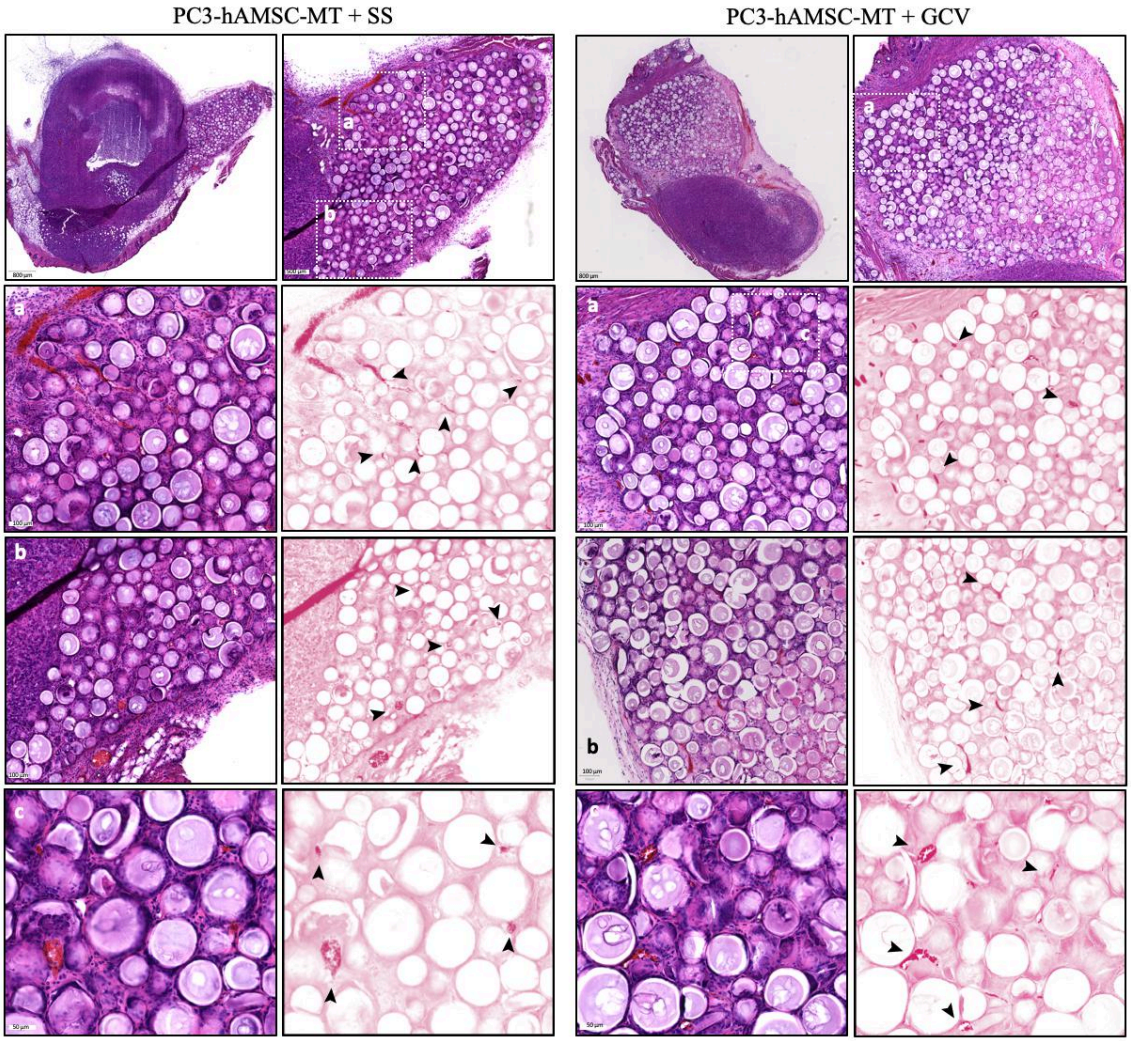

Figure 6.10 Haematoxylin-eosin histological staining of TK-hAMSCs-MT treated with saline serum retrieved after 40 days of implantation. Eosin enhanced staining of erythrocytes allows the visualization of ingrowth vessels inside the microtissues (arrowheads).

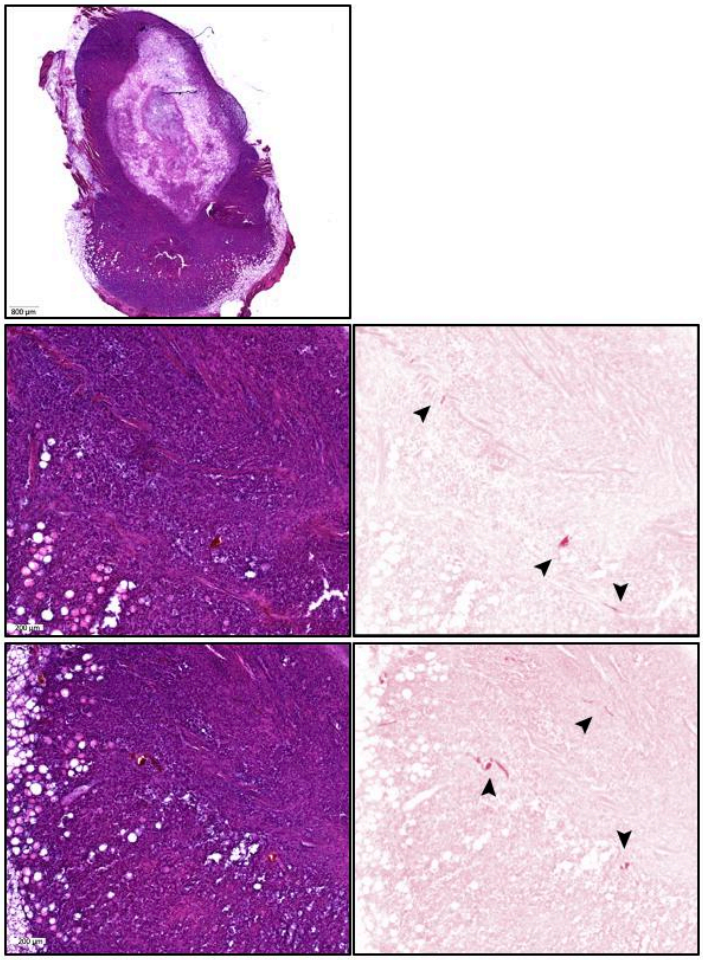

Figure 6.11 Histological H&E staining of PG-PC3 extracted tumours, after 40 days of dorsal subcutaneous implantation. Erythrocyte-positive areas were found on the outside of tumours (arrowheads), and although high cellular density was observed, little ingrowth vascularization was evidenced.

Immunofluorescent confocal imaging enabled the observation of CD31 positive cells in the inside of microtissues, conforming lumen structure (*Figure 6.12*). Moreover, immunofluorescent detection of hAMSCs with specific anti-human mitochondria antigen demonstrated cell migration towards the tumoral region, which was characterized by GFP fluorescence (Pluc-GFP-expressing PG-PC3 cells) (*Figure 6.13*). Therapeutic cell migration was observed from MT regardless the treatment (GCV and SS), demonstrating PG-PC3 potential chemokine attraction on hAMSCs. Although *in vitro* results did not confirm PC3 migration capacity (transwell migration assay), *in vivo* results clearly manifested hAMSC tropism towards tumoral cells.

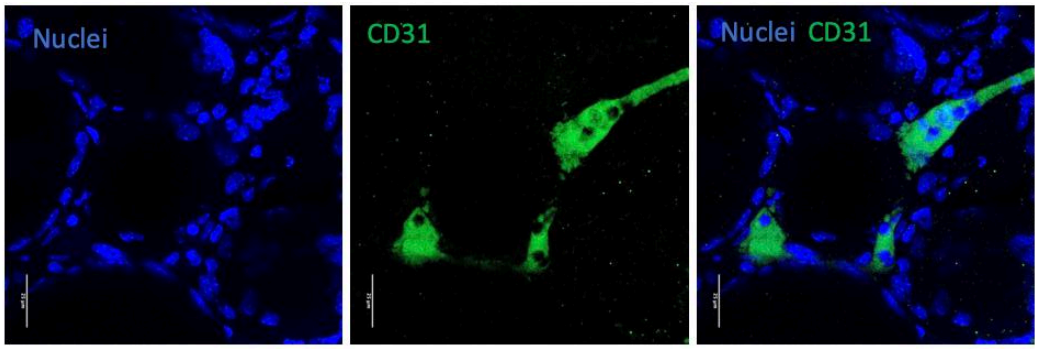

Figure 6.12 Immunofluorescence showing CD31 positive cells inside the MTs conforming a tubular lumen structure.

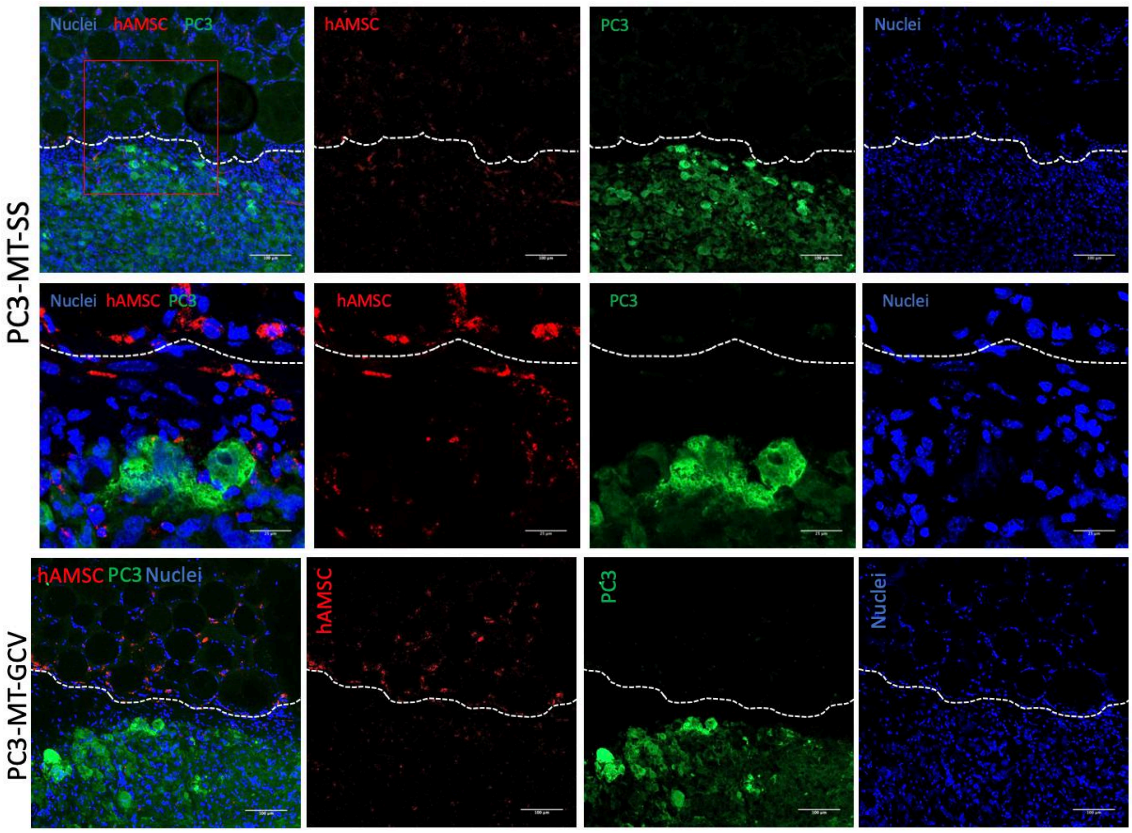

Figure 6.13 hAMSCs migration from MTs towards tumoral cells was observed using anti-human mitochondria antibody. Dashed lines show the limit of the implanted microtissues (upper side of the images), and the host tissues where the tumour cells are (lower side).

6.4 Discussion

Bystander cell based therapies including TK genes emerged as promising and sophisticated approaches against cancer progression (Moolten, 1986). The use of autologous cells as drug-delivery vehicles was previously demonstrated to be feasible (Guerra-Rebollo, 2018; Kucerova, 2007; Vilalta, 2009). However, these approaches are based in the direct administration of therapeutic cells, process that faces rapid cell

clearance, reducing therapeutic efficiency and requiring further cell inoculations. For that reason, we have developed a therapeutic cell-derived MT capable of accompanying prolonged cell retention upon implantation that remained permissive to cell tropism migration, favouring anti-tumor cell-mediated therapy. Complementing this strategy, monitoring of the therapeutic efficacy was successfully performed by *in vivo* BLI signal from both therapeutic microtissues and tumour cells.

Cell-derived ECM scaffolds have been used in several TE approaches for the regeneration of bone (Decaris, 2012; Hoshiba, 2009; Narayanan, 2009), cartilage (Cheng, 2009; Lu, 2011a), liver (Grant, 2018), skin (Schenke-Layland, 2009), vascular veins (Bourget, 2012), among others. However, little has been investigated on cell-derived ECM scaffolds for the delivery of therapeutic cells in anti-tumour approaches. Instead, a few strategies have introduced the use of hydrogels to encapsulate and retain therapeutic cells. For instance, Kauer *et al.* used polyethylene glycol diacrylate hydrogel to embed neural stem cells preventing their rapid diffusion upon implantation and allowing tropism migration towards tumour cells (Kauer, 2012). Similarly, Bagó *et al.* used a fibrin-based hydrogel to increase cell retention and enhance therapeutic effect of MSCs against glioblastoma tumours (Bagó, 2016a). We have created therapeutic cell-derived ECM scaffolds using PLA MCs. In contrast to previous studies, therapeutic cells were not embedded in hydrogels, but instead, they were themselves forming the scaffolds: cells adhered to MCs and both by proliferation and ECM deposition they synthesized therapeutic microtissues. BLI signal demonstrated the survival of therapeutic cells in MTs after 40 days of implantation, although a stepped decrease is observed during the first days. We hypothesize that the decrease in cell number was due to the restricted availability of nutrients and oxygen arriving through diffusion. Thus, subsequent BLI signal increase observed upon the 7^{th} day was the result of the vascular network growing towards the inner space of microtissues. Interestingly, Bagó *et al.* reported the use of a PLA electrospun nanofibrous scaffold in a bystander cell therapy against glioblastoma (Bagó, 2016b). Their PLA scaffold consisted in a 2D fibrous film, presenting the cells on its surface. Upon implantation, cells did not require vascularization, and thus, they did not observe any cellular loss. Instead, even after 21 days, 40% of implanted cells were still alive (Bagó, 2016b). Despite the initial cell loss, we have demonstrated the therapeutic effect of TK-hAMSCs-MT in significantly restraining tumour progression.

Bystander cell therapy occurs by different mechanisms, *i.e* by the direct cell-cell contact between therapeutic and tumour cells, release of apoptotic vesicles generated

from TK-modified cells or by the release of cytotoxic substances such as GCV phosphorylated metabolites (Van Dillen, 2002). Despite this demonstrated vesicle-mediated mechanism, the ability of hAMSC to home to tumour cells is highly relevant for the success of the bystander therapy. Although *in vitro* examination yielded low migratory capacity of hAMSCs in MTs towards PG-PC3 cells, we clearly identified hAMSCs beyond microtissue boundaries, coinciding with tumour cells. In order to increase cell mobility, alternative strategies were assessed *in vitro,* including decellularization and reseeding with therapeutic cells, and CXCR4/SDF-1α axis blocking with AMD3100. Dense ECM deposition was previously found in MC-derived microtissues, and taking advantage of this, cell-free MTs could be used for autologous cell reseeding. By this procedure, cells could be available on the surface of MTs, ready for migrating towards tumour-secreted chemokines. However, our results could not prove enhanced migration, probably due to the fact that decellularized matrix derived from MSCs still possess plenty of integrin binding sites, as well as integrated molecules that could negatively influence freshly added cells mobility (Lin 2012).

On the other hand, AMD3100 blocking of CXCR4/SDF-1α axis was previously shown to enhance stem cell mobilization from stem cell niches towards other tissues (Marquez-Curtis, 2013). CXCR4/SDF-1α axis is responsible for the homing effect of hematopoietic stem cells and mesenchymal stem cells in bone marrow. Under the influence of AMD3100, cells leave the bone marrow and enter the circulatory system, where they can achieve other tissues or they can be easily collected for subsequent autologous implantation (De Clercq, 2015). Nevertheless, SDF-1α/CXCR4 signalling is also involved in the stem cell homing to tumour tissues (Jiang, 2018). Thus, AMD3100 preconditioning could alos have antagonist effect as long preconditioning inhibits tumour tropism by blocking SDF-1α recognition (Lin, 2010; Liu, 2018). An interesting approach was able to increase cell migration towards hypoxic tumours by forcing CXCR4 overexpression, thus sensitizing hAMSCs towards SDF-1α-expressing hypoxic cells (Jiang, 2018). Although we did not tested CXCR4 expression, previous research demonstrated increased transmembrane expression of that receptor when culturing rat BM-MSCs on PLA MCs (Levato, 2015). Thus, conditioning PG-PC3 derived medium in a more realistic environment, *i.e.* hypoxia, we might obtain increased *in vitro* migration.

Particular concerns were aroused by the use of hAMSCs in bystander therapies, as the inoculation of MSCs contributed to the progression of some tumours (Hung, 2005; Zimmerlin, 2013). Nevertheless, a recent study showed innocuous effect of non-

therapeutic hAMSCs on tumour growth when included next to therapeutic TK-hAMSCs (Guerra-Rebollo, 2018). In this case however, tumour associate state (released cytokines, hypoxia, enhanced vascularization) may have contributed to the rapid vascularization of implanted microtissues, aiding in the survival of therapeutic cells.

The use of MCs for the fabrication of cell-derived MTs offers a modular approach for the obtaining of virtually any MT shape and size, with soft consistency that allows the inclusion of the TK-hAMSCs-MTs in different organs adapting to the structure of the tissue. Moreover, the choice of hAMSCs relies in their relative abundance, ease of isolation and promise for autologous cell therapies.

6.5 Conclusions

Therapeutic cell-derived extracellular matrix scaffolds prepared using biodegradable and biocompatible PLA microcarriers were here firstly reported. Delivery of HSV-TK bystander therapy against ectopic prostate tumour, successfully achieved tumour regression, prolonged cell retention and vascularization of implanted microtissues. Although hAMSCs mobility from MT was not clearly assessed *in vitro*, both *in vivo* decreased tumour volume and colocalization of hAMSCs within tumoral region, demonstrated availability of therapeutic cells from MT. This strategy was combined with BLI monitoring demonstrating feasibility of this non-invasive imaging technique to track therapeutic cell survival together with tumoral cell fate.

Chapter 7
Conclusions

Chapter 3. Study of PLA microcarrier cell seeding technique for microtissue formation

- In static conditions, MC cell seeding is not homogeneous, and a dense layer appears surrounding the MC-scaffold and the inner space is poorly colonized.
- The most appropriate MC colonization procedure for the formation of cell-derived PLA MCs microtissues is the use of a spinner flask bioreactor and intermittent agitation regime, followed by a static period with cell proliferation and ECM deposition.

Chapter 4. Cell-derived ECM scaffolds: microcarrier choice influences ECM deposition and functionality

- Cultisphere S derived microtissues are prone to express osteogenic phenotype in normal medium, but also enhance osteogenesis when directly induced.
- PLA microtissues show no spontaneous osteogenic differentiation and failed in secreting a dense extracellular matrix due to retarded cell proliferation.
- Mixed microtissues are able to maintain continuous cell proliferation, secrete an abundant ECM and promote angiogenic properties as seen in the *in vivo* CAM assay.

Chapter 5. Microtissue vascularization using a co-culture strategy

- The production of a CoC-MT by seeding cells separately on PLA MCs is not successful because HUVEC cells did not attach properly to MCs.
- Cells laden on MC deposit and extended and intricate network of ECM providing with appropriate cell-adhesion sites for HUVEC endothelial cells.

- PLA-MC microtissues enhance growth factor sensitivity and the angiogenic potential of hAMSCs when exposing them to 3D environments.
- The co-culture strategy was not capable of enhancing microtissue vascularization compared to hAMSC-MT. Nevertheless, cell-derived MT present successful peripheral vascularization.

Chapter 6. Anti-tumoral microtissue application of cell-derived MT

- Therapeutic cell-derived ECM scaffolds prepared by TK-hAMSCs using PLA microcarriers were firstly used.
- Delivery of HSV-TK bystander therapy against ectopic prostate tumour, successfully achieved tumour regression, prolonged cell retention and vascularization of implanted microtissues.
- hAMSCs mobility from MT was not clearly assessed *in vitro*, both *in vivo* decreased tumour volume and colocalization of hAMSCs within tumoral region, demonstrated availability of therapeutic cells from MT.
- This strategy was combined with BLI monitoring demonstrating feasibility of this non-invasive imaging technique to track therapeutic cell survival together with tumoral cell fate.

Scientific contributions

Publications

- Irene Cano-Torres, Lourdes Sánchez-Cid, Marta Guerra-Rebollo, Nuria Rubio, Jerónimo Blanco, Miguel Á. Mateos-Timoneda, Elisabeth Engel, Cristina Garrido. "Cell-derived extracellular matrix microtissues as vehicles for thymidine kinase/ganciclovir bystander therapy against human prostate cancer PC3 mice model." 2019. *To be submitted.*

- Irene Cano-Torres, Cristina Garrido, Nuria Rubio, Jerónimo Blanco, Miguel Á. Mateos-Timoneda, Elisabeth Engel. "Cell-derived ECM microtissue vascularization using a human adipose derived and human umbilical vein cells as a co-culture strategy". 2019. *To be submitted.*

- Irene Cano-Torres, Soledad Pérez-Amodio, Miguel Á. Mateos-Timoneda, Elisabeth Engel. "Cell-derived extracellular matrix scaffolds: microcarrier choice influences ECM deposition and functionality". 2019. *To be submitted.*

- Joan Marti-Munoz, Soledad Pérez-Amodio, Irene Cano-Torres, Josep Planell, Elisabeth Engel, Oscar Castano. "Calcium releasing pro-angiogenic PLA nanofibers. An angiogenic validation for bone healing". 2018. *Under revision.*

- Olaia F. Vila, Cristina Garrido, Irene Cano-Torres, Marta Guerra-Rebollo, Melva Navarro, Oscar Meca-Cortés, Stephen P. Ma, Elisabeth Engel, Nuria Rubio, Jerónimo Blanco. "Real-time bioluminescence imaging of cell distribution, growth, and differentiation in a three-dimensional scaffold under interstitial perfusion for tissue engineering". *Tissue Engineering Part C: Methods.* 2016. 22(9); 864-872.

- Miguel A. Mateos-Timoneda, Riccardo Levato, Xavier Punet, Irene Cano-Torres, Oscar Castano, Elisabeth Engel. "Biofunctionalization of polymeric surfaces". *37th Annual International Conference of the IEEE Engineering in Medicine and Biology Society (EMBC)*. 2015. 1745-8.

Posters and oral presentations in conferences

- Irene Cano-Torres*, Cristina Garrido*, Nuria Rubio, Jerónimo Blanco, Miguel Á. Mateos-Timoneda, Elisabeth Engel. "Anti-glioblastoma Therapeutic Microtissues". (*authors contributing equally). Reunión Anual Red de Terapia Celular, TERCEL isciii. Valladolid, Spain. 23-24th November 2017.
- Irene Cano-Torres, Cristina Garrido, Nuria Rubio, Jerónimo Blanco, Elisabeth Engel, Miguel Á. Mateos-Timoneda. "Bioluminescence monitored Microtissue Assembly in a Perfused Bioreactor". Poster presentation at the TERMIS-EU. Davos, Switzerland. 26-30th June 2017.
- Irene Cano-Torres, Soledad Pérez-Amodio, Miguel Á. Mateos-Timoneda, Elisabeth Engel. "Evaluation of angiogenic potential of cell-derived ECM scaffolds on chick embryo chorioallantoic membrane animal model". Poster presentation at the 10th Ibec Symposium: Bioengineering for Future Medicine". Barcelona, Spain. 6-7th June 2017.
- Irene Cano-Torres, Cristina Garrido, Nuria Rubio, Jerónimo Blanco, Elisabeth Engel, Miguel Á. Mateos-Timoneda. "Bioluminescence monitored Microtissue Assembly in a Perfused Bioreactor". Poster and Oral presentation at the 9th Ibec Symposium: Bioengineering for Active Aging. Barcelona, Spain. 29th June 2016.
- Irene Cano-Torres, Riccardo Levato, Miguel A. Mateos-Timoneda, Elisabeth Engel. "Cell-laden Microparticles for Microtissue Assembly: a Bottom-up Approach for Bone Tissue Engineering". Poster and Oral presentation at the 27th European Conference on Biomaterials. Kraków, Poland. 30th August – 3rd September 2015.
- Irene Cano-Torres, Riccardo Levato, Miguel A. Mateos-Timoneda, Elisabeth Engel. "Cell-laden microparticles for microtissue assembly in bone tissue engineering". Poster presentation at the 5th Advanced Summer School. Interrogations at the Biointerface – the Nano/Medicine Interface. Porto, Portugal. 29th June – 3rd July 2015.
- Irene Cano-Torres, Riccardo Levato, Miguel A. Mateos-Timoneda, Elisabeth Engel. "Cell-laden microparticles for microtissue assembly in bone tissue engineering". Poster presentation at the Scientific Workshop on Biomedical, Health and Bio-Related applications of Hybrid Materials. HINTBCN. Bellaterra, Spain. 8-9 June 2015.

- Irene Cano-Torres, Riccardo Levato, Miguel A. Mateos-Timoneda, Elisabeth Engel. "*In vitro* development of cell-derived extracellular matrix scaffolds using PLA microparticles for bone regeneration". Oral presentation at the 5th China-Europe Symposium on Biomaterials in Regenerative Medicine (CESB 2015). Hangzhou, China. 7-10th April 2015.
- Irene Cano-Torres, Riccardo Levato, Miguel A. Mateos-Timoneda, Elisabeth Engel. "*In vitro* development of cell-derived extracellular matrix scaffolds using PLA microparticles". Poster and oral presentation at the 4th Advanced Summer School: Interrogations at the Biointerface. The self-renewal differentiation interface. Barcelona, Spain. 30th June – 2nd July 2014.
- Irene Cano-Torres, Riccardo Levato, Miguel A. Mateos-Timoneda, Elisabeth Engel. "*In vitro* development of cell-derived extracellular matrix scaffolds using PLA microparticles for bone regeneration". Poster presented at IBEC's 7th annual Symposium: Bioengineering for Future Medicine. Barcelona, Spain. 29th September 2014.

Bibliography

Abagnale G, Steger M, Nguyen VH, Hersch N, Sechi A, Joussen S, Denecke B, Merkel R, Hoffmann B, Dreser A, Schnakenberg U, Gillner A, Wagner W. 2015. Surface topography enhances differentiation of mesenchymal stem cells towards osteogenic and adipogenic lineages. *Biomaterials* 61:316–326.

Aboody KS, Brown A, Rainov NG, Bower KA, Liu S, Yang W, Small JE, Herrlinger U, Ourednik V, Black PM, Breakefield XO, Snyder EY. 2000. Neural stem cells display extensive tropism for pathology in adult brain. Evidence from intracranial gliomas. *PNAS* 97(23):12846–12851.

Alfred R, Radford J, Fan J, Boon K, Krawetz R, Rancourt D, Kallos MS. 2011a. Efficient suspension bioreactor expansion of murine embryonic stem cells on microcarriers in serum-free medium. *Biotechnol Prog* 27(3):811–823.

Alfred R, Taiani JT, Krawetz RJ, Yamashita A, Rancourt DE, Kallos MS. 2011b. Large-scale production of murine embryonic stem cell-derived osteoblasts and chondrocytes on microcarriers in serum-free media. *Biomaterials* 32:6006–16.

Alieva M, Bagó JR, Aguilar E, Soler-Botija C, Vila OF, Molet J, Gambhir SS, Rubio N, Blanco J. 2012. Glioblastoma therapy with cytotoxic mesenchymal stromal cells optimized by bioluminescence imaging of tumor and therapeutic cell response. *PLoS One* 7(4):e35148.

de Almeida PE, van Rappard JRM, Wu JC. 2011. In vivo bioluminescence for tracking cell fate and function. *Am J Physiol Circ Physiol* 301(3):H663–H671.

Armentano I, Dottori M, Fortunati E, Mattioli S, Kenny JM. 2010. Biodegradable polymer matrix nanocomposites for tissue engineering: A review. *Polym Degrad Stab* 95:2126–2146.

Atala A, Bauer SB, Soker S, Yoo JJ, Retik AB. 2006. Tissue-engineered autologous bladders for patients needing cystoplasty. *Lancet* 367:1241–1246.

Badenes SM, Fernandes TG, Rodrigues CAV, Diogo MM, Cabral JMS. 2016. Microcarrier-based platforms for in vitro expansion and differentiation of human pluripotent stem cells in bioreactor culture systems. *J Biotechnol* 234:71–82.

Badylak SF, Freytes DO, Gilbert TW. 2009. Extracellular matrix as a biological scaffold material: Structure and function. *Acta Biomater* 5:1–13.

Badylak SF, Gilbert TW. 2008. Immune response to biologic scaffold materials. *Semin Immunol* 20:109–116.

Baelo A, Levato R, Julián E, Crespo A, Astola J, Gavaldà J, Engel E, Mateos-Timoneda MA, Torrents E. 2015. Disassembling bacterial extracellular matrix with DNase-coated nanoparticles to enhance antibiotic delivery in biofilm infections. *J Control Release* 209:150–158.

Bagó JR, Alieva M, Soler C, Rubio N, Blanco J. 2013a. Endothelial differentiation of adipose tissue-derived mesenchymal stromal cells in glioma tumors: Implications for cell-based therapy. *Mol Ther* 21(9):1758–1766.

Bagó JR, Pegna GJ, Okolie O, Hingtgen SD. 2016a. Fibrin matrices enhance the transplant and efficacy of cytotoxic stem cell therapy for post-surgical cancer. *Biomaterials* 84:42–53.

Bagó JR, Pegna GJ, Okolie O, Mohiti-Asli M, Loboa EG, Hingtgen SD. 2016b. Electrospun nanofibrous scaffolds increase the efficacy of stem cell-mediated therapy of surgically resected glioblastoma. *Biomaterials* 90:116–125.

Bagó JR, Aguilar E, Alieva M, Soler-botija C, Vila OF, Claros S, Andrades A. 2013b. In Vivo Bioluminescence Imaging of Cell Differentiation in Biomaterials : A Platform for Scaffold Development. *Tissue Eng Part A* 19(5-6):593–603.

Bahramsoltani M, Slosarek I, De Spiegelaere W, Plendl J. 2014. Angiogenesis and Collagen Type IV Expression in Different Endothelial Cell Culture Systems. *Anat Histol Embryol* 43:103–115.

Baras B, Benoit MA, Gillard J. 2000. Parameters influencing the antigen release from spray-dried poly(DL-lactide) microparticles. *Int J Pharm* 200:133–145.

Bariana M, Aw MS, Moore E, Voelcker NH, Losic D. 2014. Radiofrequency-triggered release for on-demand delivery of therapeutics from titania nanotube drug-eluting implants. *Nanomedicine* 9(8):1263–1275.

Bello-Morales R, López-Guerrero JA. 2018. Extracellular Vesicles in Herpes Viral Spread and Immune Evasion. *Front Microbiol* 9:1–9.

Belmar-Lopez C, Mendoza G, Oberg D, Burnet J, Simon C, Cervello I, Iglesias M, Ramirez JC, Lopez-Larrubia P, Quintanilla M, Martin-Duque P. 2013. Tissue-derived mesenchymal stromal cells used as vehicles for anti-tumor therapy exert different in vivo effects on migration capacity and tumor growth. *BMC Med* 11(139):1–16.

Beltrami AP, Barlucchi L, Torella D, Baker M, Limana F, Chimenti S, Kasahara H, Rota M, Musso E, Urbanek K, Leri A, Kajstura J, Nadal-Ginard B. 2003. Adult Cardiac Stem Cells Are Multipotent and Support Myocardial Regeneration we have documented the existence of cycling ventricu- lar myocytes in the normal and pathologic adult mam. *Cell* 114 (19):763–776.

Berkland C, Kim K, Pack DW. 2001. Fabrication of PLG microspheres with precisely controlled and monodisperse size distributions. *J Control Release* 73:59–74.

Bonanno E, Iurlaro M, Madri JA, Nicosia RF. 2000. Type IV Collagen modulates angiogenesis and neovessel survival in the rat aorta model. *Vitr Cell Dev Biol* 36:336–340.

Boo L, Selvaratnam L, Tai CC, Ahmad TS, Kamarul T. 2011. Expansion and preservation of multipotentiality of rabbit bone-marrow derived mesenchymal stem cells in dextran-based microcarrier spin culture. *J Mater Sci Mater Med* 22:1343–1356.

Borden M, Attawia M, Laurencin CT. 2002. The sintered microsphere matrix for bone tissue engineering: In vitro osteoconductivity studies. *J Biomed Mater Res* 61:421–429.

Böstman OM, Pihlajamäki HK. 2000. Adverse tissue reactions to bioabsorbable fixation devices. *Clin Orthop Relat Res* 371:216–227.

Bourget J-M, Gauvin R, Larouche D, Lavoie A, Labbé R, Auger F a, Germain L. 2012. Human fibroblast-derived ECM as a scaffold for vascular tissue engineering. *Biomaterials* 33:9205–9213.

Bourgine PE, Pippenger BE, Todorov A, Tchang L, Martin I. 2013. Tissue decellularization by activation of programmed cell death. *Biomaterials* 34:6099–6108.

Brew SA, Ingram KC. 1994. Purification of human plasma fibronectin. *J Tissue Cult Methods* 16:197–199.

Brudno Y, Ennett-Shepard AB, Chen RR, Aizenberg M, Mooney DJ. 2013. Enhancing microvascular formation and vessel maturation through temporal control over multiple pro-angiogenic and pro-maturation factors. *Biomaterials* 34:9201–9209.

Burey P, Bhandari BR, Howes T, Gidley MJ. 2008. Hydrocolloid gel particles: Formation, characterization, and application. *Crit Rev Food Sci Nutr* 48(5):361–377.

Caddeo S, Boffito M, Sartori S. 2017. Tissue Engineering Approaches in the Design of Healthy and Pathological In Vitro Tissue Models. *Front Bioeng Biotechnol* 5:1–22.

Cannas M, Bosetti M, Sabbatini M, Reno F, Renò F. 2004. Role of Extracellular Matrix Remodeling in Advanced Biocompatibility. *Tissue Eng Nov Delivey Syst* 1:1–30.

Carmeliet P, Jain RK. 2000. Angiogenesis in cancer and other diseases. *Nature* 407:249–257.

Cesarz Z, Tamama K. 2015. Spheroid Culture of Mesenchymal Stem Cells. *Stem Cells Int* 2016:9176357.

Chambers KF, Mosaad EMO, Russell PJ, Clements JA, Doran MR. 2014. 3D cultures of prostate cancer cells cultured in a novel high-throughput culture platform are more resistant to chemotherapeutics compared to cells cultured in monolayer. *PLoS One* 9(11):e111029.

Chau DYS, Agashi K, Shakesheff KM. 2008. Microparticles as tissue engineering scaffolds: manufacture, modification and manipulation. *Mater Sci Technol* 24(9):1031–1044.

Chen AK-L, Chen X, Choo ABH, Reuveny S, Oh SKW. 2011a. Critical microcarrier properties affecting the expansion of undifferentiated human embryonic stem cells. *Stem Cell Res* 7:97–111.

Chen AK-L, Chew YK, Tan HY, Reuveny S, Oh SKW. 2015. Increasing efficiency of human mesenchymal stromal cell culture by optimization of microcarrier concentration and design of medium feed. *Cytotherapy* 17:163–173.

Chen AK-L, Reuveny S, Oh SKW. 2013a. Application of human mesenchymal and pluripotent stem cell

microcarrier cultures in cellular therapy: achievements and future direction. *Biotechnol Adv* 31:1032–1046.

Chen F-M, Liu X. 2016a. Advancing biomaterials of human origin for tissue engineering. *Prog Polym Sci* 53:86–168.

Chen G, Lu Y, Guo P, Lin C, Zhang X, Yang L, Xu Z. 2013b. Matrix mechanics and fluid shear stress control stem cells fate in three dimensional microenvironments. *Curr Stem Cell Res Ther* 8(4):313–323.

Chen J, Zhang D, Li Q, Yang D, Fan Z, Ma D, Ren L. 2016b. Effect of different cell sheet ECM microenvironment on the formation of vascular network. *Tissue Cell* 48:442–451.

Chen M, Wang X, Ye Z, Zhang Y, Zhou Y, Tan W-S. 2011b. A modular approach to the engineering of a centimeter-sized bone tissue construct with human amniotic mesenchymal stem cells-laden microcarriers. *Biomaterials* 32:7532–7542.

Chen M, Zhou M, Ye Z, Zhou Y, Tan W-S. 2014. Ectopic Osteogenesis of Macroscopic Tissue Constructs Assembled from Human Mesenchymal Stem Cell-Laden Microcarriers through In Vitro Perfusion Culture. *PLoS One* 9(10):e109214.

Chen RR, Silva EA, Yuen WW, Mooney DJ. 2007a. Spatio-temporal VEGF and PDGF Delivery Patterns Blood Vessel Formation and Maturation. *Pharm Res* 24:258–264.

Chen X, Dusevich V, Feng JQ, Manolagas SC, Jilka RL, Al CET. 2007b. Extracellular Matrix Made by Bone Marrow Cells Facilitates Expansion of Marrow-Derived Mesenchymal Progenitor Cells and Prevents Their Differentiation Into Osteoblasts. *J Bone Miner Res* 22:1943–1956.

Cheng CW, Solorio LD, Alsberg E. 2014. Decellularized tissue and cell-derived extracellular matrices as scaffolds for orthopaedic tissue engineering. *Biotechnol Adv* 32:462–484.

Cheng D, Cao X, Gao H, Wang Y. 2013. Superficially porous poly(lactic-co-glycolic acid)/calcium carbonate microsphere developed by spontaneous pore-forming method for bone repair. *RSC Adv* 3:6871–6878.

Cheng H-W, Tsui Y-K, Cheung KMC, Chan D, Chan BP. 2009. Decellularization of chondrocyte-encapsulated collagen microspheres: a three-dimensional model to study the effects of acellular matrix on stem cell fate. *Tissue Eng Part C Methods* 15(4):697–706.

Chiu LLY, Radisic M. 2010. Scaffolds with covalently immobilized VEGF and Angiopoietin-1 for vascularization of engineered tissues. *Biomaterials* 31:226–241.

Choi K-H, Choi BH, Park SR, Kim BJ, Min B-H. 2010. The chondrogenic differentiation of mesenchymal stem cells on an extracellular matrix scaffold derived from porcine chondrocytes. *Biomaterials* 31:5355–65.

Chou MJ, Hsieh CH, Yeh PL, Chen PC, Wang CH, Huang YY. 2013. Application of open porous poly(D, L -lactide-co-glycolide) microspheres and the strategy of hydrophobic seeding in hepatic tissue cultivation. *J Biomed Mater Res - Part A* 1011A(10):2862–2869.

Chudakov DM, Lukyanov S, Lukyanov KA. 2005. Fluorescent proteins as a toolkit for in vivo imaging. *Trends Biotechnol* 23(12):605–613.

Chung HJ, Park TG, Ph D. 2009. Injectable cellular aggregates prepared from biodegradable porous microspheres for adipose tissue engineering. *Tissue Eng Part A* 15(6):1391–1400.

Cipurkovic A, Horozic E, Donlagic N, Maric S, Saletovic M, Ademovic Z. 2018. Biodegradable Polymers: Production, properties and application in medicine. *Technol Acta* 11(1):25–35.

Cirone P, Bourgeois JM, Austin RC, Chang PL. 2002. A Novel Approach to Tumor Suppression with Microencapsulated Recombinant Cells. *Hum Gene Ther* 13:1157–1166.

Clary JJ, Feron VJ, Van Velthuijsen JA. 1998. Safety assessment of lactate esters. *Regul Toxicol Pharmacol* 27:88–97.

De Clercq E. 2015. AMD3100/CXCR4 inhibitor. *Front Immunol* 6:276.

Colombo BM, Benedetti S, Ottolenghi S, Mora M, Pollo B, Poli G, Finocchiaro G, Al CET. 1995. The bystander effect. Association of U-87 cell death with ganciclovir-mediated apoptosis of nearby cells and lack of effect in athymic mice. *Hum Gene Ther* 772:763–772.

Colton CK. 2014. Oxygen supply to encapsulated therapeutic cells. *Adv Drug Deliv Rev* 67–68:93–110.

Conway DE, Breckenridge MT, Hinde E, Gratton E, Chen CS, Schwartz MA. 2013. Fluid shear stress on endothelial cells modulates mechanical tension across VE-cadherin and PECAM-1. *Curr Biol* 23(11):1024–1030.

Correa F, Enríquez G, Rosselló J, Lucaya J, Piqueras J, Aso C, Vázquez E, Ortega A, Gallart A. 2004. Posterior fontanelle sonography: An acoustic window into the neonatal brain. *Am J Neuroradiol* 25:1274–1282.

Correia CR, Santos TC, Pirraco RP, Cerqueira MT, Marques AP, Reis RL, Mano JF. 2017. In vivo osteogenic differentiation of stem cells inside compartmentalized capsules loaded with co-cultured endothelial cells. *Acta Biomater* 53:483–494.

Costa-Almeida R, Granja PL, Soares R, Guerreiro SG. 2014. Effect of fiber surface conditioning on the acoustic emission behavior of steel fiber reinforced concrete. *Eur Cells Mater* 28:51–67.

Crisan M, Yap S, Casteilla L, Chen CW, Corselli M, Park TS, Andriolo G, Sun B, Zheng B, Zhang L, Norotte C, Teng PN, Traas J, Schugar R, Deasy BM, Badylak S, Buhring HJ, Giacobino JP, Lazzari L, Huard J, Péault B. 2008. A Perivascular Origin for Mesenchymal Stem Cells in Multiple Human Organs. *Cell Stem Cell* 3:301–313.

Daar AS, Greenwood HL. 2007. A proposed definition of regenerative medicine. *J Tissue Eng Regen Med* 1:179–184.

Daley WP, Peters SB, Larsen M. 2008. Extracellular matrix dynamics in development and regenerative medicine. *J Cell Sci* 121(3):255–264.

Datta N, Pham QP, Sharma U, Sikavitsas VI, Jansen J a, Mikos AG. 2006. In vitro generated extracellular matrix and fluid shear stress synergistically enhance 3D osteoblastic differentiation. *Proc Natl Acad Sci U S A* 103(8):2488–2493.

Davisson T, Sah RL, Ratcliffe A. 2002. Perfusion Increases Cell Content and Matrix Synthesis in Chondrocyte Three-dimensional Cultures. *Tissue Eng* 8(5):807–816.

Decaris ML, Ph D, Binder BY, Soicher MA, Bhat A, Leach JK. 2012. Cell-Derived Matrix Coatings for Polymeric Scaffolds. *Tissue Eng Part A* 18(19-20):2148–2157.

Declercq HA, De Caluwé T, Krysko O, Bachert C, Cornelissen MJ. 2013. Bone grafts engineered from human adipose-derived stem cells in dynamic 3D-environments. *Biomaterials* 34:1004–1017.

Deryugina EI, Quigley JP. 2008. Chick embryo chorioallantoic membrane models to quantify angiogenesis induced by inflammatory and tumor cells or purified effector molecules. *Methods Enzymol* 444:21–41.

Dikina AD, Alt DS, Herberg S, McMillan A, Strobel HA, Zheng Z, Cao M, Lai BP, Jeon O, Petsinger VI, Cotton CU, Rolle MW, Alsberg E. 2018. A Modular Strategy to Engineer Complex Tissues and Organs. *Adv Sci* 5:1700402.

Dikina AD, Strobel HA, Lai BP, Rolle MW, Alsberg E. 2015. Engineered cartilaginous tubes for tracheal tissue replacement via self-assembly and fusion of human mesenchymal stem cell constructs. *Biomaterials* 52:452–462.

Van Dillen IJ, Mulder NH, Vaalburg W, De Vries EFJ, Hospers GAP. 2002. Influence of the Bystander Effect on HSV-tk/GCV Gene Therapy. A Review. *Curr Gene Ther* 2:307–322.

Discher DE. 2005. Tissue Cells Feel and Respon to the Stiffness of Their Substrate. *Science* 310(5751):1139–1143.

Dvir T, Timko BP, Kohane DS, Langer R. 2011. Nanotechnological strategies for engineering complex tissues. *Nat Nanotechnol* 6:13–20.

Eggers J, Villermaux E. 2008. Physics of liquid jets. *Reports Prog Phys* 71:036601.

Ehrbar M, Schoenmakers R, Christen EH, Fussenegger M, Weber W. 2008. Drug-sensing hydrogels for the inducible release of biopharmaceuticals. *Nat Mater* 7:800–804.

Eibes G, dos Santos F, Andrade PZ, Boura JS, Abecasis MM a, da Silva CL, Cabral JMS. 2010. Maximizing the ex vivo expansion of human mesenchymal stem cells using a microcarrier-based stirred culture system. *J Biotechnol* 146:194–197.

Elbert DL. 2011. Bottom-up tissue engineering. *Curr Opin Biotechnol* 22(5):674–680.

Endres M, Wenda N, Woehlecke H, Neumann K, Ringe J, Erggelet C, Lerche D, Kaps C. 2010.

Microencapsulation and chondrogenic differentiation of human mesenchymal progenitor cells from subchondral bone marrow in Ca-alginate for cell injection. *Acta Biomater* 6:436–444.

Engler AJ, Sen S, Sweeney HL, Discher DE. 2006. Matrix elasticity directs stem cell lineage specification. *Cell* 126:677–689.

Fabbri P, Messori M. 2017. Surface Modification of Polymers: Chemical, Physical, and Biological Routes. In: . *Modif Polym Prop*. Elsevier Inc., pp. 109–130.

Fennema E, Rivron N, Rouwkema J, van Blitterswijk C, De Boer J. 2013. Spheroid culture as a tool for creating 3D complex tissues. *Trends Biotechnol* 31(2):108–115.

Fercana GR, Yerneni S, Billaud M, Hill JC, VanRyzin P, Richards TD, Sicari BM, Johnson SA, Badylak SF, Campbell PG, Gleason TG, Phillippi JA. 2017. Perivascular extracellular matrix hydrogels mimic native matrix microarchitecture and promote angiogenesis via basic fibroblast growth factor. *Biomaterials* 123:142–154.

Fernandez-Yague MA, Abbah SA, McNamara L, Zeugolis DI, Pandit A, Biggs MJ. 2015. Biomimetic approaches in bone tissue engineering: Integrating biological and physicomechanical strategies. *Adv Drug Deliv Rev* 84:1–29.

Feugier P, Black RA, Hunt JA, How T V. 2005. Attachment, morphology and adherence of human endothelial cells to vascular prosthesis materials under the action of shear stress. *Biomaterials* 26:1457–1466.

Fitzpatrick LE, McDevitt TC. 2015. Cell-derived matrices for tissue engineering and regenerative medicine applications. *Biomater Sci* 3:12–24.

Floeth FW, Sabel M, Stoffels G, Pauleit D, Hamacher K, Steiger H-J, Langen K-J. 2008. Prognostic Value of 18F-Fluoroethyl-L-Tyrosine PET and MRI in Small Nonspecific Incidental Brain Lesions. *J Nucl Med* 49(5):730–737.

Foster GA, Headen DM, González-García C, Salmerón-Sánchez M, Shirwan H, García AJ. 2017. Protease-degradable microgels for protein delivery for vascularization. *Biomaterials* 113:170–175.

Frantz C, Stewart KM, Weaver VM. 2010. The extracellular matrix at a glance. *J Cell Sci* 123(24):4195–4200.

Frauenschuh S, Reichmann E, Ibold Y, Goetz PM, Sittinger M, Ringe J. 2007. A microcarrier-based cultivation system for expansion of primary mesenchymal stem cells. *Biotechnol Prog* 23:187–193.

Freeman SM, Abboud C, Freeman SM, Packman CH, Koeplin DS, Moolten FL, Abraham GN. 1993. The "Bystander Effect": Tumor Regression When a Fraction of the Tumor Mass Is Genetically Modified. *Cancer Res* 53:5274–5283.

Fuchs S, Hofmann A, Kirkpatrick CJ. 2007. Microvessel-Like Structures from Outgrowth Endothelial Cells from Human Peripheral Blood in 2-Dimensional and 3-Dimensional Co-Cultures with Osteoblastic Lineage Cells. *Tissue Eng* 13(10):2577–2588.

Furth ME, Atala A, Van Dyke ME. 2007. Smart biomaterials design for tissue engineering and regenerative medicine. *Biomaterials* 28:5068–5073.

Furuyama a, Mochitate K. 2000. Assembly of the exogenous extracellular matrix during basement membrane formation by alveolar epithelial cells in vitro. *J Cell Sci* 113:859–868.

Futrega K, Palmer JS, Kinney M, Lott WB, Ungrin MD, Zandstra PW, Doran MR. 2015. The microwell-mesh: A novel device and protocol for the high throughput manufacturing of cartilage microtissues. *Biomaterials* 62:1–12.

Gage FH. 2000. Mammalian Neural Stem Cells. *Science* 287:1433–1438.

Gauvin R, Sc M, Ahsan T, Ph D, Larouche D, Ph D, Le P, Sc M, Dube J. 2010. A Novel Single-Step Self-Assembly Approach for the Fabrication of Tissue-Engineered. *Tissue Eng Part A* 16(5):1737–1747.

Georgi N, Blitterswijk C Van, Karperien M, Al GET. 2014. Mesenchymal stromal/stem cell- or Chondrocyte-Seeded Microcarriers as Building Blocks for Cartilage Tissue Engineering 00:1–11.

Geudens I, Gerhardt H. 2011. Coordinating cell behaviour during blood vessel formation. *Development* 138:4569–4583.

Gilbert TW, Sellaro TL, Badylak SF. 2006. Decellularization of tissues and organs. *Biomaterials* 27:3675–3683.

Goh TK-P, Zhang Z-Y, Chen AK-L, Reuveny S, Choolani M, Chan JKY, Oh SK-W. 2013. Microcarrier Culture for Efficient Expansion and Osteogenic Differentiation of Human Fetal Mesenchymal Stem Cells. *Biores Open Access* 2(2):84–97.

Gomes ME, Sikavitsas VI, Behravesh E, Reis RL, Mikos AG. 2003. Effect of flow perfusion on the osteogenic differentiation of bone marrow stromal cells cultured on starch-based three-dimensional scaffolds. *J Biomed Mater Res Part A* 67A:87–95.

Gonsales da Rosa N, Swiech K, Picanço-Castro V, de Sousa Russo-Carbolante EM, Neto MAS, de Castilho-Fernandes A, Faça VM, Fontes AM, Covas DT. 2012. SK-HEP cells and lentiviral vector for production of human recombinant factor VIII. *Biotechnol Lett* 34:1435–1443.

González-Vázquez A, Planell J a., Engel E. 2014. Extracellular calcium and CaSR drive osteoinduction in mesenchymal stromal cells. *Acta Biomater* 10:2824–2833.

Grand View Research. 2018. Tissue Engineering Market Size, Share & Trends Analysis Report by Application and Segment Forecasts 2018-2025.

Grant R, Hay D, Callanan A. 2018. From scaffold to structure: The synthetic production of cell derived extracellular matrix for liver tissue engineering. *Biomed Phys Eng Express* 4:065015.

Grayson WL, Ma T, Bunnell B. 2004. Human mesenchymal stem cells tissue development in 3D PET matrices. *Biotechnol Prog* 20(3):905–912.

Guerra-Rebollo M, Nogueira De Moraes C, Alcoholado C, Soler-Botija C, Sanchez-Cid L, Vila OF, Meca-Cortés O, Ramos-Romero S, Rubio N, Becerra J, Blanco J, Garrido C. 2018. Glioblastoma Bystander Cell Therapy: Improvements in Treatment and Insights into the Therapy Mechanisms. *Molecuylar Ther Oncolytics* 11:39–51.

Gupta V, Khan Y, Berkland CJ, Laurencin CT, Detamore MS. 2017. Microsphere-Based Scaffolds in Regenerative Engineering. *Annu Rev Biomed Eng* 19:135–161.

Hakkinen KM, S, Jil D, Harunaga B, Doyle AD, Yamada KM. 2011. Direct Comparisons of the Morphology, Migration, Cell Adhesions, and Actin Cytoskeleton of Fibroblasts in Four different three-dimensional extracellular matrices. *Tissue Eng Part A* 17(5-6):713–724.

Han L, Tang C, Yin C. 2015. Dual-targeting and pH/redox-responsive multi-layered nanocomplexes for smart co-delivery of doxorubicin and siRNA. *Biomaterials* 60:42–52.

Herberts CA, Kwa MSG, Hermsen HPH. 2011. Risk factors in the development of stem cell therapy. *J Transl Med* 9(29):1–14.

Hernández RM, Orive G, Murua A, Pedraz JL. 2010. Microcapsules and microcarriers for in situ cell delivery. *Adv Drug Deliv Rev* 62:711–730.

Higuchi Y, Shiraki N, Yamane K, Qin Z, Mochitate K, Araki K, Senokuchi T, Yamagata K, Hara M, Kume K, Kume S. 2010. Synthesized basement membranes direct the differentiation of mouse embryonic stem cells into pancreatic lineages. *J Cell Sci* 123(16):2733–2742.

Hong S-J, Yu H-S, Kim H-W. 2009. Tissue engineering polymeric microcarriers with macroporous morphology and bone-bioactive surface. *Macromol Biosci* 9:639–645.

Hoshiba T, Cho CS, Murakawa A, Okahata Y, Akaike T. 2006. The effect of natural extracellular matrix deposited on synthetic polymers on cultured primary hepatocytes. *Biomaterials* 27:4519–4528.

Hoshiba T, Kawazoe N, Chen G. 2012. The balance of osteogenic and adipogenic differentiation in human mesenchymal stem cells by matrices that mimic stepwise tissue development. *Biomaterials* 33:2025–2031.

Hoshiba T, Kawazoe N, Tateishi T, Chen G. 2009. Development of stepwise osteogenesis-mimicking matrices for the regulation of mesenchymal stem cell functions. *J Biol Chem* 284(45):31164–31173.

Hoshiba T, Kawazoe N, Tateishi T, Chen G. 2010a. Development of extracellular matrices mimicking stepwise adipogenesis of mesenchymal stem cells. *Adv Mater* 22:3042–3047.

Hoshiba T, Lu H, Kawazoe N, Chen G. 2010b. Decellularized matrices for tissue engineering. *Expert Opin Biol Ther* 10(12):1717–1728.

Hoshiba T, Lu H, Yamada T, Kawazoe N, Tateishi T, Chen G. 2011. Effects of extracellular matrices derived from different cell sources on chondrocyte functions. *Biotechnol Prog* 27(3):788–795.

Hoshiba T, Tanaka M. 2013. Breast cancer cell behaviors on staged tumorigenesis-mimicking matrices

derived from tumor cells at various malignant stages. *Biochem Biophys Res Commun* 439:291–296.

Hung SC, Deng WP, Yang WK, Liu RS, Lee CC, Su TC, Lin RJ, Yang DM, Chang CW, Chen WH, Wei HJ, Gelovani JG. 2005. Mesenchymal stem cell targeting of microscopic tumors and tumor stroma development monitored by noninvasive in vivo positron emission tomography imaging. *Clin Cancer Res* 11(21):7749–7756.

Hynes RO. 1990. Fibronectins. Springer-Verlag New York XV, 546 p.

Imparato G, Urciuolo F, Casale C, Netti PA. 2013. The role of microscaffold properties in controlling the collagen assembly in 3D dermis equivalent using modular tissue engineering. *Biomaterials* 34:7851–7861.

Institute for Bioplastics and Biocomposites. 2018. Biopolymers facts and statistics.

Ishiguro T, Ohata H, Sato A, Yamawaki K, Enomoto T, Okamoto K. 2017. Tumor-derived spheroids: Relevance to cancer stem cells and clinical applications. *Cancer Sci* 108(3):283–289.

Jain RK, Au P, Tam J, Duda DG, Fukumura D. 2005. Engineering vascularized tissue. *Nat Biotechnol* 23(7):821–823.

Janssen FW, Oostra J, Oorschot A Van, Blitterswijk CA Van. 2006. A perfusion bioreactor system capable of producing clinically relevant volumes of tissue-engineered bone: In vivo bone formation showing proof of concept. *Biomaterials* 27:315–323.

Ji P, Manupipatpong S, Xie N, Li Y. 2016. Induced Pluripotent Stem Cells: Generation Strategy and Epigenetic Mystery behind Reprogramming. *Stem Cells Int* 2016:8415010.

Jiang X, Wang C, Fitch S, Yang F. 2018. Targeting tumor hypoxia using nanoparticle-engineered CXCR4-overexpressing adipose-derived stem cells. *Theranostics* 8(5):1350–1360.

Jin CZ, Choi BH, Park SR, Min B-H. 2009. Cartilage engineering using cell-derived extracellular matrix scaffold in vitro. *J Biomed Mater Res A* 92(4):1567–1577.

Jin GZ, Park JH, Seo SJ, Kim HW. 2014. Dynamic cell culture on porous biopolymer microcarriers in a spinner flask for bone tissue engineering: A feasibility study. *Biotechnol Lett* 36:1539–1548.

Jorgenson KD, Hart DA, Krawetz R, Sen A. 2018. Production of Adult Human Synovial Fluid-Derived Mesenchymal Stem Cells in Stirred-Suspension Culture. *Stem Cells Int* 2018:8431053.

Kadler KE, Baldock C, Bella J, Boot-Handford RP. 2007. Collagens at a glance. *J Cell Sci* 120(12):1955–1958.

Kaehler J, Zilla P, Fasol R, Deutsch M, Kadletz M. 1989. Precoating substrate and surface configuration determine adherence and spreading of seeded endothelial cells on polytetrafluoroethylene grafts. *J Vasc Surg* 9(4):535–541.

Kalluri R. 2003. Basement membranes: Structure, assembly and role in tumour angiogenesis. *Nat Rev Cancer* 3:422–433.

Kang Y, Kim S, Bishop J, Khademhosseini A, Yang Y. 2012. The osteogenic differentiation of human bone marrow MSCs on HUVEC-derived ECM and β-TCP scaffold. *Biomaterials* 33:6998–7007.

Kanke K, Masaki H, Saito T, Komiyama Y, Hojo H, Nakauchi H, Lichtler AC, Takato T, Chung U, Ohba S. 2014. Stepwise Differentiation of Pluripotent Stem Cells into Osteoblasts Using Four Small Molecules under Serum-free and Feeder-free Conditions. *Stem Cell Reports* 2:751–760.

Karagiannis ED, Popel AS. 2007. Identification of novel short peptides derived from the a 4 , a 5 , and a 6 fibrils of type IV collagen with anti-angiogenic properties. *Biochem Biophys Res Commun* 354:434–439.

Kauer TM, Figueiredo JL, Hingtgen S, Shah K. 2012. Encapsulated therapeutic stem cells implanted in the tumor resection cavity induce cell death in gliomas. *Nat Neurosci* 15(2):197–204.

Kelm JM, Breitbach M, Fischer G, Odermatt B, Agarkova I, Fleischmann BK, Hoerstrup SP. 2012. 3D Microtissue Formation of Undifferentiated Bone Marrow Mesenchymal Stem Cells Leads to Elevated Apoptosis. *Tissue Eng Part A* 18(7-8):692–702.

Keshaw H, Thapar N, Burns AJ, Mordan N, Knowles JC, Forbes A, Day RM. 2010. Microporous collagen spheres produced via thermally induced phase separation for tissue regeneration. *Acta Biomater* 6:1158–1166.

Khan OF, Voice DN, Leung BM, Sefton M V. 2015. A novel high-speed production process to create

modular components for the bottom-up assembly of large-scale tissue-engineered constructs. *Adv Healthc Mater* 4:113–120.

Kim HK, Chung HJ, Park TG. 2006. Biodegradable polymeric microspheres with "open/closed" pores for sustained release of human growth hormone. *J Control Release* 112:167–174.

Kim M-H, Sawada Y, Taya M, Kino-oka M. 2014. Influence of surface topography on the human epithelial cell response to micropatterned substrates with convex and concave architectures. *J Biol Eng* 8(13):1–9.

Klar AS, Güven S, Zimoch J, Zapiórkowska NA, Biedermann T, Böttcher-Haberzeth S, Meuli-Simmen C, Martin I, Scherberich A, Reichmann E, Meuli M. 2016. Characterization of vasculogenic potential of human adipose-derived endothelial cells in a three-dimensional vascularized skin substitute. *Pediatr Surg Int* 32:17–27.

Klimanskaya I, Chung Y, Meisner L, Johnson J, West MD, Lanza R. 2005. Human embryonic stem cells derived without feeder cells. *Lancet* 365:1636–1641.

Klyushnenkova E, Mosca JD, Zernetkina V, Majumdar MK, Beggs KJ, Simonetti DW, Deans RJ, McIntosh KR. 2005. T cell responses to allogeneic human mesenchymal stem cells: Immunogenicity, tolerance, and suppression. *J Biomed Sci* 12:47–57.

Kook Y-M, Kim H, Kim S, Heo CY, Park MH, Lee K, Koh W-G. 2018. Promotion of Vascular Morphogenesis of Endothelial Cells Co-Cultured with Human Adipose-Derived Mesenchymal Stem Cells Using Polycaprolactone/Gelatin Nanofibrous Scaffolds. *Nanomaterials* 8(117):1–16.

Kou D, Du M, Hou X, Chen B, Li X, Fang Y, Zhao Y, Wang H, Wang L, Dai J. 2016. Centimeter-sized biomimetic bone constructs fabricated via CBD-BMP2-collagen microcarriers and BMSC-gelatin microspheres. *J Mater Chem B* 4:461–470.

Kraiselburd E. 1976. Thymidine kinase gene transfer by herpes simplex virus. *Bull Cancer* 63(3):393–398.

Kucerova L, Altanerova V, Matuskova M, Tyciakova S, Altaner C. 2007. Adipose tissue-derived human mesenchymal stem cells mediated prodrug cancer gene therapy. *Cancer Res* 67(13):6304–6313.

Kunishige I, Samejima Y, Shiki Y, Moriyama A, Meruelo D, Saji F, Murata Y. 1999. Suicide gene therapy for human uterine adenocarcinoma cells using herpes simplex virus thymidine kinase. *Gynecol Oncol* 72:16–25.

Kutys ML, Doyle AD, Yamada KM. 2013. Regulation of cell adhesion and migration by cell-derived matrices. *Exp Cell Res* 319:2434–2439.

Lai Y, Sun Y, Skinner CM, Son EL, Lu Z, Tuan RS, Jilka RL, Ling J, Chen X-D. 2010. Reconstitution of marrow-derived extracellular matrix ex vivo: a robust culture system for expanding large-scale highly functional human mesenchymal stem cells. *Stem Cells Dev* 19(7):1095–1107.

Lakes R. 1993. Materials with structure hierarchy. *Nature* 361:511–515.

Lam GC, Sefton M V. 2015. Tuning Graft- and Host-Derived Vascularization in Modular Tissue Constructs: A Potential Role of HIF1 Activation. *Tissue Eng Part A* 21:803–816.

Langer R, Vacanti JP. 1993. Tissue Engineering. *Science* 260(5110):920–926.

Larrañaga A, Sarasua J-R. 2016. Poly(α-hydroxy Acids)-Based Cell Microcarriers. *Appl Sci* 6(436):1–16.

Lau TT, Lee LQP, Vo BN, Su K, Wang D-A. 2012. Inducing ossification in an engineered 3D scaffold-free living cartilage template. *Biomaterials* 33:8406–8417.

Lau TT, Wang D-A. 2011. Stromal cell-derived factor-1 (SDF-1): homing factor for engineered regenerative medicine. *Expert Opin Biol Ther* 11(2):189–197.

Layre A, Couvreur P, Chacun H, Richard J, Passirani C, Requier D, Benoit JP, Gref R. 2006. Novel composite core-shell nanoparticles as busulfan carriers. *J Control Release* 111(3):271–280.

Leber J, Barekzai J, Blumenstock M, Pospisil B, Salzig D, Czermak P. 2017. Microcarrier choice and bead-to-bead transfer for human mesenchymal stem cells in serum-containing and chemically defined media. *Process Biochem* 59:255–265.

Lee HJ, Koh WG. 2014. Hydrogel micropattern-incorporated fibrous scaffolds capable of sequential growth factor delivery for enhanced osteogenesis of hMSCs. *ACS Appl Mater Interfaces* 6:9338–9348.

Leferink AM, Hendrikson WJ, Rouwkema J, Karperien M, Blitterswijk CA van, Moroni I. 2016. Increased cell seeding efficiency in bioplotted three-dimensional PEOT/PBT scaffolds. *J tissue Eng Regen Med*

10:679–689.

Leonard A, Koria P. 2017. Growth factor functionalized biomaterial for drug delivery and tissue regeneration. *J Bioact Compat Polym* 32(6):568–581.

Leong W, Wang D-A. 2015. Cell-laden Polymeric Microspheres for Biomedical Applications. *Trends Biotechnol* 33(11):653–666.

Leung BM, Sefton M V. 2007. A modular tissue engineering construct containing smooth muscle cells and endothelial cells. *Ann Biomed Eng* 35:2039–2049.

Levato R, Mateos-Timoneda M a, Planell J a. 2012. Preparation of biodegradable polylactide microparticles via a biocompatible procedure. *Macromol Biosci* 12:557–566.

Levato R, Planell JA, Mateos-Timoneda M a., Engel E. 2015. Role of ECM/peptide coatings on SDF-1a triggered mesenchymal stromal cell migration from microcarriers for cell therapy. *Acta Biomater* 18:59–67.

Levato R, Visser J, Planell JA, Engel E, Malda J, Mateos-Timoneda MA. 2014. Biofabrication of tissue constructs by 3D bioprinting of cell-laden microcarriers. *Biofabrication* 6:035020.

Li Q, Wang Z. 2013. Influence of Mesenchymal stem cells with endothelial progenitor cells in co-culture on osteogenesis and angiogenesis: An in vitro study. *Arch Med Res* 44:504–513.

Li Y, Wu M, Zhang N, Tang C, Jiang P, Liu X, Yan F, Zheng H. 2018. Mechanisms of enhanced antiglioma efficacy of polysorbate 80-modified paclitaxel-loaded PLGA nanoparticles by focused ultrasound. *J Cell Mol Med* 22:4171–4182.

Liao J, Guo X, Grande-Allen KJ, Kasper FK, Mikos AG. 2010. Bioactive polymer/extracellular matrix scaffolds fabricated with a flow perfusion bioreactor for cartilage tissue engineering. *Biomaterials* 31:8911–8920.

Lin D, Chai Y, Ma Y, Duan B, Yuan Y, Liu C. 2017. Rapid initiation of guided bone regeneration driven by spatiotemporal delivery of IL-8 and BMP-2 from hierarchical MBG-based scaffold. *Biomaterials*:1–16.

Lin G, Yang R, Banie L, Wang G, Ning H, Li LC, Lue TF, Lin CS. 2010. Effects of transplantation of adipose tissue-derived stem cells on prostate tumor. *Prostate* 70:1066–1073.

Lin YM, Lim JF, Lee J, Choolani M, Chan JK, Reuveny S, Oh SK. 2016. Expansion in microcarrier-spinner cultures improves the chondrogenic potential of human early mesenchymal stromal cells. *Cytotherapy* 18:740–753.

Liu H, Zhou W, Ren N, Feng Z, Dong Y, Bai S, Jiao Y, Wang Z, Zhao Y. 2017. Cell Sheets of Co-cultured Endothelial Progenitor Cells and Mesenchymal Stromal Cells Promote Osseointegration in Irradiated Rat Bone. *Sci Rep* 7:3038.

Liu JS, Gartner ZJ. 2012. Directing the assembly of spatially organized multicomponent tissues from the bottom up. *Trends Cell Biol* 22(12):683–691.

Liu L, Yu Q, Fu S, Wang B, Hu K, Wang L, Hu Y, Xu Y, Yu X, Huang H. 2018. CXCR4 Antagonist AMD3100 Promotes Mesenchymal Stem Cell Mobilization in Rats Preconditioned with the Hypoxia-Mimicking Agent Cobalt Chloride. *Stem Cells Dev* 27(7):466–478.

Lock LT, Tzanakakis ES. 2009. Expansion and Differentiation of Human Embryonic Stem Cells to Endoderm Progeny in a Microcarrier Stirred-Suspension Culture. *Tissue Eng Part A* 15(8):2051–2063.

Lu H, Hoshiba T, Kawazoe N, Chen G. 2011a. Autologous extracellular matrix scaffolds for tissue engineering. *Biomaterials* 32:2489–2499.

Lu H, Hoshiba T, Kawazoe N, Koda I, Song M, Chen G. 2011b. Cultured cell-derived extracellular matrix scaffolds for tissue engineering. *Biomaterials* 32:9658–9666.

Lu J, Hou R, Yang Z, Tang Z. 2015. Development and characterization of drug-loaded biodegradable PLA microcarriers prepared by the electrospraying technique. *Int J Mol Med* 36:249–254.

Luciani A, Coccoli V, Orsi S, Ambrosio L, Netti PA. 2008. PCL microspheres based functional scaffolds by bottom-up approach with predefined microstructural properties and release profiles. *Biomaterials* 29:4800–4807.

Luo H, Chen M, Wang X, Mei Y, Ye Z, Tan W-S. 2014. Fabrication of viable centimeter-sized 3D tissue

constructs with microchannel conduits for improved tissue properties through assembly of cell-laden microbeads. *J Tissue Eng Regen Med* 8:493–504.

Mao Y, Schwarzbauer JE. 2005. Fibronectin fibrillogenesis, a cell-mediated matrix assembly process. *Matrix Biol* 24:389–399.

Marquez-Curtis LA, Janowska-Wieczorek A. 2013. Enhancing the migration ability of mesenchymal stromal cells by targeting the SDF-1/CXCR4 axis. *Biomed Res Int* 2013:561098.

Marti-Munoz J, Pérez-Amodio S, Cano-Torres I, Planell JA, Engel E, Castano O. 2018. Calcium releasing pro-angiogenic PLA nanofibers. An angiogenic validation for bone healing. *Under Revis*.

Martin I. 2014. Engineered Tissues as Customized Organ Germs. *Tissue Eng Part A* 20(7-8):2013–2014.

Martin I, Wendt D, Heberer M. 2004. The role of bioreactors in tissue engineering. *Trends Biotechnol* 22(2):80–86.

Massoud TF, Gambhir SS. 2003. Molecular imaging in living subjects: seeing fundamental biological processes in a new light. *Genes Dev* 17:545–580.

Mateos-Timoneda M a, Castano O, Planell J a, Engel E. 2014. Effect of structure, topography and chemistry on fibroblast adhesion and morphology. *J Mater Sci Mater Med* 25:1781–1787.

Matsumoto A, Matsukawa Y, Suzuki T, Yoshino H. 2005. Drug release characteristics of multi-reservoir type microspheres with poly(dl-lactide-co-glycolide) and poly(dl-lactide). *J Control Release* 106:172–180.

Matsunaga YT, Morimoto Y, Takeuchi S. 2011. Molding cell beads for rapid construction of macroscopic 3D tissue architecture. *Adv Mater* 23:H90–H94.

McGuigan AP, Leung B, Sefton M V. 2007a. Fabrication of cells containing gel modules to assemble modular tissue-engineered constructs. *Nat Protoc* 1(6):2963–2969.

McGuigan AP, Sefton M V. 2007b. Modular tissue engineering: fabrication of a gelatin-based construct. *J Tissue Eng Regen Med* 1:136–145.

McGuigan AP, Sefton M V. 2006. Vascularized organoid engineered by modular assembly enables blood perfusion. *PNAS* 103(31):11461–11466.

McGuigan AP, Sefton M V. 2007c. Design criteria for a modular tissue-engineered construct. *Tissue Eng* 13(5):1079–1089.

Meca-Cortés O, Guerra-Rebollo M, Garrido C, Borrós S, Rubio N, Blanco J. 2017. CRISPR/Cas9-Mediated Knockin Application in Cell Therapy: A Non-viral Procedure for Bystander Treatment of Glioma in Mice. *Mol Ther - Nucleic Acids* 8:395–403.

Mehta SR, Huang R, Yang M, Zhang XQ, Kolli B, Chang KP, Hoffman RM, Goto Y, Badaro R, Schooley RT. 2008. Real-time in vivo green fluorescent protein imaging of a murine leishmaniasis model as a new tool for Leishmania vaccine and drug discovery. *Clin Vaccine Immunol* 15(12):1764–1770.

Mei Y, Luo H, Tang Q, Ye Z, Zhou Y, Tan W-S. 2010. Modulating and modeling aggregation of cell-seeded microcarriers in stirred culture system for macrotissue engineering. *J Biotechnol* 150:438–446.

Melero-Martin JM, Khan ZA, Picard A, Wu X, Parachuri S, Bischoff J. 2007. An uncommon presentation of endometriosis a case report. *Blood* 109(11):4761–4768.

Merten OW. 2015. Advances in cell culture: Anchorage dependence. *Philos Trans R Soc B Biol Sci* 370:20140040.

Migonney V. 2014. History of Biomaterials. In: Véronique Migoneey, editor. *Biomaterials* First., pp. 1–10.

Mohamed F, Christopher F. 2008. Engineering Biodegradable Polyester Particles With Specific Drug Targeting and Drug Release Properties. *J Pharm Sci* 97:71–87.

Moolten FL. 1986. Tumor Chemosensitivity Conferred by Inserted Herpes Thymidine Kinase Genes: Paradigm for a Prospective Cancer Control Strategy. *Cancer Res* 46:5276–5281.

Mueller D, Tascher G, Ursula M, Knobeloch D, Nuessler AK. 2011. In-depth physiological characterization of primary human hepatocytes in a 3D hollow-fiber bioreactor. *J Tissue Eng Regen Med* 5(8):e207-218.

Mukhopadhyay A, Mukhopadhyay SN, Talwar GP. 1993. Influence of serum proteins on the kinetics of attachment of vero cells to cytodex microcarriers. *J Chem Technol Biotechnol* 56:369–374.

Mundel TM, Kalluri R. 2014. Type IV collagen-derived angiogenesis inhibitors. *Microvasc Res* 74(0):85–89.

Na XM, Gao F, Zhang LY, Su ZG, Ma GH. 2012. Biodegradable microcapsules prepared by self-healing of porous microspheres. *ACS Macro Lett* 1:697–700.

Nair A, Shen J, Lofti P, Ko C-Y, Zhang CC, Tang L. 2011. Biomaterial implants mediate autologous stem cell recruitment in mice. *Acta Biomater* 7:3887–3895.

Nair LS, Laurencin CT. 2007. Biodegradable polymers as biomaterials. *Prog Polym Sci* 32:762–798.

Nakamizo A, Marini F, Amano T, Khan A, Studeny M, Gumin J, Chen J, Hentschel S, Vecil G, Dembinski J, Andreeff M, Lang FF. 2005. Human bone marrow-derived mesenchymal stem cells in the treatment of gliomas. *Cancer Res* 65(8):3307–3318.

Narayanan K, Leck K-J, Gao S, Wan AC a. 2009. Three-dimensional reconstituted extracellular matrix scaffolds for tissue engineering. *Biomaterials* 30:4309–4317.

Navarro-Requena C, Weaver JD, Clark AY, Clift DA, Pérez-Amodio S, Castaño Ó, Zhou DW, García AJ, Engel E. 2017. PEG hydrogel containing calcium-releasing particles and mesenchymal stromal cells promote vessel maturation. *Acta Biomater* 67:53–65.

Navarro M, Engel E, Planell JA, Amaral I, Barbosa M, Ginebra MP. 2008. Surface characterization and cell response of a PLA/CaP glass biodegradable composite material. *J Biomed Mater Res - Part A* 85(2):477–486.

Nichol JW, Khademhosseini A. 2009. Modular Tissue Engineering: Engineering Biological Tissues from the Bottom Up. *Soft Matter* 5:1312–1319.

Nicholas T, Read S, Burrows F, Kruse C. 2003. Suicide gene therapy with Herpes simplex virus thymidine kinase and ganciclovir is enhanced with connexins to improve gap junctions and bystander effects. *Histol Histopathol* 18(2):495–507.

Nicosia RF, Belser P, Bonanno E, Diven AJ. 1991. Regulation of angiogenesis in vitro by collagen metabolism. *Vitr Cell Dev Biol* 27A:961–966.

Novosel EC, Kleinhans C, Kluger PJ. 2011. Vascularization is the key challenge in tissue engineering. *Adv Drug Deliv Rev* 63:300–311.

Nowak-sliwinska P, Segura T, Iruela-arispe ML. 2015. The chicken chorioallantoic membrane model in biology, medicine and bioengineering. *Angiogenesis* 17(4):779–804.

Nwabo Kamdje AH, Vecchio L, Seke Etet PF, Kamga PT, Muller JM, Bassi G, Lukong E, Goel RK, Krampera M. 2016. Mesenchymal Stem/Stromal Cell Trafficking and Homing. *Mesenchymal Stromal Cells as Tumor Stromal Modul*. Elsevier Inc. 169-191 p.

Oh SKW, Choo ABH. 2011. Stem Cells. In: . *Compr Biotechnol Second Ed*, Vol. 1, pp. 341–365.

Ojeh NO, Navsaria HA. 2014. An in vitro skin model to study the effect of mesenchymal stem cells in wound healing and epidermal regeneration. *J Biomed Mater Res - Part A* 102(8):2785–2792.

Okita K, Ichisaka T, Yamanaka S. 2007. Generation of germline-competent induced pluripotent stem cells. *Nature* 448(7151):313–317.

Okura H, Smith CA, Rutka JT. 2014. Gene therapy for malignant glioma patients. *Mol Cell Ther* 2(21):1–19.

Ott HC, Matthiesen TS, Goh S-K, Black LD, Kren SM, Netoff TI, Taylor D a. 2008. Perfusion-decellularized matrix: using nature's platform to engineer a bioartificial heart. *Nat Med* 14(2):213–221.

Palmiero C, Imparato G, Urciuolo F, Netti P. 2010. Engineered dermal equivalent tissue in vitro by assembly of microtissue precursors. *Acta Biomater* 6:2548–2553.

Park KM, Gerecht S. 2014. Harnessing developmental processes for vascular engineering and regeneration. *Development* 141:2760–2769.

Parry DAD, Squire JM. 2017. Fibrillar Collagens. In: . *Fibrous Proteins Struct Mech*. Springer Nature, pp. 457–490.

Pendleton C, Li Q, Chesler DA, Yuan K, Guerrero-Cazares H, Quinones-Hinojosa A. 2013. Mesenchymal Stem Cells Derived from Adipose Tissue vs Bone Marrow: In Vitro Comparison of Their Tropism towards Gliomas. *PLoS One* 8(3):e58198.

Perche F, Torchilin VP. 2012. Cancer cell spheroids as a model to evaluate chemotherapy protocols. *Cancer Biol Ther* 13(12):1205–1213.

Pereira RF, Bártolo PJ. 2015. 3D Photo-Fabrication for Tissue Engineering and Drug Delivery. *Engineering* 1(1):090-112.

Peterson AW, Caldwell DJ, Rioja AY, Rao RR, Putnam AJ, Stegemann JP. 2014. Vasculogenesis and Angiogenesis in Modular Collagen-Fibrin Microtissues. *Biomater Sci* 2:1497–1508.

Peticone C, Thompson DDS, Owens GJ, Kim H, Micheletti M, Knowles JC, Wall I. 2017. Towards modular bone tissue engineering using Ti – Co-doped phosphate glass microspheres : cytocompatibility and dynamic culture studies. *J Biomater Appl* 32(3):295–310.

Pham QP, Kasper FK, Scott Baggett L, Raphael RM, Jansen J a, Mikos AG. 2008. The influence of an in vitro generated bone-like extracellular matrix on osteoblastic gene expression of marrow stromal cells. *Biomaterials* 29:2729–2739.

Pill K, Hofmann S, Redl H, Holnthoner W. 2015. Vascularization mediated by mesenchymal stem cells from bone marrow and adipose tissue: A comparison. *Cell Regen* 4(8):1–10.

Pittenger MF. 1999. Multilineage Potential of Adult Human Mesenchymal Stem Cells. *Science* 284:143–147.

Place ES, Evans ND, Stevens MM. 2009. Complexity in biomaterials for tissue engineering. *Nat Mater* 8:457–470.

Portalska KJ, Leferink A, Groen N, Fernandes H, Moroni L, van Blitterswijk C, de Boer J. 2012. Endothelial Differentiation of Mesenchymal Stromal Cells. *PLoS One* 7(10):e46842.

Potapova IA, Brink PR, Cohen IS, Doronin S V. 2008. Culturing of human mesenchymal stem cells as three-dimensional aggregates induces functional expression of CXCR4 that regulates adhesion to endothelial cells. *J Biol Chem* 283(19):13100–13107.

Przyborski SA. 2005. Differentiation of Human Embryonic Stem Cells After Transplantation in Immune-Deficient Mice. *Stem Cells* 23:1242–1250.

Punet X, Mauchauffé R, Giannotti MI, Rodríguez-Cabello JC, Sanz F, Engel E, Mateos-Timoneda M a., Planell J a. 2013. Enhanced cell-material interactions through the biofunctionalization of polymeric surfaces with engineered peptides. *Biomacromolecules* 14:2690–2702.

Quiros RM, Valianou M, Kwon Y, Brown KM, Godwin AK, Cukierman E. 2008. Ovarian normal and tumor-associated fibroblasts retain in vivo stromal characteristics in a 3-D matrix-dependent manner. *Gynecol Oncol* 110:99–109.

Rafiq QA, Coopman K, Nienow AW, Hewitt CJ. 2016. Systematic microcarrier screening and agitated culture conditions improves human mesenchymal stem cell yield in bioreactors. *Biotechnol J* 11:473–486.

Rafiq QA, Ruck S, Hanga MP, Heathman TRJ, Coopman K, Nienow AW, Williams DJ, Hewitt CJ. 2018. Qualitative and quantitative demonstration of bead-to-bead transfer with bone marrow-derived human mesenchymal stem cells on microcarriers: Utilising the phenomenon to improve culture performance. *Biochem Eng J* 135:11–21.

Reardon JE. 1989. Herpes simplex virus type 1 and human DNA polymerase interactions with 2'-deoxyguanosine 5'-triphosphate analogues. Kinetics of incorporation into DNA and induction of inhibition. *J Biol Chem* 264(15):19039–19044.

Richtig E, Langmann G, Müllner K, Richtig G, Smolle J. 2004. Calculated tumour volume as a prognostic parameter for survival in choroidal melanomas. *Eye* 18:619–623.

Rivera-Cruz CM, Shearer JJ, Figueiredo Neto M, Figueiredo ML. 2017. The immunomodulatory effects of mesenchymal stem cell polarization within the tumor microenvironment niche. *Stem Cells Int* 2017:4014039.

Rivron NC, Vrij EJ, Rouwkema J, Gac S Le, Berg A van den, Truckenmüller RK, Blitterswijk CA van. 2012. Tissue deformation spatially modulates VEGF signaling and angiogenesis. *PNAS* 109(18):6886–6891.

Roam JL, Yan Y, Nguyen PK, Kinstlinger IS, Leuchter MK, Hunter DA, Wood MD, Elbert DL. 2015. A modular, plasmin-sensitive, clickable poly(ethylene glycol)-heparin-laminin microsphere system for establishing growth factor gradients in nerve guidance conduits. *Biomaterials* 72:112–124.

Rossi L, Attanasio C, Vilardi E, De Gregorio M, Netti PA. 2016. Vasculogenic potential evaluation of bottom-up, PCL scaffolds guiding early angiogenesis in tissue regeneration. *J Mater Sci Mater Med* 27(107):1–11.

Rourou S, Van Der Ark A, Majoul S, Trabelsi K, Van Der Velden T, Kallel H. 2009. A novel animal-component-free medium for rabies virus production in Vero cells grown on Cytodex 1 microcarriers in a stirred bioreactor. *Appl Microbiol Biotechnol* 85:53–63.

Rouwkema J, Koopman BFJM, Blitterswijk CAV, Dhert WJA, Malda J. 2009. Supply of nutrients to cells in engineered tissues. *Biotechnol Genet Eng Rev* 26:163–178.

Rouwkema J, Rivron NC, Blitterswijk CA Van. 2008. Vascularization in tissue engineering. *Trends in* 16(8):434–441.

Ruijtenberg S, van den Heuvel S. 2016. Coordinating cell proliferation and differentiation: Antagonism between cell cycle regulators and cell type-specific gene expression. *Cell Cycle* 15(2):196–212.

Sabel MS, Arora A, Su G, Mathiowitz E, Reineke JJ, Chang AE. 2007. Synergistic effect of intratumoral IL-12 and TNF-α microspheres: systemic anti-tumor immunity is mediated by both CD8+ CTL and NK cells. *Surgery* 142(5):749–760.

Salasznyk RM, Williams WA, Boskey A, Batorsky A, Plopper GE. 2004. Adhesion to Vitronectin and Collagen I Promotes Osteogenic Differentiation of Human Mesenchymal Stem Cells 2004(1):24–34.

Saleh F a, Whyte M, Genever PG. 2011. Effects of endothelial cells on human mesenchymal stem cell activity in a three-dimensional in vitro model. *Eur Cell Mater* 22:242–257.

Sart S, Agathos SN, Li Y. 2013. Engineering stem cell fate with biochemical and biomechanical properties of microcarriers. *Biotechnol Prog* 29(6):1354–1366.

Sart S, Errachid A, Schneider Y-J, Agathos SN. 2011. Controlled expansion and differentiation of mesenchymal stem cells in a microcarrier based stirred bioreactor. *BMC Proc* 5(Suppl 8):P55.

Sart S, Schneider YJ, Agathos SN. 2010. Influence of culture parameters on ear mesenchymal stem cells expanded on microcarriers. *J Biotechnol* 150:149–160.

Sart S, Tsai A-C, Li Y, Ma T. 2014. Three-Dimensional Aggregates of Mesenchymal Stem Cells: Cellular Mechanisms, Biological Properties, and Applications. *Tissue Eng Part B Rev* 20(5):365–380.

Schenke-Layland K, Rofail F, Heydarkhan S, Gluck JM, Ingle NP, Angelis E, Choi C-H, MacLellan WR, Beygui RE, Shemin RJ, Heydarkhan-Hagvall S. 2009. The use of three-dimensional nanostructures to instruct cells to produce extracellular matrix for regenerative medicine strategies. *Biomaterials* 30:4665–4675.

Schindelin J, Arganda-Carreras I, Frise E. 2012. Fiji: an open-source platform for biological-image analysis. *Nat Methods* 9(7):676–682.

Schittny JC, Yurchenco PD. 1989. Basement membranes: molecular organization and function in development and disease. *Curr Opin Cell Biol* 1:983–988.

Schop D, Dijkhuizen-Radersma R van, Borgart E, Janssen FW, Rozemuller H, Prins H-J, Bruijn JD De. 2010. Expansion of human mesenchymal stromal cells on microcarriers. Growth and metabolism. *J Tissue Eng Regen Med* 4:131–140.

Scudellari M. 2009. The delivery dilemma. *Nat Reports Stem Cells*. Nature Publishing Group.

Sellaro TL, Ravindra AK, Stolz DB, Badylak SF. 2007. Maintenance of hepatic sinusoidal endothelial cell phenotype in vitro using organ-specific extracellular matrix scaffolds. *Tissue Eng* 13(9):2301–2310.

Serra T, Mateos-Timoneda MA, Planell JA, Navarro M. 2013. 3D printed PLA-based scaffolds. *Organogenesis* 9(4):239–244.

Sevilla CA, Dalecki D, Hocking DC. 2010. Extracellular Matrix Fibronectin Stimulates the Self-Assembly of Microtissues on Native Collagen Gels. *Tissue Eng Part A* 16(12):3805–3819.

Shekaran A, Lam A, Sim E, Jialing LEE, Jian LI, Toh J, Wen PEI, Kok J, Chan YEN, Choolani M, Reuveny S, Birch W, Oh S. 2016. Biodegradable ECM-coated PCL microcarriers support scalable human early MSC expansion and in vivo bone formation. *Cytotherapy* 18:1332–1344.

Shekaran A, Sim E, Tan KY, Kok J, Chan Y, Choolani M, Reuveny S, Oh S. 2015. Enhanced in vitro osteogenic differentiation of human fetal MSCs attached to 3D microcarriers versus harvested from 2D monolayers. *BMC Biotechnol* 15(102):1–13.

Shi X, Wang Y, Varshney RR, Ren L, Gong Y, Wang DA. 2010. Microsphere-based drug releasing scaffolds for inducing osteogenesis of human mesenchymal stem cells in vitro. *Eur J Pharm Sci* 39:59–67.

da Silva Meirelles L, Fontes AM, Covas DT, Caplan AI. 2009. Mechanisms involved in the therapeutic properties of mesenchymal stem cells. *Cytokine Growth Factor Rev* 20:419–427.

Sisson AL, Schroeter M, Lendlein A. 2011. Polyesters. In: Lendlein, A, Sisson, AL, editors. *Handb Biodegrad Polym Isol Synth Charact Appl*. Wiley, pp. 1–21.

Soucy P a, Romer LH. 2009. Endothelial cell adhesion, signaling, and morphogenesis in fibroblast-derived matrix. *Matrix Biol* 28:273–283.

Sridhar B V., Doyle NR, Randolph MA, Anseth KS. 2014. Covalently tethered TGF-β1 with encapsulated chondrocytes in a PEG hydrogel system enhances extracellular matrix production. *J Biomed Mater Res - Part A* 102A(12):4464–4472.

Stock P, Staege MS, Müller LP, Sgodda M, Völker A, Volkmer I, Lützkendorf J, Christ B. 2008. Hepatocytes Derived From Adult Stem Cells. *Transplant Proc* 40:620–623.

Su T-M, Lan C-M, Lee T-H, Hsu S-W. 2014. Gas-containing brain abscess: Etiology, clinical characteristics, and outcome. *Kaohsiung J Med Sci* 30:619–624.

Sun Y, Li W, Lu Z, Chen R, Ling J, Ran Q, Jilka RL, Chen X-D. 2011. Rescuing replication and osteogenesis of aged mesenchymal stem cells by exposure to a young extracellular matrix. *FASEB J* 25(5):1474–1485.

Sung B, Shaffer S, Sittek M, Alboslemy T, Kim C, Kim M-H. 2016. Alternating Magnetic Field-Responsive Hybrid Gelatin Microgels for Controlled Drug Release. *J Vis Exp* 108:e53680.

Takahashi K, Yamanaka S. 2006. Induction of Pluripotent Stem Cells from Mouse Embryonic and Adult Fibroblast Cultures by Defined Factors. *Cell* 126:663–676.

Tan KY, Reuveny S, Oh SKW. 2016. Recent advances in serum-free microcarrier expansion of mesenchymal stromal cells: Parameters to be optimized. *Biochem Biophys Res Commun* 473:769–773.

Tang C, Xu Y, Jin C, Min B-H, Li Z, Pei X, Wang L. 2013. Feasibility of Autologous Bone Marrow Mesenchymal Stem Cell-Derived Extracellular Matrix Scaffold for Cartilage Tissue Engineering. *Artif Organs* 37(12):170–190.

Tang Q, Zhou Y, Chen F, Tan W. 2008. Preparing Engineered Tissues in vitro by Macroporous Microcarriers. *Chin J Biotechnol* 24(1):74–82.

Tang X, Thankappan SK, Lee P, Fard SE, Harmon MD, Tran K, Yu X. 2014. Polymeric Biomaterials in Tissue Engineering and Regenerative Medicine. *Nat Synth Biomed Polym*. Elsevier Inc. 351-371 p.

Tao J, Sun Y, Wang QG, Liu CW. 2009. Induced endothelial cells enhance osteogenesis and vascularization of mesenchymal stem cells. *Cells Tissues Organs* 190:185–193.

Thevenot PT, Nair AM, Shen J, Lotfi P, Ko CY, Tang L. 2010. The effect of incorporation of SDF-1α into PLGA scaffolds on stem cell recruitment and the inflammatory response. *Biomaterials* 31:3997–4008.

Thibault RA, Mikos AG, Kasper FK. 2013. Scaffold/Extracellular Matrix Hybrid Constructs for Bone Tissue Engineering. *Adv Heal Mater* 2(1):13–24.

Thibault R a, Scott Baggett L, Mikos AG, Kasper FK. 2010. Osteogenic differentiation of mesenchymal stem cells on pregenerated extracellular matrix scaffolds in the absence of osteogenic cell culture supplements. *Tissue Eng Part A* 16(2):431–440.

Thomson JA, Itskovitz-Eldor J, Shapiro SS, Waknitz MA, Swiergiel JJ, Marshall VS, Jones JM. 1998. Embryonic stem cell lines derived from human blastocysts. *Science* 282:1145–1147.

Tiruvannamalai-Annamalai R, Armant DR, Matthew HWT. 2014. A glycosaminoglycan based, modular tissue scaffold system for rapid assembly of perfusable, high cell density, engineered tissues. *PLoS One* 9(1):e84287.

Tomford WW. 1995. Transmission of disease through transplantation of musculoskeletal allografts. *J Bone Jt Surg - Ser A* 77:1742–1754.

Totaro A, Urciuolo F, Imparato G, Netti PA. 2016. Engineered cardiac micromodules for the in vitro fabrication of 3D endogenous macro-tissues. *Biofabrication* 8:025014.

Tour G, Wendel M, Ph D, Tcacencu I. 2011. Cell-Derived Matrix Enhances Osteogenic Properties of Hydroxyapatite. *Tissue Eng Part A* 17(1-2):127–137.

Tour G, Wendel M, Tcacencu I. 2013. Human fibroblast-derived extracellular matrix constructs for bone tissue engineering applications. *J Biomed Mater Res A* 101A(10):2826–2837.

Touraine RL, Ishii-Morita H, Ramsey WJ, Blaese RM. 1998. The bystander effect in the HSVtk/ganciclovir system and its relationship to gap junctional communication. *Gene Ther* 5:1705–1711.

Tseng P-C, Young T-H, Wang T-M, Peng H-W, Hou S-M, Yen M-L. 2012. Spontaneous osteogenesis of MSCs cultured on 3D microcarriers through alteration of cytoskeletal tension. *Biomaterials* 33:556–564.

Tsuchiya K, Chen G, Ushida T, Matsuno T, Tateishi T. 2001. Effects of cell adhesion molecules on adhesion of chondrocytes, ligament cells and mesenchymal stem cells. *Mater Sci Eng C* 17:79–82.

Twal WO, Klatt SC, Harikrishnan K, Gerges E, Cooley M a, Trusk TC, Zhou B, Gabr MG, Shazly T, Lessner SM, Markwald RR, Argraves WS. 2014. Cellularized microcarriers as adhesive building blocks for fabrication of tubular tissue constructs. *Ann Biomed Eng* 42(7):1470–1481.

Urciuolo F, Imparato G, Palmiero C, Trilli A, Netti P a. 2011. Effect of process conditions on the growth of three-dimensional dermal-equivalent tissue obtained by microtissue precursor assembly. *Tissue Eng Part C Methods* 17(2):155–164.

VanWezel AL. 1967. Growth of cell-strains and primary cells on micro-carriers in homogeneous culture. *Nature* 216(Octobe:64–65.

Verseijden F, Posthumus-van Sluijs SJ, Pavljasevic P, Hofer SOP, van Osch GJV., Farrell E. 2010. Adult Human Bone Marrow– and Adipose Tissue–Derived Stromal Cells Support the Formation of Prevascular-like Structures from Endothelial Cells In Vitro. *Tissue Eng Part A* 16(1):101–114.

Vhora I, Patil S, Bhatt P, Gandhi R, Baradia D, Misra A. 2014. Receptor-targeted drug delivery: Current perspective and challenges. *Ther Deliv* 5(9):1007–1024.

Vila OF, Bagó JR, Navarro M, Alieva M, Aguilar E, Engel E, Planell J, Rubio N, Blanco J. 2013. Calcium phosphate glass improves angiogenesis capacity of poly(lactic acid) scaffolds and stimulates differentiation of adipose tissue-derived mesenchymal stromal cells to the endothelial lineage. *J Biomed Mater Res - Part A* 101A(4):932–941.

Vila OF, Garrido C, Cano I, Guerra-Rebollo M, Navarro M, Meca-Cortés O, Ma SP, Engel E, Rubio N, Blanco J. 2016. Real-Time Bioluminescence Imaging of Cell Distribution, Growth, and Differentiation in a Three-Dimensional Scaffold Under Interstitial Perfusion for Tissue Engineering. *Tissue Eng Part C Methods* 22(9):864–872.

Vilalta M, Dégano IR, Bagó J, Aguilar E, Gambhir SS, Rubio N, Blanco J. 2009. Human adipose tissue-derived mesenchymal stromal cells as vehicles for tumor bystander effect: A model based on bioluminescence imaging. *Gene Ther* 16:547–557.

Vilalta M, Dégano IR, Bagó J, Gould D, Santos M, García-Arranz M, Ayats R, Fuster C, Chernajovsky Y, García-Olmo D, Rubio N, Blanco J. 2008. Biodistribution, Long-term Survival, and Safety of Human Adipose Tissue-derived Mesenchymal Stem Cells Transplanted in Nude Mice by High Sensitivity Non-invasive Bioluminescence Imaging. *Stem Cells Dev* 17:993–1004.

Vlahos AE, Cober N, Sefton M V. 2017. Modular tissue engineering for the vascularization of subcutaneously transplanted pancreatic islets. *PNAS* 114(35):9337–9342.

Vöpel T, Scholz R, Davico L, Groß M, Büning S, Kareth S, Weidner E, Ebbinghaus S. 2015. Infrared laser triggered release of bioactive compounds from single hard shell microcapsules. *Chem Commun* 51:6913–6916.

Waldeck HM, Kao WJ. 2011. Extracellular Matrix : Inspired Biomaterials. *Compr Biomater*. Elsevier Ltd. 113-126 p.

Wang X, Jiao Q, Zhang S, Ye Z, Zhou Y, Tan W-S. 2014. Perfusion culture induced template-assisted assembling of cell-laden microcarriers is a promising route for fabricating macrotissues. *Biotechnol*

J 9:1425–1434.

Wang Z, Wang Z, Lu WW, Zhen W, Yang D, Peng S. 2017. Novel biomaterial strategies for controlled growth factor delivery for biomedical applications. *NPG Asia Mater* 9(e435):1–17.

Wen PY, Kesari S. 2008. Malignant gliomas in adults. *N Engl J Med* 359:492–507.

Wendt D, Jakob M, Martin I. 2005. Bioreactor-based engineering of osteochondral grafts: from model systems to tissue manufacturing. *J Biosci Bioeng* 100(5):489–494.

Whitesides GM, Grzybowski B. 2002. Self-assembly at all scales. *Science* 295:2418–2421.

Wong CY, Al-Salami H, Dass CR. 2018. Microparticles, microcapsules and microspheres: A review of recent developments and prospects for oral delivery of insulin. *Int J Pharm* 537:223–244.

Wronska MA, O'Connor IB, Tilbury MA, Srivastava A, Wall JG. 2016. Adding Functions to Biomaterial Surfaces through Protein Incorporation. *Adv Mater* 28:5485–5508.

Xiao J, Zhang G, Li B, Wu Y, Liu X, Tan Y, Du B. 2017. Dioscin augments HSV-tk-mediated suicide gene therapy for melanoma by promoting connexin-based intercellular communication. *Oncotarget* 8(1):798–807.

Xu Q, Hashimoto M, Dang TT, Hoare T, Kohane DS, Whitesides GM, Langer R, Anderson DG. 2009. Preparation of monodisperse biodegradable polymer microparticles using a microfluidic flow-focusing device for controlled drug delivery. *Small* 5:1575–1581.

Yang Y, Rossi FMV, Putnins EE. 2007. Ex vivo expansion of rat bone marrow mesenchymal stromal cells on microcarrier beads in spin culture. *Biomaterials* 28:3110–3120.

Yeatts AB, Fisher JP. 2011. Bone tissue engineering bioreactors: dynamic culture and the influence of shear stress. *Bone* 48:171–181.

Yoshida Y, Yamanaka S. 2010. Recent stem cell advances: Induced pluripotent stem cells for disease modeling and stem cell-based regeneration. *Circulation* 122:80–87.

Young RM, Jamshidi A, Davis G, Sherman JH. 2015. Current trends in the surgical management and treatment of adult glioblastoma. *Ann Transl Med* 3(9):121–146.

Yuan Y, Kallos MS, Hunter C, Sen A. 2014. Improved expansion of human bone marrow-derived mesenchymal stem cells in microcarrier-based suspension culture. *J Tissue Eng Regen Med* 8:210–225.

Yunoki S, Ikoma T, Monkawa A, Marukawa E, Sotome S, Shinomiya K, Tanaka J. 2007. Three-dimensional porous hydroxyapatite/collagen composite with rubber-like elasticity. *J Biomat Sci Polym* 18:393–409.

Zhang S, Zhou M, Ye Z, Zhou Y, Tan WS. 2017. Fabrication of viable and functional pre-vascularized modular bone tissues by coculturing MSCs and HUVECs on microcarriers in spinner flasks. *Biotechnol J* 12(8):1700008.

Zhang W, Zhu Y, Li J, Guo Q, Peng J, Liu S, Yang J, Wang Y. 2016. Cell-Derived Extracellular Matrix: Basic Characteristics and Current Applications in Orthopedic Tissue Engineering. *Tissue Eng Part B Rev* 22(3):193–207.

Zhong M, Wei D, Yang Y, Sun J, Chen X, Guo L, Wei Q, Wan Y, Fan H, Zhang X. 2017. Vascularization in engineered tissue construct by assembly of cellular patterned micromodules and degradable microspheres. *ACS Appl Mater Interfaces* 9:3524–3534.

Zhou Y, Gao HL, Shen LL, Pan Z, Mao LB, Wu T, He JC, Zou DH, Zhang ZY, Yu SH. 2016a. Chitosan microspheres with an extracellular matrix-mimicking nanofibrous structure as cell-carrier building blocks for bottom-up cartilage tissue engineering. *Nanoscale* 8:309–317.

Zhou Z, Pausch F, Schlötzer-Schrehardt U, Brachvogel B, Pöschl E. 2016b. Induction of initial steps of angiogenic differentiation and maturation of endothelial cells by pericytes in vitro and the role of collagen IV. *Histochem Cell Biol* 145:511–525.

Zhu L, Li M, Liu X, Jin Y. 2017. Drug-Loaded PLGA Electrospraying Porous Microspheres for the Local Therapy of Primary Lung Cancer via Pulmonary Delivery. *ACS Omega* 2:2273–2279.

Zimmerlin L, Park TS, Zambidis ET, Donnenberg VS, Donnenberg AD. 2013. Mesenchymal stem cell secretome and regenerative therapy after cancer. *Biochimie* 95:2235–2245.

Zorlutuna P, Vrana NE, Khademhosseini A. 2013. The expanding world of tissue engineering: The building

blocks and new applications of tissue engineered constructs. *IEEE Rev Biomed Eng* 6:47–62.